MATHEMATICAL MODELLING OF CATALYTIC DISTILLATION IN A 1-HEXENE HYDROGENATION SYSTEM

by

JOSIAS JAKOBUS NIEUWOUDT
B.Eng. (Chem. Eng.) University of Stellenbosch
M.Sc.Eng. (Chem. Eng.) University of Stellenbosch

Thesis presented for the Degree of

DOCTOR OF PHILOSOPHY IN ENGINEERING

in the

CENTRE FOR CATALYSIS RESEARCH

in the department of

CHEMICAL ENGINEERING

at the

UNIVERSITY OF CAPE TOWN

SUPERVISOR

Professor K.P. MöLLER

GRADUATION DATE

JUNE 2010

Declaration

I, the undersigned, hereby declare that the work contained in this thesis is my own original work and that I have not previously in its entirety or in part submitted it at any university for a degree.

_____
J.J. Nieuwoudt

26th May 2010
Date

Summary

Catalytic Distillation (CD) is a form of process intensification were a heterogeneously catalyzed reaction is performed in a distillation unit. This fusion of functions has been shown to have the potential to reduce capital costs, operating costs and environmental impacts.

It is hypothesized that a fundamental mathematical model of both the mass/heat transfer and reaction kinetics is required to accurately predict the behaviour of even perceived "simple" kinetic equation reactions performed in a CD column, and that such a validated model can yield a deeper understanding of the dynamics in such systems.

The hypothesis was proven successfully. To achieve this, 1-hexene hydrogenation Langmuir-Hinshelwood kinetics were derived and fitted to experimental semi-batch data. The reaction kinetics were then included in a non-equilibrium distillation model which was compared to experimental CD hydrogenation data. The reaction kinetics and mass transfer correlation coefficients were then fitted to the CD data.

The pre-exponential Arrhenius factors and activation energies of the reaction rate constants were fitted with an acceptable level of statistical variance. A sensitivity analysis showed that, within the region of interest, the dissociative hydrogen adsorption and 1-hexene adsorption are rate controlling rather than, as was expected from literature, the first hydrogen transferral, though the latter becomes more significant as the temperature is increased.

The resulting CD model was found to be extremely non-linear and sensitive to the mass transfer effects to and from the catalyst and between the vapour and liquid phases. Incorporation of the reaction kinetics and a subsequent understanding of the catalyst surface species concentrations is required to adequately simulate the experimentally observed values. The conversions and selectivities were found to be most sensitive to changes in pressure and hydrogen feed flow rate, both of which significantly affect the column temperature and hence the reaction kinetics and mass transfer. The model thus not only yielded a deeper understanding of the dynamics in the system, but also showed that rigorous reaction kinetics can add value to our understanding of the system dynamics.

The models were developed based on a sound combination of experimental, theoretical and statistical techniques. The study also supplies statistically weighted liquid

phase 1-hexene hydrogenation kinetics on a Ni/Al_2O_3 catalyst, which, after an exhaustive search, could not be found in literature. Maxwell-Stefan mass transfer was approximated by using the linearized approach to reduce computational time and complexity. The resulting CD model solves for the surface species concentrations described by fundamental, fitted Langmuir-Hinshelwood kinetics, thus tracking the effects on the surface and elucidating its effect on the overall CD column dynamics.

Viva Scientia!

Acknowledgements

When I started this PhD, I expected an exciting journey and I was not disappointed! I can honestly say that everything you read here is my own work, that I walked this road to the end with sheer determination often despite the continuous boulders thrown in my way by supposed support structures and services...

...and that I am very proud of it. I made it!

But, there are people and individuals who made a significant contribution to my finishing the thesis by today. They deserve my gratitude and, sometimes, admiration either because they do what they do well or because they assisted and supported me during critical periods of the PhD.

Bill and Granville from the electrical workshop: you were always willing to help, you did it promptly and you did it well. Mr Roberts, thank you for allowing me to use your online micro-GC for my off-gas analyses despite the outside risk of high levels of hydrocarbons getting into it. Without your micro-GC, I would not have been able to finish this thesis. You Qi, thank you that I could hijack your reactor system for the kinetic studies - there is an entire chapter in this thesis devoted to it! I am also grateful to Roelof Coetzer who taught me a couple of tricks when performing statistical data analyses. Pieter and Maureen, thank you for temporarily increasing my computer resources 3-fold! Also thanks to the UCT library for having excellent electronic and hardcopy resources to facilitate academic research.

Klaus, I would not have been able to finish this thing without you...

Many people and friends have crossed my way over the years. They may not have had a direct impact on the PhD, but walked the road with me nonetheless. These guys know who they are, but might not know how important they were. Thank you!

'n Spesiale woord van dank aan my familie: ma, pa, Allan, Gerdus, Ouma Onie en Oupa John, Oupa Joos en Ouma Hasie. Dankie vir julle ondersteuning, julle geloof en julle inspirasie.

And then to the friend who, I'm glad to say, decided to marry me and see the road out to the end. Cathrin, you have more then made up for the time you were writing your thesis up. For the last couple of years, you have been sharing me with work, PhD and (of course) my first wife - Sally the CD column ;-) I hope to be served the divorce papers soon! Ich liebe dich, mein Schätzle!

Lastly, I thank God. He will know what for.

Knowledge is like the first spring rains in Namakwaland. It decorates a barren wilderness filled with tough, thorny bushes with a magical array of flowers that resiliently push their way up through the sun-cracked soil. We have so much information nowadays, that it is sometimes difficult to find those flowers of thought that we are seeking. In time, these flowers will wither and die. But for the lucky ones, someone may come along and be inspired by them, and this cross-polination of ideas will then lie in wait for the next rains. Then, a small part of them will live on into the future and never die. If, one day, you should open this thesis among all the zillions of books and zettabytes of information and find any inspiration - let me know.

Jako Nieuwoudt

Vanderbijlpark

29 November 2009

Contents

Nomenclature

Variables in **bold** are matrices or vectors. SI units or SI derived units will be used in all equations throughout the thesis, except for kmol instead of mol. Specifications (such as catalyst or structured packing) will be supplied in units most convenient to the specific application.

Symb.	Definition	Unit(s)
	Normal Letters	
a	Interfacial surface area per stage	m^2/stage
a	Species dependent constant (Section B.2 only)	$kg.m^5/kmol^2.s^2$
a_d	Specific packing surface area density	m^2/m^3
a_p	Specific packing surface area	m^2/m^3
A	Area	m^2
A	Species dependent constant (Section B.2 only)	-
A	Constant in eq. 5.43	-
A_{rh}	Pre-exponential Arrhenius constant	Varies
$A_{contact}$	Contact area	m^2
A_p	Surface area of particle	m^2
b	Species dependent constant (Section B.2 only)	m^3/kmol
B	Channel base (structured packing)	m
B	Species dependent constant (Section B.2 only)	-
c	Number of components	-
cor	Correlation matrix	-
cov	Covariance matrix	-
c_i	Constant i	Varies
c_p	Specific heat capacity	J/kmol.K
C	Concentration	$kmol/m^3$
C_i	Concentration of component i	$kmol/m^3$
C_{WP}	Weisz-Prater criterion	-
Ca_L	Capillary number	-
CV	Coefficient of variation	-
$C_{n,m}^{UNIFAC}$	Vector of 3 UNIFAC constants [Horstmann et al., 2005]	Varies

Symb.	Definition	Unit(s)
d	Diameter	m
d_p	Particle diameter	m
d_{eq}	Equivalent diameter	m
D	Diffusion coefficient	m^2/s
e^a	Energy transfer rate through stagnant film of phase a	W
E_a	Reaction activation energy	J/kmol
eqE^a	Error term for energy balance around boundary a	W
$eqFlux$	Error term for rate equation	-
$eqHydr$	Error term for pressure drop equation	Pa
eqM_i^a	Error term for component i mole balance in phase a	kmol/s
eqQ_i	Error term for vapour-liquid equilibrium of component i	-
eqS	Error term for summation equation	-
$eq\theta_V$	Error term for surface species balance	mol/kg_{cat}
f_{ass}	Association factor	-
f_ω	Function of acentric factor (Appendix B)	-
F^a	Feed molar flow rate of phase a	kmol/s
F_{aux}	Auxiliar property of component i (Appendix B)	-
F_P	Packing factor [Seader & Henley, 1998]	ft^2/ft^3
g	Gravitational acceleration (9.81 m/s^2)	m/s^2
G	Gibbs free energy	J/kmol.K
G^E	Gibbs excess energy	J/kmol.K
h_a	Heat transfer coefficient in phase a	$W/m^2.K$
h_c	Crimp height (structured packing)	m
H	Height of section of packing	m
H_i^a	Specific enthalpy of i in phase a	J/kmol
k_c^a	Heat conductivity in phase a	$W/m^2.K$
k_i^a	Intrinsic forward reaction rate constant for reaction i, type a	$kmol/s.kg_{cat}$
$k_{i,k}^a$	Binary mass transfer coefficient of component i in phase a	m/s
K_i^a	Reaction equilibrium constant for reaction i of type a	Varies
$K_{eq,i}$	Vapour-liquid equilibrium constant of component i	-
L	Liquid molar flow rate	kmol/s
Le	Lewis number $Le = \frac{\lambda}{D^{ave} c_p \rho}$	-
M_i	Molecular weight	kg/kmol
$\dot{m}$	Mass flow rate	kg/s
n_i	Number of moles	kmol
n_{iso}	Number of alkene isomers	-
n_{pars}	Number of parameters	-

Symb.	Definition	Unit(s)
n_{peaks}	Number of peaks	-
n_{points}	Number of points	-
$n_{rxnorder}$	Reaction order	-
$n_{i,k}^{subgroups}$	Number of subgroups k in component i (Appendix B)	-
N_{stages}	Total number of stages	kmol/m^2.s
N_i^a	Molar flow rate of i through stagnant film of phase a	kmol/s
N_i^a	Number of moles of i in phase a (batch systems)	kmol
par	Vector of parameters	Varies
P	Pressure	Pa
P	Perimeter per cross-sectional area (structured packing)	m/m^2
q	q-factor used in constant molar overflow	-
q_i	Relative van-der-Waal's surface area of component i (Appendix B)	-
Q	Heat transferred added to (+) or removed from (-) a	W
Q_k	Relative van-der-Waal's surface area of subgroup k (Appendix B)	-
r_i	Rate of formation of i	kmol/s.kg$_{cat}$
r_i	Relative van-der-Waal's volume of component i (Appendix B)	-
r_j^a	Fraction of phase a leaving stage j that is drawn off in a sidestream	-
R	Recycle ratio (ratio of recycle and distillate liquid molar flow rates)	-
R_0	Ideal gas constant (8314 J/kmol.K)	J/kmol.K
R^2	R^2 statistical value	-
R_k	Relative van-der-Waal's volume of subgroup k (Appendix B)	-
R_i^a	Rate of consumption of i in reaction of type a	kmol/s.kg$_{cat}$
Re	Reynolds number $Re = \frac{\rho u d}{\eta}$	-
s	Standard error	Varies
s^2	Sum of squares	Varies
$S_{i,k}$	Selectivity of component i based on component k consumed	kmol$_i$/kmol$_k$
S	Channel side (structured packing)	m
Sc	Schmidt number $Sc = \frac{\eta}{\rho^{mass} D^{ave}}$	-
Sh	Sherwood number $Sh = \frac{k d_{eq}}{D^{ave}}$	-
SE	Standard error	Varies
sns	Vector of deviations parameters considered in fitting of the CD system	Varies

Symb.	Definition	Unit(s)
t	Time	s
t_L	Exposure time	s
T^a	Temperature of phase a	K
u	Superficial velocity	m/s
v	Linear velocity	m/s
V	Vapour molar flow rate	kmol/s
V^a	Volume of a	m^3
V_{aux}	Auxiliary property for component i (Appendix B)	-
V_{emp}	Empirically modified V_{aux} for component i (Appendix B)	-
$V_{Fuller,i}$	Fuller volume of component i	cm^3/mol
$\dot{V}$	Volumetric flow rate	m^3/s
W	Weight	kg
x_i	Molar fraction of i in a liquid mixture	-
x^{exp}	Experimentally set independent variable	Varies
X	Conversion	kmol/kmol
X_m	Group mole fraction of group m in the liquid phase (Appendix B)	-
y_i	Molar fraction of i in a vapour mixture	-
y^{exp}	Experimentally determined dependent variable	Varies
y^{model}	Theoretically determined dependent variable	Varies
z	Distance in the z direction	m
z_i	Total molar fraction of i in the liquid and vapour phases	kmol/kmol
Z	Compressibility factor	-
	Subscripts	
ave	Average	-
c	Critical	-
C	Alkene	-
CH	Half-hydrogenated state on catalyst surface	-
cat	Catalyst	-
F	Feed to column	-
H	Dissociatively adsorbed hydrogen on catalyst surface	-
H2	Diatomic hydrogen	-
i	Indicates component i in the mixture	-
I	Interface	-
j	Indicates stage j in the distillation system	-
k	Indicates component k in the mixture	-
L	Liquid phase	-

Symb.	Definition	Unit(s)
LF	Liquid feed	-
nC	n-Alkane	-
p	Catalyst particle	-
r	Reduced	-
T	Total	-
vap	Refers to vapourization	-
V	Vapour phase or vacant sites	-
VF	Vapour feed	-
	Superscripts	
$\overline{\mathbf{a}}$	Arithmetical average of matrix **a**	-
ads	Adsorption of alkene in the Horiuti-Polanyi mechanism	-
ave	Average	-
bed	Catalyst bed	-
cat	Catalyst	-
des	Desorption of alkane in the Horiuti-Polanyi mechanism	-
F	Feed to column	-
id	Ideal	-
iso1	First hydrogen transferral in the Horiuti-Polanyi mechanism	-
iso2	First hydrogen transferral in the Horiuti-Polanyi mechanism onto the alternative carbon involved in the double bond	-
inf	Infinity	-
I	Vapour-liquid interface	-
L	Liquid phase	-
LI	Liquid phase interface	-
mix	Mixture	-
rxn	Reaction	-
sat	Indicates saturation	-
vap	Refers to vapourization	-
V	Vapour phase	-
VI	Vapour phase interface	-
	Greek letters	
δ	Indicates a small change	Varies
Δ	Indicates a large change	Varies
ϵ	Void fraction	-
$\hat{\phi}_i$	Fugacity coefficient of species i in solution	-
γ_i	Activity coefficient of i	-

Symb.	Definition	Unit(s)
Γ	Liquid molar flow rate per unit of perimeter (structured packing)	kmol/s.m
Γ_k	Group activity coefficient of group k in the mixture (Appendix B)	-
Γ_k^I	Group activity coefficient of group k in the pure substance (Appendix B)	-
η	Viscosity	Pa.s
λ	Heat conductivity	W/m.K
μ	Chemical potential	J/kmol
π	3.14159265358979...	-
θ	Catalyst surface concentration	kmol/kg$_{cat}$
θ	Channel flow angle from horizontal (structured packing)	$^\circ$
θ_m	Surface fraction of group m in the liquid phase (Appendix B)	-
ρ	Density	kmol/m^3
σ_i	Surface Tension of component i	N/m
σ_{ii}^2	Variance of parameter i	Varies
σ_{ik}^2	Covariance of parameters i and k	Varies
υ_i	Stoichiometric coefficient of component i	-
υ	Molar volume (Appendix B)	m^3/kmol
ω	Acentric factor	-
$\psi_{n,m}$	UNIFAC group interaction parameter between main groups n and m (Appendix B)	-
	Other	
∇	Mathematical operator for "gradient"	-
$\aleph_{i,j}$	Interaction parameter between components i and j (Appendix B)	-
	Abbreviations	
CD	**C**atalytic **D**istillation	-
CFD	**C**omputational **F**luid **D**ynamics	-
CMO	**C**onstant **M**olar **O**verflow	-
CR&L	**C**hemical **R**esearch and **L**icensing	-
CSTR	**C**ontinuous **S**tirred **T**ank **R**eactor	-
DAE	**D**ifferential **A**lgebraic **E**quation	-
EOS	**E**quation **o**f **S**tate	-
EQ	**Eq**uilibrium	-
GUI	**G**raphical **U**ser **I**nterface	-
HETP	**H**eight **E**quivalent of a **T**heoretical **P**late	-

Symb.	Definition	Unit(s)
HPLC	**H**igh **P**ressure **L**iquid **C**hromatography	-
JaKaD	Computer algorithm developed in this thesis to model the CD 1-hexene system	-
KD	**K**atalitiese **D**istillasie	-
KPI	**K**ey **P**erformance **I**ndicator	-
MERSHH	**M**aterial balance, **E**quilibria, **R**ate, **S**ummation, Energy (**H**) balance and **H**ydraulic equations	-
MESH	**M**aterial balance, **E**quilibria, **S**ummation and Energy (**H**) balance equations	-
MOC	**M**aterials **o**f **c**onstruction	-
MSS	**M**ultiple **S**teady **S**tates	-
MTBE	**M**ethyl **t**ertiary **b**utyl **e**ther (IUPAC name: 2-methoxy-2-methylpropane)	-
NEQ	**N**on-**eq**uilibrium	-
NTP	**N**ormal **T**emperature and **P**ressure (273.15 K; 101325 Pa)	-
PBR	**P**acked **B**ed **R**eactor	-
PFR	**P**lug **F**low **R**eactor	-
PID	**P**roportional-**I**ntegral-**D**erivative (in control systems)	-
P&ID	**P**ipe and **I**nstrumentation **D**iagram	-
PR	**P**eng-**R**obinson EOS	-
PSRK	**P**redictive **S**oave-**R**edlich-**K**wong	-
RD	**R**eactive **D**istillation	-
RK	**R**edlich-**K**wong EOS	-
SCD	**S**uspension **C**atalytic **D**istillation	-
SRK	**S**oave-**R**edlich-**K**wong EOS	-
STP	**S**tandard **T**emperature and **P**ressure (298.15 K; 101325 Pa)	-
TAME	**T**ertiary-**a**myl **m**ethyl **e**ther (IUPAC name: 2-methoxy-2-methylbutane)	-
TEM	**T**ransmission **E**lectron **M**icroscopy	-
TPR	**T**emperature **P**rogrammed **R**eduction	-
UCT	**U**niversity of **C**ape **T**own	-
UNIFAC	**Uni**versal **F**unctional **A**ctivity **C**oefficient	-
UPS	**U**ninterrupted **P**ower **S**upply	-
VI	**V**irtual **I**nstrument (main program in LabVIEW)	-
VLE	**V**apour-**L**iquid **E**quilibrium	-

List of Figures

List of Tables

Part I

LITERATURE REVIEW & PROJECT DEFINITION

Chapter 1

Reactive Distillation

1.1 History and background

Catalytic Distillation (CD) is a form of process intensification were a heterogeneously catalyzed reaction is performed in a distillation unit. Reactive distillation (RD) is similar and should strictly refer to the use of a homogeneously rather than heterogeneously catalyzed reaction (e.g. as in Podrebarac et al. [1997]). However, in this thesis (as is more often the case in literature, e.g. Lei et al. [2004]) the term RD will be used to refer to the general case of a simultaneous reaction and distillative separation and CD will be used to refer to the specific case of where the reaction is catalyzed heterogeneously - i.e. by a solid catalyst.

In a certain sense, RD is as old as distillation itself, though a reaction was usually seen as something to be avoided rather than encouraged [Doherty & Buzad, 1992]. Only in the late 1910's did the possible benefits of RD capture the imagination of scientists and engineers and in the early 1920's four patents were awarded to Backhaus [1921, 1922, 1923a,b]. This was followed by several decades of little or no development in this field where the intrinsic benefits of RD were often recognized without apparent knowledge of the 1920 patents (cf. Saito et al. [1971])

In 1980, approximately 6 decades after the first RD patents appeared, the first commercial-scale CD column was put into operation by Charter Oil's Houston, Texas refinery for the production of methyl tertiary butyl ether (MTBE) - an octane enhancer in fuels [Rock et al., 1997]. The process was developed by Chemical Research & Licensing (CR&L), which was founded in 1977 [Siegel et al., 2005]. It was found to be so successful that by 1997 CD-based MTBE processes outnumbered rival installations [Podrebarac et al., 1997].

The success of CD is due to its well established advantages. One of the best summaries thereof by Podrebarac et al. [1997] is adapted here:

Heat integration The heat released in the exothermic reaction is used directly in the

column to generate more vapour thus enhancing separation via distillation and increasing energy efficiency - the synergistic effect.

Reduced danger of hot spots Since the CD column contains boiling liquid the danger of hot spots is reduced, as the temperature of the liquid cannot exceed its boiling point. Additionally, as long as the catalyst is properly wetted it will have a similar temperature to the liquid.

Precise isothermal reaction control This is essentially an extension of the previous point and is achieved by keeping the catalyst particle temperature close to the liquid boiling point. Radial and axial temperature gradients are also minimized.

Reduced capital and operating costs Instead of having a reactor and subsequent separation units, one can achieve both product formation and separation in the same column, thus cutting back on costs.

Reduced corrosion It is unnecessary to use corrosion resistant material to construct the column walls or internals when using corrosive or hazardous catalysts, as there is no contact between them in CD.

Increased conversion CD can effectively "cheat" equilibrium and circumvent thermodynamic restrictions by immediately removing the products from the system upon formation. According to Le Chatelier's principle[a] this favours the forward reaction thus increasing the product formation rate in an equilibrium limited reaction and subsequently the conversion.

Improved selectivity Consecutive reactions are minimized by the relatively fast removal of products from the CD column's reactive zone.

Increased catalyst life Reduced catalyst poisoning is possible by correct placement of the reactive zone relative to the feed point.

Azeotropes can disappear Non-reactive azeotropes may disappear when a reaction takes place [Krishna & Wesselingh, 1997].

Despite the considerable commercial success of the CD MTBE process, it required a keynote paper by Doherty & Buzad in 1992 to spark a renewed interest in the subject. In fact, in an update to this review by Taylor & Krishna [2000], it is pointed out that over 150 of the 300 papers related to RD and CD cited in the year 2000 were written after 1992. On the commercial front CR&L and Lummus Technology partnered 50/50

[a]From e.g. Atkins [1998], Le Chatelier's principle states that "a system at equilibrium, when subjected to a disturbance, responds in a way that tends to minimize the effect of the disturbance". The original principle was formulated by Le Chatelier [1884, 1888].

in 1988 to form CDTECH [CDTech, 2009] and has since become one of the (if not the) main contributors to commercial CD products (see Section 2.4 for examples).

A rough search on `www.freepatentsonline.com` for RD and CD finds 708 patents of which CR&L and Lummus contribute 89 (12%). Of the 708 patents 7.8% are related to hydrogenation, though hydrogenation of olefins totals only 1.0%. Hiwale et al. [2004] supplies an interesting list of systems considered for CD applications while Harmsen [2007] supplies an updated review of CD with a list of commercial products available from CDTECH. Several hybrid versions of CD have also been considered - see Section 1.2.

Despite the possible benefits, CD is inherently limited by physical and commercial constraints (list adapted from Podrebarac et al. [1997]):

1. Distillation must be a viable method of separation.

2. The reaction must take place in the liquid phase.

3. Conditions within the column must preferably ensure both acceptable reaction and distillation performances. The boiling temperature within the column can be changed by changing the pressure, but at least one component must always be below its critical point.

4. The reaction must preferably be exothermic otherwise the advantage of heat integration is lost. If not, the extent of the additionally required energy input will have to be balanced against the projected benefits.

5. Catalyst replacement is usually expensive and labour intensive and the catalyst lifespan can thus weigh heavily against the other economic incentives of CD. Usually, a catalyst lifetime of 1 to 2 years is preferred.

6. From Turton et al. [1998], the increased capital and operating costs involved in operating a distillation column outside 1-10·10^5 Pa(a) and 313.15-523.15 K (40-250°C) must be weighed carefully against the economic incentives. This limits the economic viability of CD as many reactions of interest occur optimally outside of this operational space.

7. CD is not trivial to model and scale up as it requires a thorough understanding of both the reaction and distillation dynamics. Additionally, work by Sneesby et al. [1999] suggested that conventional rules of thumb (in this case specifically with regards to the number of trays in a column) for distillation do not always apply to CD. Although Al-Arfaj & Luyben [2000] challenged this, it cannot be denied that the (possibly extreme) non-linearity that can be introduced by a reaction(s) can potentially lead to unexpected behaviour.

8. Compared to the number of variables, CD has less degrees of freedom than conventional distillation-reactor systems and can thus be more difficult to control [Kaymak & Luyben, 2008].

Despite these limitations, developments in CD will probably continue as more stringent environmental awareness and legislation drive companies toward process intensification. It is this "green" aspect of CD coupled with potential savings in capital and operating costs that sustain commercial interests and demand a more fundamental understanding of reaction kinetics and mass transfer.

1.2 The physical system

In its simplest form, a CD system comprises a distillation column with one or more reactive zones interspersed between the non-reactive internals along the height of the column.

In terms of *column internals*, standard trays, random packing, or structured packing can be used in the non-reactive sections of the column. Random (or dumped) packing consist of a multitude of metal, ceramic, plastic (or other) elements with a specific geometry that is randomly dumped (or "poured") into a distillation column to optimize the phase contact area. Distillation textbooks, such as Seader & Henley [1998], supply more information regarding the available materials of construction, geometries and sizes available. Structured packing consists of vertical metal, plastic, carbon, etc. layers with a predefined geometry held together in an ordered manner to supply the necessary phase contact area. Again, Seader & Henley [1998] can supply more information regarding the different materials of construction, types and specifications available.

Several similar options are available for the reactive section internals as depicted in Figure 1.1. In general, the packing must allow good reactant-catalyst contact for the reaction and must cause a pressure drop sufficiently low for distillation purposes. Options include tea bag configurations, catalyst bales, horizontally disposed configurations, and catalyst containers vertically inserted into structured packing such as Sulzer Katapak-SP [Chemtech, 2003]. Mass transfer in bale type packings are considered by Manduca et al. [2003], on granules by Yuxiang & Xien [1992], and on Sulzer Katapak-SP by Kolodziej et al. [2004, 2005], van Baten et al. [2001] and van Baten & Krishna [2002]. Some have also looked at covering a structured packing surface with a thin catalyst layer [Oudshoorn et al., 1999].

Different *column configurations* have also been considered. Wang et al. [2002] investigated placing the catalyst within the liquid downcomers in trayed columns, effectively creating reactive downcomers. The authors claim that this approach facilitates easier replacement of the spent catalyst, which is economically advantageous in CD - see Sec-

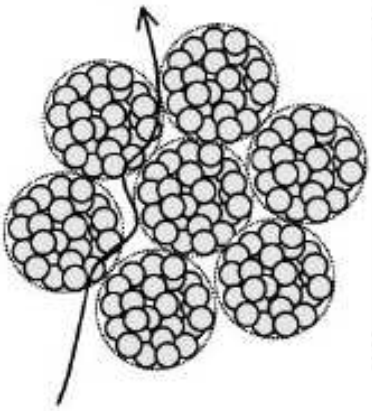

(a) Tea bag: spherical basket.

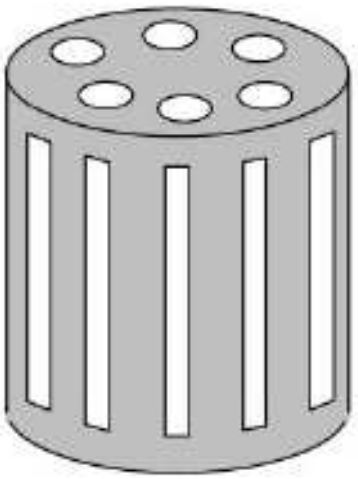

(b) Tea bag: Cylindrical container.

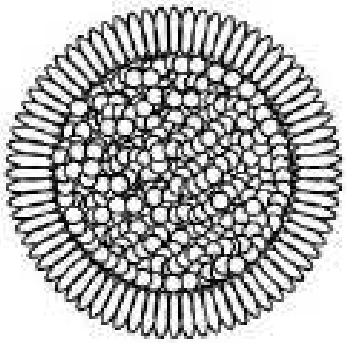

(c) Tea bag: Wire gauze envelopes.

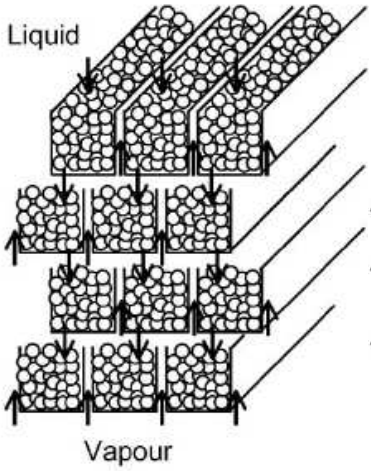

(d) Horizontally disposed gutters.

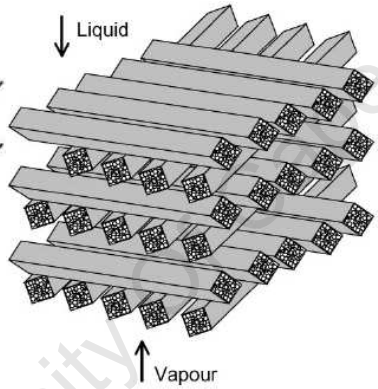

(e) Horizontally disposed wire gauze tubes.

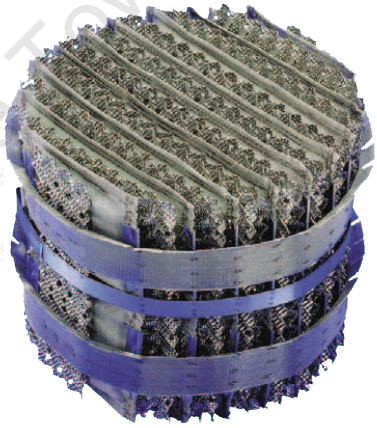

(f) Sulzer Katapak-SP [Chemtech, 2003].

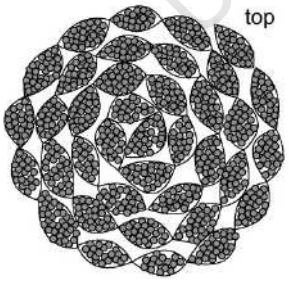

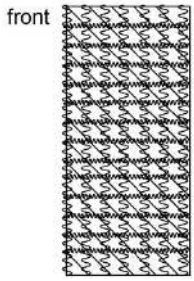

(g) Catalyst bales.

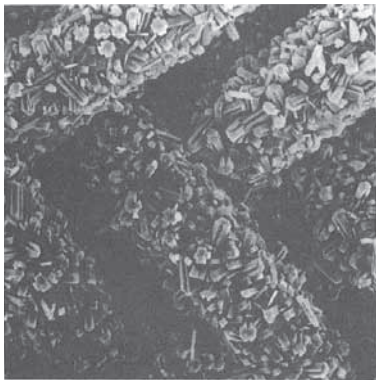

(h) Binderless film of zeolite H-ZSM-5 grown on 35 μm diameter stainless steel wire mesh [Oudshoorn et al., 1999]

Figure 1.1: Reaction zone internals in CD copied from Taylor & Krishna [2000] unless otherwise stated.

tion 1.1. Hybrid RD systems have also been investigated. Mueller & Kenig [2007], Hernandez et al. [2009], Harmsen [2006] and Sander et al. [2007] considered RD in a dividing wall column, Buchaly et al. [2007] presents a combination between RD and membrane separation, Wentink et al. [2007] looks at reactive extractive distillation, Steyer et al. [2008] at RD with a reactive entrainer, and Radulescu et al. [2009] at RD with potential liquid phase splitting. Wen et al. [2000] introduced a suspension catalytic distillation (SCD) column where a fine catalyst is blended into the liquid feed, thus enhancing liquid-solid mass transfer, and avoiding the need for catalyst replacement shutdowns and structured catalyst packing. Lei et al. [2007] considers fixed-bed CD, SCD and ionic-liquid distillation columns on a mathematical basis. As an interesting alternative to CD, Baur & Krishna [2003, 2004] presented the concept of "reactive pump arounds" where a sidestream of a distillation column is withdrawn, circulated through an external reactor, and returned to the column. Apart from practical considerations regarding catalyst replacement, this has the advantage above conventional CD that the reaction operating conditions can differ from that in the distillation column. However, it loses many of the advantages of CD, especially those related to system integration. Strictly speaking, such systems are not CD systems, though they fall under process intensification and present interesting flowsheeting challenges.

Research into RD has clearly been prolific during the last 2 decades.

There is also work performed on *operation and control* of CD systems. Adams et al. [2009] document a semi-continuous system that alternates between RD and reactive extraction. Grüner et al. [2003], Chandra & Venkateswarlu [2007], Kaymak & Luyben [2008], Luyben [2007], Kumar & Kaistha [2007, 2008b,a,c,d, 2009b,a] and Lai et al. [2008] investigate CD control issues. Kumar & Kaistha [2008d] and Rosales-Quintero & Vargas-Villamil [2009] consider control issues with regards to multiple steady states (see Section 1.3), Alejski & Duprat [1996], Peng et al. [2003], Segovia-Hernndez et al. [2005], Scenna et al. [1998] focus on dynamic and start-up issues, while Sumana & Venkateswarlu [2007] wrote an interesting article regarding inference of a metathesis CD column's stream compositions to affect control.

1.3 Modelling and design

There is a vast amount of publications in the open literature regarding simulation of non-reactive distillation systems. An undergraduate chemical engineering textbook such as Seader & Henley [1998] supplies a general overview of separation processes with significant emphasis on both practical and theoretical concepts in distillation.

Several commercial software packages such as Aspen Plus, Pro II and Chemsep are available to solve non-reactive distillation problems in terms of either the EQ or NEQ model. However, these packages are limited with regards to the upper level of complexity

that is possible for the reaction. Often, the reaction is incorporated in the form of a power rate law. Also, these packages do not allow access to their source codes and one is thus limited in terms of flexibility when interested in the fundamentals of mass transfer and reaction.

1.3.1 General

Many tools are available to simulate distillation columns, progressing from the simple graphical approaches for binary systems to complex non-equilibrium (NEQ) models requiring significant computer resources. Similarly, simple reactor models such as continuous stirred tank reactors (CSTR's), plug flow reactors (PFR's) and the related packed bed reactors (PBR), and batch reactors can be combined in several configurations to model more complex reactor dynamics.

RD modelling is usually approached from a distillation perspective with superimposed reaction kinetics. Thus, Saito et al. [1971] intuitively models a "new distillation process" using constant molar overflow, vapour-liquid equilibrium (VLE) on a stage, and instantaneous chemical equilibrium[b].

Though reminiscent of the McCabe-Thiele graphical approach, Saito et al. [1971] could not employ this method as the system contained 6 components (too much for a graphical technique unless they can be lumped) and a chemical reaction. Barbosa & Doherty [1987, 1988] suggested the use of transformed variables and residue curve maps to serve as initial screening tools for RD systems. Their graphical approach is limited to quaternary systems and the assumption that chemical equilibrium is reached instantaneously. Hauan et al. [2000], Lee et al. [2000] and Hoffmaster & Hauan [2004, 2005] introduced RD difference points. This was built upon by Mulopo et al. [2008] who presented a reactive column profile map, which, combined with the concepts introduced by the latter papers, could identify feasible column operating regions and hence assist in its design. Their case study was limited to a single equimolar reaction. Graphical methods are useful largely in initial screening of feasible RD operating regions and may more easily elucidate unexpected behaviour due to their visual nature. However, the technique is intrinsically limited to simpler systems that lend themselves to graphical methodologies.

As in non-reactive distillation, multicomponent RD can be simulated more rigorously using either the equilibrium (EQ) or non-equilibrium (NEQ, rates-based) models or variations of these. Higler [1999] supplies a good overview of initial approaches in simulating CD by using the EQ model. Essentially, such a model assumes that the vapour and liquid *streams* leaving a stage in the column had sufficient contact to be in equilibrium and

[b]The calculation was performed on a NEAC-2200 digital computer and took 20 minutes and 100 iterations to solve a 10-stage problem.

reaction terms are then included in the mass balance equations to compensate for the reaction. In contrast, the NEQ model assumes the vapour-liquid *interface* on the stage to be in equilibrium, thus requiring knowledge of the mass and energy transfer between phases on a stage which are functions of the geometry of the phase contact areas. The complexity of each model can vary depending on the thermodynamic, hydrodynamic, and mass/heat transfer approaches used. For distillation textbooks, Seader & Henley [1998] and Taylor & Krishna [1993] may be consulted, while thermodynamics is covered by Smith et al. [1996] and Sandler [1999].

In terms of RD, several authors have compared the EQ and NEQ models. Work by Baur et al. [2000a] showed that in cases where multiple steady states (MSS's) exist, the more robust NEQ model can minimize the number of infeasible steady state operating conditions when compared to that predicted by the EQ model. MSS are known from non-reactive distillation, but the existence of 5-9 steady states in ethylene glycol RD is quite striking [Taylor & Krishna, 2000]. In the study by Baur et al. [2000a], it was found that several steady states identified by the EQ model were physically unrealizable when investigated by the NEQ model. MSS is of great concern when operating an RD system (cf. Section 1.2). Baur et al. [2000a] concludes his comparison by saying: "It is concluded that for design of RD columns we must routinely resort to nonequilibrium stage modelling.".

1.3.2 Mass transfer, heat transfer and hydrodynamics

Although the NEQ model is fundamentally more correct, industry often favours the simpler EQ model and corrects for incomplete VLE by introducing empirical Murphree efficiencies. This is especially true for complex systems containing a large number of components where the added complexity and subsequent estimations and approximations required by the NEQ model may offset the benefit of fundamentality by compounded inaccuracies [Nieuwoudt, 2008].

To elaborate: mass and heat transfer are integral to the NEQ distillation model (see Section 5.4.1). However, mass and heat transfer coefficients are dependent on a significant number of variables which can broadly be divided into fluid properties and the geometry of the phase interface (cf. Appendices B and C), which are dependent on the distillation internals' geometry. Whereas the EQ model essentially only requires the prediction of the vapour-liquid equilibrium coefficients and enthalpies, the NEQ model additionally requires estimation of pure component liquid and vapour densities, viscosities, heat conductivities, surface tensions, molar volumes, molecular weights, critical properties and diffusivities and additionally requires mixing rules for the equivalent mixture properties. Most of these values are based on predictive or fitted equations (unless experimental data is available) each contributing its own uncertainties.

For a more detailed understanding of the mass and heat transfer involved during distillation, the books of Bird et al. [2002] and Taylor & Krishna [1993] are good starting points, while Krishna & Wesselingh [1997] provide a quick overview of the Maxwell-Stefan approach to mass transfer, which is fundamentally more sound than the Fickian approach as it is based on chemical potential rather than concentration driving forces (see Section 5.4.2).

Further refinement of the reactive and non-reactive NEQ models are possible and research is ongoing. For example, though it is fundamentally more accurate to include mass transfer on a stage, the normal hydrodynamic assumption of proper phase distribution is not necessarily valid. Baur et al. [2000b, 2001] introduced the use of multiple homogeneously mixed cells to incorporate radial gradients within tray columns: the NEQ cell model. Though it is undoubtedly fundamentally more sound to consider rigorous computational fluid dynamic (CFD) calculations and although Taylor & Krishna [2000] notes a lack of CFD research in the field of RD systems to better predict hydrodynamic effects, the required computational resources and time are often unavailable and in most cases the added complexity might outweigh the potential benefits introduced by a more rigorous approach.

1.3.3 The reaction

Incorporation of the heterogeneous reaction into the EQ and NEQ models can take several forms, the simplest of which is assuming a certain conversion within the reactive zone(s). More accurately, the catalyst can be approached either as an additional phase in a three-phase NEQ approach (thus requiring knowledge of the mass and heat transfer to and from the catalyst), or as part of a pseudo-homogeneous liquid phase where the catalyst and liquid phases are lumped - a standard reactor engineering technique [Fogler, 1999]. A comparison by Xu et al. [2005] cautions the use of the pseudo-homogeneous approach except in cases where the reaction is known to be kinetically controlled, i.e. where the mass transfer limitations between the bulk liquid and catalyst are not significant. Higler et al. [2000] presents a three-phase NEQ model that also incorporates internal mass transfer effects within the catalyst particle itself by using the dusty fluid model, where the porous catalyst structure is seen as an additional pseudo-phase in the mass transfer equations [Krishna & Wesselingh, 1997]. Though both the pseudo-homogeneous and dusty fluid model approaches adequately predicted Higler et al.'s tertiary-amyl methyl ether (TAME) case study, the more mass transfer sensitive MTBE process required the dusty fluid model to eliminate infeasible conditions that were predicted by the MSS solution of the pseudo-homogeneous approach.

As mentioned at the beginning of this section, it is tempting to approach RD as a distillation column and superimpose a reactive term on it (in its simplest form a conver-

sion specification). In this doctoral thesis, it was desired to put more emphasis on the mathematical description of the reaction than is generally the case in open literature. In fact, Schmitt et al. [2008] concludes that determination of a suitable level of complexity for a specific problem reduces to a thorough understanding both of the reaction kinetics and thermodynamics of the RD system. Schmitt et al. [2008] states that mastering the reaction is key to successfully designing a CD column.

It is believed that the (often) non-linear surface reactions may yield macroscopically observed effects that can only be explained by thoroughly understanding, not only the mass transfer, but also the reaction kinetics, the latter of which encompasses the potential non-linearity introduced by heterogeneous catalyst surface reactions.

However, a survey clearly indicates that the emphasis in literature usually falls on the mass transfer effects. Although the reaction kinetics are sometimes derived from first-principle Langmuir-Hinshelwood kinetics, there are usually accompanying simplifications. A review of open literature appears to indicate that no-one has yet attempted to solve the NEQ model with reaction kinetics expressed as functions of the fundamental intermediary surface species concentrations.

Chapter 2

1-Hexene hydrogenation

Hydrogenation is arguably the oldest known heterogeneous catalytic system, dating back to 1838 and the work of Kulmann [Sabatier, 1912]. Progress was intermittent until 1897 when Sabatier and Senderens hydrogenated unsaturated hydrocarbons over usually Ni catalysts [Sabatier, 1912; Morachevskii, 2004], followed by detailed mechanistic studies in the 1930's (such as Farkas et al. [1934], Horiuti & Polanyi [1934] and Twigg & Rideal [1939]) when classification between ortho- and para-alkenes, and isotopes of hydrogen became available [Pines, 1981].

Olefin hydrogenation over Ni thus follows a well-known mechanism making it ideal for first approach studies into reactive distillation. Although usually not of industrial interest to convert olefins into lower value alkanes, olefin hydrogenation is economical in several cases such as where they may deactivate downstream catalysts or where the alkane may increase the fuel octane (as in the case with iso-octene [Lylykangas, 2004]).

2.1 Mechanism

The hydrogenation mechanism of pure alkenes on metal catalysts is well understood due to research conducted especially in the 1930's and 1960's [Farkas et al., 1934; Twigg & Rideal, 1939; Bond & Wells, 1964] though there is still scope in understanding competitive systems containing additional compounds [Jackson & Monaghan, 2007].

Hydrogenation on a metal catalyst is generally understood to occur via the Horiuti-Polanyi mechanism depicted in Figure 2.1 [Horiuti & Polanyi, 1934]. To illustrate, consider the left alkene isomer in Figure 2.1. Here, dissociatively adsorbed hydrogen transfers reversibly to one carbon participating in the adsorbed alkene's double bond (say, the α-carbon) to produce a "half-hydrogenated" state, followed by irreversible transferal of another hydrogen to the remaining carbon originally participating in the double bound (the β-carbon) and formation and simultaneous desorption of the alkane.

Alkene adsorption can occur either via classic Horiuti-Polanyi σ-diadsorption, cor-

responding to adsorption of the carbons participating in the double bond via sp^3 hybridization (see Figure 2.2) onto two metal atoms, or π-adsorption, which corresponds to adsorption onto only one metal atom as depicted in Figure 2.1 [Bond & Wells, 1964]. Both allow for isomerization, though the latter is thought to encourage it through reversal of the half-hydrogenated state to an adsorbed alkene via an allylic carbon-hydrogen bond onto a carbon initially adjacent to the double bound (the γ-carbon in the example). This at least partially accounts for the relatively high isomerization observed on π-allyl promoting Pd and Ni when compared to Rh, Ru, Os, Ir and Pt metal catalysts [Augustine, 1996].

Isomerization is more dominant during low surface hydrogen availability, which generally corresponds to low pressure, insufficient component mixing or excess catalyst. This inhibits fast transferal of hydrogen to the adsorbed alkene or half-hydrogenated state. However, an increase in hydrogen pressure increases the hydrogenation rate faster than that of isomerization. E.g., for iso-octenes isomerization is negligible at at least $10{\cdot}10^5$ Pa [Lylykangas et al., 2003]. Increasing temperature favours hydrogenation, though the reaction occurs readily at 298.15 K (25°C). The ease of hydrogenation decreases in the order Pd $\geq$ Rh $>$ Pt $\geq$ Ni $>>$ Ru [Augustine, 1996]. While Pd is commonly used, Ni is more favourable from a cost perspective[a].

Campelo et al. [1982] investigated the effect of different supports on 1-hexene hydrogenation with 20wt% Ni catalyst loadings and found the extent of support-Ni interactions to increase in the order $Ni/SiO_2 < Ni/AlPO_4\text{-}SiO_2 < Ni/AlPO_4\text{-}Al_2O_3 < Ni/Al_2O_3$, with Ni/SiO_2 being the most active. However, they found the reaction structure-insensitive (cf. Singh & Vannice [2001]). It must be noted that isomerization can occur on acidic supports, such as Al_2O_3.

2.2 Reaction kinetics

Despite the fact that hydrogenation is a commonly used reaction, exhaustive searches failed to find reaction kinetics for liquid phase 1-hexene hydrogenation on the 18wt% Ni/Al_2O_3 catalyst used in this study - at least not in open literature nor after queries to the catalyst supplier, Kata-Leuna.

Campelo et al. [1982] reported Arrhenius constants for 1-hexene hydrogenation over a 20wt% Ni/Al_2O_3 catalyst in a batch (Parr low pressure) hydrogenator for an initial hydrogen partial pressure of $4.1{\cdot}10^5$ Pa and methanol diluted 1-hexene solution of 1 M. However, the reported reaction kinetics and data analyses were conducted only at almost complete hydrogen coverage of the catalyst surface and very low 1-hexene liquid concentrations - the opposite to what is expected in the reactive zone of a CD column. At these

[a]For example, in February 2010 Pd was in excess of 500 times more expensive than Ni according to `www.icmj.com` and `www.metalprices.com`.

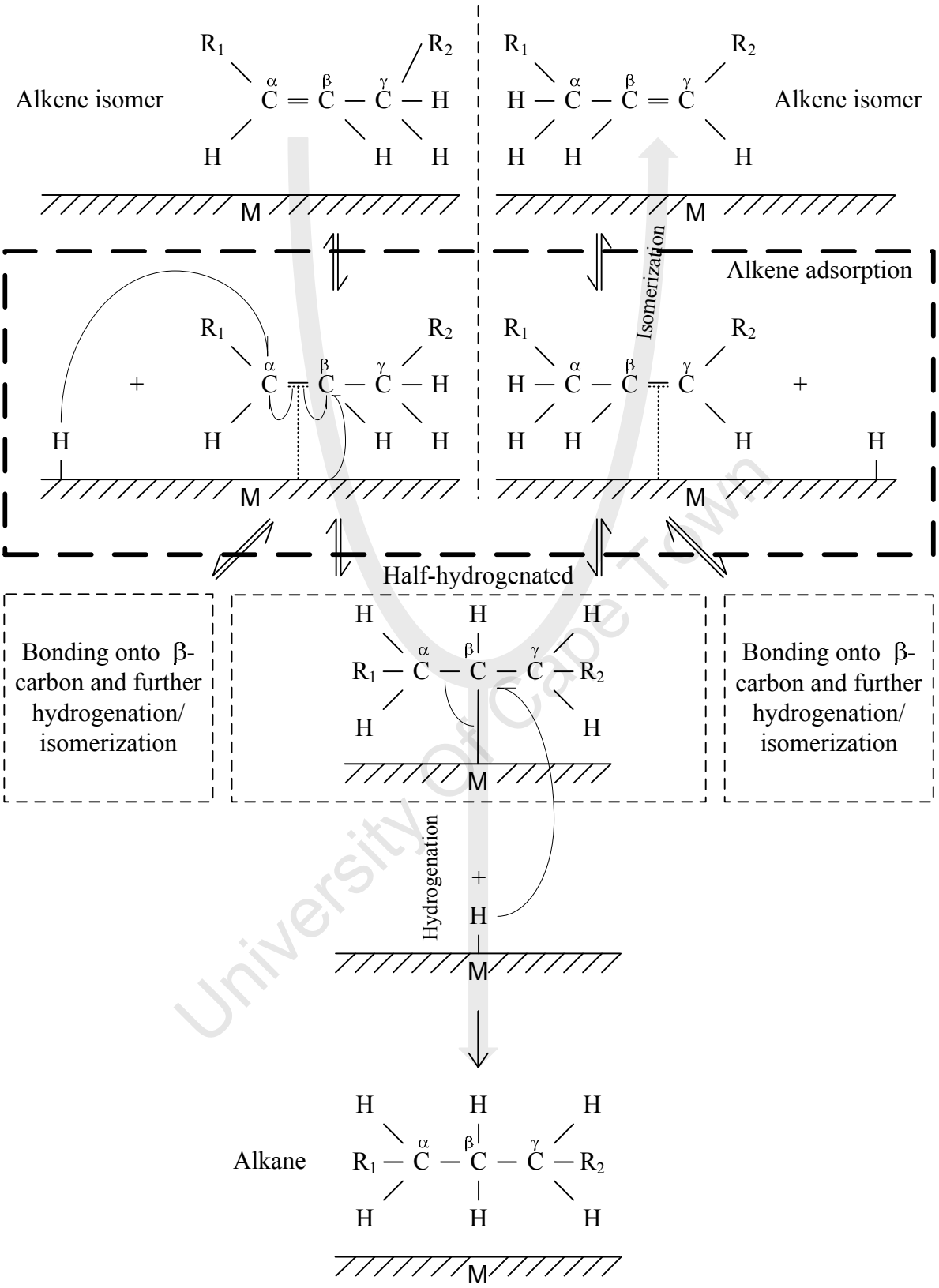

Figure 2.1: Horiuti-Polanyi mechanism with π-allyl intermediate for alkene hydrogenation over a metal (M) catalyst with arbitrary residual carbon chains R_1 and R_2 on either side of the double bond (adapted from Augustine [1996]). See Figure 2.2 for the alternative adsorped alkene intermediate via sp^3 hybridization.

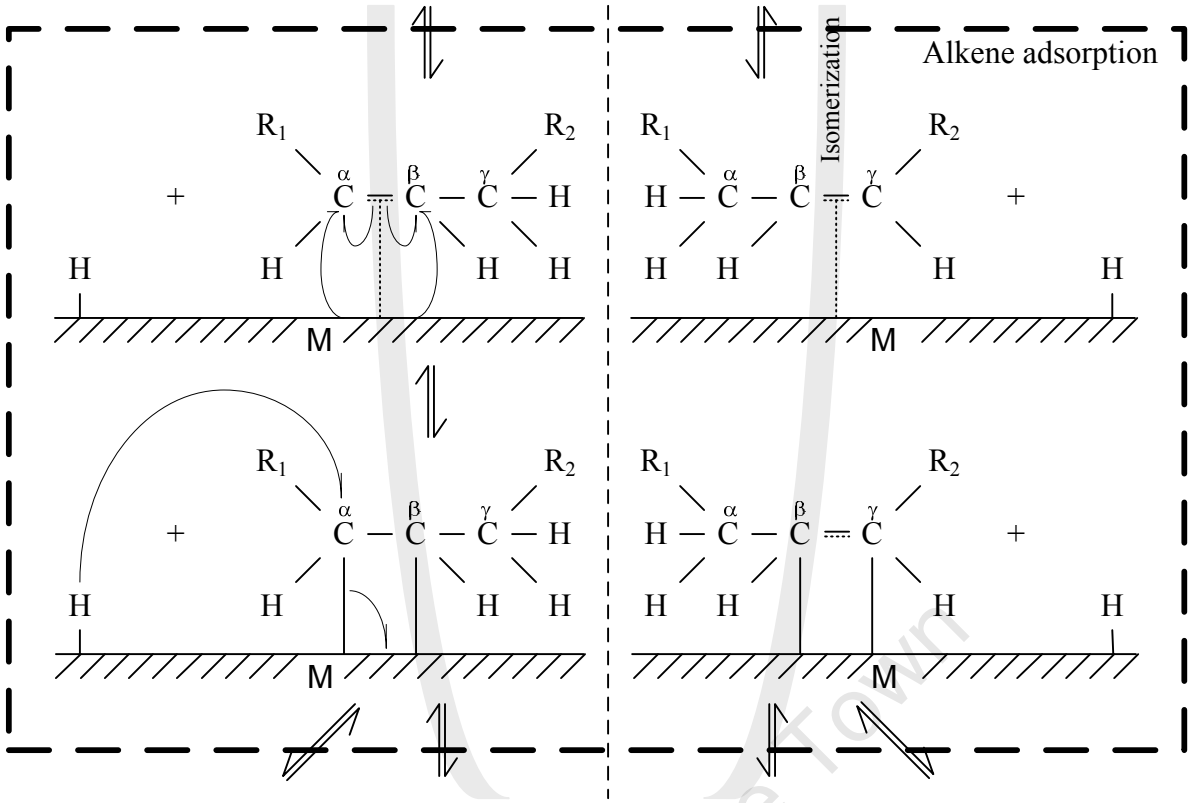

Figure 2.2: Horiuti-Polanyi mechanism with sp^3 hybridization intermediate. See Figure 2.1 for the rest of the mechanism.

conditions, the reaction rate was independent of both the hydrogen partial pressure and olefin concentration. Thus, the results are based on a simple reaction kinetic system which fails to deconvolute the complex intermediary reactions that take place. For this zero-order reaction (in the reactants and products), non-mass transfer limited system, Campelo et al. [1982] found the apparent activation energy of the overall system to be $7.1{\cdot}10^7$ J/kmol, which at least supplies an idea of the order of magnitude to be expected.

More recently, Lylykangas and co-workers [Lylykangas et al., 2003; Lylykangas, 2004] investigated the hydrogenation of varying iso-octene (in particular 2,4,4-trimethyl-1-pentene and 2,4,4-trimethyl-2-pentene) feed concentrations over a 16.6wt% Ni/Al_2O_3 catalyst in a CSTR at 308.15-368.15 K (35-95°C) and $10\text{-}40{\cdot}10^5$ Pa. The treatment by Lylykangas et al. [2003] is represented in Table 2.2. A π-absorption mechanism was assumed for the alkene (cf. previous section). It was further assumed that there is only one type of active site, that the reactant adsorption is at equilibrium, that the first hydrogen insertion is rate limiting (cf. Jonker et al. [1997]) and that desorption of the alkane is rapid and irreversible so that the surface concentration of the adsorbed alkane is zero ($\theta_{alkane} = 0$). The active intermediate (the half-hydrogenated state Y) is assumed to be highly reactive, justifying a pseudo-steady-state hypothesis. Combining these assumptions with a molar balance of the surface species led to equations that encompassed both hydrogenation and double-bond migration between the terminal and

Table 2.1: Lylykangas [2004] results for hydrogenation of iso-octenes over a 16.6wt% Ni/Al_2O_3 catalyst.

Parameter	Unit(s)	Value
$k_{65^\circ C,\alpha-olefin}$	$mol^{1/3}(m^3)^{3/2}/g_{Ni}.h$	3.1 ± 0.1 x 10^{-3}
$k_{65^\circ C,\beta-olefin}$	$mol^{1/3}(m^3)^{3/2}/g_{Ni}.h$	1.3 ± 0.2 x 10^{-3}
$E_{a,\alpha-olefin}$ (apparent)	J/kmol	3.4 ± 0.2 x 10^{+7}
$E_{a,\beta-olefin}$ (apparent)	J/kmol	4.9 ± 0.6 x 10^{+7}
K_H	m^3/kmol	1.6 ± 0.3 x 10^{-2}

Table 2.2: Kinetic model for 1-hexene hydrogenation if the approach of Lylykangas et al. [2003] for iso-octenes is applied to the 1-hexene system (symbols are that used by Lylykangas et al. [2003]).

Reaction equation			Rate equation		
$H_2 + 2*$	$\leftrightarrow$	$2H*$	$k_H C_{H_2}\theta_v^2$	$-$	$k_{-H}\theta_H^2$
$C_{1-Hexene} + *$	$\leftrightarrow$	$C_{1-Hexene}*$	$k_1 C_{1-Hexene}\theta_v$	$-$	$k_{-1}\theta_{1-Hexene}$
$C_{1-Hexene} * + H*$	$\leftrightarrow$	$Y * + *$	$k_2\theta_{1-Hexene}\theta_H$	$-$	$k_{-2}\theta_Y\theta_v$
$Y * + H*$	$\leftrightarrow$	$C_{n-Hexane} * + *$	$k_3\theta_Y\theta_H$	$-$	$k_{-3}\theta_{n-Hexane}\theta_v$
$C_{n-Hexane}*$	$\rightarrow$	$C_{n-Hexane} + *$	$k_4\theta_{n-Hexane}$		
$C_{2-Hexene} + *$	$\leftrightarrow$	$C_{2-Hexene}*$	$k_5 C_{2-Hexene}\theta_v$	$-$	$k_{-5}\theta_{2-Hexene}$
$C_{2-Hexene} * + H*$	$\leftrightarrow$	$Y * + *$	$k_6\theta_{2-Hexene}\theta_H$	$-$	$k_{-6}\theta_Y\theta_v$

β positions (further isomerization was not considered).

Experimentally generated data indicated that the vapour-liquid mass transfer was not rate limiting and (importantly) that isomerization could be neglected at the conditions investigated. Lylykangas et al. [2003] were consequently able to derive simple reaction kinetics equations for the iso-octene system, which, combined with a suitable reactor model, fit the experimental data.

However, these results cannot be used directly in the current studies as the catalyst had a different metal loading (16.6 vs. 18wt%), as the feed alkene was longer and branched (with possible different stereo effects), and as the experiments were performed above $10{\cdot}10^5$ Pa rather than at $1\text{-}6{\cdot}10^5$ Pa(a) where Lylykangas et al. [2003] report that isomerization becomes more significant, thus requiring isomerization to be included in the kinetic equations. Furthermore, the assumption that the adsorption steps are at equilibrium may not be valid in the CD system where mass transfer limitations between the bulk liquid and catalyst surface may be more significant. Lylykangas and co-workers do, however, supply a good base from which to derive the hydrogenation kinetics [Lylykangas et al., 2003; Lylykangas, 2004].

Table 2.3: 1-Hexene hydrogenation thermodynamics at 298.15 K (based on data from Perry et al. [1997])

Parameter	Ideal gas enthalpy of formation ΔH_f^0 kJ/mol	Ideal gas Gibbs energy of formation ΔG_f^0 kJ/mol	Thermodynamic equilibrium coefficient -
Hydrogen	0	0	
1-hexene	-42.0	87.4	
2-hexene	-42.0	87.4	
n-hexane	-166.9	-0.07	
Hydrogenation reaction	-124.9	-87.5	2.10E+15
Isomerization reaction	0	0	1

2.3 Thermodynamics

Table 2.3 supplies a basic overview of the hydrogenation and isomerization reactions at standard conditions of 298.15 K and $1.01325 \cdot 10^5$ Pa. It is clear that, even at low temperatures, hydrogenation is very exothermic, with a heat of reaction in the order of -125 kJ/mol. Isomerization is essentially thermoneutral as the 1-hexene reactant and 2-hexene product have approximately the same enthalpies of formation. Hydrogenation thus has a very high thermodynamic equilibrium constant (ca. 2.1E+15), which implies that the n-hexane product is thermodynamically very much preferred.

Although the reaction kinetics will determine the rate of reaction, it cannot exceed the thermodynamic limit.

2.4 CD hydrogenation systems

In 1997 CDTech reported that they could install more than nine different CD selective hydrogenation units into a process [Rock et al., 1997]. The main applications included buta-, penta-, and hexadiene selective hydrogenation as well as benzene total hydrogenation.

The selective hydrogenation of butadiene is of particular importance in industry. Diolefins in hydrocarbon streams can deactivate downstream catalysts and participate in undesirable side reactions [Podrebarac et al., 1997]. It is also of special interest to refiners who selectively hydrogenate C_4 streams to increase the n-butane content available for alkylation, which in turn reduces acid consumption during alkylation. This reduces costs and environmental impacts due to effluents from, for example, acid regeneration. Ultimately, it enhances the octane number[b] of the fuel emanating from the hydrofluoric

[b]Figure indicating the anti-knock properties of a fuel [Thompson, 1996]. More specifically, it is

alkylation units [Rock et al., 1997]. The CD system for selective hydrogenation of butadiene is discussed by Podrebarac et al. [1997]. It achieves simultaneous selective hydrogenation of butadiene, separation of the C_4 and C_{5+} fraction and hydrogenation of the light sulphur compounds to H_2S, which is subsequently removed from the system through the off-gas stream. Consequently it produces a sulphur-free C_4 fraction while the heavier sulphur compounds exit with the C_{5+} bottoms product.

More recent reference to Harmsen [2007] and the CDTech website (`www.cdtech.com`) in August 2009 yields several CD hydrogenation technologies specifically aimed at selective hydrogenation. CD*Hydro*® allows selective hydrogenation of methyl acetylene and propadiene to propylene, C_{4-6} diolefin reduction technologies, and hydrogenation of benzene to name a few. The CD*Etherol*® system effects simultaneous hydrogenation, isomerization and etherification, though this is achieved in a separate reactor as part of a CD system and not in the CD column itself. BASF SELOP is also available from CDTech for selective hydrogenation of C_{4-5} diolefin reductions.

Not surprisingly CD 1-hexene hydrogenation has not been investigated (at least not in the open literature) as n-hexane has a considerably lower monetary value than 1-hexene, although a patent was filed by Stark & Swart [2006] for bulk CD hydrogenation of a stream containing multiple olefinic compounds. The system was envisaged to operate at 1.5-3.0·10^5 Pa(a) and (as example) at 160-200°C for a C_3 to C_7 based olefinic stream.

In general, it does not appear that CD mono-olefin hydrogenation has been investigated thoroughly in open literature.

the percentage 2,2,4-trimethylpentane in heptane that has the same knocking characteristics as a petrol tested in a standard engine. Premature ignition of the fuel-air mixture in an engine is termed "knocking" [Hartmann-Petersen et al., 2001].

Chapter 3

Project background, definition and novelty

This thesis continues from an M.Sc.Eng. (Chem. Eng.) project completed by the researcher and documented in Nieuwoudt [2005]. The goal of that project was to design and commission the University of Cape Town's (UCT's) first laboratory-scale Catalytic Distillation (CD) column. 1-Hexene hydrogenation was chosen as a test reaction as it was a relatively simple, exothermic, liquid phase reaction and simple distillation system that allowed sufficient reaction and distillative separation at similar process conditions. The long-term plan was to exploit this simple system to isolate the effect of more complex mass transfer phenomena.

At the end of the project, it was shown that the commissioned CD column could sustain a simultaneous reaction and separation. However, the system proved to be imperfect and additional time was required to ensure high quality data. The changes to the system to achieve this are documented in Appendix A.

It is *hypothesized* that a fundamental mathematical model of both the mass/heat transfer and reaction kinetics is required to accurately predict the behaviour of even perceived "simple" kinetic equation reactions performed in a CD column, and that such a validated model can supply a deeper understanding of the dynamics in such systems.

In order to prove the hypothesis, the *goal* is to develop models that accurately describe the dynamics of both the intrinsic reaction kinetics and the CD column, to rigorously fit these models to experimental data, and to investigate the behaviour of the resulting CD model to both sensitive parameters and operating conditions.

Several *key questions* must be asked:

- What is the impact of internal and external mass transfer limitations on both the reaction kinetic and CD experiments?
- How can the mass transfer effects be incorporated into the model and what level of detail is necessary?

- How can the validity of the regressed process parameters and their impacts on the model be properly quantified?

In terms of *novelty*, the thesis will build up the models based on a sound combination of experimental, theoretical and statistical techniques. Secondary to this, it will supply statistically weighted liquid phase 1-hexene hydrogenation kinetics on a Ni/Al_2O_3 catalyst, which, after an exhaustive search, could not be found in literature, though much work has been done on hydrogenation in other systems. Maxwell-Stefan mass transfer will be approximated by using the linearized approach to reduce computational time and complexity. The resulting model will simultaneously solve for the surface species concentrations described by fundamental, fitted Langmuir-Hinshelwood kinetics, thus tracking the effects on the surface and elucidating its effect on the overall CD column dynamics.

Part II

METHODOLOGY

Part II details the methodology followed to achieve the goals and hypothesis (Section 3). Essentially, experiments (Section 4) are performed to regress (Section 6) unknown parameters and validate the models developed theoretically (Section 5). Using these parameters and validated models it is then possible to simulate various different scenarios and process conditions (Section 6).

To ensure an accurate model, the 1-hexene hydrogenation reaction rate constants and the mass transfer correlation parameters for the reactive zone in the CD column is regressed from experimental data as they are respectively catalyst and geometry specific and unavailable from literature. In contrast, the structured Sulzer CY packing used in the column has well defined and investigated mass transfer correlations. Reaction kinetic data is generated in an available semi-batch reactor, and CD data in the designed and constructed CD column [Nieuwoudt, 2005]. A reaction mechanism, semi-batch model and catalytic distillation model is then developed to perform the regression.

Chapter 4

Experimental methodology

4.1 The consumables used

The purities of the 1-hexene, n-hexane, argon, hydrogen and nitrogen used, as well as the catalyst specifications are supplied in Table 4.1.

Argon, hydrogen and nitrogen were supplied by houselines, while 1-hexene and n-hexane were procured and stored in dark containers.

The catalyst consists of dark-gray commercially available Kata-Leuna Ni/Al_2O_3 extrudates with an 18wt% Ni loading. Supported Ni is a common hydrogenation catalyst partially due to its low cost even though it allows more double bond migration [Rylander, 1994]. For consistency, the used catalyst was retained from the previous work by Nieuwoudt [2005]. The *ex-situ* catalyst reduction procedures and its transferal into the reactive system under an inert atmosphere are supplied in Appendix A.3.

4.2 The semi-batch system

To prevent deactivation, the used catalyst (Section 4.1) was reduced as described in Table A.6 and transferred under an argon atmosphere into vials filled with 1-hexene bubbled through with argon. The filled vials were weighed just prior to and after addition of catalyst to determine the catalyst weight (ca. 0.50 g).

A clean, 600 ml SS316 autoclave was filled with 250 ml of the pure 1-hexene standard (see Section 4.1 for details). Excess 1-hexene was removed via pipette from the catalyst vial, the catalyst swiftly dumped into the 250 ml 1-hexene and the vessel closed.

The autoclave system depicted in Figure 4.1 consists of pressure regulated house-line argon and hydrogen supplies, each of which can be fed directly or via an MFC into the autoclave. The MFC was calibrated using a bubble meter. A check valve (CV-Feed) and several ball valves protect the MFC from liquid pushing back from the reactor. Reactor temperature is measured via a j-type thermocouple and controlled using a Gefran 500

Table 4.1: Standard consumables used and the catalyst specifications.

Parameter	Unit(s)	Value
General consumables		
1-hexene purity	wt%	99.5
n-hexane purity	wt%	99.3
hydrogen purity	wt%	99.9
argon purity	wt%	99.9
nitrogen purity	wt%	99.9
Catalyst specifications		
Manufacturer	-	Kata-Leuna, CRI, Houston, Texas, USA
Catalyst type	-	KL6560-TL2.5
Catalyst shape	-	Extrudates
Nickel content	wt%	$\pm$ 18
Alumina content	wt%	$\pm$ 82
Bulk density	kg/m^3	650-750
Average length	mm	3-5
BET surface area	m^2/g	120-140
Pore volume	cm^3/g	0.48-0.57
Side crush length	N/mm	$\leq$ 12
Approximate diameter	mm	2.5

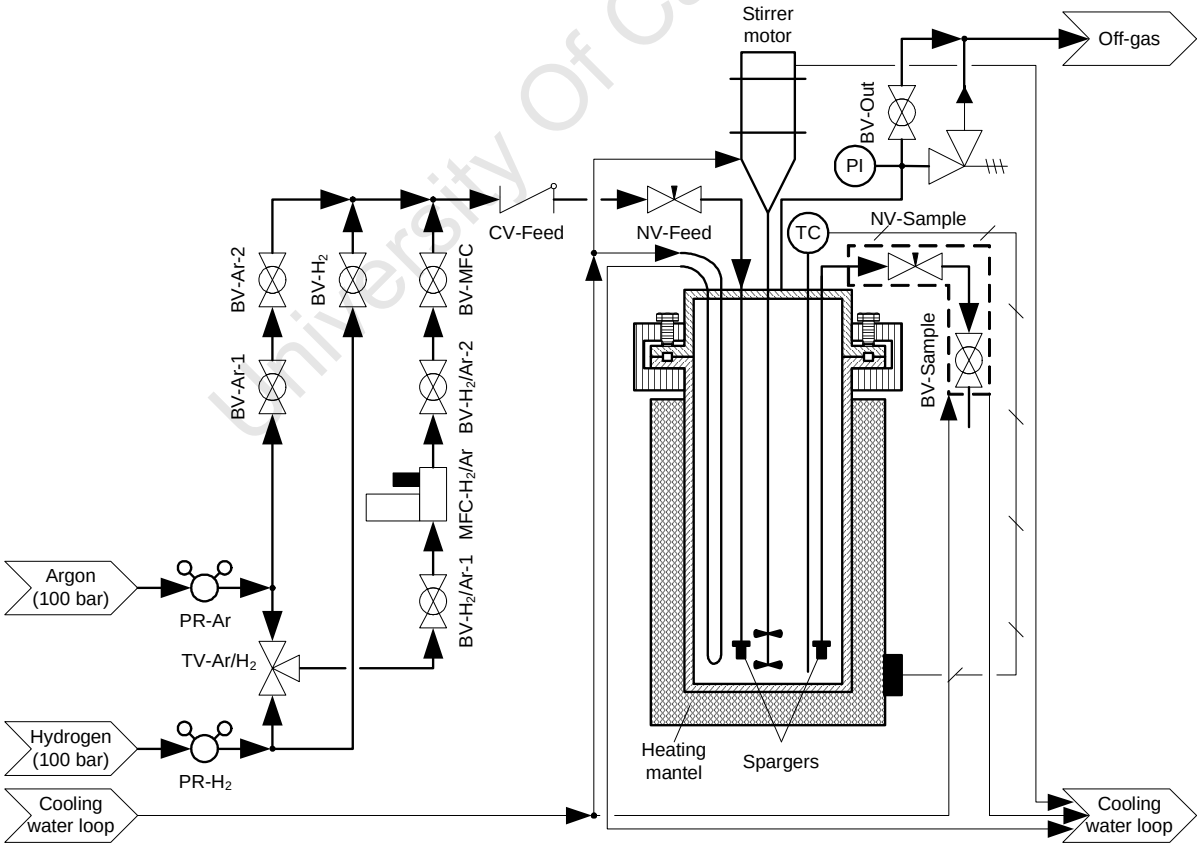

Figure 4.1: Experimental system used to generate 1-hexene hydrogenation kinetic data (see CD system's P&ID in Section 4.3 for symbol definitions).

controller connected to an external element heating jacket. An internal water cooling loop with a constant flow rate and temperature is used to counter the heater. A sparger on the feed gas inlet distributes gas bubbles into the stirrer mixed autoclave liquid. The vessel outlet contains a pressure indicator and pressure relief valve. Liquid samples for GC-analyses could be taken via needle valves NV-Sample and BV-Sample, provided the liquid sample line was flushed prior to sampling.

Consider Figure 4.1 with all valves closed unless otherwise stated.

A minimum $20{\cdot}10^5$ Pa(g) argon pressure test was performed by opening BV-Ar-1/2 and NV-Feed. Once nearly pressurized, BV-Ar-1/2 and NV-Feed were closed, TV-Ar/H_2 set to argon, and MFC-H_2/Ar set to 100%. BV-H_2/Ar-1/2, BV-MFC and NV-Feed were then sequentially opened, waiting each time (for ca. 5-10 s) for the MFC reading to drop to 0% to preclude the presence of leaks.

Following a successful pressure test, MFC-H_2/Ar was set to 95% ($2.36{\cdot}10^{-6}$ m_n^3/s) and BV-Out opened for 30 min to replace air with an argon atmosphere. The argon supply and hence vessel pressure was then dropped to atmospheric pressure and BV-out, NV-Feed, BV-MFC and BV-Ar-1/2 closed before resetting MFC-H_2/Ar to 100%. The desired total vessel pressure was then chosen by setting the hydrogen supply pressure and turning TV-Ar/H_2 to hydrogen.

The stirrer speed was set as desired (usually 20 Hz) to create proper phase and thermal mixing, and the reactor temperature increased step-wise to prevent overshooting of the desired setpoint.

BV-H_2 and NV-Feed were then respectively opened to quickly pressurize the autoclave to the reaction pressure. BV-H_2 was then closed and BV-H_2/Ar-1/2 again sequentially opened, waiting each time (for ca. 5-10 s) for the MFC reading to drop to 0%, before opening BV-MFC. The hydrogen consumption (as indicated by the MFC), reactor temperature and reactor pressure were then logged manually over several hours with reading intervals based on the rate of change of the readings. The pressure gauge could be read to approximately $0.1 \cdot 10^5$ Pa accuracy and was thus insufficient to capture very small pressure fluctuations. Temperature usually varied by no more than 0 to +1 K. Liquid sampling was not performed during the run as it significantly disturbed the reactor pressure.

After several hours the increase in the hydrogen consumption rate became approximately linear and the minimum number of data points required for fitting of the 20 intrinsic reaction rate constants (at the specific isothermal reaction temperature) were reached. At this point, 3 consecutive liquid samples were taken for GC analyses. BV-H_2/Ar-1/2, BV-MFC and NV-Feed were closed, the vessel allowed to cool to ambient, and BV-Out opened to release the pressure, before finally measuring the remaining liquid volume left in the vessel.

This experiment was performed several times at different isothermal reaction tem-

peratures between 333.15 K (60°C) and 373.15 K (100°C). For each isothermal run, an absolute minimum of 20 data points (preferably more) were required to fit 20 reaction rate constants, whereas across the different temperatures, an absolute minimum of 40 data points (preferably more) were desired in order to fit the 20 pre-exponential Arrhenius factors and 20 activation energies used in the model (see Section 5.2).

4.3 The CD system

The original continuous CD system [Nieuwoudt, 2005] has undergone extensive changes to make it more efficient, versatile and easier to use. The updated P&ID is shown on pages 31 to 34, while a complete description of both it and the control system may be found in Appendix A.

4.3.1 Mass Balances

The filtered liquid *feed* flow rate to the column is controlled to within 0.1 ml/min via an HPLC pump (with a 0.0-10.0 ml/min range) connected to a 5000 ml glass bottle. Its composition is verified with off-line GC-FID analyses (see Section 4.4 for analyses methods). The HPLC pump head can be cooled to prevent flashing of volatile components. The houseline gas feed flow rate to the column is controlled with a mass flow controller (MFC). Nine access points along the height of the column allow easy variation of the feed point locations if required. As a first approach, the feed point location was chosen as halfway up the height of the column.

Internally, the reflux pump flow rate is set by the control program and is thus known.

Optical level controllers maintain a constant reboiler liquid level by draining its liquid inventory into the transiently weighed (ca. every 15 s) bottoms *product* tank. The distillate flow rate is set via a fine metering needle valve and measured via the transiently weighed distillate product tank. Off-line GC-FID analyses of the bottoms and distillate are performed on samples taken from the reboiler and reflux line respectively. Product drain tubes are sufficiently long to convectively subcool the products below their normal boiling points and cooling of the sampling lines and valves via cooling water is possible to prevent flashing. Off-gas compositional analyses are made by feeding a nitrogen reference gas with an MFC controlled flow rate to the atmospheric section of the off-gas line. A back-pressure regulator maintains a slight super atmospheric column pressure to prevent pressure fluctuations in the off-gas line from influencing the internal VLE. Online off-gas compositional analyses are made in a multi-functional micro-GC-TCD (see Section 4.4) that can analyse both for non-condensable and volatile components simultaneously. The off-gas flow rate is then calculated based on the obtained composition and set reference gas flow rate. Please see Appendix A.3 for sampling procedures and Section 4.4 for more

sampling information.

Possible mass *losses* are anticipated and reduced by thorough system pressure testing and monitored in post-processing of the data via a mass balance.

4.3.2 Energy Balances

The energy *fed* to the reboiler is set through a pulse-width modulator (PWM) connected to an external heating band around the reboiler vessel. Energy *removed* from the system in the two-stage partial condenser is calculated from the energy change in the tap water and ethylene-glycol/water cooling media, which is based on their known flow rates, and inlet and outlet temperatures. Note that cooling media flow rates and inlets temperatures are controlled directly rather than the condenser heat duty itself.

The mass balance discussed in the previous section is combined with feed, reboiler and condensate temperature measurements to determine their energy *contributions*. The reaction heat cannot be measured directly and must be calculated based on overall conversion and free energies of formation.

Heat losses were determined experimentally by measuring the amount of reboiler heat duty required to boil a 50/50 mixture of 1-hexene/n-hexane up to the partial condenser. In the middle of the temperature range of interest (i.e. at ca. 365 K or 93°C) this was found to be in the order of 70 W. In the model, an average heat loss was estimated for the column and divided amongst the stages (See Section 5.4).

4.3.3 Column Internals

Non-reactive packing

The choice of Sulzer CY gauze type packing (Sulzer CY) as non-reactive packing as well as the chosen internal flow rates, are discussed in Nieuwoudt [2005]. From the Kister and Gill equation and $F_P = 229.66$ m^2/m^3 (eq. 4.1 [Seader & Henley, 1998]), the flooding point is calculated to be $0.0184{\cdot}10^5$ Pa/m:

$$\Delta P_{flood} = 40.87 \cdot F_P^{0.7} \tag{4.1}$$

For a column with 1.280 m of packing, this translates to a top-bottom differential pressure of $0.0235{\cdot}10^5$ Pa. Manometer readings did not exceed this value and it is thus unlikely that flooding occurred.

Geometric data required for simulation purposes are supplied in Table 4.2.

V-1,2,3	FEED AND PRODUCT TANKS		HPLC-1	HYDROCARBON FEED PUMP		MFC-1	MASS FLOW CONTROLLER		P-2	Submersible water pump		CD-1	CD COLUMN		P-RD	REFLUX
Temperature	Ambient	°C	Flow	0.01 - 10.0	ml/min	Capacity	0 - 3670	ml/min	Type	Centrifugal	-	Temperature	< 240	°C	Type	Dosing
Pressure	1.01325	bar	Pressure	0 - 172	bar	Pressure (out)	1 - 6	bar	Flow		l/h	Pressure	1 - 6	bar	Flow	0 - 14.2
Orientation	Horizontal	-	Fluid density	662	kg/m^3	Pressure (max)	100	bar	Pressure (max)	6	mH$_2$O	MOC	SS316	-	Pressure (max)	20
MOC	Glass	-	Type	HPLC	-	Temperature	70	°C	MOC	Plastic	-	Size			Fluid density	ca. 662
Size			MOC	SS	-	Valve MOC	Viton	-	Motor	220	V	Height	2000	mm	MOC	SS316
Height	240	mm	Remote	RS232	-	Valve normal	Closed	-				ID	47	mm	Diaphragm	PTFE
OD	130 (base)	mm	Power	220/60	V/Hz	Power	24	V(dc)				Internals	Sulzer CY	-	Motor	230
Internals	None	-										Reboiler	Banded heater	-		3/4
													1000	W	Power (shaft)	250

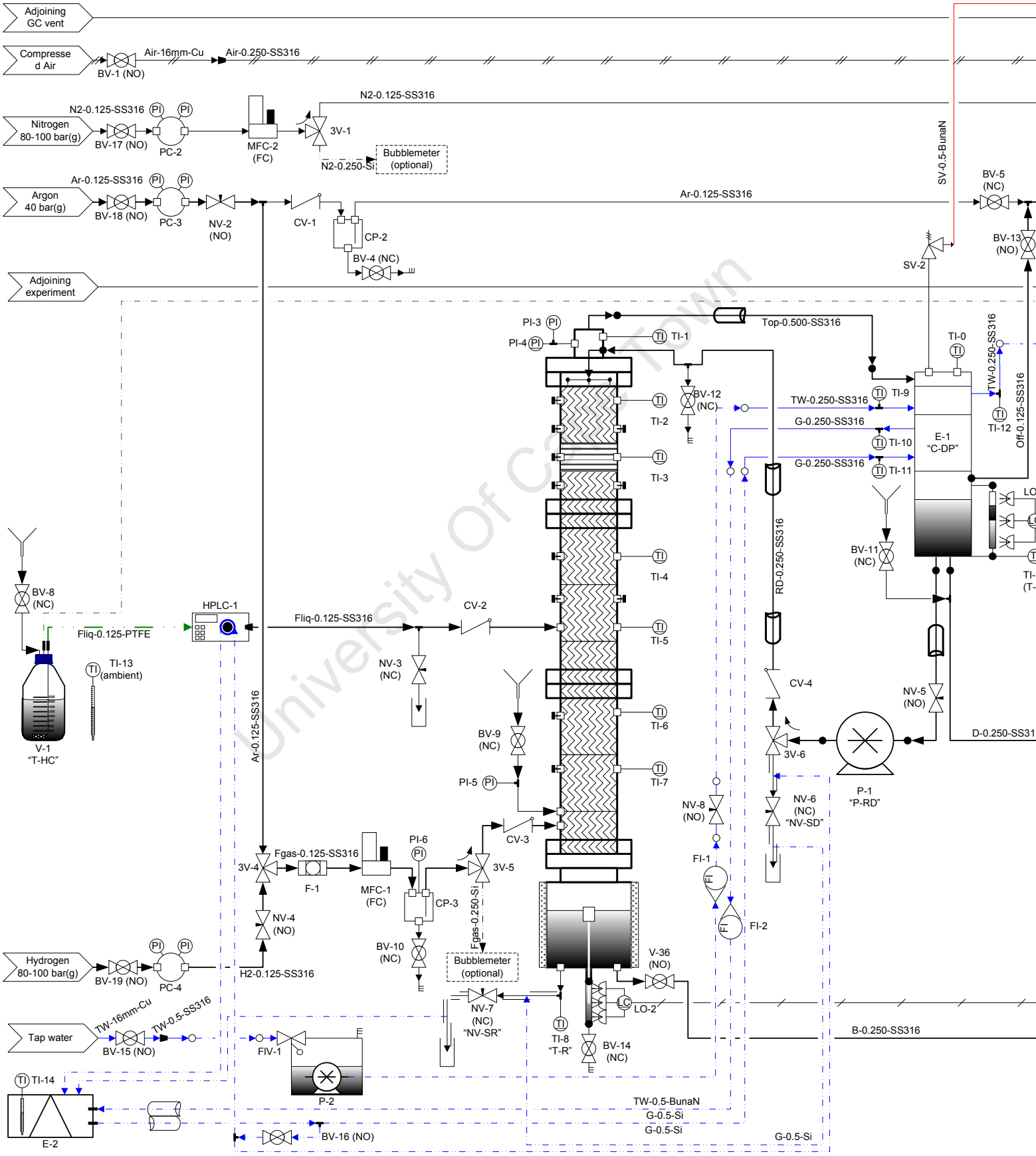

PUMP		C-DP	PARTIAL CONDENSER		
-		Type	Shell and tube		-
l/h		Area	57453		mm^2
bar		Duty	650		W
kg/m^3			Shell	Tube	
-		Temp. (tap)	30/40	124/60	°C
-		Temp. (ref)	2/7	60/7	°C
V		Pressure	1	6	bar
ph/pole		Phase	L	G/V	-
W		MOC	SS316	SS316	-

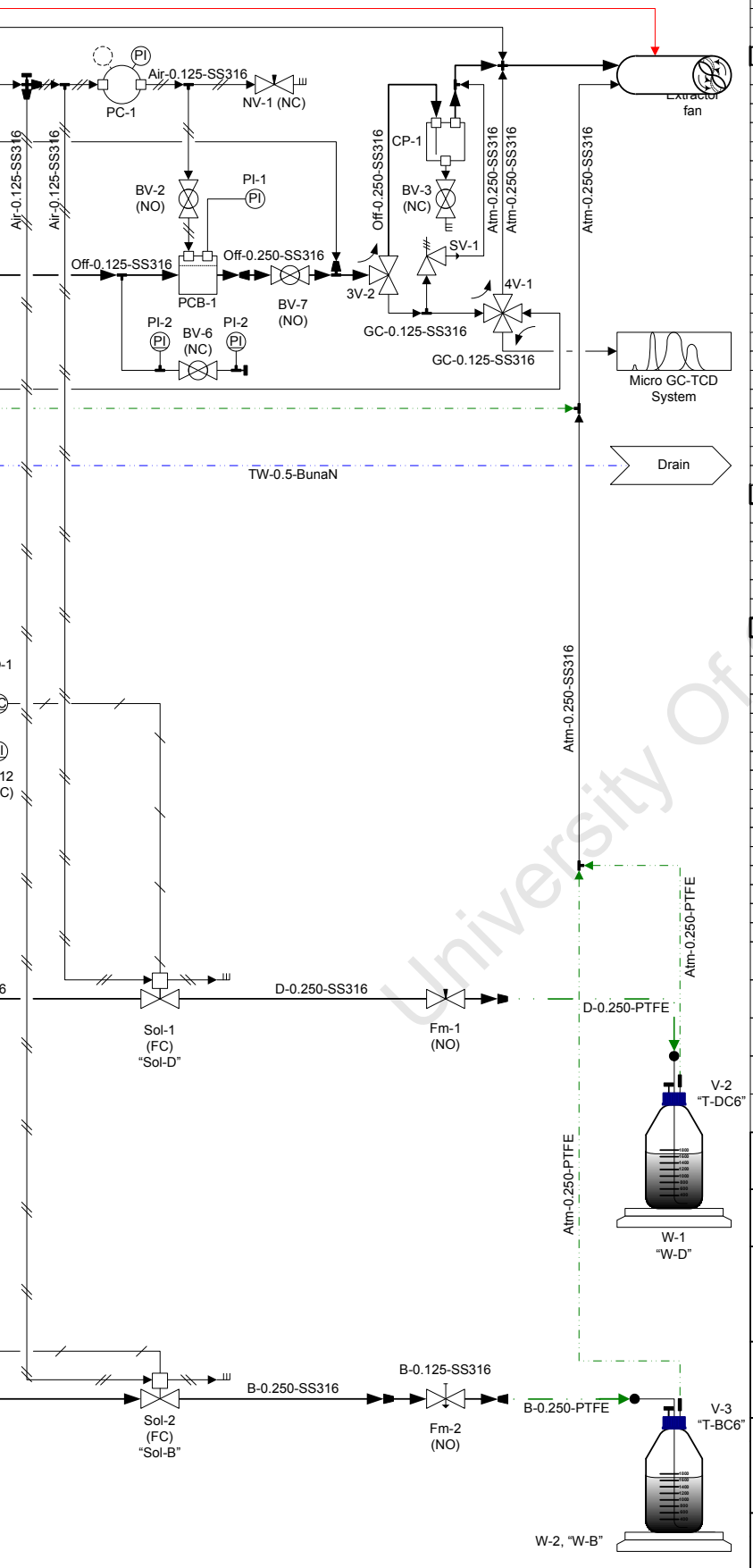

PIPE SPECIFCATIONS

Material prefix - OD[inch] - Pipe MOC

MATERIAL PREFIXES

( )	Usually contains	H2	Hydrogen
Atm	Atmospheric	N2	Nitrogen
Air	Compressed Air	Off	Off-gas
B	Bottoms	PTFE	Teflon
BunaN	BunaN	RD	Reflux distillate
D	Distillate	Si	Silicon
Fgas	Feed gas	SS316	Stainless steel 316
Fliq	Feed liquid	Top	Vapour exiting top
G	Glycol	TW	Tap water
GC	Gas Chromatogram		

INSTRUMENT IDENTIFICATION LETTERS

	1st letter	2nd letter	3rd letter
A		Analysis	Alarm
B	Ball		Back
C	Check	Control	Control
Cp	Catch pot		
D			
E	Heat exchanger		
F	Flow/Filter	Flow	
Fl	Float		
Fm	Fine metering		
L	Level		
M	Mass		
N	Needle		
O		Optical	
P	Pressure/Pump		
S	Safety		
Sol	Solenoid		
T	Temperature		
V	Vessel	Valve	Valve
W	Weight		

GENERAL ABBREVIATIONS

B	Bottoms	HPLC	HPLC pump
C	Condenser	NC	Normally closed
CD	Catalytic distillation	NO	Normally open
D	Distillate		Normally open direction
FC	Fail closed		
FO	Fail open		

SYMBOLS

Line types			Needle valve		Balance
	Stiff				
	Flexible		Fine metering needle valve		Back pressure regulator
	Pneumatic				
	PID signal				
	Cooled		Float valve		Thermo-meter
Fittings					
	Union		Check valve		Optical sensor
	T-piece				
	Cross		Filter		**Miscellaneous**
	Reducer				Sample bottles
	Plug/Cap	**Instruments**			
	Hose clamp		Pump		Tube insulation
	Slipped on				
	NPT thread	FI	Rotameter		Read manually
Piping items					
	Ball valve		Mass flow controller		Read by PC
	3-way valve		Catch pot		Float
	4-way valve		Pressure regulator		Atmosphere
					Sulzer CY
	Safety valve		Funnel		Catalyst
					Heater
	Solenoid valve		Refrigerator		

SCALE

Not drawn to scale

DRAWN BY:	REVISED:
J.J. Nieuwoudt	2009/09/06

P&ID

CATALYTIC DISTILLATION PROJECT

Continuous system

CD SYSTEM

DESCRIPTION

Pipe and instrumentation diagram of the catalytic distillation system

DRAWING NUMBER	REVISION NO.
JJN/09112003-01	2

Reactive packing

The catalyst used in this study is discussed in Section 4.1. Two different reactive zone designs were considered. In both cases, the reactive zone was placed above the Sulzer CY packing at the highest 1-hexene liquid concentration in the column. To prevent channeling and to ensure good liquid distribution two layers of wire mesh were placed above the catalyst: the upper one rough and part of an outer catalyst cage; the second finer and part of an inner catalyst cage.

In design 1, 21 g of the catalyst extrudates were randomly dumped into a cylindrical cage spanning the entire perpendicular flow area in the column. Essentially, it used a teabag configuration protected by a catalyst cage as shown in Figure 4.2. This configuration promoted bubbling of the hydrogen through the liquid zone to effect higher vapour-liquid contact in the reactive zone. The design lent itself to simulation as random packing, for which there are well defined correlations (see Section 5).

Design 2 had several semi-circular catalyst filled bags perpendicular to the flow area except for a removed segment 25% of the column diameter in length. These semi-circular bags were staggered along the height of the column and separated with sufficient voidage to allow an easy criss-cross upward/downward path for material. The aim was to reduce the pressure drop across the catalyst zone, though this design also lent itself to possible catalyst bypassing and incomplete catalyst wetting (see Figure A.1).

4.3.4 Other considerations

The *materials of construction* (MOC) were discussed in Nieuwoudt [2005]. In the case of metals, stainless steel SS316L was the material of choice as it is resistant against hydrogen attack and the other components found in the hexene system [Perry et al., 1997]. Similarly, Teflon was preferred as plastic where atmospheric flexible tubes were required or as sealant. At temperatures above 523.15 K (250°C) and in metal-glass connections, graphite was used. Glass was used for pressurized applications where transparency was required. Experiments with reactants, but no catalyst, were performed at conditions similar to those investigated to ascertain the contribution of the metal sites in the MOC's on the conversion. No significant reactions were detected.

The presence of an off-gas line made the use of a back-pressure regulator convenient for pressure control. It also isolated the internal system from downstream pressure fluctuations. The system was qualitatively found to be very sensitive to pressure effects and tight pressure control was thus maintained.

Figure 4.2: Reactive zone packing showing strong outer catalyst cage encapsulating a finer inner teabag containing catalyst. The upper lid of the outer cage is not shown.

Table 4.2: Sulzer CY geometric data.

Specification	**Symbol**	**Value**	**Units**
Void fraction	ϵ	0.965	none
Packing surface area	a_p	708	m^2/m^3
Crimp height	h_c	4.25	mm
Channel base	B	7.5	mm
Channel side	S	5.65	mm
Channel flow angle from horizontal	θ	45	$^\circ$

4.3.5 System Operation

Detailed operating instructions are supplied in Appendix A.3, but the broad methodology will be discussed here. Generally, the sequence was first to create a safe working environment, then catalyst characterization, pressure testing of the system, catalyst reduction, catalyst loading into the system, start-up and operation of the system, and analyses of the generated data and samples.

In general, before each new experiment the column itself was pressure tested with argon up to $6{\cdot}10^5$ Pa(g) and either a soap bubble solution or commercially available Snoop® used to detect leaks.

The desired amount of Ni/Al_2O_3 catalyst was then weighed out and reduced at atmospheric pressure under 70 ml/min hydrogen over a 20 hour period, consisting of an initial 4 hour temperature ramp from ambient to a reduction temperature of 623.15 K (350°C). The catalyst was then allowed to cool down to ambient in the hydrogen atmosphere. To prevent catalyst oxidation in air, the reduced catalyst was poured into tetradecane and then scooped into the reactive zone container - in both cases under an argon atmosphere. It was then transported under tetradecane to the open CD column (filled with flowing argon) and sealed into the argon pressurized system.

A ca. 50/50 molar mixture of 1-hexene and n-hexane was prepared and loaded into the reboiler via the HPLC pump. The reboiler was initially slightly overfilled to supply enough material to satisfy the required column hold-up during operation. Liquid feed to the column was then initiated via the HPLC pump.

Following this, the desired *non-condensable, non-reactive* argon feed flow rate was set and the column allowed to pressurize to the desired operating pressure via the off-gas backpressure regulator. An initial reboiler heat duty was then chosen on the computer control program and the reflux pump allowed to find the subcooled reflux flow rate required for a *pseudo*-total reflux system in terms of the condensable components. Once the system had stabilized, the reflux flow rate was set to automatic to control the condenser liquid level at a constant value, the distillate flow rate set to a constant value, and the bottoms valve allowed to drain into the product tanks until a continuous steady state was reached.

Table 4.3: Offline Varian 3900 GC FID analyses (units as required by the instrument).

Parameter	Unit(s)	Value
Gas chromatograph	-	Varian model 3900
Autosamples	-	Varian model 8400
Detector	-	Flame ionization detector (FID)
Carrier gas		Helium
Carrier gas flow rate	ml/min	2
Make-up gas	-	Nitrogen
Liquid sample volume	μl	0.1
Column type	-	Plot fused silica column
Stationary phase	-	Al_2O_3 / Na_2SO_4
Column manufacturer	-	Varian - CP7568
Column length	m	50
Column internal diameter	mm	0.53
Film thickness	μm	10
Injector temperature	°C	180
Detector temperature	°C	250
Temperature program		
Rate	Time	Total time
°C/min	min	min
Initial	0.0	0.0
5.0	0.0	22.0
20.0	3.0	26.0

Once steady state was achieved, liquid samples were taken of the feed, reflux (distillate) and bottoms for three analyses in an off-line GC-FID and three online gas GC-TCD samples of the off-gas (see Section 4.3.1 and Table A.13). The three compositions were then averaged in each case.

To investigate CD, i.e. to introduce a reaction into the system, the argon feed was replaced with a *non-condensable, reactive* hydrogen feed of equal molar flow rate, the system allowed to reach a steady state and samples taken as before.

After shutdown the column feeds and exits were closed and the system pressurized with inert argon to protect the catalyst from oxygen and to prevent vacuum formation during cooling.

4.4 Analyses

Off-line analyses of liquid samples were performed on a Varian 3900 GC FID with specifications and temperature program as shown in Table 4.3.

On-line analyses of the off-gas were performed on a Varian CP-4900 micro-GC TCD with three channels (Table 4.4).

Table 4.4: Off-gas on-line Varian CP-4900 GC TCD analyses (units as required by the instrument).

Parameter	Unit(s)	Channel 1	Channel 2	Channel 3
Detection of...	-	Non-condensables	N/A	Volatiles
Carrier gas	-	Argon	Hydrogen	Hydrogen
Column type	-	Molecular sieve 5A PLOT	Pora PLOT Q	CP-Sil 5 CB
Column length	m	10	10	8
Injector temperature	°C	unheated	50	40
Analysis temperature	°C	70	60	40
Analysis pressure	kPa	160	80	60
Analysis time	s	480	480	480

GC-TCD errors are usually in the order of 3-5%, while that for GC-FID's are usually 1-2% [Welker-Nieuwoudt, 2008]. In the case of the GC-FID, the correction factors were approximately unity for the components of interest [Roberts, 2007] and the composition could be determined by the areas under the GC peaks:

$$x_i = \frac{A_{peak,i}}{\sum_{i=1}^{n_{peaks}} A_{peak,i}} \tag{4.2}$$

For the micro-GC TCD a calibration had to be performed with the assistance of Roberts [2007] to relate the TCD reading to the actual composition of the component. The calibration results are shown in Table 4.5 and the resulting equation to calculate the composition (including a nitrogen reference as depicted by the apostrophe ') supplied in equation 4.3.

$$(y')_i^{off-gas} = \frac{\frac{A_{peak,i}}{f_i^{calibration}}}{\sum_{i=1}^{n_{peaks}} \frac{A_{peak,i}}{f_i^{calibration}}} \tag{4.3}$$

A known amount of nitrogen ($1.90.10^{-7}$ kmol/s) was co-fed with the off-gas to calculate the off-gas flow rates based on the resulting compositions. The nitrogen usually comprised ca. 25 mol% of the combined stream to make its composition significant, thus minimizing potential experimental errors. The off-gas flow rate was thus calculated as follows:

$$V^{off-gas} = \frac{1.90.10^{-7}}{(y')_{N2}^{off-gas}} - 1.90.10^{-7} \tag{4.4}$$

Table 4.5: Micro-GC TCD calibration values.

Component	Calibration value
Hydrogen	43892
Nitrogen	4879
1-Hexene	7559
n-Hexane	7815

and the nitrogen composition of the reference gas removed to yield the true off-gas composition of component i:

$$y_i^{off-gas} = \frac{(y')_i^{off-gas}}{1 - (y')_{N2}^{off-gas}} \tag{4.5}$$

Chapter 5

Theoretical methodology

5.1 Property estimations

As will become apparent in this chapter, a large variety of liquid and vapour properties must be estimated in the current study. The property estimation techniques and equations are summarized in Appendix B for information purposes, but a short note regarding equations of states (EOS's) will be highlighted here.

The presence of non-condensable hydrogen precludes the use of Raoult's law which requires pure component vapour pressures. An EOS is thus required to calculate the equilibrium coefficient and vapour and liquid molar volumes. Several EOS's are available, of which the ideal gas law, and generalized gas law (which accounts for compressibility) are probably best known. Other well-known EOS's include Van der Waals (now infrequently used), Redlich-Kwong (RK), Soave-Redlich-Kwong (SRK) and Peng-Robinson (PR) [Seader & Henley, 1998]. In this study the current version of the PSRK-Unifac method [Horstmann et al., 2005] will be used. The PSRK-Unifac method forms a bridge between traditional EOS's and activity coefficient models and can thus predict both highly non-ideal liquids and gases. See Appendix B for more detailed information regarding the above EOS's.

5.2 Reaction Kinetics

Based on the Horiuti-Polanyi mechanism (Figures 2.1 and 2.2), the Langmuir-Hinshelwood kinetics can be developed for each elementary reaction rate of consumption. In the following derivation, n_{iso} is the number of possible alkene isomers, carbon i arbitrarily the carbon to the left of the double bond as shown in Figure 5.1, and $*$ a vacant site. The classic Horiuti-Polanyi mechanism via sp^3 hybridization is shown here.

Based on the elementary reaction steps, the *adsorption rate* of hydrogen and the n_{iso}

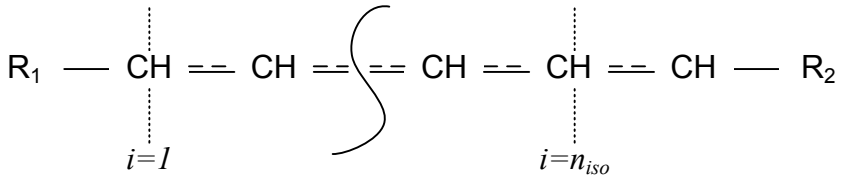

Figure 5.1: An arbitrary section of a linear alkene containing n_{iso} possible positions for the double bond (delineated by the dashed lines) and involving $n_{iso}+1$ carbons during isomerization/hydrogenation. R_1 and R_2 are the residual chains on either sides.

possible isomers are derived in equations 5.1 and 5.2.

$$\begin{aligned} H_2 + 2* &\rightleftharpoons 2H* \\ \left(R_1 - C^iH = C^{i+1}H - R_2\right) + 2* &\rightleftharpoons \left(R_1 - C^iH - C^{i+1}H - R_2\right)** \end{aligned}$$

$$R^{H2} = k^{H2}(x_{H2}\theta_V^2 - \frac{\theta_H^2}{K^{H2}}) \tag{5.1}$$

$$R_i^{ads} = k_i^{ads}(x_{C,i}\theta_V^2 - \frac{\theta_{C,i}}{K_i^{ads}}) \tag{5.2}$$

The *first hydrogen transferral* to the adsorbed alkene may occur onto either of the two carbons involved in the double bond, i.e. either onto carbon i or $i+1$.

$$\begin{aligned} \left(R_1 - C^iH - C^{i+1}H - R_2\right)** + H* &\rightleftharpoons \left(R_1 - C^iH_2 - C^{i+1}H - R_2\right)* + 2* \\ \left(R_1 - C^iH - C^{i+1}H - R_2\right)** + H* &\rightleftharpoons \left(R_1 - C^iH - C^{i+1}H_2 - R_2\right)* + 2* \end{aligned}$$

$$R_i^{iso1} = k_i^{iso1}(\theta_{C,i}\theta_H - \frac{\theta_{CH,i}\theta_V^2}{K_i^{iso1}}) \tag{5.3}$$

$$R_i^{iso2} = k_i^{iso2}(\theta_{C,i}\theta_H - \frac{\theta_{CH,i+1}\theta_V^2}{K_i^{iso2}}) \tag{5.4}$$

Following the assumption that alkane desorption is rapid (Section 2), the first hydrogen transferral is followed by the *second hydrogen transferral and simultaneous desorption* of the resulting alkane (or stated differently: the adsorbed alkane concentration is zero). If desorption is irreversible, regression analyses should show $\mathbf{K^{des}}$ to be very large.

$$\left(R_1 - C^iH_2 - C^{i+1}H - R_2\right)* + H* \rightarrow Alkane + 2*$$

$$R_i^{des} = k_i^{des}(\theta_{CH,i}\theta_H - \frac{\theta_V^2 x_{nC}}{K_i^{des}}) \tag{5.5}$$

The reaction rate of formation for each species can then be computed from the

elementary rates of consumption:

$$r^{H2} = -R^{H2} \tag{5.6}$$

$$r_{i-alkene} = -R_i^{ads} \tag{5.7}$$

$$r_{alkane} = \sum_{i=1}^{n_{iso}+1} R_i^{des} \tag{5.8}$$

$$r_{\theta H} = 2R^{H2} - (\sum_{i=1}^{n_{iso}} R_i^{iso1} + \sum_{i=1}^{n_{iso}} R_i^{iso2} + \sum_{i=1}^{n_{iso}+1} R_i^{des}) \tag{5.9}$$

$$r_{\theta C,i} = R_i^{ads} - (R_i^{iso1} + R_i^{iso2}) \tag{5.10}$$

$$r_{\theta CH,i} = R_i^{iso1} - R_i^{des} + R_{i-1}^{iso2} \tag{5.11}$$

Lastly, θ_v may be solved for via a surface species balance if the total number of available surface sites (θ_S) is known:

$$\theta_S = \theta_V + 2\sum_{i=1}^{n_{iso}} \theta_{C,i} + \sum_{i=1}^{n_{iso}+1} \theta_{CH,i} + \theta_H$$

$$eq\theta_V = \theta_S - \left(\theta_V + 2\sum_{i=1}^{n_{iso}} \theta_{C,i} + \sum_{i=1}^{n_{iso}+1} \theta_{CH,i} + \theta_H\right) \tag{5.12}$$

At steady state the surface species' rates of formation ($r_{\theta H}$, $r_{\theta C,i}$, $r_{\theta CH,i}$) are zero if a pseudo-steady-state approach is assumed and it is thus possible to express the rate of hydrogenation as a function of only the bulk concentrations. Attempts by hand proved too time-consuming and the algebraic solver Maxima was thus used. Maxima could reach the following maximum level of simplification:

$$0 = c_0 + c_1\theta_H + c_2\theta_H^2 + c_3\theta_H^3 + c_4\theta_H^4 + c_5\theta_H^5 + c_6\theta_H^6 + c_7\theta_H^7 \tag{5.13}$$

$$\theta_{\mathbf{C}} = f\left(\text{reaction rate constants}, x_{H2}, \mathbf{x_C}, \mathbf{x_{nC}}, \theta_V^2, \theta_H\right) \tag{5.14}$$

$$\theta_{\mathbf{CH}} = f\left(\text{reaction rate constants}, x_{H2}, \mathbf{x_C}, \mathbf{x_{nC}}, \theta_V^2, \theta_H\right) \tag{5.15}$$

where $\mathbf{c} = f$ (reaction rate constants, $x_{H2}, \mathbf{x_C}, \mathbf{x_{nC}}, \theta_V^2$) and where the reaction rate constants include the intrinsic reaction rates and equilibrium coefficients: $\mathbf{k^{H2}}$, $\mathbf{K^{H2}}$, $\mathbf{k^{ads}}$, $\mathbf{K^{ads}}$, $\mathbf{k^{iso1}}$, $\mathbf{K^{iso1}}$, $\mathbf{k^{iso2}}$, $\mathbf{K^{iso2}}$, $\mathbf{k^{des}}$, $\mathbf{K^{des}}$. Beyond this the equations become too complex for Maxima to solve. However, this set of equations can now be numerically solved relatively easily for a set of bulk input concentrations (i.e. x_{H2}, $\mathbf{x_C}$ and $\mathbf{x_{nC}}$) by supplying a suitable guess for $\theta_V = [0 : \theta_S]$, solving equation 5.13 for θ_H via a polynomial solver (such as the Fortran subroutine *rpoly.for*), calculating $\theta_{\mathbf{C}}$ and $\theta_{\mathbf{CH}}$ via equations 5.14 and 5.15 and minimizing error equation 5.12 to zero by varying θ_V. Of the seven possible roots, only those lying within the range $[0 : \theta_S]$ need be considered. By using different

Table 5.1: Variables and equations used in the semi-batch reactor model.

Equations	No.	Variables
5.18	c	n_i^T
5.19	1	θ_H
5.20	n_{iso}	$\theta_{C,i}$
5.21	$n_{iso}+1$	$\theta_{CH,i}$
5.22	c	n_i^L
5.23	1	P or F_{H2}
5.24	1	T
$2c+2n_{iso}+4$		

initial guesses, it was possible to confirm that, at least in the cases considered, only one apparent (the same root may appear more than once) root was found within this range.

Lastly, it is necessary to determine whether external and/or internal mass transfer limitations within the porous catalyst are significant. For external mass transfer limitations, Mear's criterion [Fogler, 1999] may be used, where Mear found that external mass transfer effects may be neglected when:

$$0.15 \quad > \quad \frac{r_i^{observed}\rho^L(0.5d_p)n_{\text{rxnorder}}}{k^S\rho_i^L} \tag{5.16}$$

where the overall reaction order both for the hydrogenation and isomerization is 1. The Weisz-Prater criterion is the equivalent for internal diffusion [Fogler, 1999]:

$$C_{WP,i} \quad = \quad \frac{r_i^{observed}\rho_{cat}(0.5d_p)^2}{D_i^{S,effective}C_i^S} \tag{5.17}$$

If $C_{WP} << 1$, there are no internal diffision limitations. The diffusivity and mass transfer values will be discussed in Section 5.4.2.

5.3 Modelling reactors: Semi-batch 1-hexene hydrogenation

Kinetic studies were conducted in a semi-batch reactor and thus required a model for regression analyses. The experimental set-up is shown in Figure 4.1. The system may be modelled with a set of differential algebraic equations (DAE's). Table 5.1 summarizes the variables and associated equations.

As the catalyst is dispersed in the liquid phase, it was assumed that the reaction occurs only on the catalyst surface in the liquid phase with no reaction in the gas phase. The $2n_{iso}+2$ material balances on the adsorbed hydrogen, n_{iso} adsorbed alkene

and $n_{iso}+1$ half-hydrogenated surface species reduce to an accumulation term and the product of the reaction rates and catalyst weight. For the c bulk species the amount fed must additionally be accounted for.

$$\frac{dn_i^T}{dt} = r_i^L W_{cat} + F_i^{in} \tag{5.18}$$

$$\frac{d\theta_H}{dt} = r_{\theta H} W_{cat} \tag{5.19}$$

$$\frac{d\theta_{C,i}}{dt} = r_{\theta C,i} W_{cat} \tag{5.20}$$

$$\frac{d\theta_{CH,i}}{dt} = r_{\theta CH,i} W_{cat} \tag{5.21}$$

In the absence of rigorous mass transfer coefficient correlations for the semi-batch reactor and given the vigorous mixing of the vessel, mass transfer limitations were assumed negligible and the vapour and liquid phases assumed to be in equilibrium. Mass transfer effects between the liquid and solid phases are captured by the regressed adsorption and desorption reaction rate coefficients, and internal mass transfer limitations are not considered as the particles used were ground to a fine dust in the reactor via attrition. The liquid and vapour volumes are constrained by the physical dimensions of the reactor, yielding an additional equation, and the temperature is set by the operating philosophy described in Section 4.2.

$$0 = \frac{n_i^V}{\sum_{i=1}^{c} n_i^V} - K_{eq,i} \frac{n_i^L}{\sum_{i=1}^{c} n_i^L} \tag{5.22}$$

$$0 = V^T - (V^L + V^V) \tag{5.23}$$

$$\frac{dT}{dt} = Gradient \tag{5.24}$$

5.4 Modelling reactive non-equilibrium distillation

The approach followed here is to divide the column height into many incremental segments, or stages, to characterize each and to calculate the change in column conditions height wise so as to satisfy the set inputs, and top and bottoms boundary conditions if physically feasible. Other techniques are available [Seader & Henley, 1998; Taylor & Krishna, 1993, 2000], but this approach is commonly used. The methodology is based on that found in Kooijman & Taylor [1998].

5.4.1 MERSHH equations

To characterize each stage the **m**aterial balance, **e**quilibrium equations, **r**ate equations, **s**ummation equations, energy (ent**h**alpy) balance, and **h**ydraulic equations (MERSHH

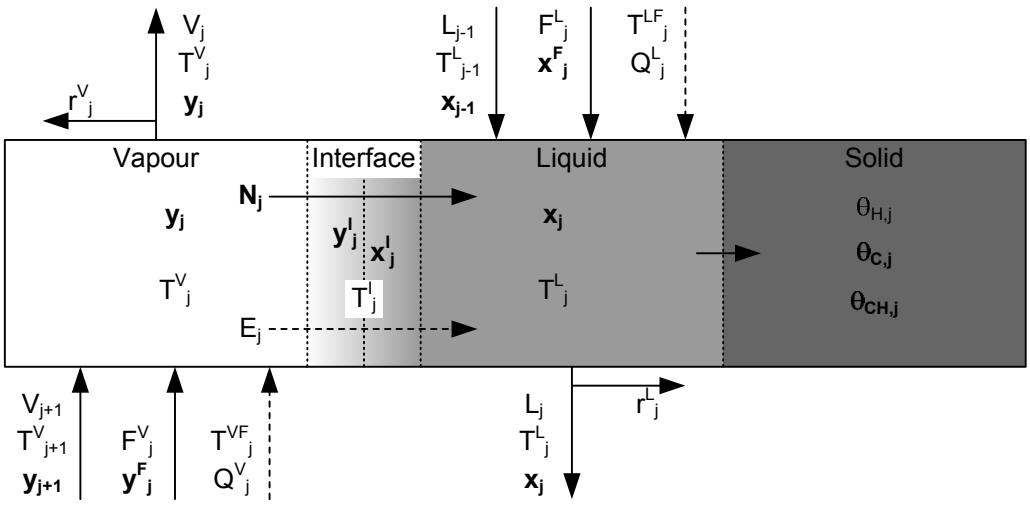

Figure 5.2: Non-equilibrium (NEQ) model with reaction (variables in bold are component vectors).

equations) must be satisfied. Figure 5.2 shows a schematic diagram of a stage with vectors assumed to be positive in the arrow direction. Table 5.2 summarizes the number of equations and variables required. The error equations developed here (such as $eqM^L_{i,j}$) will be optimized towards zero by numerical solution algorithms discussed in Section 5.5.

(2c) Material balances

Component material balances must be performed on c components in 2 phases resulting in $2c$ material balances per stage. The liquid and vapour component material balances are shown in equations 5.25 and 5.26 respectively. Note the c component molar flux variables ($N_{i,j}$) and c component reaction terms $r^L_{i,j}$ which will be discussed later. In the specific case considered in this work it is assumed that the reaction occurs in the liquid phase only and that $\mathbf{r_V} = \mathbf{0}$.

$$eqM^L_{i,j} = (1 + r^L_j)L_j x_{i,j} - L_{j-1}x_{i,j-1} - F^L_j x^F_{i,j} + r^L_{i,j}W_{cat} - N_{i,j} \quad (5.25)$$

$$eqM^V_{i,j} = (1 + r^V_j)V_j y_{i,j} - V_{j+1}y_{i,j+1} - F^V_j y^F_{i,j} + r^V_{i,j}W_{cat} + N_{i,j} \quad (5.26)$$

$$eqM_{i,j} = (1 + r^L_j)L_j x_{i,j} - L_{j-1}x_{i,j-1} - F^L_j x^F_{i,j} + r^L_{i,j}W_{cat} + (1 + r^V_j)V_j y_{i,j} - V_{j+1}y_{i,j+1} - F^V_j y^F_{i,j} + r^V_{i,j}W_{cat} \quad (5.27)$$

(1) Equilibrium equation

The vapour-liquid equilibrium is assumed to exist at the vapour-liquid interface at the interfacial temperature and between the interfacial vapour and liquid component compositions, as shown in equation 5.28.

$$eqQ^I_{i,j} = K_{eq,i,j}x^I_{i,j} - y^I_{i,j} \quad (5.28)$$

Table 5.2: Equations and variables required by the MERSHH equations per stage.

Equations	No.	Variables	No.
$eqM^L_{i,j}$	c	$x_{i,j}$	c
$eqM^V_{i,j}$	c	$y_{i,j}$	c
$eqE_{i,j}$	c	L_j	1
$eqR^L_{i,j}$	$c-1$	V_j	1
$eqR^V_{i,j}$	$c-1$	$N_{i,j}$	c
eqS^L_j	1	$x^I_{i,j}$	c
eqS^V_j	1	$y^I_{i,j}$	c
eqS^{LI}_j	1	T^L_j	1
eqS^{VI}_j	1	T^V_j	1
eqE^L_j	1	T^I_j	1
eqE^V_j	1	P_j	1
eqE^I_j	1		
$eqHydr_j$	1		
	$5c+6$		$5c+6$

($\mathbf{2c-2}$) Rate equations

Interphase mass transfer may be modelled in several ways. Firstly, the hydrodynamics may be described via film, two-film, penetration, film penetration and turbulent boundary layer models [Nieuwoudt, 2005; Seader & Henley, 1998]. Two-film theory assumes the existence of two perfectly mixed ("bulk") phases separated by two diffusion controlled stagnant films (one in each phase) and a phase equilibrium interface between the films. Diffusional flux may be modelled via Fickian or Maxwell-Stefan diffusion of which Maxwell-Stefan will be used as it is thermodynamically more rigorous [Taylor & Krishna, 2000] - see Section 5.4.2. Assuming no accumulation at the interface, the $c-1$ equations (the last not being independent) for each phase are shown in equations 5.29 and 5.30.

$$eqFlux^L_{i,j} = N_{i,j} - N^L_{i,j} \tag{5.29}$$

$$eqFlux^V_{i,j} = N_{i,j} - N^V_{i,j} \tag{5.30}$$

where $N^L_{i,j}$ and $N^V_{i,j}$ are functions calculated by the method described in Section 5.4.2.

(4) Summation Equations

The 4 mole fraction summation equations close the liquid, vapour, interfacial liquid and interfacial vapour material balances and are shown in equations 5.31 to 5.34.

$$eqS_j^L = \sum_{i=1}^{c} x_{i,j} - 1 \tag{5.31}$$

$$eqS_j^V = \sum_{i=1}^{c} y_{i,j} - 1 \tag{5.32}$$

$$eqS_j^{LI} = \sum_{i=1}^{c} x_{i,j}^I - 1 \tag{5.33}$$

$$eqS_j^{VI} = \sum_{i=1}^{c} y_{i,j}^I - 1 \tag{5.34}$$

(3) Energy (enthalpy) balances

The 3 liquid (eq. 5.36), vapour (eq. 5.37) and interfacial (eq. 5.35) energy balances close the overall energy balance. Note the enthalpy (H) and energy transfer (e) functions that are required and which will be discussed below.

$$eqE_j^I = e_j^V - e_j^L \tag{5.35}$$

$$eqE_j^L = (1 + r_j^L)L_j H_j^L - L_{j-1}H_{j-1}^L - F_j^L H_j^{LF} - Q_j^L - e_j^L \tag{5.36}$$

$$eqE_j^V = (1 + r_j^V)V_j H_j^V - V_{j+1}H_{j+1}^V - F_j^V H_j^{VF} - Q_j^V + e_j^V \tag{5.37}$$

$$eqE_j = (1 + r_j^L)L_j H_j^L - L_{j-1}H_{j-1}^L - F_j^L H_j^{LF} - Q_j^L$$
$$(1 + r_j^V)V_j H_j^V - V_{j+1}H_{j+1}^V - F_j^V H_j^{VF} - Q_j^V \tag{5.38}$$

(1) Hydraulic equation

Lastly, the single hydraulic equation takes the pressure drop through the column into account. As a first approach, the pressure drop through the column was assumed to be zero.

$$eqHYDR_j = P_j - P_{\text{condenser}} \tag{5.39}$$

5.4.2 Mass and energy interphase transfer

Mass transfer

Numerous methods are available to estimate liquid and vapour mass transfer coefficients [Wang et al., 2005].

The estimation techniques recommended by Kooijman & Taylor [1998] for *structured packing* are used here:

$$k_{i,k,j}^{L,\text{structured}} = 2\sqrt{\frac{D_{i,k,j}^{L}}{\pi t_{L,j}}} \tag{5.40}$$

$$k_{i,k,j}^{V,\text{structured}} = \frac{Sh_j^V D_{i,k,j}^{V}}{d_{eq}} \tag{5.41}$$

where $t_{L,j}$, Re_j, Sh_j and Sc_j are defined in terms of effective diameters, and superficial vapour and liquid velocities, which are supplied in Appendix C based on the internals' geometric properties. The average stage diffusion or mass transfer coefficient is calculated at the average film compositions and temperatures.

Similarly, equations 5.42 and 5.43 are suggested for random packing.

$$k_{i,k,j}^{L,\text{random}} = 0.0051\left(\text{Re}_j^{I,L}\right)^{0.667}(Sc_j^L)^{-0.5}(a_p d_p)^{0.4}\left(\frac{\rho_{mix,j}^L}{\eta_{mix,j}^L g}\right)^{-0.33} \tag{5.42}$$

$$k_{i,k,j}^{V,\text{random}} = A(\text{Re}_j^V)^{0.7}(Sc_j^V)^{0.333}(a_p d_p)^{-2}\left(a_p D_{i,k,j}^V\right) \tag{5.43}$$

where A is a constant determined by the size of the random packing, the Reynolds and Schmidt numbers are modified, and where $\text{Re}_j^{I,L}$ is a modified Reynolds number based on the interfacial area density (see Appendix C).

Generally, mass transfer rates are correlated using dimensionless numbers which not only require estimation of numerous physical and thermodynamic properties, but also knowledge of the hydrodynamic environment inside the system (see Section 4.3.3). Tables B.1 and B.2 list the estimated properties, the methods used and their applicability to the systems at hand for both the liquid and vapour phases. In particular, note the use of an EOS in systems where species without vapour pressures (i.e. non-condensables) are present, as in this work.

The Maxwell-Stefan approach to mass transfer will be used here rather than the Fickian approach. Krishna & Wesselingh [1997] give an excellent overview of the derivation and application of the Maxwell-Stefan approach as well as examples of where the Fickian approach fails. In fact, Fick's Law is shown to be a special case of the Maxwell-Stefan approach. Essentially, a force balance is performed on the molecules of a component, where the driving force must be balanced by the frictional ("drag") force exerted on the component by the other components in the mixture. Krishna & Wesselingh [1997]

readily shows that this simplifies to a chemical potential gradient driving force, rather than the somewhat arbitrary concentration gradient driving force utilized by Fick's Law. For a multicomponent liquid mixture, eq. 5.44 can be derived for component i as modified from Krishna & Wesselingh [1997] for symbol continuity and the application to distillation stages.

$$\frac{x_{i,j}}{R_0 T}\nabla_T \mu_i = \sum_{k=1}^{c} \frac{x_{i,j}N^L_{k,j} - x_{k,j}N^L_{i,j}}{D^L_{i,k,j}C^L_{ave,j}A_{contact}} \tag{5.44}$$

The following assumptions can now be applied to eq. 5.44:

- The driving force across the film thickness is mono-directional from the bulk phase to the phase interface, i.e. $\nabla_T \mu_i = \frac{d\mu_i}{dz}$.
- There are no external driving forces such as electrostatic or centrifugal forces.
- The solution is ideal, which should be valid for a system containing 1-hexene, 2-hexene, n-hexane and hydrogen. The following thermodynamic relationship is thus applicable: $\mu_i = G^{id}_i + R_0 T ln(x_i)$ [Smith et al., 1996]

Consequently, based on the above assumptions:

$$\begin{aligned} \frac{d\mu_i}{dz} &= \frac{dG^{id}_i}{dz} + R_0 T \frac{dln(x_i)}{dz} \\ &= R_0 T \frac{1}{x_i}\frac{dx_i}{dz} \\ \frac{x_i}{R_0 T}\frac{d\mu_i}{dz} &= \frac{dx_i}{dz} \end{aligned} \tag{5.45}$$

and thus the general Maxwell-Stefan equation for an ideal liquid solution can be derived via substitution of eq. 5.45 into eq. 5.44 as shown in equation 5.46. The Maxwell-Stefan equation for an ideal vapour solution is similar to that for the liquid.

$$\frac{dx_i}{dz} = \sum_{k=1}^{c} \frac{x_{i,j}N^L_{k,j} - x_{k,j}N^L_{i,j}}{D^L_{i,k,j}C^L_{ave,j}A_{contact}} \tag{5.46}$$

Assuming a linear film concentration, eq. 5.46 may be discretized between the bulk and interfacial concentrations. Additionally, invoking the relation that $k_{i,j} = \frac{D_{i,j}}{\delta z}$ (where δz is the film thickness) results in eq. 5.47.

$$2A_{contact}C^L_{ave,j}\left(x_{i,j} - x^I_{i,j}\right) = \sum_{\substack{k=1 \\ k\neq i}}^{c}\left(\frac{x_{i,j} + x^I_{i,j}}{k^L_{i,k,j}}N^L_{k,j}\right) + \left(\frac{x_{i,j} + x^I_{i,j}}{k^L_{i,i,k}} - \sum_{k=1}^{c}\frac{x_{k,j} + x^I_{k,j}}{k^L_{i,k,j}}\right)N^L_{i,j} \tag{5.47}$$

which for a specific stage j may be represented in matrix form by eq. 5.48 in terms of vector $\mathbf{B}$ $(c \times 1)$, matrix $\mathbf{A}$ $(c \times c)$ and vector $\mathbf{N^L}$ $(c \times 1)$:

$$\begin{aligned} \mathbf{B} &= \mathbf{A}\mathbf{N^L} \\ B_i &= 2A_{contact}C^L_{ave}\left(x_i - x^I_i\right) \\ A_{i,k} &= \frac{x_i + x^I_i}{k^L_{i,k}} ... k \neq i \\ A_{i,i} &= \frac{x_i + x^I_i}{k^L_{i,i}} - \sum_{k=1}^{c} \frac{x_k + x^I_k}{k^L_{i,k}} \end{aligned} \tag{5.48}$$

To bootstrap the $c-1$ independent equations an overall material balance is invoked on stage j:

$$N^L_{total} = \sum_{i=1}^{c} N^L_i \tag{5.49}$$

with $B_c = N^L_{total}$ and $A_{i,c} = 1$. The resulting set of c linear equations are solved for N^L using linear algebra. A similar method is used to calculate N^V, remembering to use a driving force direction consistent with that of eq. 5.47:

$$2A_{contact}C^V_{ave,j}\left(y^I_{i,j} - y_{i,j}\right) = \sum_{\substack{k=1 \\ k\neq i}}^{c} \left(\frac{y_{i,j} + y^I_{i,j}}{k^V_{i,k,j}} N^V_{k,j} \right) + \left(\frac{y_{i,j} + y^I_{i,j}}{k^V_{i,i,j}} - \sum_{k=1}^{c} \frac{y_{k,j} + y^I_{k,j}}{k^V_{i,k,j}} \right) N^V_{i,j} \tag{5.50}$$

In CD it is also necessary to include mass transfer to/from and in the catalyst itself. Mass transfer to and from the catalyst surface is incorporated into the adsorption and desorption reaction coefficients and will thus not be calculated, but rather regressed from experimental data. This simplifies the set of unknowns as it means that molar fluxes to and from the catalyst surface need not be calculated. However, it is still prudent to perform the tests for external and internal mass transfer limitations discussed in Section 5.2. Fogler [1999] supplies the following correlations for external mass transfer coefficients in fixed beds:

$$k^S_{i,k,j} = \left[0.765(Re^L_j)^{0.18} + 0.365(Re^L_j)^{0.614}\right] \epsilon_{bed}(Sc^L_j)^{0.333} D^L_{i,k,j}(d_{eq})^{-1} \tag{5.51}$$

where $d_{eq} = d_p$ for a spherical particle and $d_{eq} = \sqrt{A_p/\pi}$ for a non-spherical particle and where A_p is the external surface area of the particle.

When considering mass transfer in a porous catalyst, the bulk diffusivity must be adjusted via the tortuosity (τ_{cat}) and constriction (σ_{cat}) factors to compensate for non-linearities both in the pore directions and pore cross sectional areas. As a first approach,

these values were set to unity.

$$D^{S,effective} = \frac{D^{l}\epsilon_{cat}\sigma_{cat}}{\tau} \tag{5.52}$$

Since the catalyst is specifically designed for industrial hydrogenation reactions, it is (as a first approach) assumed that there are no internal mass transfer limitations. However, these assumptions must be tested during analyis of the experimental data.

Energy transfer

Interphase energy transferred comprises a convection and mass diffusion term as shown in equations 5.53 and 5.54.

$$e_j^L = A_{contact}h_j^L\left(T_j^I - T_j^L\right) + \sum_{i=1}^{c} N_{i,j}H_{i,j}^{LI} \tag{5.53}$$

$$e_j^V = A_{contact}h_j^V\left(T_j^V - T_j^I\right) + \sum_{i=1}^{c} N_{i,j}H_{i,j}^{VI} \tag{5.54}$$

Heat transfer coefficients for the complex hydrodynamics in distillation are difficult to estimate accurately, but required by the convective component in interphase energy transfer. Following the method of Kooijman & Taylor [1998], the heat transfer coefficients are estimated via the penetration model for the liquid (eq. 5.55) and via the Chilton-Colburn analogy for the vapour (eq. 5.56) phases.

$$h_j^L = k_{ave,j}^L\rho_{mix,j}^L c_{p,mix}^L (Le_j^L)^{0.5} \tag{5.55}$$

$$h_j^V = k_{ave,j}^V\rho_{mix,j}^V c_{p,mix}^V (Le_j^V)^{\frac{2}{3}} \tag{5.56}$$

where Le is the Lewis number as defined in Appendix B.

In terms of the catalyst, it is assumed that there are no external or internal heat transfer limitations as a first approach.

5.4.3 Material and energy intraphase conversion

The presence of a reaction causes intraphase mass and energy conversion to occur.

To calculate *material* conversion, reaction specific kinetics are required if reaction equilibrium cannot be assumed. The reaction kinetics can be explicitly defined as functions, solved simultaneously in an independent loop within the MERSHH equations or added to the MERSHH equations. As discussed in Section 5.2, the set of equations describing the surface species concentrations and both bulk and intermediary reaction rates will be solved in an internal root finding loop to supply ($r_{i,j}^L$).

Table 5.3: Reduction in complexity from the reactive NEQ to reactive EQ model.

Reactive NEQ $n_{equations/unknowns} = 5c + 6$						Reactive EQ		
Constraints		Unknowns less		Equations less				
$N_{i,j} = 0$	c	$N_{i,j}$	$-c$	$eqM^V_{i,j}$	$-c$	$eqM_{i,j}$	$x_{i,j}$	c
$x^I_{i,j} = x_{i,j}$	c	$x_{i,j}$	$-c$	$eqR^L_{i,j}$	$-(c-1)$	$eqQ^I_{i,j}$	$y_{i,j}$	c
$y^I_{i,j} = y_{i,j}$	c	$y_{i,j}$	$-c$	$eqR^V_{i,j}$	$-(c-1)$	eqS^L_j	L_j	1
$T_L = T^I_j$	1	T^L_j	-1	eqS^{LI}_j	-1	eqS^V_j	V_j	1
$T_L = T^I_j$	1	T^V_j	-1	eqS^{VI}_j	-1	eqE_j	T_j	1
				eqE^I_j	-1			
				eqE^V_j	-1			
Reactive EQ $n_{equations/unknowns} = 2c + 4$								$2c + 4$

The *heat* generated by the reaction is implicitly calculated by including the free heats of formation in component enthalpy estimations.

5.4.4 Special cases

The reactive non-equilibrium distillation model historically developed as a natural progression from the special case of the constant molar overflow non-reactive equilibrium model.

Non-reactive distillation as a special case simply requires the reaction term to be zero regardless of the model. Equilibrium distillation as a special case, however, can drastically reduce the number of MERSHH equations and related physical properties, with further reductions when using constant molar overflow. Depending on the simplicity and ideality of the system either may be an accurate model, though their interest here is to supply initial estimates for the numerical solution algorithms (see Section 5.5)

Reactive equilibrium distillation

The reactive equilibrium model assumes vapour-liquid equilibrium between the vapour and liquid streams leaving a stage, rather than at an interface *on* a stage. Mathematically, this is equivalent to assuming infinitely large interphase mass transfer coefficients and significantly reduces the number of equations and unknowns as shown in Table 5.3. Specifically, the EQ model is described by equations 5.27, 5.28, 5.31, 5.32, 5.38 and 5.39.

Additionally, since calculation of the mass and heat transfer coefficients is not necessary, hydrodynamic and geometric knowledge of the stage internals are also not required and the number of physical properties to estimate are significantly reduced. Overall this drastically reduces the complexity and required computational system resources.

Non-reactive constant molar overflow

Further simplification is possible by assuming that the mixture enthalpy and vapourization enthalpy along the column is approximately constant - a relatively safe assumption across small temperature ranges - leading to eq. 5.57 (see Appendix D).

$$\frac{(1+r_j^L)L_j - L_{j-1}}{F_j^T} = \frac{H_j^V - (\frac{F_j^L}{F_j^T}H_j^{LF} + \frac{F_j^V}{F_j^T}H_j^{VF})}{\Delta H^{vap}} - \frac{R_{i,j}^L H_j^V}{F_j^T \Delta H^{vap}} - \frac{Q_j^T}{F_j^T \Delta H^{vap}} \tag{5.57}$$

Defining a column section as a consecutive number of stages where there are no material or energy disturbances (such as feeds, sidestreams, heat exchange or reactions) equation 5.57 shows that the liquid (and similarly for the vapour) molar flow rates in sections remain constant, hence constant molar overflow (CMO). The energy balance thus becomes redundant except on stages where material and energy disturbances take place. On these stages a q-factor (for example) is introduced to account for the change in molar flux across the stage (eq. 5.58).

$$q = \frac{H_j^V - (\frac{F_j^L}{F_j^T}H_j^{LF} + \frac{F_j^V}{F_j^T}H_j^{VF})}{\Delta H^{vap}} - \frac{R_{i,j}^L H_j^V}{F_j^T \Delta H^{vap}} - \frac{Q_j^T}{F_j^T \Delta H^{vap}} \tag{5.58}$$

Eq. 5.58 reduces to the more familiar definition of the q-factor [Seader & Henley, 1998] in cases where no reaction occurs nor additional heat is added on the feed stage. In such cases $q < 0$ corresponds to a superheated vapour feed, $q = 0$ to a saturated vapour feed, $q = 1$ to a saturated liquid feed and $q > 1$ to a subcooled liquid feed.

5.4.5 Condenser configurations

The reboiler and condenser stages are modelled using the EQ model, resulting in a total of $(N_{stages} - 2)(5c + 6)$ unknowns and variables for the reactive NEQ model and $N_{\text{degrees of freedom}}$.

However, the theoretical model must reflect that the physical system can operate either with a subcooled condenser, saturated liquid product condenser or a partial condenser.

The *partial* condenser is the simplest case, requiring an input specification such as the cooling duty (Q_1^V) or a constraint on the condenser temperature (T_1^L) with variable Q_1^V if $N_{\text{degrees of freedom}}$ is to be conserved. Similarly, a *total liquid* product condenser implicitly constrains $V_1 = 0$ and Q_1^V can replace it as variable. A *subcooled* condenser also physically constrains $V_1 = 0$, but additionally constrains the subcooled T_1^L and implicitly defines c vapour molar fractions on the condenser stage ($y_{i,1}$), which do not

exist (no equilibrium). To match the number of equations and unknowns, the equilibrium (eq. 5.28) and vapour unity summation (eq. 5.32) equations must thus be dropped for the condenser stage.

5.5 Solving the models

Unless otherwise stated, the models were solved using Digital Visual Fortran subroutines and coded in f90 format. Refer to Appendix G for a summary of the publically available subroutines used.

5.5.1 Semi-batch 1-hexene hydrogenation

Two regions may be identified during the semi-batch experiment, namely an initial period with variable temperature and pressure, but no hydrogen feed, and a second isothermal, isobaric period with variable hydrogen feed.

In the first region, the temperature gradient and a zero hydrogen feed flow rate are supplied and the pressure varied to satisfy the DAE system of equations. The DAE's require initial conditions for temperature, pressure, and moles of 1-hexene and hydrogen in the vapour and liquid phases. The initial temperature and pressure are known, but the initial amount of moles must be calculated from the knowledge of the initial volume of 1-hexene (the liquid volume displaced by the catalyst is negligible) in equilibrium with the surrounding argon and the amount of 1-hexene adsorbed onto the catalyst surface. Since the catalyst was protected from air via submersion in 1-hexene, it is assumed that the rate of 1-hexene adsorption is zero at $t = 0$. The initial conditions may thus be solved via equations 5.59 to 5.63.

$$0 = \frac{n^V_{1-hexene}}{\sum_{i=1}^{c} n^V_i} - K_{eq,1-hexene}\frac{n^L_{1-hexene}}{\sum_{i=1}^{c} n^L_i} \tag{5.59}$$

$$0 = \frac{n^V_{argon}}{\sum_{i=1}^{c} n^V_i} - K_{eq,argon}\frac{n^L_{argon}}{\sum_{i=1}^{c} n^L_i} \tag{5.60}$$

$$0 = V^T - (V^L + V^V) \tag{5.61}$$

$$0 = V^L_0 - V^L \tag{5.62}$$

$$0 = r_{\theta C,1-hexene} W_{cat} \tag{5.63}$$

The first region may be solved via the Fortran subroutine *DDASAC.f90*. The initial conditions to the second region assume an instantaneous pressure increase to the setpoint hydrogen pressure. To calculate the moles of hydrogen added and the distribution in

the liquid and vapour phases:

$$0 = \frac{n^V_{1-hexene}}{\sum_{i=1}^{c} n^V_i} - K_{eq,1-hexene}\frac{n^L_{1-hexene}}{\sum_{i=1}^{c} n^L_i} \quad (5.64)$$

$$0 = \frac{n^V_{argon}}{\sum_{i=1}^{c} n^V_i} - K_{eq,argon}\frac{n^L_{argon}}{\sum_{i=1}^{c} n^L_i} \quad (5.65)$$

$$0 = \frac{n^V_{hydrogen}}{\sum_{i=1}^{c} n^V_i} - K_{eq,hydrogen}\frac{n^L_{hydrogen}}{\sum_{i=1}^{c} N^L_i} \quad (5.66)$$

$$0 = V^T_0 - (V^L + V^V) \quad (5.67)$$

$$0 = n^T_{1-hexene} - (n^L_{1-hexene} + n^V_{1-hexene}) \quad (5.68)$$

$$0 = n^T_{argon} - (n^L_{argon} + n^V_{argon}) \quad (5.69)$$

In the second region the temperature gradient is zero (isothermal), pressure isobaric, and the hydrogen feed a variable. Since the hydrogen feed is no longer constant, the set of DAE equations becomes an index 2 problem[a] and *DDASAC.f90* must thus be replaced by *Besirk.f90* [Kooijman, 1995].

5.5.2 JaKaD: MERSHH equations

JaKaD is shown schematically in Figure 5.3 and is based on the methodological approach outlined by Kooijman & Taylor [1998]. The user is led through several questions to define the system which is then saved in a .jkd text file similar to the .sep file in Chemsep. The .jkd file includes input information regarding the number and names of components used, the number of stages and the associated internals' geometric information, the number of feeds and their conditions, the reaction stoichiometry (if applicable), whether the EQ or NEQ model is to be used and what the desired heat duty is. Additionally, several condenser configurations are available including subcooled, total liquid product and partial. Due to the varied nature of reaction kinetics and kinetic equations, reaction kinetics are programmed directly into Fortran and are not saved in the .jkd file.

Essentially, JaKaD reads the .jkd input specifications, reads the component data required for property estimation, makes an initial estimate assuming CMO, solves the EQ model, uses the solution as initial estimate to solve the NEQ model (if required), outputs the final iteration to file, and outputs selected graphs to screen using GNUplot. During analyses it was found that a rudimentary homotopy approach facilitated solution

[a]The index of DAE $F(t, y, y') = 0$ is the minimum number of times that the DAE must be differentiated with respect to t to extract an underlying ordinary differential equation or ODE [Gear & Petzold, 1983]. I.e., the index of a DAE essentially indicates to what degree it differs from an ODE and the index of an ODE is thus 0.

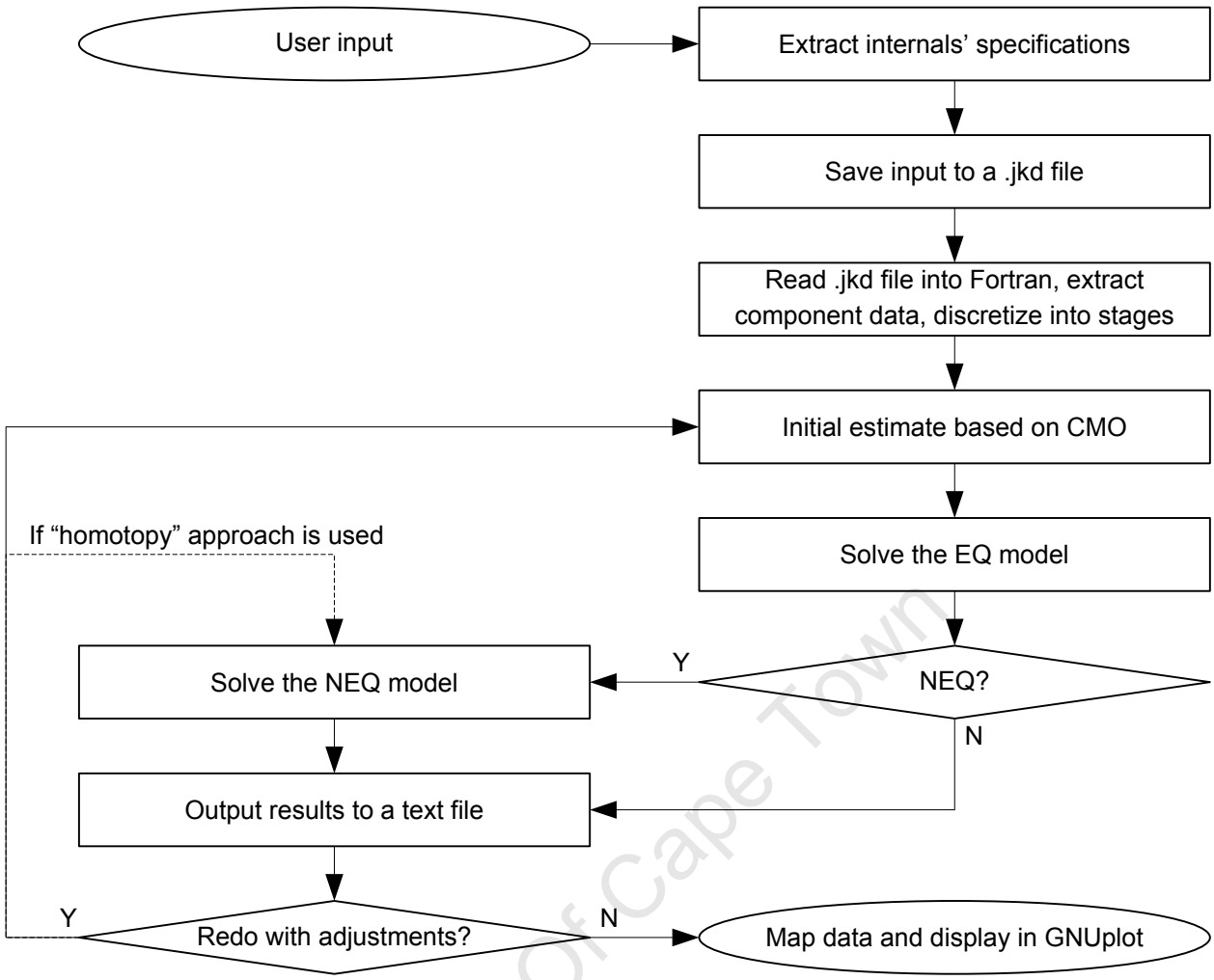

Figure 5.3: Schematic representation of JaKaD.

of the reactive NEQ model. This will be discussed in Section 8.2.

Wherever possible, linear algebra routines from LAPACK were used. For rootfinding of non-linear problems with one variable *DFZERO.f* was used with suitable bounds supplied for the roots. *Cubicroots.for* was used for cubic equations (such as for EOS calculations) and *cpoly.for* for other polynomials. *cpoly.for* includes complex roots and was found to be more reliable for the current application when compared to *rpqr79.for* and *rpoly.for*.

Several (unbounded) numerical rootfinding Fortran subroutines using modified Newton-Raphson techniques are available to solve the MERSHH equations, differing mainly in the rate-limiting computation of the finite difference approximation of the Jacobian matrix. The MERSHH equations' Jacobian matrix to solve for is a sparse matrix and a drastic reduction in computational time is thus possible from computing each element of the Jacobian (*minpack.f90*) to computing the banded Jacobian (*NLEQ1.f* or *minpack.f90*) to computing the sparse Jacobian (*NLEQ1S.f*). Due to time constraints and the complexity involved, the Jacobian was not solved analytically, though this would

considerably speed up the calculations [Kooijman & Taylor, 1998]. *NLEQ1S.f* was thus used.

Chapter 6

Analysis methodology

Combining theoretical models and experimental data is not always trivial and will be discussed here. Mass transfer correlations for standard structured and random packing are well-defined and documented in the literature [Onda et al., 1968; Taylor & Krishna, 1993; Perry et al., 1997; Seader & Henley, 1998; Kooijman & Taylor, 1998] or by suppliers. However, the mass transfer coefficients and elementary reaction rates for the used hydrogenation catalyst is catalyst specific and not available from either literature or the supplier. As discussed in Chapter 5 the semi-batch experiments and model can be used to regress for the reaction rates, while the CD experiments and CD model can regress for the mass transfer coefficients. This section details the methodology followed to achieve this.

6.1 Parameter estimation: semi-batch kinetic experiments

6.1.1 Non-linear least squares optimization

In this work, the Fortran subroutine *lmdif.f90* is used to estimate model parameters via least squares minimization of the errors between the theoretically and experimentally obtained values, normalized to the experimental values, as shown in eq. 6.1, to facilitate numerical convergence of *lmdif.f90*.

$$\begin{aligned} s^2 &= \sum_{i=1}^{n_{points}} (error_i)^2 \\ &= \sum_{i=1}^{n_{points}} \left(1 - \frac{y_i^{model}(t_i, \mathbf{x_i^{exp}}, \mathbf{par})}{y_i^{exp}(t_i, \mathbf{x_i^{exp}}, \mathbf{par})}\right)^2 \\ &= \frac{}{n_{points} - n_{pars}} \end{aligned} \tag{6.1}$$

where $\mathbf{y^{exp}}$ is the experimentally obtained value, $\mathbf{y^{model}}$ the model predicted value, t_i is the moment in time (unnecessary in steady state systems), **par** is the vector of parameters that are being fitted and $\mathbf{x_i^{exp}}$ is the column i in matrix $\mathbf{x^{exp}}$ that specifies the experimentally set values at time t_i. In this thesis, R^2 will generally not be used as an indication of the accuracy of a non-linear fit as it is strictly defined for linear systems. Instead, the accuracy of the model will be determined using the coefficient of variation (CV), model error and standard errors of parameters.

The standard error, s, is the square root of eq. 6.1 while the CV is defined as shown in eq. 6.2. The less the CV, the more variance can be explained by the model. A CV of 0 - 40% is typically considered as acceptable. Since s^2 is minimized based on the *normalized* experimental values, CV conveniently reduces to s.

$$\begin{aligned} CV &= \frac{s}{\left[\frac{y_i^{exp}}{\overline{y_i^{exp}}}\right]} \cdot 100 \\ &= s \end{aligned} \tag{6.2}$$

The covariance matrix (eq. 6.3) contains useful information such as the variance (σ_{ii}^2) of each parameter and the covariance of 2 parameters (σ_{ij}^2).

$$Covar = \begin{bmatrix} \sigma_1^2 = \sigma_{11}^2 & \cdots & \cdots & \cdots & \sigma_{n_{pars}1}^2 \\ \vdots & \ddots & & & \vdots \\ \sigma_{i1}^2 & & \sigma_i^2 = \sigma_{ii}^2 & & \vdots \\ \vdots & & & \ddots & \vdots \\ \sigma_{n_{pars}1}^2 & \cdots & \sigma_{n_{pars}j}^2 & \cdots & \sigma_{n_{pars}}^2 = \sigma_{n_{pars}n_{pars}}^2 \end{bmatrix} \tag{6.3}$$

The covariance matrix is defined as shown in eq. 6.4.

$$\begin{aligned} V_{i,j} &= \frac{\partial y^{model}\left(t_i, \mathbf{x^{exp}}, \mathbf{par}\right)}{\partial par_j} ....i = 1, 2...n_{points}; j = 1, 2...n_{pars} \\ \mathbf{cov} &= s^2(V^T V)^{-1} \end{aligned} \tag{6.4}$$

Normalization of the covariance with respect to the parameter variances, as shown in equations 6.5 and 6.6, yields the square symmetrical correlation matrix, with 0 indicating no correlation and 1 indicating complete correlation between two parameters.

$$\begin{aligned}\mathbf{Cor} &= \mathbf{W}\cdot\mathbf{cov}\cdot\mathbf{W} \\ &= \begin{bmatrix} 1 & \cdots & \cdots & \cdots & \frac{\sigma^2_{n_{pars}1}}{\sqrt{\sigma^2_{n_{pars}}\sigma^2_1}} \\ \vdots & \ddots & & & \vdots \\ \frac{\sigma^2_{i1}}{\sqrt{\sigma^2_i\sigma^2_1}} & & 1 & & \vdots \\ \vdots & & & \ddots & \vdots \\ \frac{\sigma^2_{n_{pars}1}}{\sqrt{\sigma^2_{n_{pars}}\sigma^2_1}} & \cdots & \frac{\sigma^2_{n_{pars}j}}{\sqrt{\sigma^2_{n_{pars}}\sigma^2_j}} & \cdots & 1 \end{bmatrix}\end{aligned} \tag{6.5}$$

where the matrix W is defined as:

$$\mathbf{W} = \begin{bmatrix} \frac{1}{\sqrt{\sigma^2_1}} & \cdots & \cdots & \cdots & 0 \\ \vdots & \ddots & & & \vdots \\ 0 & & \frac{1}{\sqrt{\sigma^2_i}} & & \vdots \\ \vdots & & & \ddots & \vdots \\ 0 & \cdots & 0 & \cdots & \frac{1}{\sqrt{\sigma^2_{n_{pars}}}} \end{bmatrix} \tag{6.6}$$

Interdependency between parameters makes it difficult to isolate the true value of each individual parameter. Stated differently, if parameters are highly correlated the relationship between the parameters is "fitted" rather than the parameters themselves. Such parameter values may thus be completely incorrect. This does not affect the validity of the model predictions, but indicates that the number of parameters (and possibly complexity) of the model may be reduced. It also has statistical implications if the regressed, possibly erroneous, values are used for further regression analyses (cf. Section 6.1.3).

The error associated with each parameter and with each experimental data point can be calculated as respectively shown in equations 6.7 and 6.8.

$$SE_i^{parameters} = \sqrt{cov_{i,i}} \tag{6.7}$$

$$SE_i^{predictions} = \left[\sqrt{s^2 V_0^T cov V_0}\right]_{i,i} \tag{6.8}$$

Standard errors as calculated above implicitly assume a normalized error distribution. This assumption can be tested by performing a non-parametric analysis such as the bootstrap analysis. Essentially, a bootstrap analysis randomly samples data points with replacement (i.e. each data point can be selected more than once) from the original data set to generate a new, equisized dataset for regression analyses. 200 iterations of the

aforementioned is generally considered as sufficient to yield a good approximation as to the actual parameter distribution and, hence, to the actual variance in each parameter [Sharrock & Coetzer, 2007]. Here, Fortran's implicit pseudo-random number generator function *random_number* was seeded via the implicit *random_seed* to generate a random selection of data points. A frequency histogram was then generated using the statistical programming language R[a].

6.1.2 Linear regression

Linear regression was also performed via least squares minimization (eq. 6.1). Due to the linear nature of the regression, R^2 could be used to quantify the accuracy of the fit with $R^2 = 1$ indicating a perfect fit of the model to the experimental data. The linear regression was performed in *Microsoft Office Excel 2003*.

6.1.3 Estimation of the Arrhenius constants

Arrhenius constants were fitted to the data from the semi-batch hydrogenation experiments (Section 4.2) via the semi-batch theoretical model (Section 5.3). As the Arrhenius equations are functions of temperature (eq. 6.9), the model should preferably be fitted to all of the available isothermal experiments simultaneously. However, referring to the reaction mechanism in Section 5.2, this would require a suitable initial guess for each Arrhenius constant (A) and activation energy (E_a) for 10 *reversible* reactions, i.e. 40 parameters in total if 2 alkene isomers are involved. To directly find suitable initial guesses for each of these parameters to apply non-linear regression is not trivial.

However, given sufficient experimental data points, it is possible to estimate Arrhenuis constants indirectly *if* each of the forward and backward reaction rate constants are known at at least 2 temperatures. Here, the Arrhenius equation is linearized as shown in eq. 6.10. A plot of $\ln k^{rxn}$ *vs.* $\frac{-1}{R_0 T}$ then yields E_a as the gradient and $\ln A_{rh}$ as the intercept of the resulting straight line [Fogler, 1999].

$$k^{rxn} = A_{rh} e^{\frac{-E_a}{R_0 T}} \tag{6.9}$$

$$\ln k^{rxn} = E_a \frac{-1}{R_0 T} + \ln A_{rh} \tag{6.10}$$

The reaction rate constants k were thus fitted to the semi-batch 1-hexene hydrogenation data as described in Section 6.1.1 to generate reaction rate constants at different temperatures. The experimental data points used for model fitting were the recorded transient hydrogen consumption rate (F_{H2}) and the final liquid molar compositions. Fitting of the rate constants implies that the number of required initial parameter guesses

[a]Virtually all modelling and statistical analyses were programmed in Fortran, but R was used on several occasions for quick calculations.

are halved and that the computational time required is drastically reduced. It is thus faster and easier to arrive at good initial guesses via trial and error running of the model. The fitted parameters were then evaluated based on the tools described in Section 6.1.1.

An initial guess of the Arrhenius constants was then made by using eq. 6.10. If the variance of and the cross-correlation between the regressed reaction rate constants were small, the linearly regressed values for the Arrhenius constants should be close to that of the optimum values.

The initial guess was then used as described before fitting the Arrhenius constants and activiation energies simultaneously to all the isothermal runs, again using the statistical tools described in Section 6.1.1.

6.1.4 Sensitivity analysis

As defined in eq. 6.11 sensitivity analysis is used to indicate the significance of an independent variable on a key/investigated model output (dependent variable) by comparing the relative changes in their values from a base case when perturbing the independent variable by a known factor, say, δ. A respectively small, equivalent or large change in a key output parameter relative to the change in the independent variable indicates its insensitivity, linear dependence or sensitivity to the independent variable.

$$Sensitivity = \frac{dy^{model}}{dx^{model}} \tag{6.11}$$

As in Dennis & Schnabel [1996] and Heath [2002], the x^{model} will be perturbed by a constant factor to calculate the gradient differentially, i.e. a constant relative perturbation rather than a constant absolute perturbation will be made to x^{model}, which circumvents that issue that the parameters may not have the same units or order of magnitudes. Here, the size of the perturbation factor δ will always (arbitrarily) be $\pm 1\%$, and dx^{model} is thus calcualted numerically as shown in eq. 6.12.

$$\begin{aligned} dx^{model} &= \frac{\delta}{100} x_{base}^{model} \\ &= \left(\%\text{ change in } \mathrm{x}_{base}^{model}\right) x_{base}^{model} \end{aligned} \tag{6.12}$$

The change in the dependent value or (in this case) dy^{model} is then calculated based on the difference between the solutions for x_{base}^{model} and $x_{base}^{model} + \frac{\delta}{100} x_{base}^{model}$ at the time of interest. Via manipulation, dy^{model} can then be expressed as a percentage change from

its value at x_{base}^{model} as shown in eq. 6.13.

$$\begin{aligned} dy^{model} &= y\left(t, x_{base}^{model} + \frac{\delta}{100} x_{base}^{model}\right) - y\left(t, x_{base}^{model}\right) \\ &= \frac{y\left(t, x_{base}^{model} + \frac{\delta}{100} x_{base}^{model}\right) - y\left(t, x_{base}^{model}\right)}{y\left(t, x_{base}^{model}\right)} y\left(t, x_{base}^{model}\right) \\ &= \left(\%\text{ change in y}^{model}\right) y\left(t, x_{base}^{model}\right) \end{aligned} \tag{6.13}$$

Eq. 6.11 can thus be expressed as in eq. 6.14

$$\begin{aligned} Sensitivity &= \frac{dy^{model}}{dx^{model}} \\ &= \frac{\left(\%\text{ change in y}^{model}\right)}{\left(\%\text{ change in x}_{base}^{model}\right)} \cdot \frac{y\left(t, x_{base}^{model}\right)}{x_{base}^{model}} \end{aligned} \tag{6.14}$$

Since the reaction rate constants have varying units it is convenient to express sensitivity via the dimensionless first factor of eq. 6.14 for comparison purposes since the value of $\frac{y\left(t, x_{base}^{model}\right)}{x_{base}^{model}}$ is constant for a set of x^{model} values if applied to the same model.

For the semi-batch system, to simplify the sensitivity analyses on the dependent hydrogen consumption rate to a single value, the integral of the absolute difference between the base hydrogen consumption and investigated case will be used as expressed in eq. 6.15.

$$\%\text{ change in F}_{H2} = \left[1 - \frac{\int_0^{t_f} \left|F_{H2}\left(t, x_{base}^{model} + \frac{\delta}{100} x_{base}^{model}\right) - F_{H2}\left(t, x_{base}^{model}\right)\right| dt}{\int_0^{t_f} F_{H2}\left(t, x_{base}^{model}\right) dt}\right] \tag{6.15}$$

where t_f is the end time of interest. An absolute value is used to prevent positive and negative errors cancelling out and eq. 6.15 thus indicates the total deviation of the hydrogen flow rate from the base.

6.2 Parameter estimation: CD experiments

6.2.1 Non-linear least squares optimization

To perform least squares optimization on the 1-hexene hydrogenation CD experimental data the bounded, double precision version of NL2SOL, namely *DN2FB.f*, was used. A bounded non-linear least squares parameter estimator was required as attempts to prevent *lmdif.f90* from straying outside of the feasible region of parameter values failed, causing the program to crash. The least squares approach as detailed in Section 6.1

Table 6.1: Parameters investigated and their initial values. Once optimized, these parameters will indicate the deviation of the actual mass transfer and reaction coefficients from that predicted.

Parameter	Initial value	Equations
k_L^{random}	$sns_1 = 0.0051$	$sns_1 \left(\text{Re}_L^I\right)^{0.667} Sc_L^{-0.5} \left(a_p d_p\right)^{0.4} \left(\frac{\rho_L^{mix}}{\eta_L^{mix} g}\right)^{-0.33}$
k_V^{random}	$sns_2 = 1.0$	$sns_2 A \text{Re}_V^{0.7} Sc_V^{0.333} \left(a_p d_p\right)^{-2} \left(a_p D_V^{ave}\right)$
k^{des}	$sns_3 = 1.0$	$sns_3 k^{des}$
k^{iso1}	$sns_4 = 1.0$	$sns_4 k^{iso1}$
K^{iso1}, K^{iso2}	$sns_5 = 1.0$	$sns_5 K^{iso1}, sns_5 K^{iso2}$
K^{des}	$sns_6 = 1.0$	$sns_6 K^{des}$
k^{H2}	$sns_7 = 1.0$	$sns_7 k^{H2}$
K^{H2}	$sns_8 = 1.0$	$sns_8 K^{H2}$
k^{ads}	$sns_9 = 1.0$	$sns_9 k^{ads}$
K^{ads}	$sns_{10} = 1.0$	$sns_{10} K^{ads}$

was followed. Given the extensive computational times (see Section 8.2) involved, a bootstrap analysis was not performed on the data.

Section 6.1 specifically focused on the reaction kinetics and it was thus clear that the parameters to be fitted were the reaction rate and equilibrium constants as defined in Section 5.2. Here it is less clear as a combination of mass transfer and reaction kinetic effects in the reactive zone could be involved. Table 6.1 lists the parameters that were considered along with the initial values for each. A sensitivity analysis was performed on each parameter to see whether it effected the model outputs (see below). An iterative approach was then followed by hand until a suitable initial guess was found for *DN2FB.f*. The sensitivity of the model outputs to each parameter was checked on a regular basis during this process. Once a suitable initial guess was found, it could be supplied to *DN2FB.f* to regress for the parameters.

The following model outputs were chosen for the sum of squares calculations:

- Distillate and bottoms molar compositions of 1-hexene, 2-hexene and n-hexane. The liquid hydrogen concentrations could not be measured experimentally.
- Complete off-gas compositional analysis.
- Distillate, bottoms and off-gas molar flow rates.

The column temperature profile was not considered as it is essentially dependent on the column pressure, especially for such a close-boiling system, rather than the dynamics in the reactive zone. Furthermore, due to concerns regarding the accuracy of the measured condenser heat duty, its calculated error was also not included in the sum of squares.

After completion of the regression analysis a sensitivity analysis was then again performed on the final solution set. This solution set essentially indicates the deviation of the predicted mass transfer coefficients and reaction rate constants from reality if the proposed CD model is used to predict reality at the different conditions of the different runs. These deviations were then fitted as functions of the process variables.

For the liquid and vapour phase mass transfer coefficient, it was assumed that the deviation would be directly proportional to $\frac{T^{1.75}}{P}$. This was based on the fact that, for the vapour phase coefficient, vapour diffusivity includes this factor (see Table B.2). For the constants describing deviation from the predicted reaction rate constants, it is possible to show that an Arrhenius type equation can be used:

$$\begin{aligned} k^{CD}_{regressed} &= sns_i k_{predicted} \\ A^{CD}_{rh,regressed} exp\left(\frac{-E^{CD}_{a,regressed}}{R_0 T^L}\right) &= sns_i A^{semi-batch}_{rh,regressed} exp\left(\frac{-E^{semi-batch}_{a,regressed}}{R_0 T^L}\right) \\ sns_i &= A'_{regressed} exp\left(\frac{-E'_a}{R_0 T^L}\right) \end{aligned} \tag{6.16}$$

6.2.2 Effect of process variables

To evaluate the system, the following key performance indicators (KPI's) were considered and compared at different process conditions:

- hydrogen conversion (X_{H2}).
- 1-hexene conversion (X_{1Hx}).
- n-hexane selectivity based on the 1-hexene fed to the column (S_{nHx1Hx}).
- n-hexane yield based on the 1-hexene fed to the column (Y_{nHx1Hx}).
- n-hexane recovery to the bottoms product based on the 1-hexene fed to the column (R_{nHx1Hx}).

For a CD column with no sidedraws other than the distillate, it is possible to define the total molar flow rate of an arbitrary component into and out of the column as follows:

$$F^{in}_i = \sum_{j=1}^{Nstages} \left(x^F_{i,j} F^L_j + y^F_{i,j} F^V_j\right) \tag{6.17}$$

$$F^{out}_i = x_{i,1} r^L_1 L_1 + y_{i,1} V_1 + x_{i,Nstages} L_{NStages} \tag{6.18}$$

Using equations 6.18 and 6.17 it is thus possible to calculate the key performance indicators as follows:

$$S_{n-hexane,1-hexene} = \frac{F^{out}_{n-hexane} - F^{in}_{n-hexane}}{F^{in}_{1-hexene} - F^{out}_{1-hexene}} \cdot 100 \quad (6.19)$$

$$X_{1-hexene} = \frac{F^{in}_{1-hexene} - F^{out}_{1-hexene}}{F^{in}_{1-hexene}} \cdot 100 \quad (6.20)$$

$$X_{H2} = \frac{F^{in}_{H2} - F^{out}_{H2}}{F^{in}_{H2}} \cdot 100 \quad (6.21)$$

Since the reaction kinetic model developed in Section 5.2 considers only isomerization and hydrogenation, for every mole of n-hexane formed an equal amount of hydrogen must be consumed:

$$F^{out}_{n-hexane} - F^{in}_{n-hexane} = F^{in}_{H2} - F^{out}_{H2} \quad (6.22)$$

Thus, by combining equations 6.20, 6.21 and 6.22 and substituting it into equation 6.19, it is easy to show that:

$$S^{theoretical}_{n-hexane} = \frac{X_{H2}}{X_{1-hexene}} \cdot \frac{F^{in}_{H2}}{F^{in}_{1-hexene}} \quad (6.23)$$

which supplies an additional sanity check to identify errors. In the case of the model $S^{theoretical}_{n-hexane}$ should equal $S_{n-hexane,1-hexene}$ virtually exactly. For the experimental data this check can be combined with the mass balance error to give an indication as to the quality of the data. The mass balance error will be reported as a relative percentage and will be defined as follows:

$$MB_{error} = \frac{\dot{m}_{out} - \dot{m}_{in}}{\dot{m}_{in}} \cdot 100 \quad (6.24)$$

Table 6.2 lists the variables who's effects on the KPI's will be considered as well as the range over which each will be varied.

Table 6.2: Data space considered.

Parameter	Minimum	Maximum	Units
Condenser pressure	170000	600000	Pa(a)
Condenser temperature	270	290	K
1-Hexene feed flow rate	4.77E-7	1.09E-6	kmol/s
1-Hexene feed composition	0.5	1.0	kmol/kmol
1-Hexene feed location	0.0	1.3	m from top
Hydrogen feed flow rate	9.00E-8	1.30E-7	kmol/s
Hydrogen feed location	0.6	1.4	m from top
Recycle ratio	10	500	-

Part III

RESULTS AND DISCUSSION

The methodologies developed in Part II will now be applied. Firstly, the reaction kinetics will be determined in Section 7 and its accuracy quantified as described. Using this basis, the reacion kinetics will be incorporated into the CD 1-hexene hydrogenation model and the mass transfer and reacion kinetics adapted to fit the experimentally generated data in Section 8. The degree by which the parameters are modified will yield valuable insight into the working of the system. The model will then be used to study the effect of various control parameters on the KPI's.

Chapter 7

1-Hexene hydrogenation kinetics

The generated semi-batch 1-hexene hydrogenation results will first be considered based on qualitative observations. Having ascertained whether the data is qualitatively consistent, the reaction kinetic constants of each elementary Langmuir-Hinshelwood reaction will then be fitted via the semi-batch model (see Section 5.3) to the data of each individual experimental run. The following statistical techniques described in Part II will then be applied to the fitted values:

- Coefficient of variation.
- Standard error of parameters and prediction.
- Error of parameters calculated via the bootstrap method.
- Sensitivity of the model output (hydrogen consumption rate) to each kinetic constant.

Finally, these kinetic constants will by used as a first estimate to fit the Arrhenius and activation energies of each reaction simultaneously across all the experimental runs to determine the temperature dependence of the kinetic constants.

7.1 Catalyst characterization

Most of the catalyst characteristics were available from the supplier, Kata-Leuna and are supplied in Section 4.1. The catalyst reduction procedure in Table A.7 was determined via TPR measurements as described in Appendix A.3 and was also confirmed by the supplier. From the TPR measurements (not shown) it was found that 623.15 K (350°C) is necessary for complete reduction of the catalyst.

Using hydrogen chemisorption the average nickel metal crystallite size was determined to be 4.4 nm. This average crystallite size was confirmed by TEM measurements of the reduced catalyst (see Figure 7.1). It was established that the reduced catalyst

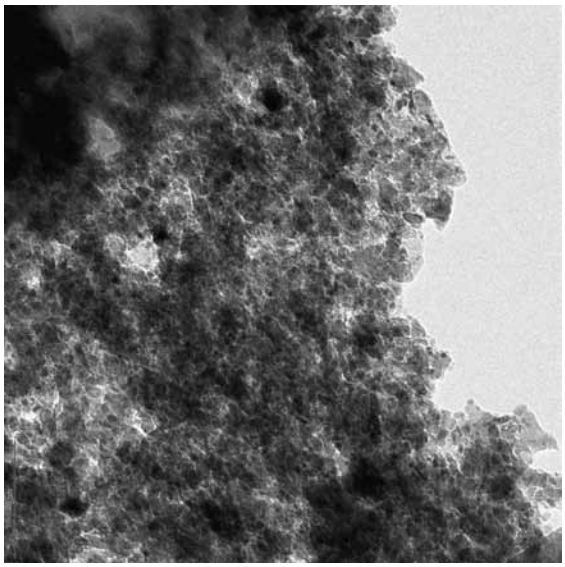

Figure 7.1: TEM image of the Ni/Al_2O_3 catalyst used in the experiments.

consists of a relatively narrow crystallite size distribution with spherical metallic nickel crystallites (the dark, small spots on the TEM image). Using the nickel metal dispersion of 25.2%, obtained from the hydrogen chemisorption, and the known nickel loading of 18wt%, the number of active metal surface sites was found to be 7.74E-04 mol/g_{cat}.

7.2 Qualitative observations

Table 7.1 summarizes the experiments of interest, namely runs 10-13. Experiments preceding run 10 were used to refine the experimental methodology and the data was not considered to be of a sufficiently high quality for regression purposes. The recorded hydrogen consumption as measured by the MFC are shown in Figures 7.2 and 7.3 for representative runs 10-13. In these graphs, hydrogen is introduced after 1800 s (30 min) as per the experimental methodology in Section 4.2.

As expected, Figures 7.2 and 7.3 show an increase in the hydrogen consumption rate with an increase in temperature. This is best shown for runs 10, 12 and 13, which were performed at the same pressure but at increasing temperatures of 60, 70 and 80° respectively.

At 323.15 K (50°C - not shown as the hydrogen consumption was very low) the low hydrogen consumption rate observed initially quickly diminishes to zero or below the detectable limit, whereas a relatively rapid hydrogen consumption is observed at 353.15 K (80°C). For the conditions and time period considered, it thus appears that little/slow reaction occurs at 323.15 K (50°C). Each of the runs performed at or above 333.15 K (60°C) exhibits a characteristically high initial hydrogen consumption rate. This consumption rate passes through a minimum prior to a rapid increase followed by

a lower, effectively linear, increase. It should be noted that even at 323.15 K (50°C) this initially high hydrogen consumption rate is observed.

Given the methodology as described in Section 4.2, the initially high hydrogen consumption can be explained by two phenomena. Firstly, it is possible that initial pressurization of the reactor vessel to the pressure gauge setting was incomplete and that the high hydrogen consumption is due to residual pressure equalization. However, this effect should be small given the experimental methodology (see Section 4). Additionally, this does not account for the ensuing rapid increase in hydrogen consumption and subsequent leveling off.

However, the observed trend can be fully described by considering the reaction kinetics equations in Section 5.2. The qualitative approach here will be verified in later sections. Since the catalyst was submerged, stored and slowly heated to reaction temperature in a 1-hexene environment, it may safely be assumed that the surface sites are occupied by an equilibrium amount of 1-hexene at the point when hydrogen is introduced. When introduced, hydrogen dissolves into the liquid phase and adsorbs (as dictated by the equilibrium) onto the remaining vacant sites resulting in a high initial hydrogen consumption, which decreases as the adsorption reaction approaches equilibrium. Competitively, adsorbed hydrogen reacts faster with the adsorbed alkene as the surface concentration of adsorbed hydrogen increases. These two opposing, superimposed effects result in a minimum consumption rate followed by a regime in which hydrogen consumption via hydrogenation is dominant. As the initially high surface concentration of 1-hexene is reduced via hydrogenation towards its new equilibrium after the introduction of hydrogen, the rate of hydrogen consumption decreases until another effect becomes rate controlling. This latter effect may be the result of the transferral of the first hydrogen to the adsorbed 1-hexene (Section 7.4) becoming rate limiting as reported in literature (Section 2) or because an equilibrium is reached between the rate of hydrogen and alkene adsorption.

7.3 Fitting of the reaction rate constants

Data fitting was performed on the data using least squares optimization as described in Section 6.1. From Table 7.1, there were sufficient data points in each run to fit the 20 desired reaction rate constants at isothermal conditions. Attempts to make the model converge using the *pi*-adsorption mechanisms failed and the classic sp^3 hybridization route was thus followed (see Section 5.2). The statistical results are included in Table 7.1. The coefficients of variation for runs 10 to 12 are within the acceptable range of 0.15 - 0.40. The lower this value, the more variance is accounted for by the model. The coefficient of variation for run 13 (0.422) is just outside this range and should thus be used cautiously.

Table 7.1: Summary of semi-batch 1-hexene experiments runs 10-13 with the associated statistical results.

Parameter	Units	10	11	12	13
Temperature	K	333.15	343.15	343.15	353.15
	(°C)	(60)	(70)	(70)	(80)
Pressure	$\cdot 10^5$ Pa(a)	6.1	11.1	6.1	6.1
Catalyst mass	g_{cat}	0.48	0.49	0.47	0.45
Sample					
Time taken into run	s	27000	13080	16800	6000
n-hexane	mol/mol	0.39	0.47	0.32	0.23
1-hexene	mol/mol	0.55	0.47	0.62	0.74
2-hexene	mol/mol	0.06	0.06	0.05	0.04
Summation test	mol/mol	1.00	1.00	1.00	1.00
Model Statistics					
Number of data points	-	40	30	37	25
s^2	-	0.082	0.076	0.078	0.178
Coefficient of Variance	-	0.286	0.275	0.279	0.422
Standard error of prediction					
H_2 consumption	%	9-26	15-27	12-27	26-42
n-hexane	%	13	15	22	36
1-hexene	%	19	15	15	40
2-hexene	%	11	17	22	41

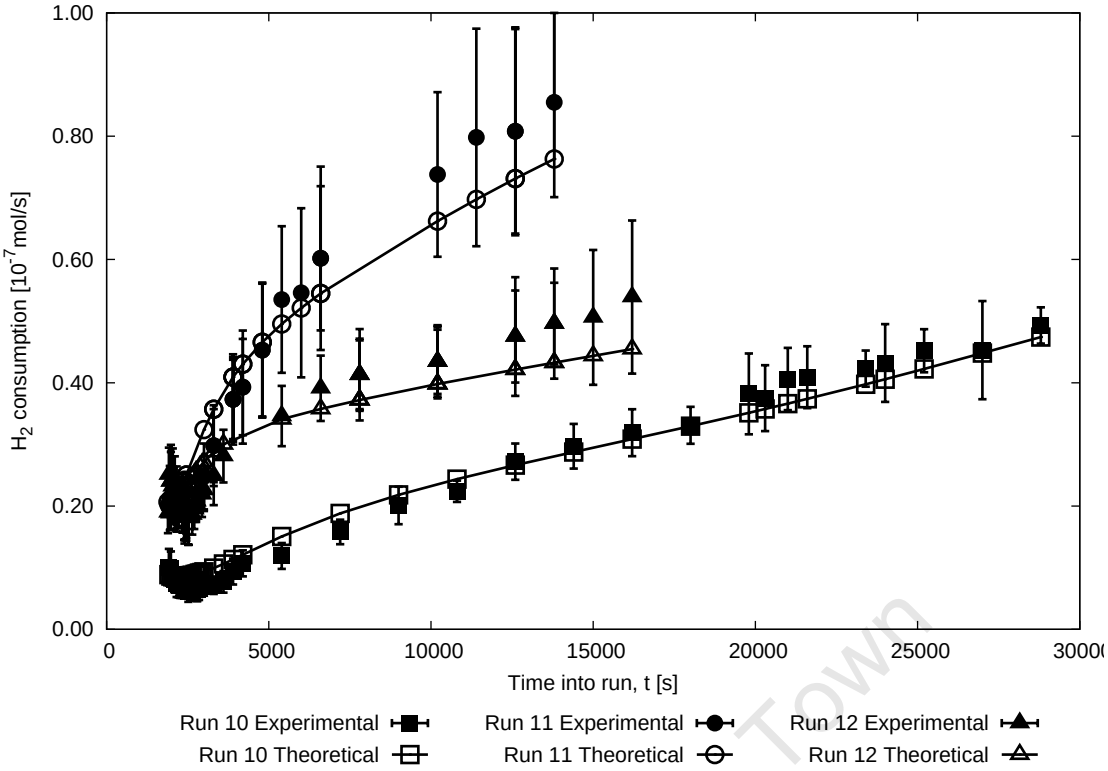

Figure 7.2: Model predictions and experimental data with errors of prediction for runs 10 to 12.

Figures 7.2 and 7.3 show the experimentally and calculated datapoints with errors of prediction and the corresponding model predictions. In general, for runs 10-12 there is ± 9-27% uncertainty when predicting the hydrogen consumption and ± 11-22% when predicting the n-hexane, 1-hexene and 2-hexene compositions. As expected from its unfavourable coefficient of variance, this is higher for run 13: respectively ± 26-42% and ± 36-41%. This is high, but the data is still useful. More measuring errors were expected at higher temperatures and pressures as this sped up the hydrogen consumption rate and thus made it more difficult to accurately determine the measured variables manually. This is indeed observed in Figures 7.2 and 7.3. The errors or prediction increase with increasing temperature (run 10 < 11 < 13) and increasing pressure (run 11 < 12). A recommendation may be to install an automated data capturing system, as built into the CD column, in order to supply high frequency, accurate measurements [Nieuwoudt, 2005].

From Table 7.2 the standard error in the parameters are large, but not unexpected given the experimental nature of the data. Again, for run 13 the standard errors of parameters are less favourable. As a check, the standard error of each parameter can be compared to the sensitivity of the model to that parameter. Generally, the model should be less sensitive to a parameter with a large variance (error) and *vice versa*. This will be discussed in the following section.

Table 7.2: Parameter values and standard error of parameters for the reaction rate constants in runs 10-13.

Parameter	Units	Run 10		Run 11		Run 12		Run 13	
		Value	Error %	Value	Error %	Value	Error %	Value	Error %
k^{H2}	$g_{cat}.m^3/kmol^2.s$	4.47E+05	10.7	7.58E+05	5.6	8.54E+05	4.8	2.30E+06	7.1
K^{H2}	$kmol/m^3$	8.54E+04	28.1	9.03E+04	20.0	9.56E+04	5.6	9.11E+04	6.3
k_1^{ads}	$m^3/kmol.s$	2.85E+03	19.3	9.77E+03	8.8	7.14E+03	15.5	9.27E+03	21.7
k_2^{ads}	$m^3/kmol.s$	2.87E+03	17.9	1.06E+04	21.5	1.16E+04	33.9	1.18E+04	25.7
K_1^{ads}	$kmol/m^3$	4.00E+04	13.4	6.96E+04	6.8	3.75E+04	15.3	3.88E+04	7.1
K_2^{ads}	$kmol/m^3$	3.44E+04	17.2	5.83E+04	25.1	4.39E+04	21.8	2.12E+04	39.3
k_1^{iso1}	$g_{cat}/kmol.s$	1.14E+04	30.9	9.84E+03	5.0	1.60E+04	17.1	4.45E+03	28.4
k_2^{iso1}	$g_{cat}/kmol.s$	1.09E+04	25.0	1.81E+04	15.0	1.27E+04	9.6	2.61E+03	19.3
K_1^{iso1}	$kmol/g_{cat}$	1.55E-06	6.3	2.33E-06	16.0	1.55E-06	71.0	1.29E-05	20.2
K_2^{iso1}	$kmol/g_{cat}$	1.36E-06	29.9	2.00E-06	39.6	8.48E-06	16.3	5.34E-06	25.9
k_1^{iso2}	$g_{cat}/kmol.s$	1.19E+04	23.5	3.12E+04	7.5	3.39E+04	15.5	4.54E+03	51.7
k_2^{iso2}	$g_{cat}/kmol.s$	1.05E+04	37.6	1.39E+04	21.3	9.28E+03	5.3	1.87E+03	18.0
K_1^{iso2}	$kmol/g_{cat}$	1.46E-06	38.3	1.57E-06	14.3	7.15E-06	25.0	1.04E-05	20.6
K_2^{iso2}	$kmol/g_{cat}$	1.47E-06	12.3	2.13E-06	3.0	1.26E-06	19.0	1.26E-05	15.8
k_1^{des}	$g_{cat}/kmol.s$	1.21E+05	25.6	2.84E+05	37.5	2.63E+05	29.6	3.00E+03	33.1
k_2^{des}	$g_{cat}/kmol.s$	1.22E+05	25.8	2.16E+05	19.3	2.99E+05	11.8	3.38E+03	26.6
k_3^{des}	$g_{cat}/kmol.s$	1.17E+05	19.5	3.07E+05	33.3	2.45E+05	17.6	2.60E+03	14.6
K_1^{des}	$kmol/m^3$	1.52E+01	22.4	1.73E+00	18.7	3.10E+00	27.3	1.13E+00	26.7
K_2^{des}	$kmol/m^3$	1.70E+01	15.7	1.54E+00	15.1	2.22E+00	23.3	1.81E+00	18.7
K_3^{des}	$kmol/m^3$	1.70E+01	26.1	1.70E+00	16.7	2.33E+00	16.5	1.82E+00	2.6

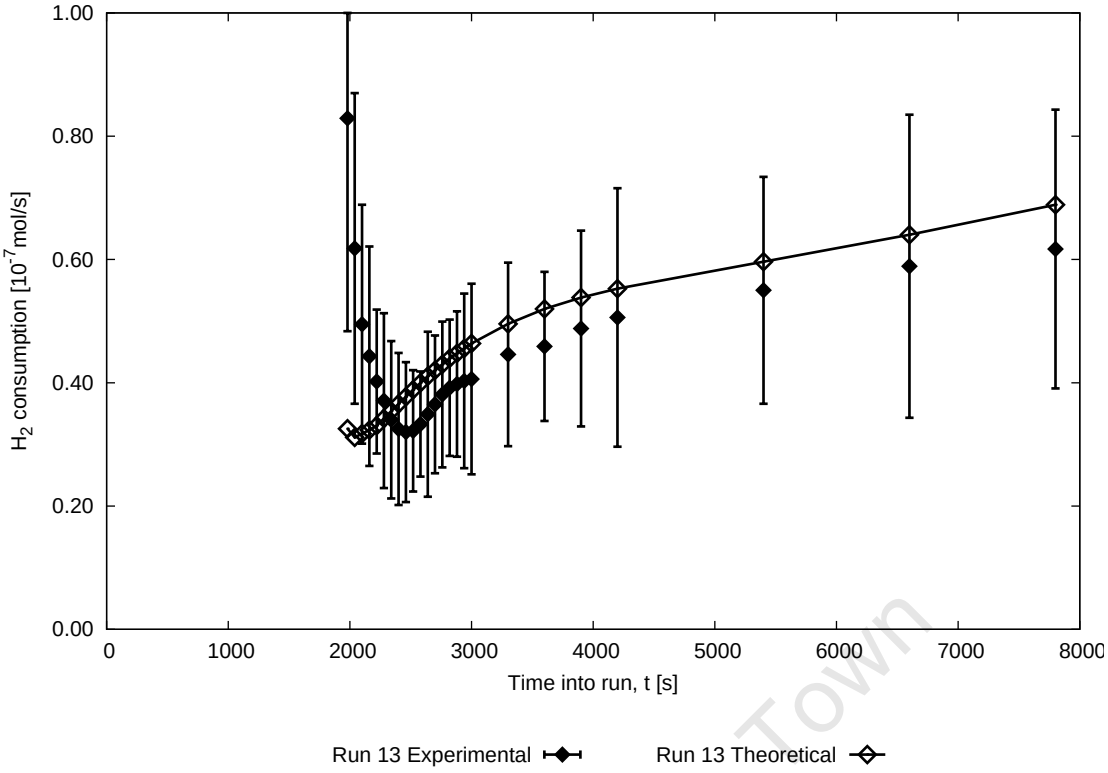

Figure 7.3: Model prediction and experimental data with errors of prediction for run 13.

7.4 Sensitivity analysis

7.4.1 Sensitivity of the hydrogen consumption rate to the model inputs

As example, the sensitivity of the hydrogen consumption in run 10 to a change in each parameter is graphed in Figure 7.4. Accurate prediction of a parameter value requires some sensitivity of the model to that parameter as the effect of the parameter on the model is used to determine its value. If the parameter has no effect on the model (i.e. has a large variance), the model is insensitive to that parameter and the variance in the parameter will be large.

From Figure 7.4 and also from the integrated summary value in Figure 7.5, it is clear that the model is more sensitive to the first reaction steps in the sequence - i.e. the adsorption steps. The implication of this will be discussed shortly.

However, what is of concern is that the sensitivity profile does not correspond to the variances calculated in Table 7.2. For example, the model appears to be very sensitive to the hydrogen adsorption rate (k^{H2}), yet this parameter also has a relatively high variance when compared to, e.g., K_1^{iso1} which has a very low sensitivity. This effect can be explained when considering the bootstrap analysis (see Section 6.1) of the parameters

in Table 7.3.

From Table 7.3 it is clear that some variances are highly non-normally distributed (skew) and that the use of normalized variances in fact gives an inaccurate indication of the true parameter variances. For example, although k^{H2} in Run 11 has a relatively large error of parameter of 35%, the bootstrap analysis indicates that the true error is only 9-13%. It is thus possible to match the variance and sensitivity, resulting in the statistical analysis thus far being consistent.

It is important to note that the insensitivity of the model in the region of certain of the reaction rate coefficients reduces their significance and limits the regression accuracy of these constants. The reaction steps associated with these constants can thus be removed without a significant loss in model accuracy. However, to keep the model robust for later analyses, this will not be done here.

The model is exceptionally sensitive to pressure (see Table F.1), but its sensitivity to this variable decreases as the reaction temperature is increased, which could indicate vapour-liquid mass transfer limitations. The sensitivity of the model to pressure suggests that finer pressure measurements and feed lines with minimized resistance could add to minimizing the observed variance. The model appears to be very insensitive to possible experimental errors in the initial 1-hexene liquid volume. This is encouraging as it reduces the effect of errors introduced by estimation of the amount of 1-hexene removed via vapourization during initial argon purging.

7.4.2 Rate limiting reaction step

The sensitivity analyses can also be used to determine the rate limiting reaction step(s) by using the reaction rate constants as independent variables. The effect was quantified by integrating the *absolute* difference in hydrogen consumption for the -1% and +1% case over the run time and expressing the difference as a percentage relative to the base case (see Section 6.1.4). The base case conditions for each run is defined by Table 7.1 and the regressed reaction rate constants to perturb is that shown in Table 7.2.

It is interesting to note that, contrary to what is observed in literature, Figure 7.5 indicates that the dissociative hydrogen adsorption and 1-hexene adsorption onto the catalyst surface are the rate determining steps. However, from Figure 7.6 it is clear that an increase in temperature shifts the rate limiting step in the direction of the first hydrogen transferal as expected from literature (Section 2). Note that the high changes in the case of $\mathbf{K^{des}}$ is negligible as, despite the increase in sensitivity of the model to these parameters, the model is still relatively insensitive to it.

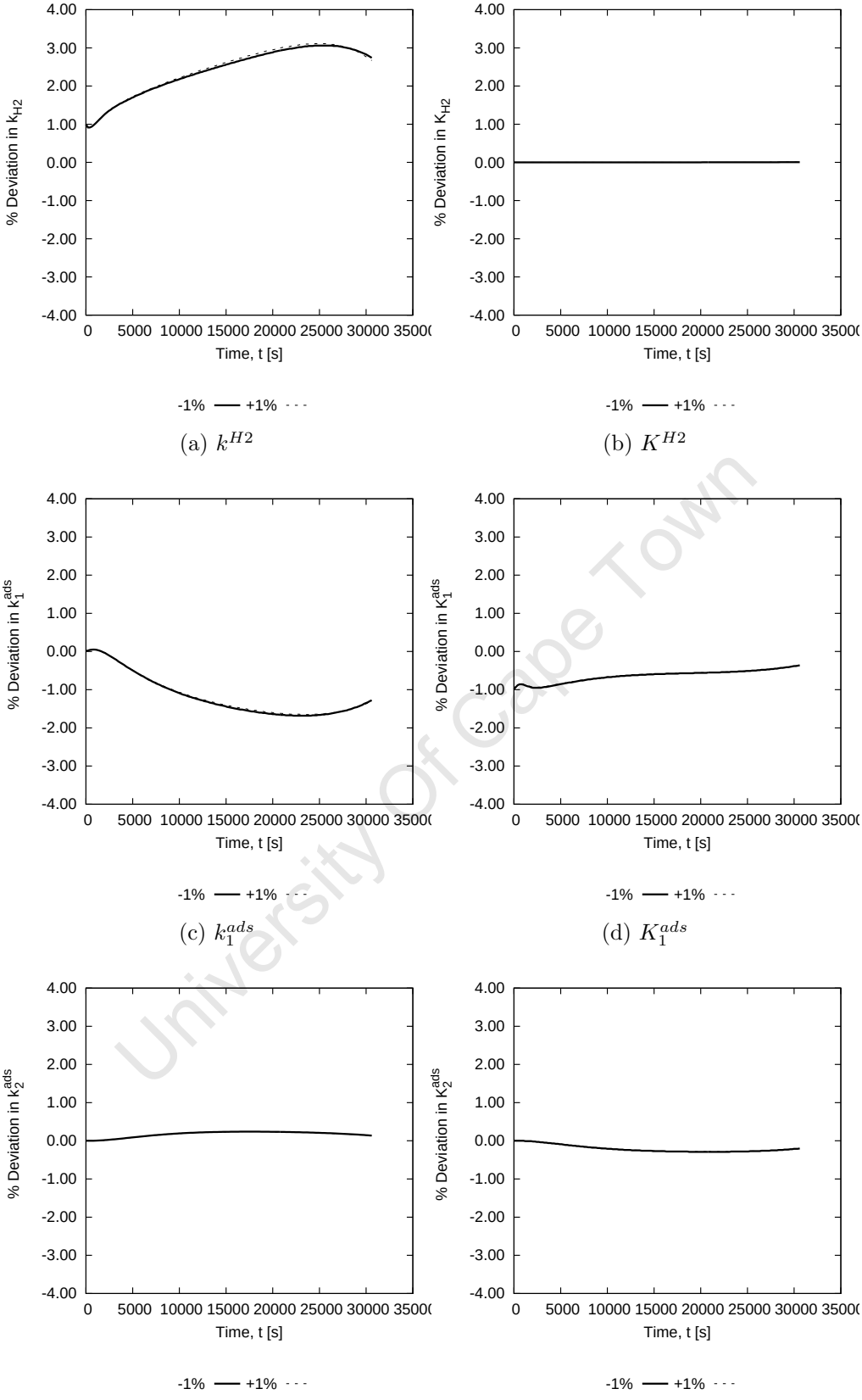

(a) k^{H2} (b) K^{H2}

(c) k_1^{ads} (d) K_1^{ads}

(e) k_2^{ads} (f) K_2^{ads}

Figure 7.4: Selected sensitivity analyses of the reaction rate constants for Run 10.

Table 7.3: Bootstrap parameter values and error of parameters with errors indicated as lower/upper percentage errors relative to the predicted parameter value.

Parameter	Units	Run 10		Run 11		Run 12		Run 13	
		Value	Error %	Value	Error %	Value	Error %	Value	Error %
k^{H2}	$g_{cat}.m^3/kmol^2.s$	4.55E+05	13/9	7.50E+05	8 /13	8.50E+05	8 /11	2.29E+06	15/3
K^{H2}	$kmol/m^3$	8.25E+04	17/17	9.25E+04	14/26	9.30E+04	4 /14	9.12E+04	5/19
k_1^{ads}	$m^3/kmol.s$	2.85E+03	16/18	9.75E+03	22/9	7.30E+03	22/8	9.13E+03	2/26
k_2^{ads}	$m^3/kmol.s$	2.70E+03	11/38	1.03E+04	22/27	1.18E+04	22/7	1.18E+04	4/8
K_1^{ads}	$kmol/m^3$	4.15E+04	11/19	6.75E+04	8 /29	3.73E+04	6 /7	3.87E+04	4/6
K_2^{ads}	$kmol/m^3$	3.50E+04	29/14	5.75E+04	34/35	4.45E+04	2 /23	2.14E+04	27/2
k_1^{iso1}	$g_{cat}/kmol.s$	1.18E+04	23/23	1.05E+04	47/35	1.58E+04	13/16	4.44E+03	12/8
k_2^{iso1}	$g_{cat}/kmol.s$	1.08E+04	11/25	1.85E+04	26/25	1.23E+04	7 /10	2.55E+03	1/14
K_1^{iso1}	$kmol/g_{cat}$	1.53E-06	19/19	2.25E-06	15/24	1.53E-06	5 /16	1.27E-05	1/14
K_2^{iso1}	$kmol/g_{cat}$	1.35E-06	28/25	1.75E-06	68/83	8.50E-06	15/8	5.41E-06	13/9
k_1^{iso2}	$g_{cat}/kmol.s$	1.18E+04	13/13	2.90E+04	31/17	3.38E+04	9 /7	4.50E+03	12/11
k_2^{iso2}	$g_{cat}/kmol.s$	1.03E+04	25/29	1.43E+04	12/13	9.25E+03	20/14	1.88E+03	6/19
K_1^{iso2}	$kmol/g_{cat}$	1.45E-06	29/18	1.55E-06	20/24	7.25E-06	24/16	1.04E-05	6/2
K_2^{iso2}	$kmol/g_{cat}$	1.45E-06	22/41	2.25E-06	31/23	1.26E-06	5 /3	1.26E-05	7/4
k_1^{des}	$g_{cat}/kmol.s$	1.18E+05	23/10	2.95E+05	23/13	2.65E+05	18/25	3.02E+03	2/19
k_2^{des}	$g_{cat}/kmol.s$	1.25E+05	23/37	2.15E+05	24/32	2.95E+05	6 /16	3.38E+03	31/4
k_3^{des}	$g_{cat}/kmol.s$	1.18E+05	27/18	3.10E+05	55/21	2.48E+05	7 /12	2.62E+03	8/4
K_1^{des}	$kmol/m^3$	1.55E+01	30/28	1.68E+00	15/21	3.05E+00	5 /18	1.13E+00	18/6
K_2^{des}	$kmol/m^3$	1.65E+01	23/35	1.55E+00	36/41	2.23E+00	10/5	1.81E+00	7/4
K_3^{des}	$kmol/m^3$	1.75E+01	19/18	1.65E+00	32/10	2.33E+00	9 /18	1.85E+00	16/4

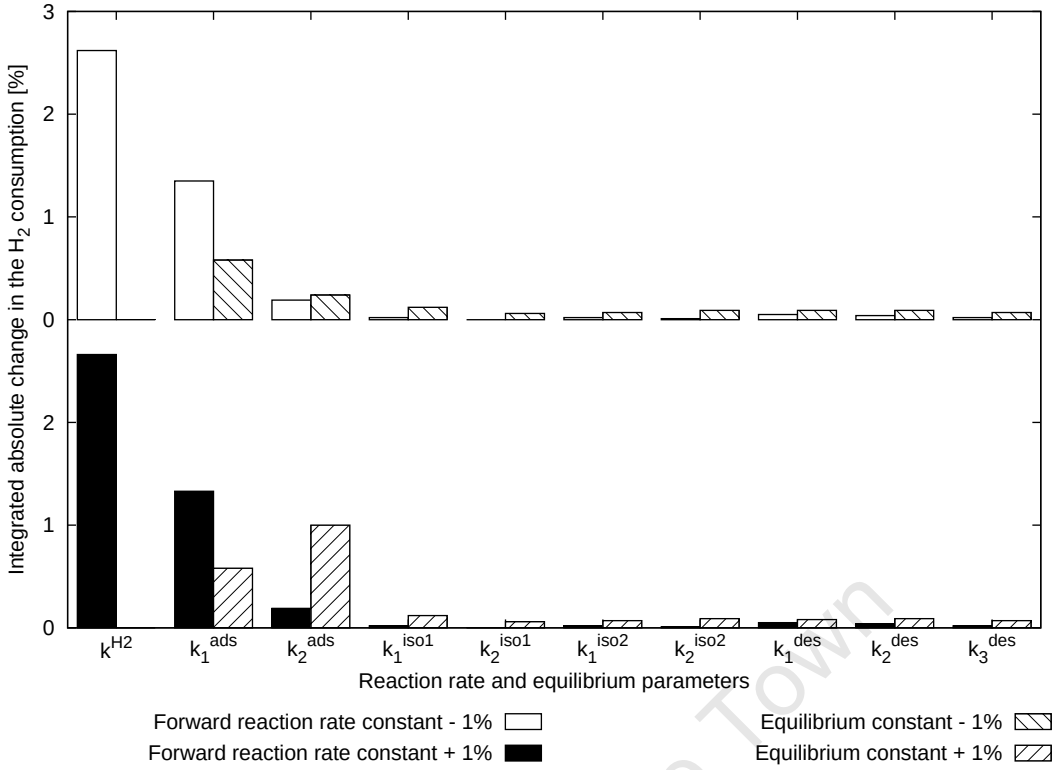

(a) Run 10

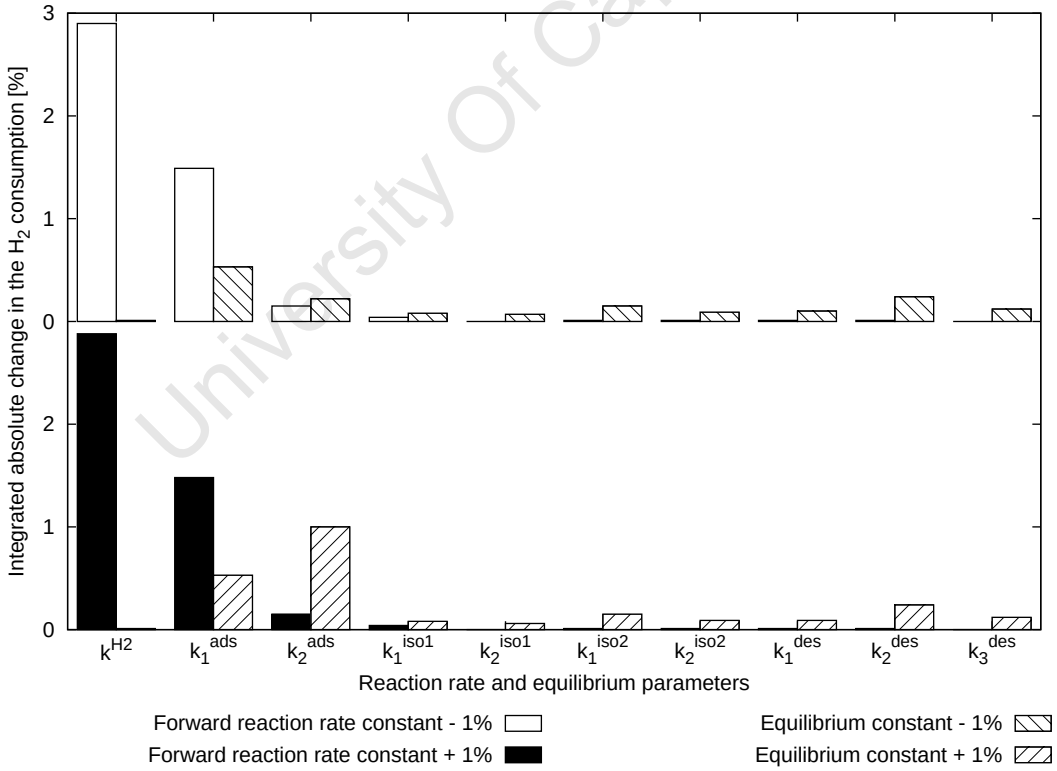

(b) Run 11

Figure 7.5: Integrated absolute percentage difference in the hydrogen flow rate between a base case and when either a reaction rate or equilibrium constants is perturbed by $\pm 1\%$ (cf. eq. (6.15)).

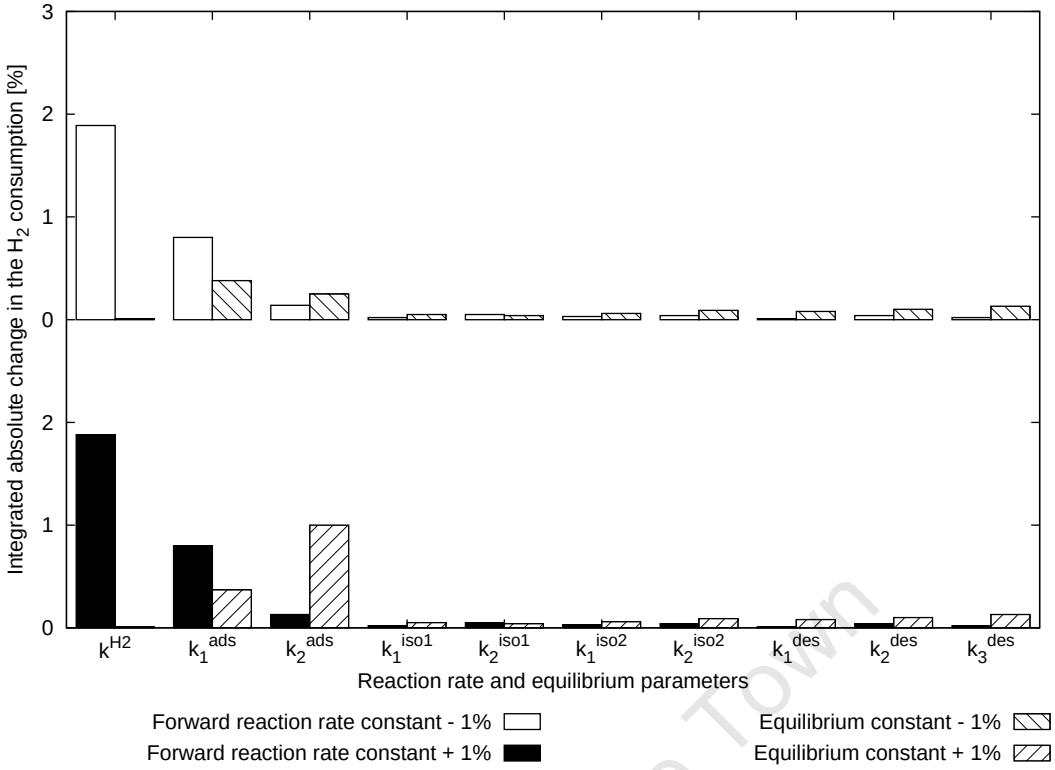

(c) Run 12

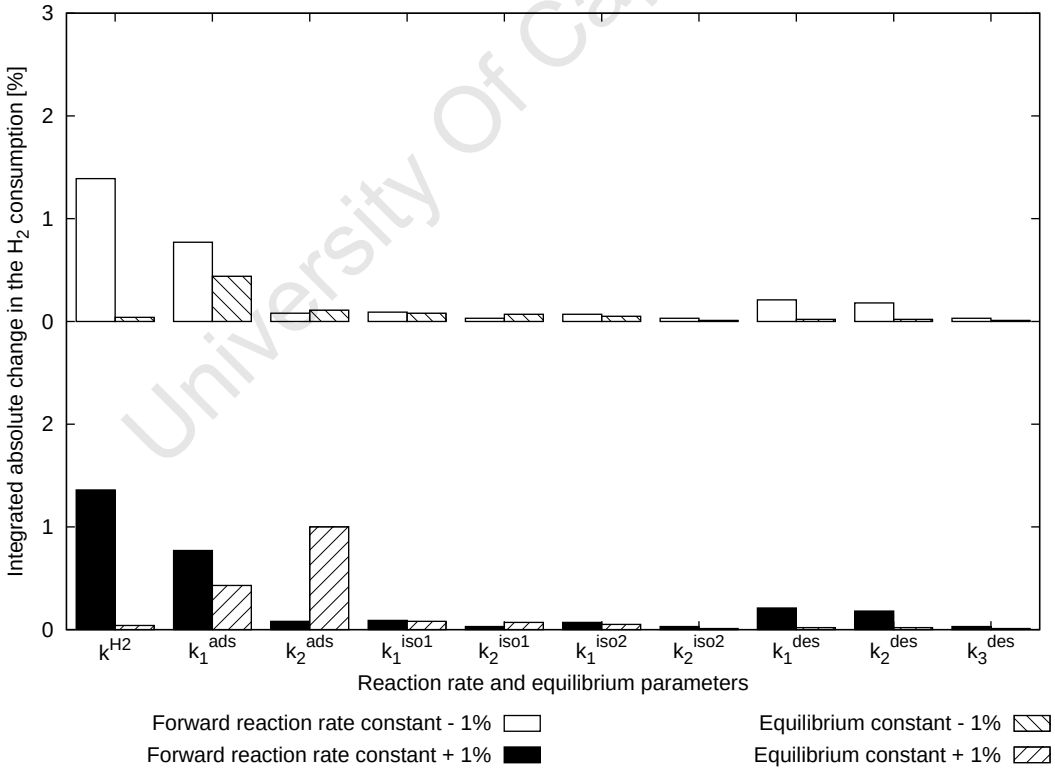

(d) Run 13

Figure 7.5: Integrated absolute percentage difference in the hydrogen flow rate between a base case and when either a reaction rate or equilibrium constants is perturbed by $\pm 1\%$ (cf. eq. (6.15)) - (cont'd).

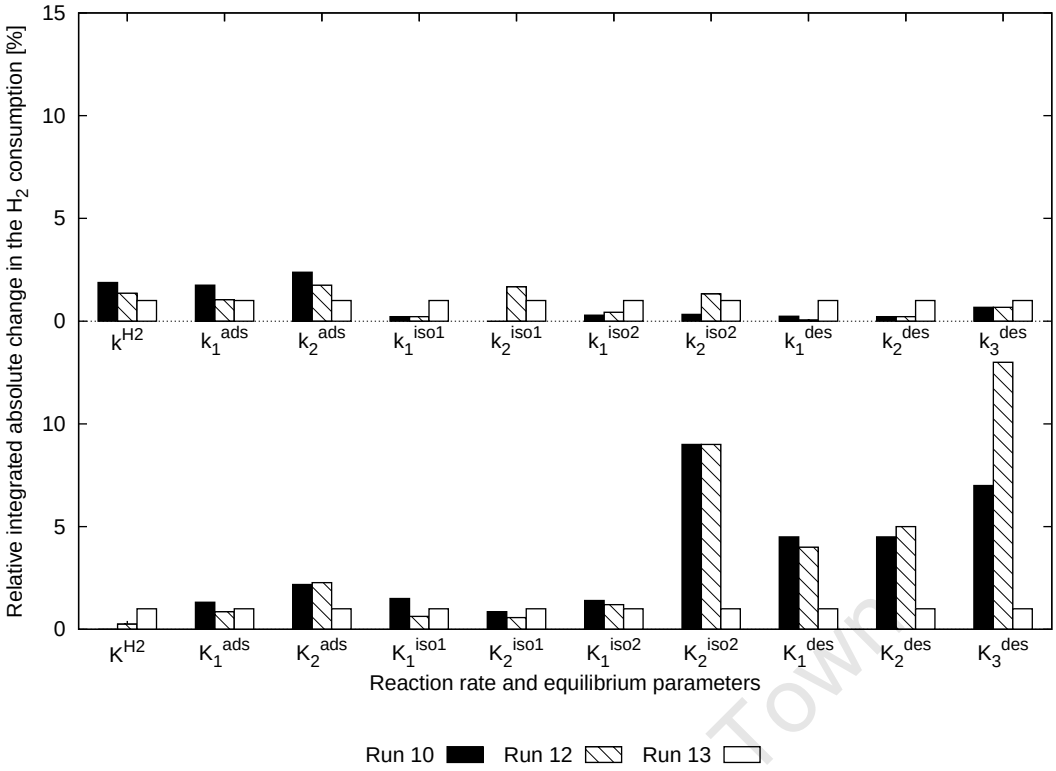

Figure 7.6: Integrated absolute percentage difference in the hydrogen flow rate between a base case and a ±1% perturbation in the reaction rate or equilibrium constant relative to that of run 13.

7.5 Correlation matrices

Tables 7.4 to 7.7 show simplified correlation matrices for runs 10 to 13. The complete matrices are available in Appendix F. There appears to be relatively strong correlations between several of the parameters, which indicates that several of the parameters are in fact interdependent. This, coupled with the large variances; low sensitivities of especially the reaction rate constants from the first hydrogen transferal onwards, suggest that linear fits to determine the Arrhenius constants by using eq. 6.10 will probably have low accuracies (i.e. low R^2 values).

The high degree of correlation in Runs 11 and 13 explains the relatively high variance and low CV values observed for these runs. Predictions from Run 11 and Run 13 parameter values must thus be used with care as the effect of all the parameters are properly separated.

Nonetheless, as this approach is simply used to arrive at an initial estimate for the Arrhenuis constants, these approximate reaction rate constants are sufficient for the current purposes.

Table 7.4: Simplified correlation matrix for run 10.

k^{H2}	#																			
K^{H2}	*	#																		
k_1^{ads}	o	*	#																	
k_2^{ads}	o	*	.	#																
K_1^{ads}		.		.	#															
K_2^{ads}	*	.	.	.	.	#														
k_1^{iso1}	o	.	*	o		*	#													
k_2^{iso1}	o	o	*	*			.	#												
K_1^{iso1}		o	.		*	.		.	#											
K_2^{iso1}		*	.	.		*	.	.	o	#										
k_1^{iso2}		o			*	*		o	.	*	#									
k_2^{iso2}	o	#	o	o			o	o	*	.	.	#								
K_1^{iso2}		o			*	.		o	*	*	#	.	#							
K_2^{iso2}	.	*	o				.	.	*	.		o		#						
k_1^{des}	*	*	*					o	*	*	*	*	*	.	#					
k_2^{des}		*		.	.	o		*	.	.	o	.	*		.	#				
k_3^{des}	.		.	.		.	.		.			.					#			
K_1^{des}	.	o	*				.	.	o	.		o	.	o	.		.	#		
K_2^{des}	.			.			.	.		.	.		*				*		#	
K_3^{des}	.	o	.		.	*		o	*	o	#	*	o	.	o	o		.	.	#

Key to degree of correlation: blank $\equiv <$ 0.2;. $\equiv 0.2 - 0.4$; $* \equiv 0.4 - 0.6$; $o \equiv 0.6 - 0.8$; $\# \equiv 0.8 - 1.0$.

Table 7.5: Simplified correlation matrix for run 11.

k^{H2}	#																		
K^{H2}	o	#																	
k_1^{ads}	.		#																
k_2^{ads}	.	.	*	#															
K_1^{ads}	o	*	.	o	#														
K_2^{ads}	.		*	*	*	#													
k_1^{iso1}	*	.	*	*	.	o	#												
k_2^{iso1}	#	o	*	*	o	.	*	#											
K_1^{iso1}	o	o	*	o	o	o	o	o	#										
K_2^{iso1}	o	o	*	o	o	o	o	o	#	#									
k_1^{iso2}		.		.		*	o		*	*	#								
k_2^{iso2}	.	.	o	o	o	o	*	*	o	o	*	#							
K_1^{iso2}	o	*	*	o	#	o	o	o	#	#	*	#	#						
K_2^{iso2}	*	.	o	o	o	o	#	*	#	o	*	#	#	#					
k_1^{des}	o	.		.		.	.	*			*	.		.	#				
k_2^{des}	#	*	*	*	o	*	.	o	o	o		o	#	*	.	#			
k_3^{des}	*	.	*	*	.	o	o	*	o	o	*	o	o	#		*	#		
K_1^{des}	o	*	*	o	o	o	o	o	#	#	*	#	#	#		o	o	#	
K_2^{des}			.	*	.	o	o		o	*	o	o	*	o	o		*	*	#	
K_3^{des}		.	#	o	*	*	.	.	*	.		o	o	o	.	*	*	*	*	#

Key to degree of correlation: blank $\equiv< 0.2$;. $\equiv 0.2 - 0.4$; $* \equiv 0.4 - 0.6$; $o \equiv 0.6 - 0.8$; $\# \equiv 0.8 - 1.0$.

Table 7.6: Simplified correlation matrix for run 12.

k^{H2}	#																			
K^{H2}	*	#																		
k_1^{ads}			#																	
k_2^{ads}	*	*		#																
K_1^{ads}	*	#		.	#															
K_2^{ads}	*	#	.	.	#	#														
k_1^{iso1}	.		.	o		.	#													
k_2^{iso1}			.	.			*	#												
K_1^{iso1}	o	*	.	o	*	.	*	*	#											
K_2^{iso1}			.	*			.			#										
k_1^{iso2}	.	.	.		.	*		o	.		#									
k_2^{iso2}	*	#	.	.	#	o			*			#								
K_1^{iso2}		.	o	.	.	*	.	*		*	o		#							
K_2^{iso2}	o	o		*	o	o	.	.	o			o		#						
k_1^{des}		*	*		.		.	.	.			o	*	.	#					
k_2^{des}	.	*	*		.	.	*	*	.	.	o	*	*	o	#					
k_3^{des}	*	*		*	*	.	.	.	.			.	.		.		#			
K_1^{des}	o	o		o	o	o	.	.	o	.	*	*	*	o				#		
K_2^{des}	.	o	.	*	o	o	.		.	.		o	.	*	.		*	*	#	
K_3^{des}	.	.	o	*	.	.	*	*		*	*		#		.	*		o	.	#

Key to degree of correlation: blank $\equiv <$ 0.2;. $\equiv 0.2 - 0.4$; $* \equiv 0.4 - 0.6$; $o \equiv 0.6 - 0.8$; $\# \equiv 0.8 - 1.0$.

Table 7.7: Simplified correlation matrix for run 13.

k^{H2}	#																		
K^{H2}	*	#																	
k_1^{ads}	#	.	#																
k_2^{ads}	*	*	.	#															
K_1^{ads}	#	*	#	*	#														
K_2^{ads}		*		*		#													
k_1^{iso1}	#	o	o	o	#		#												
k_2^{iso1}	#	.	o	o	#		#	#											
K_1^{iso1}	.	*	.	.	.	#		.	#										
K_2^{iso1}	#	*	o	o	#	.	#	#	.	#									
k_1^{iso2}		.	.	*		#	.		#	.	#								
k_2^{iso2}	.	.	.	.	.	*	o	*	*	#	*	#							
K_1^{iso2}	o		*	*	o	.	.	o		*	.		#						
K_2^{iso2}	*	.		#	*		*	o	.	o		o	*	#					
k_1^{des}	.	.	*	.	.						.		.	o	#				
k_2^{des}		o				.	.	.	*				*	*	o	#			
k_3^{des}	*		o		*	o	*	*	o	*	#	o			.		#		
K_1^{des}	o	*	#		o		o	*	.	*	*	.			#	*	o	#	
K_2^{des}	o	*	*	o	o	.	#	#	.	#	.	#	.	#			*	*	#
K_3^{des}			.	o		o		.	*	.	o		*	o	o	*	o	*	#

Key to degree of correlation: blank $\equiv < 0.2$;. $\equiv 0.2 - 0.4$; $* \equiv 0.4 - 0.6$; $o \equiv 0.6 - 0.8$; $\# \equiv 0.8 - 1.0$.

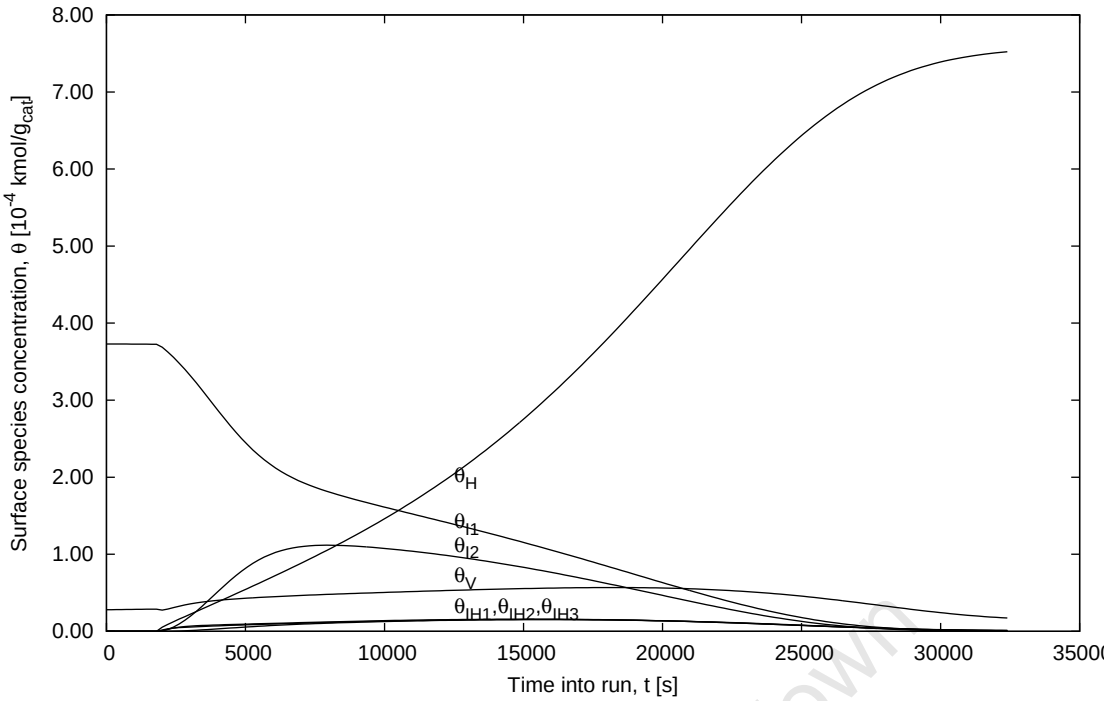

Figure 7.7: Surface species concentrations (run 11): $\theta_H \equiv$ adsorbed hydrogen; $\theta_{I1} \equiv$ adsorbed 1-hexene; $\theta_{I2} \equiv$ adsorbed 2-hexene; $\theta_V \equiv$ vacant sites; $\theta_{IH1}, \theta_{IH2}, \theta_{IH3} \equiv$ half-hydrogenated states.

7.6 1-Hexene model predictions

For illustration purposes, Figures 7.7 and 7.8 show the representative model predictions of respectively the catalyst surface loading and total reactor molar compositions of run 11.

In run 11 the catalyst surface is initially 96.4% covered with adsorbed 1-hexene. Introduction of the hydrogen leads to a rapid conversion of adsorbed 1-hexene to adsorbed 2-hexene and desorped n-hexane via a half-hydrogenated intermediate. This agrees with the observations made in Section 7.2. The adsorbed 2-hexene surface concentration reaches a maximum quite early in Figure 7.7, which is also reflected in its bulk overall liquid and vapour composition as shown in Figure 7.8.

Hydrogenation of each adsorbed alkene yields two vacant sites, accelerating hydrogen dissociative adsorption. From Section 7.4 the straight line section of the graph is not due to rate limitations introduced by the first hydrogen transferral. Rather, it is because the excess adsorbed 1-hexene has been removed and because a balance now exists between the hydrogen and alkene adsorption rates.

As the bulk 1-hexene concentration diminishes, the reaction rates and change in concentrations gradually start slowing down. At the final time shown in the figures, 97.2% of the catalyst surface is covered with dissociated hydrogen. This high coverage

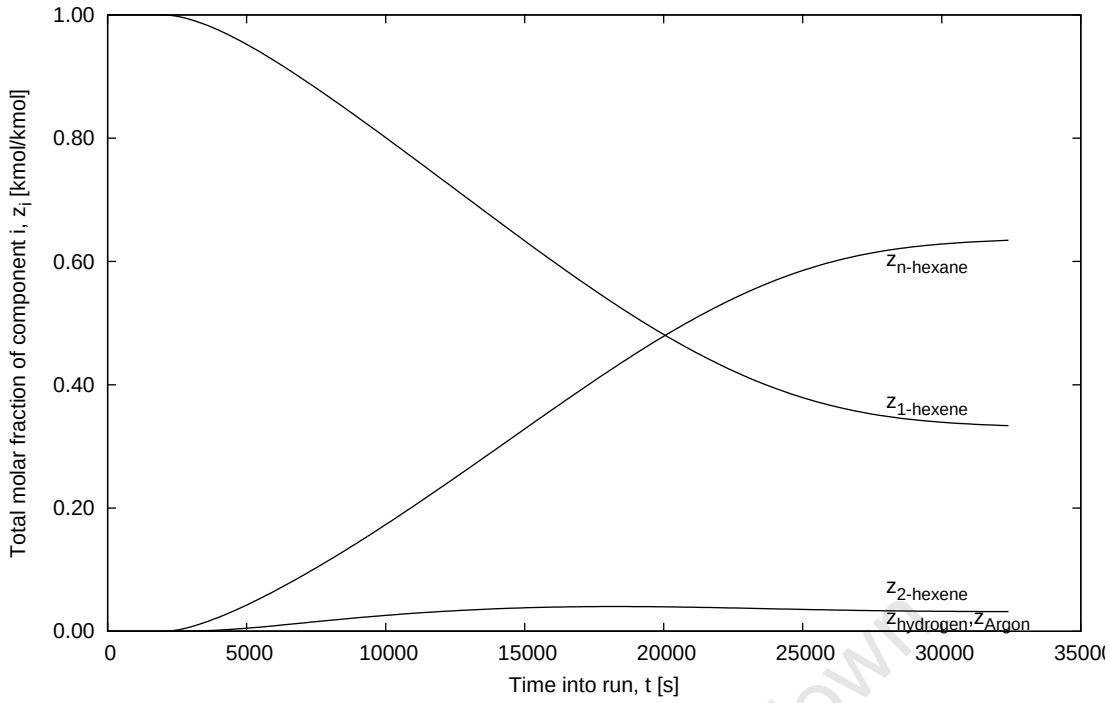

Figure 7.8: Total molar compositions of the bulk liquid and vapour phases for run 11. Note that the hydrogen and argon compositions are very small compared to that of n-hexane, 1-hexene and 2-hexene.

of hydrogen is not unexpected. TPD work by Znak & Zielinski [2008] indicates 98% hydrogen surface coverage on a Ni/Al_2O_3 catalyst at 273 K (0°C) and $1.01325 \cdot 10^5$ Pa(a).

7.7 Fitting of the Arrhenius constants

The Arrhenius rate constants were calculated as described in Section 6.1.2. From Table 7.1, 132 data points were available to fit the 40 Arrhenius constants. The results are shown in Table 7.8. The low R^2 values for the first hydrogen transferral and desorption steps are expected given the sensitivity analyses results in Section 7.4. The excellent R^2 values for dissociative hydrogen adsorption and 1-hexene adsorption are statistically significant. The estimated errors of parameters are relatively small and the coefficient of variation value is 0.35, which is within the recommended range of 0-0.4. A bootstrap analysis was performed, but not included as it did not yield any significant additional information.

From Table 7.8, the activation energies of $5.65 \cdot 10^7$ J/kmol and $7.17 \cdot 10^7$ J/kmol for respectively the 1-hexene and 2-hexene adsorptions are in the same order of magnitude and follow the same trend as that obtained by Lylykangas [2004] for the adsorption of iso-octene, namely $3.4 \cdot 10^7$ J/kmol and $4.9 \cdot 10^7$ J/kmol for respectively the primary and

secondary alkene isomers.

The hydrogen forward and reverse (i.e. adsorption and desorption) activation energies of $7.67 \cdot 10^7$ J/kmol and $8.07 \cdot 10^7$ J/kmol respectively are in very good agreement with that of Christmann et al. [1974] who investigated the adsorption of hydrogen onto single nickel crystal surfaces (Ni(111),Ni(110),Ni(100)) and found values in the order of $8.37 \cdot 10^7$ J/kmol (20 kcal/mol) and $9.63 \cdot 10^7$ J/kmol (23 kcal/mol) respectively. Rautanen et al. [2002] estimated the adsorption enthalpy to be 4.1-4.5$\cdot 10^7$ J/kmol, though this was for the hydrogenation of naphtalene on a 16wt% Ni/Al_2O_3 catalyst.

Furthermore, since the sensitivity analysis indicates that the adsorption of hydrogen and 1-hexene are rate controlling, with the model being slightly more sensitive towards hydrogen adsorption (cf. the values in Table F.1), it is not surprising to find that the apparent activation energy measured by Campelo et al. [1982] for 1-hexene hydrogenation on a 20wt% Ni/Al_2O_3 catalyst is $7.10 \cdot 10^7$ J/kmol. Several other comparisons were also made for verification purposes. For example, the activation energies are higher than that found for 1-butene hydrogenation of *ca.* $5.23 \cdot 10^7$ J/kmol [Bond & Winterbottom, 1969]. As shown by, for example, Uchytil et al. [1981], the reaction rate decreases significantly as the chain length increases and the apparent activation energy for 1-butene should thus not be higher than that for 1-hexene.

However, the model predicts negative activation energies, which is highly unlikely. Negative activation energies are associated with barrierless reactions, i.e. reactions that occur spontaneously. Based on the Arrhenius equation, an increase in temperature increases a reaction rate if the activation energy is positive. However, in the case of a negative activation energy, an increase in temperature decreases the raction rate. Thus, a negative activation energy slows down the reaction with increasing temperature.

Negative activiation energies may be due to numerical convergence errors, experimental errors, activation energies close to zero that direct the search algorithm to negative values, the insensitivity of the model to those parameters within the region of interest, a high degree of correlation between parameters (see Section 6.1) and/or the fact that the model is fundamentally not an accurate description of the system. The model converged to this solution given various initial guesses. That, coupled with the CV of 0.35, yields a high level of trust in the regression itself. However, the observed negative activation energies imply that the model is not a fundamental description of the system despite the fact that it describes the data.

I.e., the model can be used for further modelling, but with caution.

From Table 7.9 there are several parameters that are highly correlated with each other. The 1-hexene adsorption rate and equilibrium constants, n-hexane desorption rate and equilibrium constants, and hydrogen adsorption rate constants are highly correlated with each other. This is probably partially due to the fact that 1-hexene and hydrogen are both available in high concentrations in the liquid and are competitively adsorbing

onto the limited number of surface sites on the catalyst. Additionally, they are all related via the mass balance in the bulk liquid.

The desorption related constants are relatively highly correlated to each other as well. This is not unexpected as they essentially represent the same reaction mechanism, namely that of breaking the last carbon-metal bond, with the only difference that the carbons involved are further from the terminal point of the alkene. Additionally, the model is insensitive to these parameters and they may thus simply appear correlated as they could not be accurately determined. This is supported by the curious fact that these desorption rate related constants of the terminal and beta-carbons (i.e. k_1^{des} and k_1^{des}) are so highly correlated to the addition of the first hydrogen onto the terminal carbon of the adsorbed 1-hexene (k_1^{iso1} and K_1^{iso1}).

Note that the insensitivity of the model to the desorption constants and the fact that the they are highly correlated, make it easier to justify their lumping in Section 8.

Finally, via attrition the stirrer reduced the extrudated catalyst particles to a fine dust of less then a $1{\cdot}10^{-4}$ m in size. Application of the Weisz-Prater criterium at 6 bar, where the highest reaction rates were observed, results in $C_{WP} = 0.009 << 1$, which indicates that no internal mass transfer limitations were present.

7.8 Summary of results

A thorough and comprehensive experimental, theoretical and statistical approach has been used to evaluate the 1-hexene semi-batch hydrogenation data in order to determine the temperature dependent behaviour of the kinetic rate constants and the trust that may be vested in each.

The resulting model was shown to be sufficiently fundamental to be able to explain observed macroscopic phenomena, such as the hydrogen consumption rate, based on the effect of input variables, such as pressure, on the catalyst surface species' concentration. Furthermore, it was possible to show how this approach can determine the rate limiting step by applying a sensitivity analysis to run 10 (the low pressure; low temperature case). For this specific example, the 1-hexene and hydrogen adsorption rate constants were shown to be limiting.

In terms of the regression itself, the CV values for the rate and equilibrium constants fitted at constant temperatures for each of the 4 individual runs were below the targeted 0.4, except in the case of run 13 where it was 0.42. However, this was sufficiently accurate to be used as an initial guess to express each reaction rate and equilibrium constant in terms of temperature by regressing the Arrhenius equations for the Arrhenius constant and activation energy. Here, the CV was below the target of 0.4 with a good value of 0.35.

The resulting desorption coefficients were found to be highly correlated. Because

Table 7.8: Arrhenius constants fitted simultaneously across runs 10-13.

Parameter	Units	via linear regression			via direct non-linear regression			
		A_{rh} [a]	E_a/R_0 K	R^2	A_{rh} [a]	Error %	E_a/R_0 K	Error %
k^{H2}	$g_{cat}.m^3/kmol^2.s$	1.05E+18	9.53E+03	0.946	1.04E+18	0.49	9.22E+03	0.56
k_{-}^{H2}	$g_{cat}/kmol.s$	3.76E+12	9.14E+03	0.916	3.77E+12	1.13	9.71E+03	1.13
k_1^{ads}	$m^3/kmol.s$	3.28E+12	6.87E+03	0.712	3.25E+12	2.24	6.80E+03	0.99
k_2^{ads}	$m^3/kmol.s$	4.55E+14	8.50E+03	0.742	4.81E+14	1.14	8.62E+03	1.06
k_{-1}^{ads}	s^{-1}	1.08E+08	7.00E+03	0.871	1.04E+08	1.46	7.18E+03	0.91
k_{-2}^{ads}	s^{-1}	3.42E+13	1.12E+04	0.949	3.49E+13	1.37	1.06E+04	1.10
k_1^{iso1}	$g_{cat}/kmol.s$	1.34E-03	-5.41E+03	0.482	1.36E-03	1.31	-5.27E+03	-1.73
k_2^{iso1}	$g_{cat}/kmol.s$	2.22E-07	-8.38E+03	0.449	2.38E-07	1.37	-8.35E+03	-1.76
k_{-1}^{iso1}	$g_{cat}^2/kmol^2.s$	1.92E-13	-1.76E+04	0.634	1.90E-13	1.24	-1.89E+04	-0.90
k_{-2}^{iso1}	$g_{cat}^2/kmol^2.s$	2.70E-12	-1.66E+04	0.638	2.71E-12	0.98	-1.65E+04	-0.65
k_1^{iso2}	$g_{cat}/kmol.s$	2.00E-03	-5.43E+03	0.160	1.92E-03	0.91	-5.48E+03	-1.07
k_2^{iso2}	$g_{cat}/kmol.s$	1.62E-09	-9.99E+03	0.579	1.61E-09	1.43	-1.01E+04	-0.82
k_{-1}^{iso2}	$g_{cat}^2/kmol^2.s$	1.38E-12	-1.70E+04	0.617	1.35E-12	1.47	-1.75E+04	-0.85
k_{-2}^{iso2}	$g_{cat}^2/kmol^2.s$	1.00E-19	-2.24E+04	0.658	9.89E-20	0.74	-2.16E+04	-1.91
k_1^{des}	$g_{cat}/kmol.s$	9.01E-23	-2.13E+04	0.466	9.21E-23	1.74	-2.10E+04	-1.27
k_2^{des}	$g_{cat}/kmol.s$	9.01E-23	-2.13E+04	0.466	8.82E-23	1.29	-2.04E+04	-0.90
k_3^{des}	$g_{cat}/kmol.s$	9.01E-23	-2.13E+04	0.466	8.87E-23	1.19	-2.06E+04	-1.01
k_{-1}^{des}	$g_{cat}.m^3/kmol^2.s$	9.24E-04	-5.86E+03	0.042	8.88E-04	1.36	-5.82E+03	-1.73
k_{-2}^{des}	$g_{cat}.m^3/kmol^2.s$	9.24E-04	-5.86E+03	0.042	9.31E-04	1.46	-5.91E+03	-1.25
k_{-3}^{des}	$g_{cat}.m^3/kmol^2.s$	9.24E-04	-5.86E+03	0.042	9.02E-04	1.41	-5.86E+03	-1.37

[a] The units of the Arrhenius constant are the same as that of the rate constant.

Table 7.9: Simplified correlation matrix for the Arrhenius constants and activation energies.

Key to degree of correlation: . $\equiv 0.2 - 0.4$; * $\equiv 0.4 - 0.6$; o $\equiv 0.6 - 0.8$; # $\equiv 0.8 - 1.0$

of this *and* the fact that they essentially all describe the breaking of the final carbon-metal bond, their effects may thus safely be lumped. The correlation of several other coefficients were also found. However, to ensure robustness in the kinetic model used in the next section and to prevent the loss of information, these coefficients will be retained.

Chapter 8

CD analyses

In this chapter, a combination of experimental data, simulation and parameter estimation will be used to deepen the understanding of the fundamental mechanisms involved during CD hydrogenation in the experimental sample space and system considered. To evaluate the system, the following key performance indicators (KPI's) were investigated as discussed:

- hydrogen conversion (X_{H2}).
- 1-hexene conversion (X_{1Hx}).
- n-hexane selectivity based on the 1-hexene fed to the column (S_{nHx1Hx}).
- n-hexane yield based on the 1-hexene fed to the column (Y_{nHx1Hx}).
- n-hexane recovery to the bottoms product based on the 1-hexene fed to the column (R_{nHx1Hx}).

Firstly, the experimental data accuracy, consistency and validity will be discussed and determined. The model will then be fitted to the experimental data to optimize the accuracy of the model within the data space of interest. Once this has been achieved, the effect of perturbations to variables on the KPI's will be discussed.

8.1 Experimental CD data

Details of the data generation methods and enhancements to the original control system [Nieuwoudt, 2005] are shown in Appendix A and discussed in Section A.

8.1.1 Variables investigated

The CD system can be used to investigate the variables shown in Table 8.1. The variables chosen for investigation are:

Table 8.1: Control variables available for investigation on the CD column.

Category	Type	Parameter
Flows	Feed	Flow rate(s), composition(s), number, location(s).
	Sidestream	Flow rate(s), phase(s), number, location(s).
	Internal	Reboiler heat duty, recycle ratio.
Conditions	Pressure	Feeds, condenser.
	Temperature	Feeds, condenser.
Reactive zone	Mechanical	Hydrodynamic design, number, locations, catalyst.
	Catalyst	Type, composition, mass.
Non-reactive zone	Mechanical	Design, height.

- catalyst cage design.
- reboiler heat duty.
- 1-hexene feed composition.
- hydrogen feed flow rate.
- condenser pressure and (effectively) average column temperature.

These variables were considered to have the most significant influence on the mass transfer effects within the CD system. Mass transfer coefficient correlations (see Section C) are mainly functions of the internals' geometric properties, liquid and vapour flow rates, composition, and temperature. Geometric properties may be varied by employing different packing, the internal liquid and vapour flow rates are easily manipulable via the reboiler heat duty, the compositions in the reactive zone via different feed compositions and/or reaction conditions such as temperature or pressure, and the temperature via a change in the column pressure.

Catalyst cage design

The investigation of a different catalyst cage design was the result of troubleshooting to identify the cause of a high pressure drop across the reactive zone. It was originally intended to remove the geometric variables as unknowns when investigating the effect of a superimposed reaction on mass transfer coefficients by keeping the variables related to the catalyst, reactive zone, column design and distillation packing constant.

As discussed in Section 4.3, two reactive zone structural designs were used. Design 1 consisted of the catalyst extrudates dumped into a cylindrical cage spanning the entire perpendicular flow area in the column. Design 2 had several semi-circular catalyst filled bags encompassing the flow area except for a removed segment 25% of the diameter in length. These semi-circular bags were staggered along the height of the column. Design 1 could be modelled relatively easily with existing random packing correlations (see

Section 5), while design 2 could potentially reduce the pressure drop across the reactive zone. However, design 2 could also encourage bypassing of the catalyst and incomplete wetting.

Reboiler heat duty

Varying the reboiler heat duty affects the separation efficiency in the column (and reactive zone) by altering the recycle ratio and changing the mass transfer coefficients. From distillation theory [Seader & Henley, 1998], an increase in the recycle ratio increases the separation efficiency towards a maximum value by increasing the residence time (and thus the opportunity for mass transfer) of a component in the distillation system. Beyond this point, the separation efficiency remains constant. The mass transfer coefficients are affected as they are dependent on the vapour and liquid flow rates (cf. Section C).

Thus, a change in the reboiler heat duty can potentially affect the 1-hexene conversion by changing the liquid and vapour compositions in the reactive zone. Additionally, it can affect the conversion by increasing the residence time of a component in the reactive zone, supplying more opportunity for the component to participate in the reaction.

Hydrogen feed flow rate

A change in the hydrogen feed flow rate affects the reaction dynamics by changing the WHSV in terms of the hydrogen. Additionally, as a result of the non-condensable nature of hydrogen, it also affects the VLE and separation performance of the column. As discussed previously, both can have an effect on the overall conversion.

Pressure (and temperature)

The effect of pressure and (via the VLE) coupled effect of temperature affect not only the separation, but also the reaction kinetics.

8.1.2 Experimental data quality

An essentially two-factorial design approach, that uses the variables selected in Section 8.1.1, was followed. Table 8.2 summarizes the experimental design and results.

The relative mass balance errors are acceptable, with most lying between ±4wt% and all lying between ±8wt%.

However several of the 1-hexene conversions and selectivities are either negative, such as the n-hexane selectivity of -346.46 mol% in run number 2.2, or very large, such as the n-hexane selectivities in runs 1.1 and 2.3, which are 147.04 and 649.73 mol% respectively. Note that this is only the case for the low pressure runs of cage design 2, namely runs

Table 8.2: Extract of experimental results performed on the 1-hexene CD hydrogenation system showing mass balance errors and reaction performance indicators for different liquid phase compositions, feed gas flow rates, reboiler heat duties, column pressures and reactive zone mechanical designs (see Appendix E for the full set of results).

Run No	1-hexene : n-hexane	Feed gas	Reboiler duty	Condenser pressure	Average column temp.	Cage Design	Mass balance error	Conversion		Selectivity	
								Hydrogen	1-Hexene	n-Hexane	2-Hexene
	-	kmol/s	W	10^5 Pa(a)	K	-	kg/kg%	mol/mol%	mol/mol%	mol/mol%	mol/mol%
1.1	50:50	5.43E-07	150	1.6	337.33	2	-3.2	0.4	11.6	147	7
2.1	50:50	5.43E-07	250	1.6	344.79	2	-3.1	0.8	-4.4	-21	-27
2.2	50:50	5.43E-07	350	1.7	345.24	2	0.6	2.9	0.6	-346	240
2.3	50:50	5.43E-07	250	1.7	344.85	2	-0.2	1.1	-0.2	650	-758
2.4	50:50	5.43E-07	250	2.0	349.98	2	1.3	1.2	4.7	5	40
2.5	66:33	5.43E-07	250	2.0	349.42	2	1.5	1.4	5.5	25	34
3.1	100:00	5.43E-07	350	4.5	380.59	2	3.2	12.3	29.0	43	46
3.2	100:00	5.43E-07	350	6.3	393.89	2	5.6	21.8	46.7	45	42
4.1	100:00	5.43E-07	350	1.7	342.94	1	1.4	2.8	5.2	38	35
4.2	50:50	5.43E-07	350	1.7	344.11	1	-0.8	1.7	4.8	45	89
4.3	100:00	1.09E-06	350	6.0	388.39	1	5.9	21.8	66.0	56	35
4.4	100:00	1.09E-06	350	6.0	388.91	1	8.0	22.2	66.2	53	34
4.5	100:00	1.09E-06	350	6.3	390.74	1	5.9	22.6	66.7	56	35

1.1-2.3. This can be explained by firstly considering that cage design 2 allows bypassing of the catalyst (see Section 8.1.1) and secondly that lower pressures, and thus via the VLE also lower temperatures, lead to lower hydrogen and 1-hexene conversions. Thus, in these cases, small errors in the compositional and mass balance analyses are significant. It is especially the hydrocarbon mass balances that are affected as it is dependent on accurate measurement/control of four streams' flow rates and compositions, namely the hydrocarbon feed, bottoms, distillate and off-gas streams. The hydrogen conversion is by far the most accurate indicator as it is dependent on only two, well defined, more accurately measurable streams, namely the hydrogen feed and offgas streams.

The data generated in runs 1.1-2.3 are thus suspect. It is also important to note in runs 2.1 and 2.3 that the 1-hexene conversion follows the mass balance error, suggesting that the reflected 1-hexene conversions for these runs are probably not real, but the result of the mass balance error. Similarly, for run 2.2, the 1-hexene conversion (0.56 mol% or 0.56 wt%) is less than the mass balance error (0.64 wt%), implying that the conversion should not be used as it falls within the margin of error. In all cases where the 1-hexene conversion cannot be used, the n-hexane and 2-hexene selectivities are also suspect as they are dependent on the number of moles of 1-hexene converted.

Reconsidering Table 8.2, only the hydrogen conversion can be used in runs 2.2 and 2.3 - that of 1.1 and 2.1 are 0.42 and 0.82% and fall within the mass balance errors of respectively -3.15 and -3.09 wt% (see Section 4.4).

As a last data quality check, it should be noted that, if only hydrogenation and isomerization occurs, the 1-hexene conversion must always be higher than the hydrogen conversion as the 1-hexene can be converted both via hydrogenation as well as isomerization. Although hydrogen participates in isomerization, there is no nett change in its amount. This is the case in runs 4.2 and 4.3.

The data in Table 8.2 for runs 4.1 to 4.4 is qualitatively consistent. As expected a pressure (and hence temperature) and hydrogen feed flow rate increase, increases the conversions from run 4.1 to 4.3, in this case from 2.79% to 21.84%. A decrease in the 1-hexene feed flow rate from run 4.1 to 4.2 apparently decreases the hydrogen conversion - probably as the 1-hexene concentration within the reactive zone is decreased. Note that run 4.4 is a repeatability test of run 4.3 and that the conditions after run 4.3 were changed prior to resetting it and performing run 4.4. From runs 4.3 and 4.4 it is clear that results can be repeated.

From runs 2.2 and 4.2, the different reaction zone designs show different hydrogen and 1-hexene conversions for similar order of magnitude mass balance errors *and* the same conditions, namely 2.85 mol% and 1.69 mol%: a 69% difference. It is thus not advisable to compare values across the different catalyst zone designs. Furthermore, the data generated using cage design 2 has been shown to be suspect in most cases. Subsequently, the data set of design 1, namely runs 4.1-4.5, was chosen for further parameter

estimation as the mass balance errors were generally small compared to the calculated conversions and selectivities, as the mass transfer lent itself to standard random packing mass transfer correlations due to the catalyst design, and as the data set spanned different feed compositions, feed flow rates, internal flow rates and pressures. Although the n-hexane and 2-hexene selectivities should sum to 100%, this is not the case in all the runs. Specifically, in the cases of runs 4.3 to 4.5, the totals of ca. 90% are believed to be within the error margin. However, the values for runs 4.1 and 4.2 show a ±30% discrepancy, which is probably the result of low conversion exacerbating measurement errors.

The exclusion of runs 1.1-3.2 is unfortunate as investigation of the effect of the reboiler duty cannot be included: runs 4.1-4.5 are all at 350 W. Thus, investigation of the effect of different internal flow rates will be limited. However, having screened the data, the resulting data set has a higher quality, it is possible to vest more trust in the results, and the limitation of the model are more clearly understood.

Lastly, using a manometer, it was possible to show that flooding did not occur if the flooding top-bottom differential pressure criterion in Section 4.3.3 is applied.

8.2 Comparing the model to experiment

The model converged successfully for the equilibrium and non-equilibrium non-reactive distillation cases. However, initial attempts at CD simulation failed due to the difficulty in determining a suitable initial guess and the stiffness introduced into the system by the addition of the Langmuir-Hinshelwood reaction kinetics. This was partly resolved by solving the model repeatedly for increasing extents of reaction (from 10 to 100% in 5% increments) and using the converged solution of each as the initial guess for the next (cf. *homotopy*). This allows the good initial guess that nothing is initially adsorbed onto the catalyst surface ($\theta_V = \theta_S$). However, for the higher pressure cases of ca. $6{\cdot}10^5$ Pa(a)), the Jacobian became ill-conditioned in the vicinity of the solution (usually at ca. 80% of the full reaction). An additional gradual ramping of the pressure in 10% increments from 50% to 100% of that desired solved this problem.

Incrementally increasing the extent of reaction, combined with employing a numerically calculated rather than analytical Jacobian and the non-linearity introduced by the reaction, significantly increased the solution time of the model - especially for the high pressure cases where convergence could take as long as 40 min. In practice, the effort involved to differentiate the equations so as to obtain an analytical Jacobian is not only strongly advised, but is indeed implemented [Kooijman & Taylor, 1998]. A numerical Jacobian was used here as it allows for faster, more flexible changes to the system of equations, though an analytical approach should be considered for future work. The final simulations were performed on an Intel(R) Core(TM)2 Duo CPU T7300 at 2.00 GHz

with 3.00 GB of RAM. The Fortran compiler was set to maximum optimization and the calculation processes given the highest CPU priority. Two regression calculations could be run simultaneously on the separate CPU's.

The standard inputs to the model are supplied in Table 8.3 and the geometry depicted in Figure 8.1. The pressures, condenser temperature, reflux ratio, feed flow rates and feed compositions were adjusted depending on the experimental run considered.

Lastly, in the discussion to follow, low pressure runs will refer to experiments 4.1 and 4.2 at ca. $1.7{\cdot}10^5$ Pa(a), while high pressure runs will refer to experiments 4.3-4.5 at ca. $6{\cdot}10^5$ Pa(a). Note that due to the VLE, high pressure also implies a high average column temperature and *vice versa*.

8.2.1 Initial guess and bounds

The parameters identified in Table 6.1 were first varied by hand to identify both initial values and upper/lower bounds for input into *n2f2b.f*, the bounded version of the Fortran package NL2SOL. The reason for using bounded regression will be discussed shortly. As discussed in Section 6.2, the variables to which the model parameters were fitted are as follows:

- Distillate and bottoms molar compositions of 1-hexene, 2-hexene and n-hexane. The liquid hydrogen concentrations could not be measured experimentally.
- Complete off-gas compositional analysis.
- Distillate, bottoms and off-gas molar flow rates.

To determine the *bounds* within which to search for the parameter values, the effect of mass transfer on each fitted parameter as well as its expected error, was carefully considered. Bounded optimization was used to prevent the search algorithm from choosing infeasible parameter values in a highly non-linear problem. If *n2f2b.f* converged to a bound of a parameter, this bound was set wider and the regression restarted.

The reaction rate constants were based on the analysis in Section 7, specifically targeting the catalyst, temperature, pressure and components in the CD column. Additionally, the standard errors for each of the regressed reaction rate constants are clearly defined in Table 7.8. As was shown previously in Section 7.7, the internal mass transfer limitations were not found to be rate limiting when fitting the reaction kinetics. Although, the catalyst in the the CD column's reactive zone is in the form of extrudates and not a fine dust as in the kinetic experiments, it was, as a first approach, assumed that internal mass transfer limitations are negligible, especially since this is a commercial catalyst specifically designed for hydrogenation. Surface reaction rate constant bounds were thus initially limited to the standard errors predicted in Table 7.8.

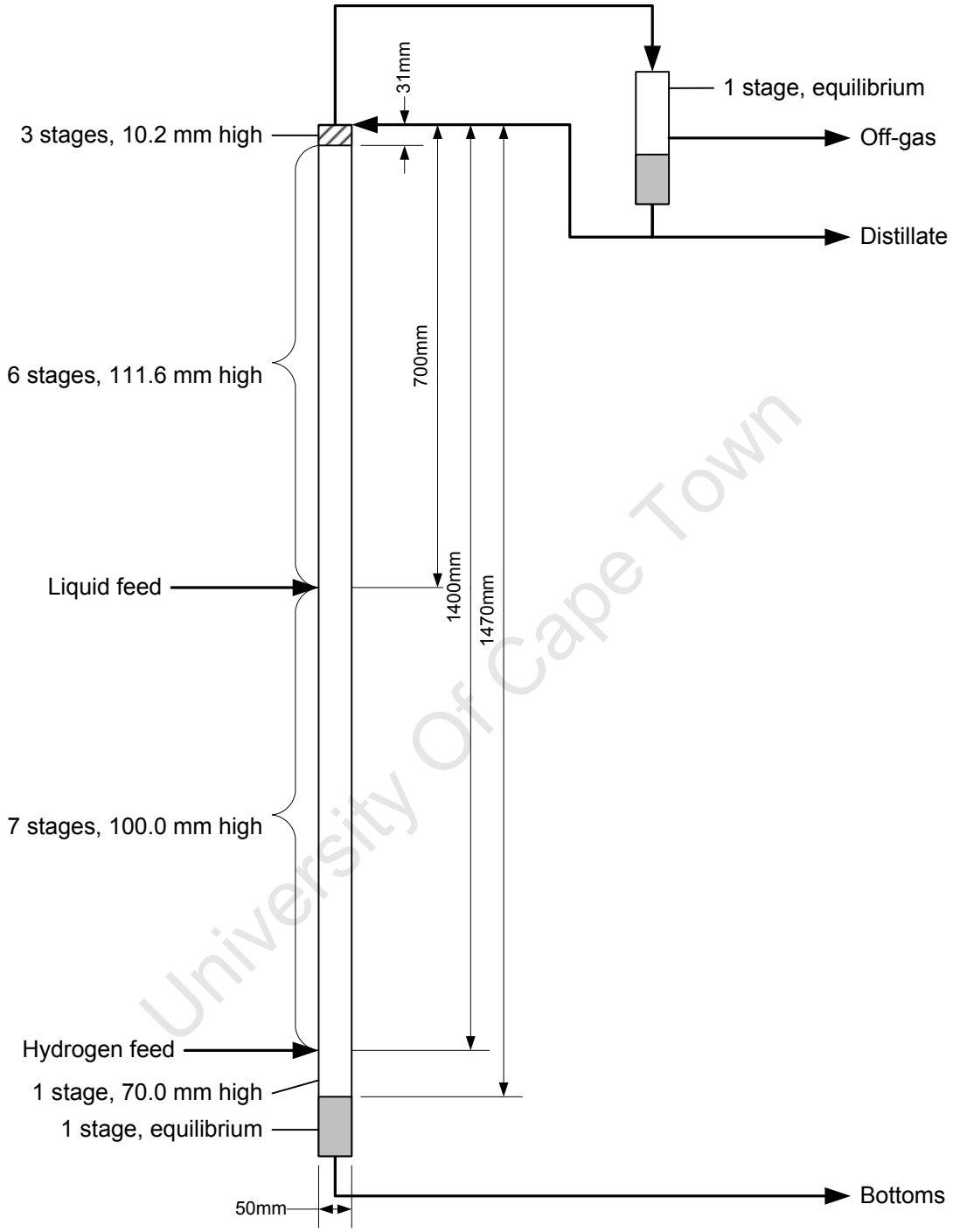

Figure 8.1: Geometric input to the CD system simulation (also see Section 4.3), where *stages* refers to the theoretical stages used in the CD column simulation. Note that the partial condenser and reboiler are always simulated as EQ stages (see Section 5.4.5).

Table 8.3: Input specifications to the model.

Category	Parameter	Units	Value 1	Value 2
Components	Number	None	4	
	Component 1	None	Hydrogen	
	Component 2	None	1-Hexene	
	Component 3	None	2-Hexene	
	Component 4	None	n-Hexane	
Operation	Mode	None	NEQ	
	Column height	m	1.47	
	Number of feed stages	None	2	
	Number of sections	None	2[a]	
Sections	Type	None	Catalyst	Structured
	Stage Height	m	0.01[b]	0.10
	Column diameter	m	0.0500	0.0500
	Packing height	m	0.0306	1.4400
	Catalyst weight	kg	0.0210	
	Bulk density	kg/m^3	700.0	
	BET	m^2/g	130.0	
	Packing density	m^2/m^3	1700.0[c]	
	Nominal size	m	0.0025	
	Specific packing surface	m^2/m^3		492.0000
	Void fraction	m^3/m^3		0.9000
	Channel base	m		0.0127
	Crimp height	m		0.0064
	Channel side	m		0.0089
	Channel flow angle	radians		1.0472
Feeds	Feed state	None	1[d]	1
	Height	m	0.70	1.40
	Temperature	K	298.15	298.15
	Pressure	Pa(a)	400000.00	400000.00
	Vapour fraction	m^3/m^3	Not specified	Not specified
	Component flow rates			
	Hydrogen	kmol/s	0.0	1.0E-06
	1-Hexene	kmol/s	0.5E-06	0.0
	2-Hexene	kmol/s	0.0	0.0
	n-Hexane	kmol/s	0.0	0.0
Condenser	Configuration	None	Partial	
	Reflux ratio	None	40.0	
	Condenser temperature	K	280.0	
	Condenser pressure	Pa(a)	400000.0	
Reboiler	Heat duty	W	350.0	

[a] This is the number of different sections containing one type of packing. The program creates additional sections to ensure that the feed points do not enter in the middle or bottom of a stage.

[b] This is the desired stage height. The program chooses the closest value to this that will ensure a whole number of stages.

[c] This value is estimated and based on the dimensions of the catalyst extrudates (see Section 4.1).

[d] 1 ≡ temperature and pressure specified.

Table 8.4: Table 6.1 deviations of predicted parameter values when regressed against CD 1-hexene hydrogenation data using the CD model.

Parameter	sns[a]	Run number				
		4.1	4.2	4.3	4.4	4.5
Regressed values						
k_L^{random}	1	0.20	-	0.75	1.06	1.06
k_V^{random}	2	0.20	-	0.05	0.05	0.05
k^{des}	3	0.96	-	1.97	2.00	2.00
$k^{iso1/2}$	4	0.20	-	2.00	2.00	2.00
$K^{iso1/2}$	5	2.10	-	1.01	1.00	1.00
K^{des}	6	1.76	-	1.02	1.00	1.00
k^{H2}	7	1.42	-	1.43	1.57	1.57
K^{H2}	8	1.00	-	1.14	1.13	1.13
k^{ads}	9	0.26	-	3.65	3.50	3.50
K^{ads}	10	2.00	-	0.45	0.44	0.44
Statistics						
s		3.67E-02	-	8.43E-02	1.33E-01	1.32E-01
CV		15.94	-	37.25	58.88	58.20

[a] The scaling factor used in the regression analyses.

However, the particle size used in the reaction kinetic experiments was small compared to the size of the extrudates. The external mass transfer limitations in the CD column could thus be very different to that in the kinetic experiments. Thus, the trust in the accuracy of the regressed adsorption and desorption reaction rate constants, which include external mass transfer effects, were low and their initial bounds were thus chosen widely.

Both the liquid and vapour phase mass transfer coefficients were determined based on correlations for random packing in a non-reactive environment. Furthermore, these correlations are based on random packing used in industry, which have much larger effective diameters than the catalyst used in the CD column. It was thus expected that there could be a larger error in the predicted liquid and vapour mass transfer coefficients as applied to this specific application in the CD hydrogenation column. Again, wider initial bounds were chosen.

8.2.2 Regression analysis

Table 8.4 shows the regression results. Due to the extreme non-linearity of the problem and the fact that numerical calculation of the Jacobian is computer resource intensive, it was very difficult to converge the model to a solution. For example, run 4.2 did not converge. This could be due to a bad initial guess. However, the main difficulty was that the damping factor, which is involved in choosing the step length towards the solution, reached it's minimum value - i.e. the system of equations became stiff and

the optimum could not be determined accurately. Investigation of the Jacobian showed several orders of magnitude differences between some of the differential elements: mainly those concerned with the energy balance and reaction rates.

In the case of run 4.2, attempts to scale the Jacobian, the independent variables, and the MESH and regression error equations failed. Also, neither lowering the minimum step length nor different paths to full reaction and pressure (see Section 8.2) succeeded. It should be noted that at high pressures and temperatures, such as in runs 4.3-4.5, convergence became more difficult. This was probably due to the higher temperature increasing the stiffness of the problem by significantly increasing the reaction rate constants via the Arrhenius equations thus increasing the influence of the non-linear Langmuir-Hinshelwood kinetics on the system of equations. However, in the cases of runs 4.3-4.5 convergence was possible by slowly (in 5% increments) increasing the column pressure.

Run 4.1 could be fit to a reasonable accuracy with a CV of 16%, while the best fit for the highe pressure runs was obtained for run 4.3 with an acceptable CV (less than 40%) of 37.25%. At low pressures, $\mathbf{K^{H2}}$ was predicted well with virtually no adjustment required, whereas at high pressures an adjustment of ca. 14% was required. At higher pressures, $\mathbf{K^{iso1/2}}$ and $\mathbf{K^{des}}$ were predicted correctly, while at lower pressure significant adjustment (ca. 100%) was required.

In general the liquid mass transfer coefficient of 0.0051 used in the Onda et al. [1968] correlation (eq. 5.42) is out be less than 6% at high pressures, though it is 80% at out at the low pressure runs. However, the vapour phase mass transfer coefficient had to be reduced significantly by 80-95%. As discussed earlier, it is not surprising that adjustment is required as the used random packing correlation was not fit on catalysts. The adjustment could also be due to incorrect estimation of the packing density (1700 m^2/m^3).

From Table 8.2, runs 4.3-4.5 have the largest mass balance errors (5.9-8.0%). It is thus not surprising that the 4.3-4.5 fits exhibit poor accuracy and that it is associated with a large error (84%) in one of the main streams, namely the distillate. In the case of run 4.1, prediction of the distillate 2-hexene value is out by an order of magnitude, namely 108%. This also has an effect on the distillate n-hexane and 1-hexene off-gas errors.

In terms of the KPI's, they appear to be poorly predicted at the lower pressure runs. The hydrogen conversion is out by -36% and the 1-hexene by -27.8%. In constrast, the values at the high pressure runs are respectively 2.3 and -2.5%. However, note that a small absolute error for the small conversions in run 4.1 (2.8 and 5.2%) will have a much larger relative effect than for the same error in the high pressure runs (21.7 and 66%). In general, the CV values still indicate that the lower pressure runs are better predicted. Furthermore, the trends observed in the KPI's are similar to that observed experimentally, i.e. the conversion and selectivity increase from runs 4.1 to 4.8.

Table 8.5: Comparison between the experimental and predicted fitted parameters for runs 4.1 and 4.4 as examples of low and high pressure runs respectively.

Parameters	Component	Run 4.1			Run 4.4		
		Exp.	Model	Error %	Exp.	Model	Error %
Composition [mol/mol]							
Distillate	1-Hexene	0.98	0.97	-1	0.34	0.38	12
	2-Hexene	0.01	0.02	179	0.25	0.32	25
	n-Hexane	0.01	0.01	-38	0.37	0.30	-20
Bottoms	1-Hexene	0.95	0.96	1	0.36	0.35	-2
	2-Hexene	0.02	0.02	-21	0.23	0.17	-25
	n-Hexane	0.03	0.02	-17	0.39	0.48	21
Off-gas	Hydrogen	0.89	0.93	5	0.97	0.98	1
	1-Hexene	0.11	0.07	-40	0.01	0.01	-29
	2-Hexene	0.00	0.00	[a]	0.00	0.01	[a]
	n-Hexane	0.00	0.00	[a]	0.01	0.01	-54
Flow Rates [kmol/s]							
Distillate	Mixture	1.11E-07	8.80E-08	-20.3	1.23E-07	1.96E-08	-84.1
Bottoms	Mixture	3.48E-07	4.03E-07	15.7	3.66E-07	4.93E-07	34.5
Off-gas	Mixture	5.91E-07	5.71E-07	-3.3	8.72E-07	8.62E-07	-1.1
KPI's [mol%]							
X_{H2}		2.8	1.8	-36.0	21.8	22.3	2.3
X_{1Hx}		5.2	3.8	-27.8	66.0	64.3	-2.5
S_{nHx1Hx}		38.2	48.7	27.6	55.8	71.8	28.7

[a] The relative errors for these value are not available as their experimental values are 0.0.

Table 8.6: Sensitivity analysis for the regressed parameters for the low and high pressure cases (runs 4.1 and 4.4).

Parameter		Run 4.1			Run 4.4		
		X_{H2}	X_{1Hx}	S_{nHx1Hx}	X_{H2}	X_{1Hx}	S_{nHx1Hx}
k^L	-1%	-0.41	-0.37	-0.03	-0.28	-0.28	0.00
	+1%	0.41	0.34	0.08	0.27	0.28	0.00
k^V	-1%	-0.07	-0.04	0.01	0.16	0.16	-0.04
	+1%	0.07	0.01	0.05	-0.16	-0.16	0.03
k^{des}	-1%	0.00	-0.09	0.09	-0.07	-0.07	-0.02
	+1%	0.00	0.08	-0.08	0.07	0.07	0.02
$k^{iso1/2}$	-1%	0.07	0.58	-0.52	-0.03	-0.03	-0.04
	+1%	-0.07	-0.59	0.56	0.03	0.03	0.03
$K^{iso1/2}$	-1%	-0.07	-0.31	0.28	-0.10	-0.10	-0.11
	+1%	0.00	0.30	-0.27	0.09	0.09	0.10
K^{des}	-1%	0.00	-0.19	0.19	-0.11	-0.11	-0.13
	+1%	0.00	0.18	-0.15	0.11	0.11	0.12
k^{H2}	-1%	0.34	0.19	0.16	-0.10	-0.11	0.00
	+1%	-0.34	-0.22	-0.13	0.10	0.11	0.00
K^{H2}	-1%	0.00	0.00	0.00	0.02	0.02	0.01
	+1%	0.00	0.00	0.00	-0.02	-0.02	-0.01
k^{ads}	-1%	-0.07	0.03	-0.09	-0.03	-0.03	-0.14
	+1%	0.07	-0.03	0.09	0.03	0.03	0.14
K^{ads}	-1%	-0.34	-0.73	0.41	-0.10	-0.10	-0.10
	+1%	0.34	0.69	-0.38	0.10	0.10	0.10

Table 8.7: Equations and averaged values describing the deviation of mass transfer and reaction rates from that predicted.

Correlation	R^2
$sns(1) = 7.71 \cdot 10^{-5} \frac{\left(T_3^L\right)^{1.75}}{P_3} - 2.43 \cdot 10^{-2}$	0.908
$sns(2) = 1.57 \cdot 10^{0} \frac{\left(T_3^L\right)^{1.75}}{P_3} - 3.36 \cdot 10^{-2}$	1.000
$sns(3) = 2.15 \cdot 10^{2} exp\left(\frac{-1.77 \cdot 10^{3}}{T_3^L}\right)$	0.999
$sns(4) = 7.79 \cdot 10^{-8} exp\left(\frac{4.50 \cdot 10^{-2}}{T_3^L}\right)$	0.997
$sns(5) = 2.41 \cdot 10^{2} exp\left(\frac{-1.45 \cdot 10^{-2}}{T_3^L}\right)$	0.998
$sns(6) = 6.28 \cdot 10^{1} exp\left(\frac{-1.09 \cdot 10^{-2}}{T_3^L}\right)$	1.000
$sns(7) = 1.50$	Average
$sns(8) = 1.10$	Average
$sns(9) = 1.27 \cdot 10^{-8} exp\left(\frac{5.13 \cdot 10^{-2}}{T_3^L}\right)$	0.995
$sns(10) = 2.76 \cdot 10^{-5} exp\left(\frac{3.67 \cdot 10^{3}}{T_3^L}\right)$	0.998

The parameters were then fit as discussed in Section 6.2 and the results are shown in Table 8.7. Since the model is already very non-linear and difficult to converge, it was decided to minimize the addition of more non-linearity. As the adjustments for $\mathbf{k^{H2}}$ and $\mathbf{K^{H2}}$ do not vary much, these values were averaged.

The equations in Table 8.7 indicate very good fits, i.e. an R^2 close to 1. This is misleading as, although four points were used, the three runs 4.3-4.5 data points are at very similar temperatures with only run 4.1 at the lower temperature since run 4.2 did not converge. *Thus, neither the equations nor constants should be extrapolated outside the range of 350-380 K!*

8.2.3 Mass transfer coefficients and reaction rate constants

The liquid phase mass transfer coefficient (k^L) appears to be very well predicted by the standard random packing correlations at the higher temperatures and pressures of runs 4.3 to 4.5 where the standard 0.0051 is out by only 6%. At the lower pressures (and temperatures) of run 4.1 the current regression analyses require a significant adjustment of 80%.

The vapour phase mass transfer coefficient is significantly smaller than that predicted from the standard correlations and ranges by a factor of 0.20 to 0.05.

From Table 8.6 it is interesting to note that at low pressures (run 4.1) the hydrogen

conversion is most sensitive to the liquid phase mass transfer coefficient, which would indicate a relatively fast reaction compared to VLE interphase mass transfer. This also holds for the higher pressure runs where a 1% change in the liquid phase mass transfer coefficient results in a 0.28% change in the hydrogen conversion - the largest response in Table 8.6 at high pressures. Additionally, the vapour phase coefficient also has a significant influence on the hydrogen conversion. It should be noted that, at low pressures, the effect of $\mathbf{k^{H2}}$ and $\mathbf{K^{ads}}$ are in the same order of magnitude. However, in terms of hydrogen conversion, it appears that the liquid and vapour mass transfer coefficients are most significant.

The 1-hexene conversion is most sensitive to the 1-hexene absorption equilibrium coefficient at lower pressures. At higher pressures, the mass transfer coefficients also dominate as with the hydrogen conversion.

At low pressures, the sensitivity is most affected by the rate of addition of the first hydrogen to the adsorbed alkene. At higher pressures, this appears to shift to the rate of alkene adsorption and the desorption equilibrium coefficient. The interphase mass transfer coefficients appear to have a negligible effect on the selectivity.

The deviation in the predictions of the alkene adsorption reaction rate constant ($\mathbf{k^{ads}}$), the rate of addition of the first hydrogen to the adsorbed alkene ($\mathbf{k^{iso1/2}}$), and the rate of desorption ($\mathbf{k^{des}}$) all increase significantly from the low to high pressure runs. At the higher pressures, these parameters are underpredicted. In contrast, the deviation in the alkene adsorption equilibrium coefficient ($\mathbf{K^{ads}}$) decreases and it is overpredicted at the higher pressures. From Table 8.6, at high pressures the model appears to be most sensitive to these parameters. The standard error of these parameters are thus low and a high confidence is attached to their regressed values.

In terms of the adsorption and desorption coefficients, it is possible that external mass transfer limitations may be prevalent in the CD column, thus altering the effective rate coefficients. However, these values appear to be underpredicted, which is curious as it is unlikely that the external mass transfer around the catalyst extrudates in the CD column would be better than that of the fine catalyst used in the semi-batch reactor.

Another explanation (and one which was not incorporated in the model) is that of heat transfer limitations. If heat transfer to and from the catalyst is limited, the catalyst temperature will increase as heat generated by the exothermic reaction cannot be removed quickly enough.

If this hypothesis is true, the reaction rates to which the model are sensitive should be underpredicted and would require an adjustment larger than one. Similarly, it would require an overprediction in the equilibrium constants to which the model are sensitive. As shown above, this is true for the high pressure cases.

To verify the assumption, the Mears and Weisz-Prater criteria for external and internal mass transfer (and by analogy heat transfer) limitations (see Section 5.2) were applied

to the average conditions observed for low pressure runs 4.1 and 4.2, and high pressure runs 4.3-4.5. The analysis indicated that for runs 4.1 and 4.2 there are no external (Mears: $0.0483 < 0.15$) nor internal ($C_{WP} = 0.53 << 1$) mass transfer limitations. However, for runs 4.3-4.5 external (Mears: $1.29 > 0.15$) and internal ($C_{WP} = 12.77 >> 1$) mass transfer limitations cannot be neglected. This strengthens the hypothesis that internal heat and mass transfer limitations become significant towards the higher pressure expressions.

Consequently, the equations in Table 8.7 are applicable only to the current system and within the sample space considered. These equations are empirical and compensate for the fact that internal and external mass and heat transfer limitations were not incorporated in the model. *They are specific to the current system and should not be applied outside of the sample space used to fit them.* Despite their empirical nature, they can still supply valuable insight into the CD hydrogenation system considered in this study.

With this information, it is now possible to explore the effect of process variables on the KPI's within the sample space of interest.

8.3 Effect of different variables on the CD hydrogenation system

In the following discussions, all the y-axes of a specific KPI or variable will be plotted on the same axis scale to allow direct order of magnitude trend comparisons between different graphs. In some cases a data point may thus fall outside a graph. The data was generated at $4.0{\cdot}10^5$ Pa, which is central to the 1.7-$6.3{\cdot}10^5$ Pa sample space considered. The full set of base conditions is supplied in Table 8.3.

The liquid and vapour phase compositions at these base conditions are shown in Figure 8.2. Starting just above the reboiler, ca. 1.5 m from the top of the column, there is a step change in (especially) the vapour phase compositions where the non-condensable hydrogen feed point is located. Moving up along the height of the system, it is clear that the hydrocarbon feed point does not have a marked effect on the compositions, but that there is a significant change close to the top, on stages 2-4, where the reactive zone is located. This is followed by large changes in the partial condenser where the temperature is dropped to ca. 280 K (6.25°C).

Figure 8.3 illustrates the temperature profile at these base conditions. Since the components are very close boiling the temperature gradient along the height of the column is less than 1 K, except in the reactive zone where the cold liquid reflux first enters the column. It is thus not surprising that there is a very steep temperature gradient within the reactive zone. Note that the liquid and vapour temperatures follow

each other closely, which is the results both of the good vapour-liquid heat transfer and close-boiling nature of the components.

8.3.1 Pressure

From Section 2, literature indicates that an increase in pressure increases the alkene conversion and also increases the selectivity towards the alkane rather than the isomeric product. This increase in selectivity is clearly reflected in Figure 8.4a. Since the model assumes that hydrogen is consumed only in the hydrogenation reaction and not in the isomerization reaction, the hydrogen conversion also increases as expected.

The reason for the observed trends in conversion and selectivity is a complex interaction between several reaction rates, equilibrium coefficients and vapour mass transfer coefficients.

Figure 8.4b shows the temperature increase in the reactive zone as a function of the changing pressure. This increase has a significant effect on the reaction rate constants as shown in Figure 8.4c and also decreases the vapour phase mass transfer coefficient. The fact that the liquid temperature on stage 2 passes a maximum is difficult to explain. However, it is probable that the reduction in the 2-hexene reactant concentration in the reactive zone (Figure 8.4e) is reducing the amount of exothermic reaction heat generated. Where the liquid temperatures for stages 3 and 4 are leveling off, stage 2 is more quickly affected as it is in direct contact with the cold, falling condenser reflux, which starts to cool it down.

In terms of the reaction rate constants, Figure 8.4c indicates a rapid increase in the 1-hexene adsorption rate, yet Figure 8.4f indicates that the surface concentration of adsorbed 1-hexene decreases. This can be because of 3 possibilities: (1) the driving force is less, i.e. the liquid concentration of 1-hexene is decreasing, (2) there is another reaction rate that is also increasing to consume adsorbed 1-hexene and/or (3) another surface species is displacing the 1-hexene from the surface.

Figure 8.4f indicates that the hydrogen surface concentration is increasing rapidly and adsorbing competitively with the 1-hexene. Therefore, although the 1-hexene bulk concentration remains relatively constant (Figure 8.4e) while its surface coverage decreases, thus increasing its adsorption driving force, the hydrogen adsorption is still preferred.

It is interesting to note that the hydrogen liquid concentration is essentially zero (Figure 8.4e) indicating that vapour-liquid interphase mass transfer limitations cannot be neglected, as was also seen in Table 8.6.

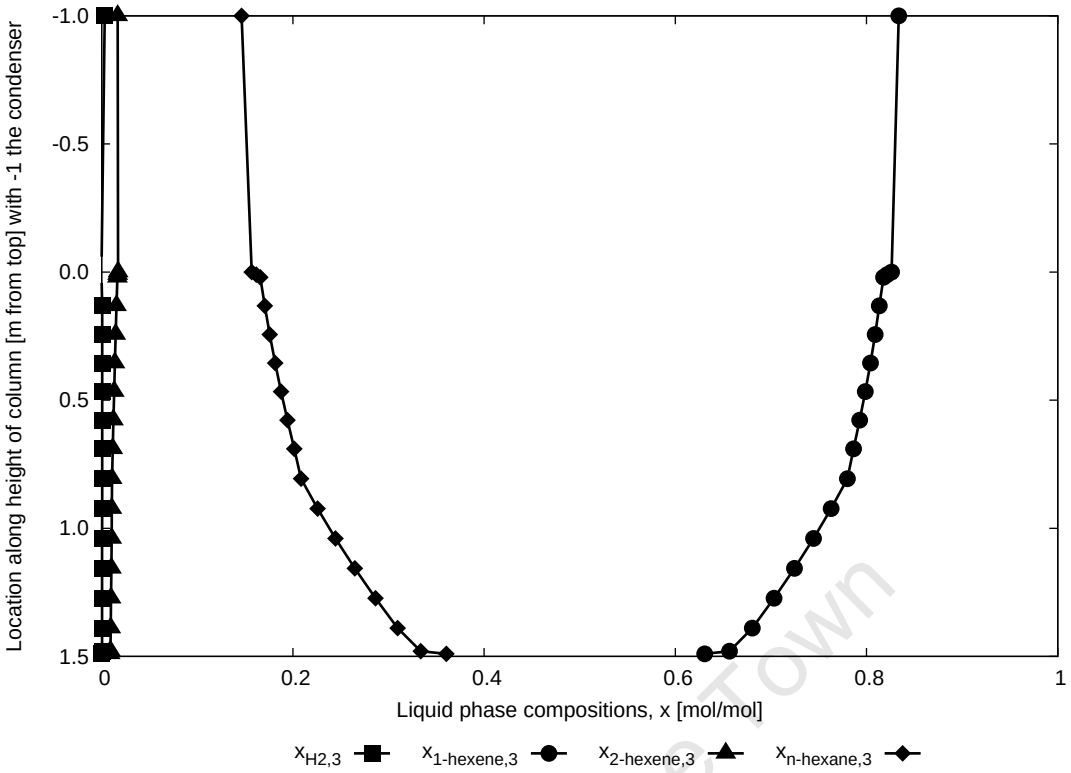

(a) Liquid compositions

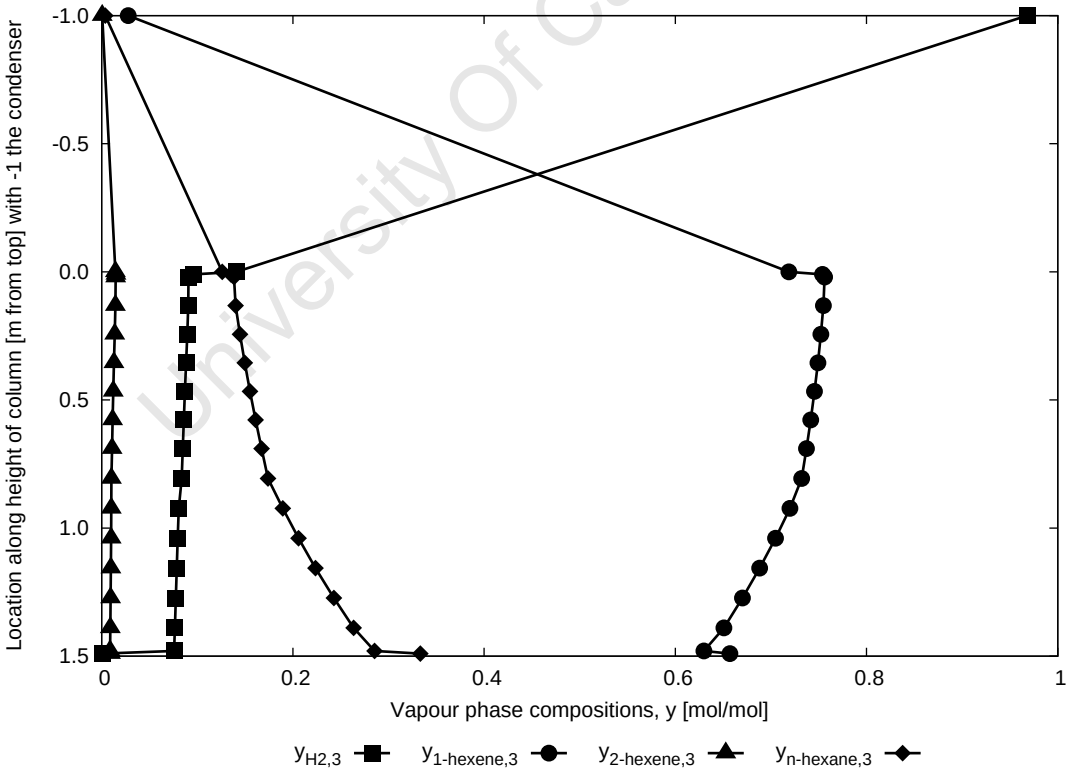

(b) Vapour compositions

Figure 8.2: Predicted composition profiles for the input specifications defined in Table 8.3.

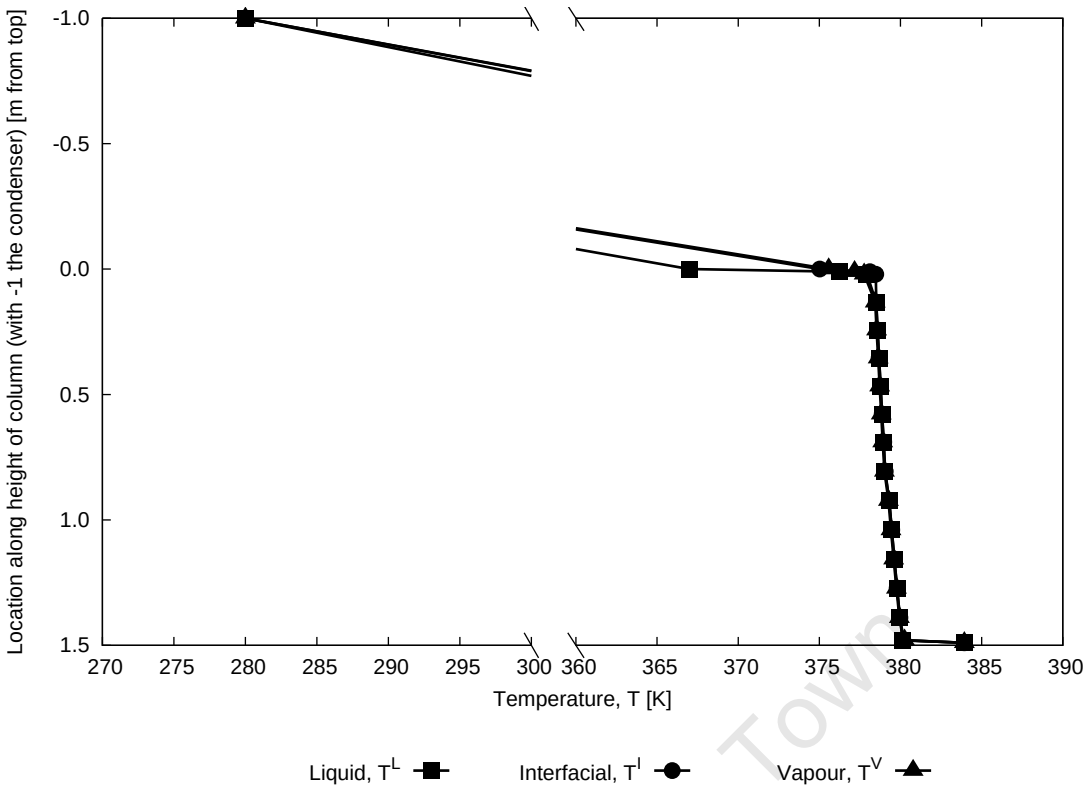

Figure 8.3: Predicted temperature profile for the input specifications defined in Table 8.3.

8.3.2 Hydrogen feed flow rate

From Figure 8.5a, an increase in the hydrogen feed flow rate decreases the hydrogen conversion, but increases the 1-hexene conversion. At first glance the increase in selectivity thus appears counter-intuitive. Since the model assumes only isomerization and hydrogenation to occur, the moles of hydrogen converted are equal to the n-hexane produced. A decrease in hydrogen conversion should thus prompt n-hexane production to decrease while the fact that 1-hexene conversion still increases should indicate an increase in 2-hexene production to compensate: thus the selectivity of 1-hexene towards n-hexane should decrease. However, from eq. 6.23, this is only true at a constant hydrogen feed flow rate and in this case the increase in the latter dominates the equation and effects an increase in selectivity.

As expected, an increase in the non-condensable hydrogen decreases the temperature in the reactive zone, as indicated in Figure 8.5b. From Figure 8.5f, the hydrogen availability on the surface increases, which must be because the hydrogen adsorption equilibrium constant dominates, since the VLE equilibrium constant increases by 5-12% and the adsorbtion reaction rate constant (Figure 8.5c) decreases by ca. 70% - both of which should decrease the hydrogen availability. Note that, since the equations are non-linear, the magnitude of the input disturbance does not necessarily cause an equally large effect in the output disturbance.

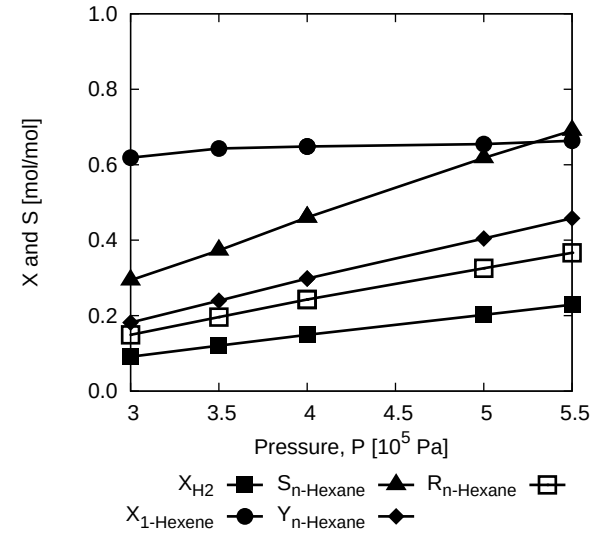

(a) Conversion and selectivity

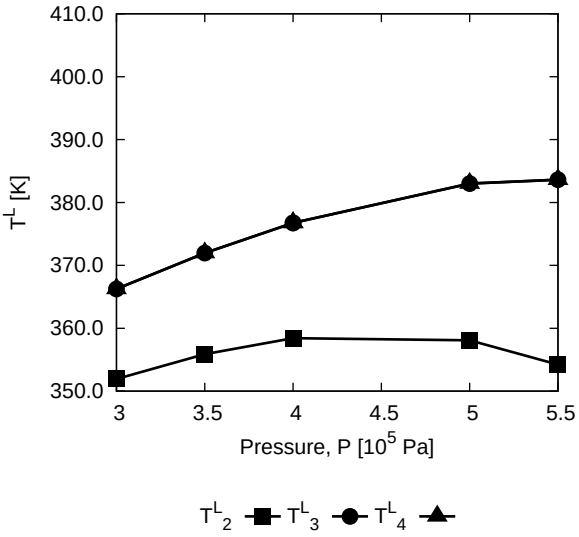

(b) Liquid temperature on stages 2 to 4

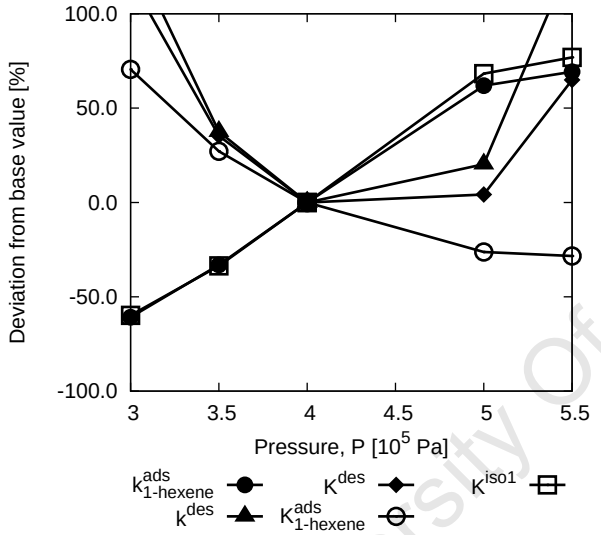

(c) Reaction kinetics

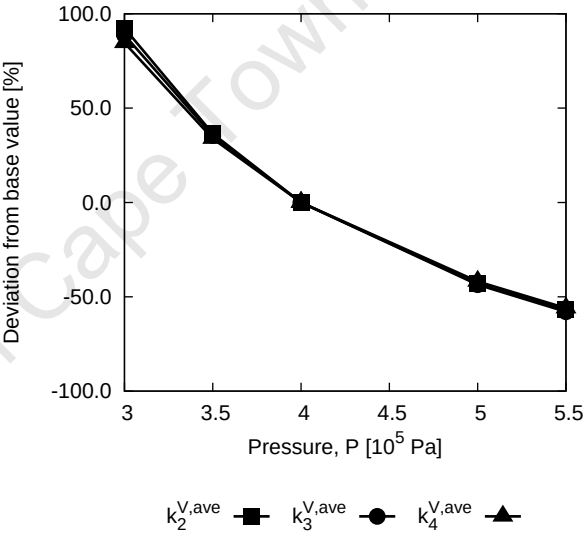

(d) Vapour phase mass transfer coefficient

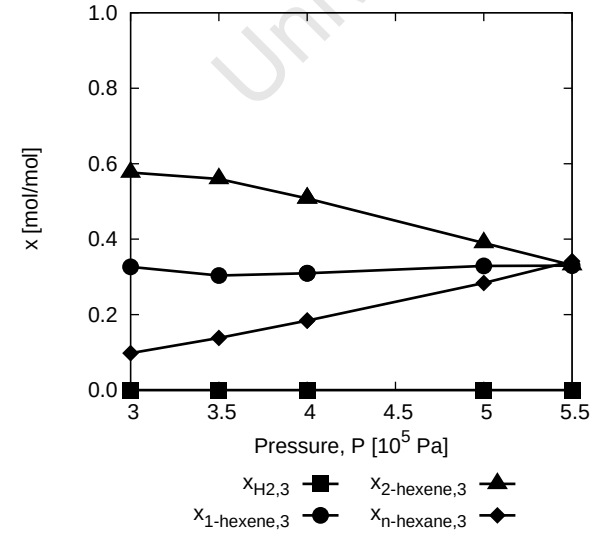

(e) Middle reactive zone liquid phase compositions

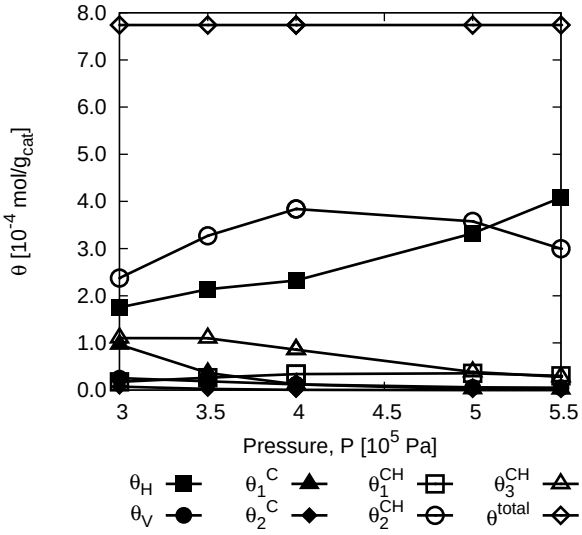

(f) Surface species concentrations

Figure 8.4: Effect of the condenser pressure on the KPI's.

From Figure 8.5a, the increase in the hydrogen feed flow rate increases the yield of n-hexane (based on the 1-hexene fed and the n-hexane reporting to the bottoms stream) from 6.8 to 26.9 mol% and also increases the purity of the bottoms product from 9.5 to 41.1 mol% n-hexane. However, there is an 8% reduction in the bottoms molar flow rate as more organics now exit with the off-gas due to a higher fraction in the non-condensable.

8.3.3 Recycle ratio

From Figure 8.6a, there is very little benefit in terms of the conversions, yield and selectivity to increase *reflux ratio*. Again, the reactive zone temperature is not significantly affected and there are thus negligible changes in the reaction kinetics and vapour mass transfer coefficient. However, there is a significant improvement of ca. 0.10 to 0.22 $\mathrm{mol}_{n-hexaneinbottoms}/\mathrm{mol}_{1-hexenefed}$ in the n-hexane recovery to the bottoms stream by increasing the recycle ratio from 15 to 50. This is expected from distillation theory since (with all other variables constant) there is a maximum separation efficiency that can be achieved in any distillation column as the recycle ratio is increased [Seader & Henley, 1998]. Thus, there is a recycle ratio beyond which no improvement in separation can be achieved. Since neither the conversions, yield nor selectivity change significantly, the improvement in the n-hexane recovery is essentially solely attributable to the enhanced separation.

8.3.4 1-Hexene feed flow rate

As is clear from Figure 8.7, a decrease in the 1-hexene conversion significantly decreases the 1-hexene conversion from ca. 80 to 40%. The yield and selectivity of n-hexane also decreases significantly. The hydrogen conversion increases slightly (less than 1%). All these variables appear to approach some optimum as their gradients start to decrease. The recovery of the n-hexane to the bottoms passes a maximum of ca. 14% at ca. a 5 kmol/s 1-hexene feed flow rate.

The reactive zone liquid temperature indicates a negligible change, which is reflected in a negligible change in the reaction rate constants. The vapour phase mass transfer coefficient also essentially remains constant.

From Figure 8.7f, it appears that the decrease in the 1-hexene conversion is attributable to the reaction rate constants, which preferentially allows one of the half-hydrogenated states to build up on the catalyst surface. This increase causes a similar decrease in the hydrogen availability on the surface. Both the half-hydrogenated state and adsorbed hydrogen surface concentration appear to approach an optimum value, which explains the observation made earlier that the conversions, selectivity and yield are approaching optima.

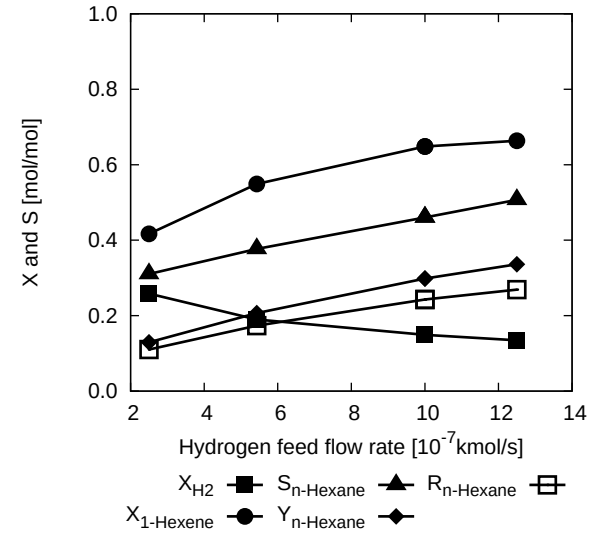

(a) Conversion and selectivity

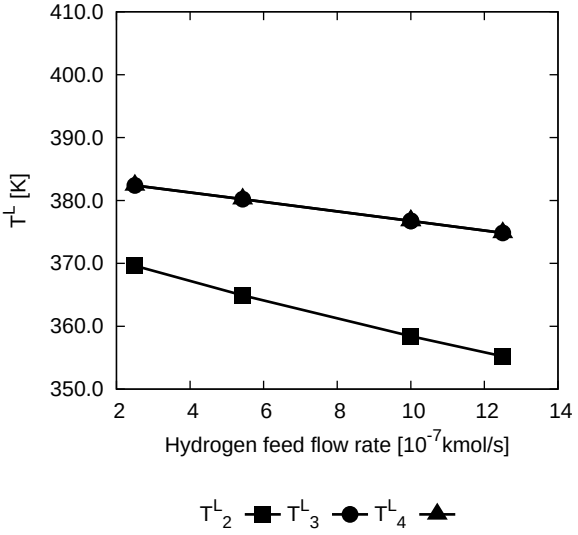

(b) Liquid temperature on stages 2 to 4

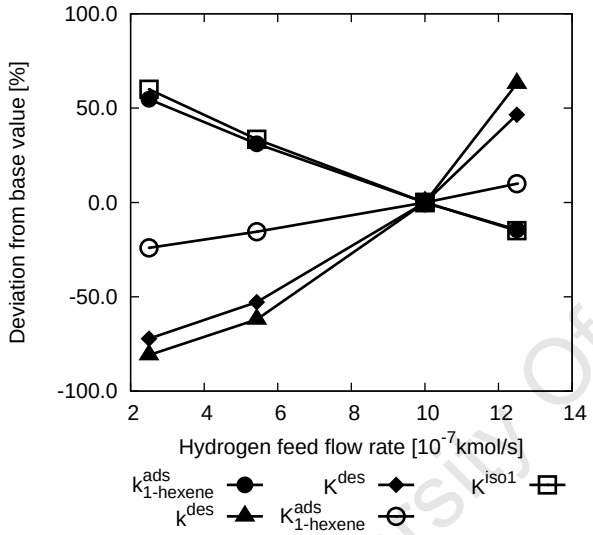

(c) Reaction kinetics

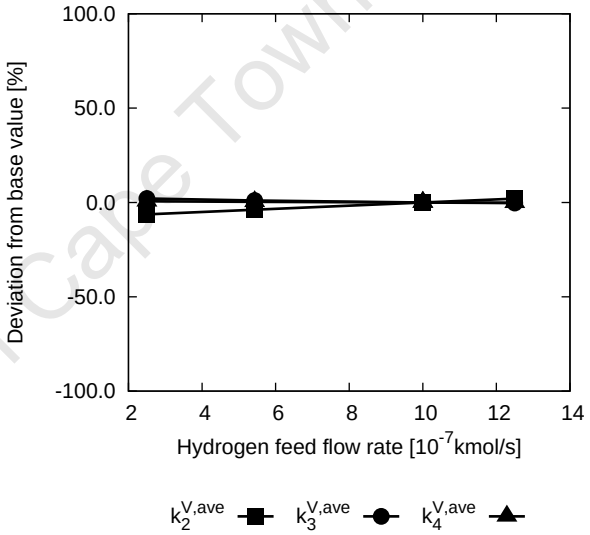

(d) Vapour phase mass transfer coefficient

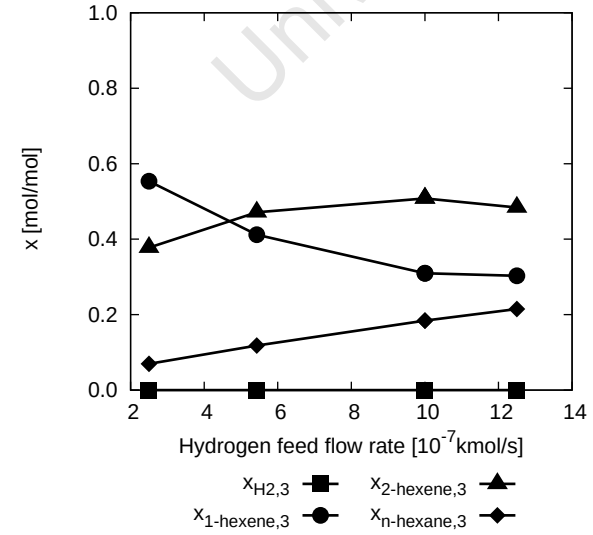

(e) Middle reactive zone liquid phase compositions

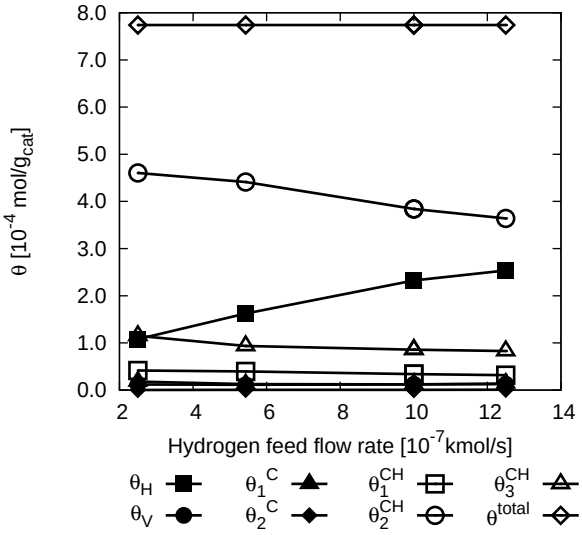

(f) Surface species concentrations

Figure 8.5: Effect of the hydrogen feed flow rate on the KPI's.

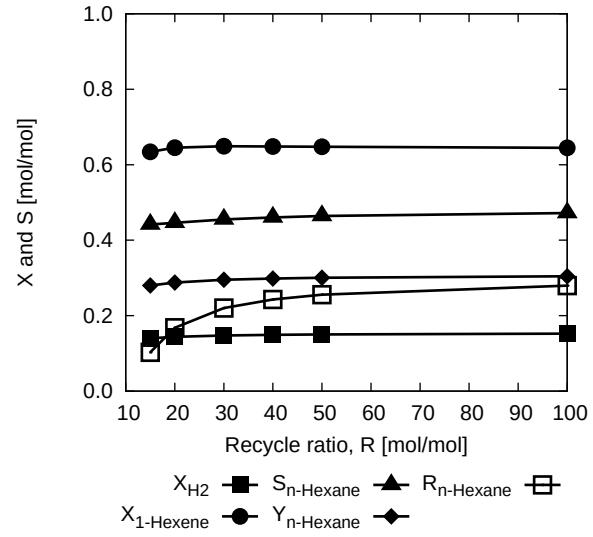

(a) Conversion and selectivity

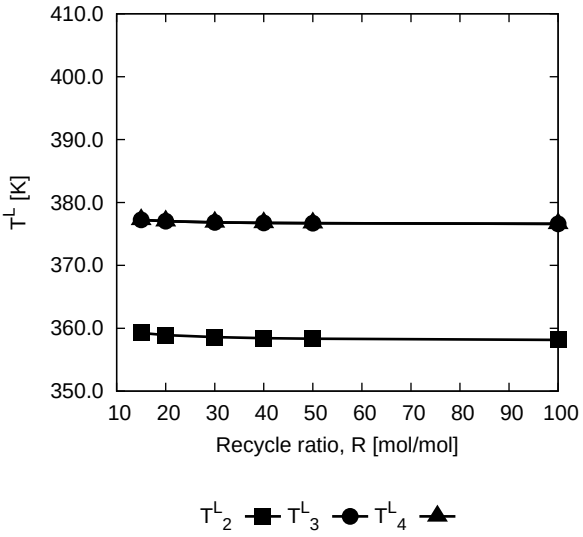

(b) Liquid temperature on stages 2 to 4

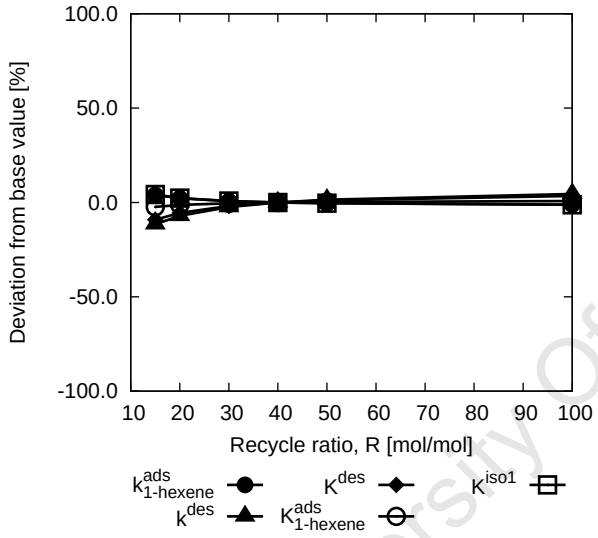

(c) Reaction kinetics

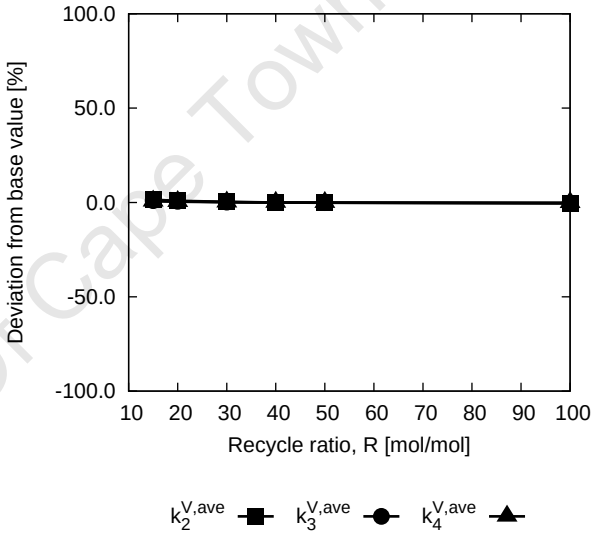

(d) Vapour phase mass transfer coefficient

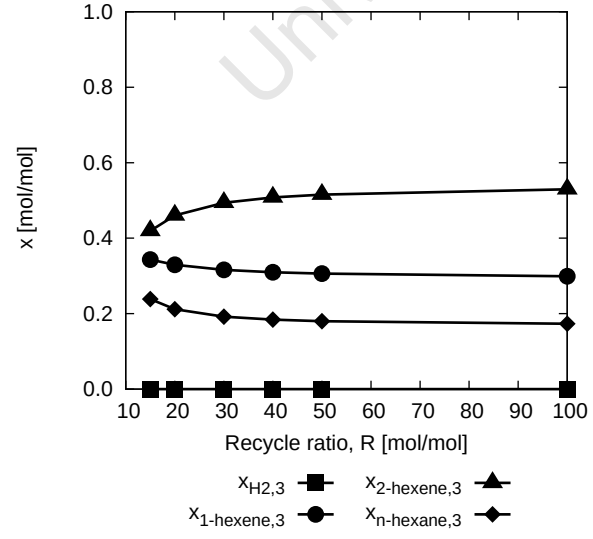

(e) Middle reactive zone liquid phase compositions

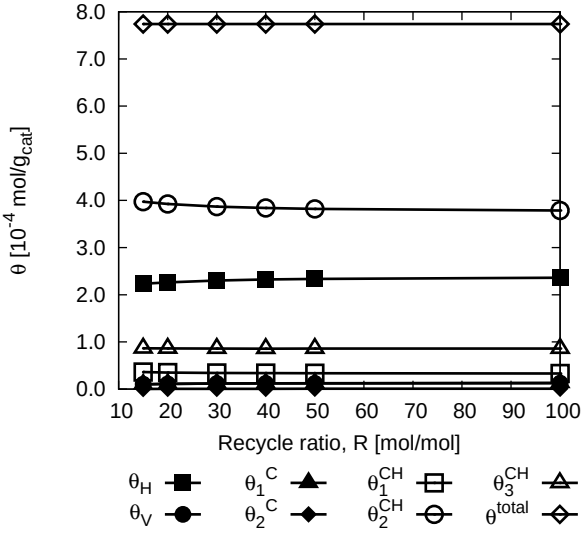

(f) Surface species concentrations

Figure 8.6: Effect of the recycle ratio on the KPI's.

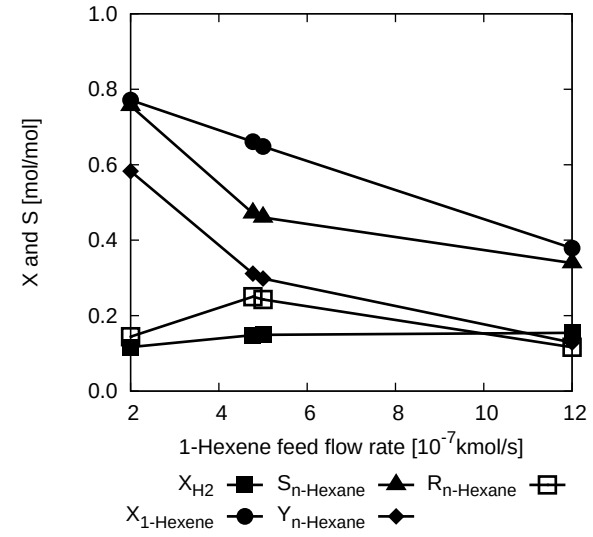

(a) Conversion and selectivity

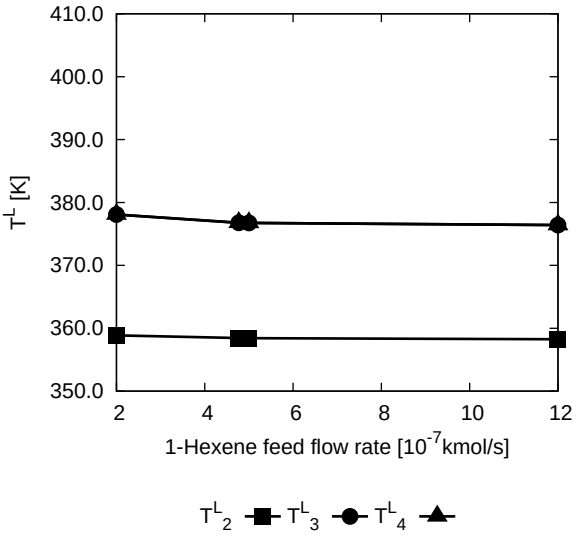

(b) Liquid temperature on stages 2 to 4

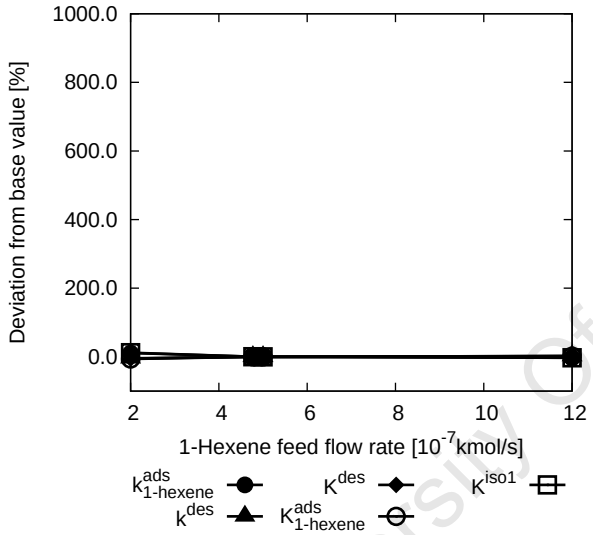

(c) Reaction kinetics

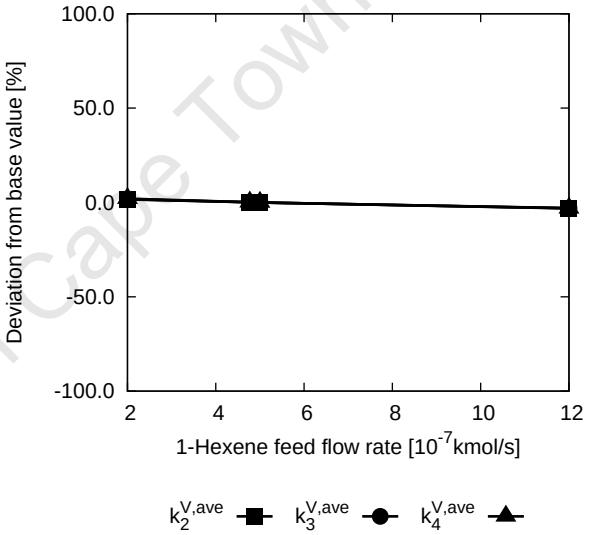

(d) Vapour phase mass transfer coefficient

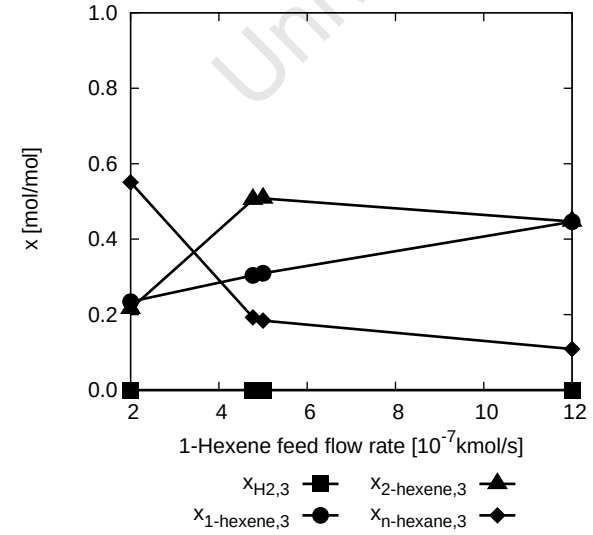

(e) Middle reactive zone liquid phase compositions

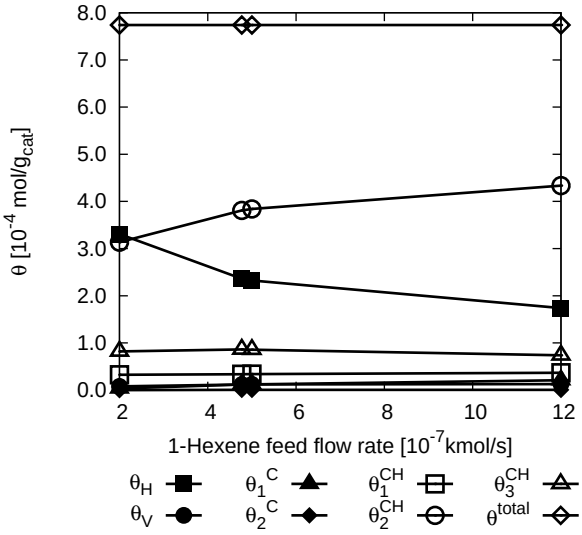

(f) Surface species concentrations

Figure 8.7: Effect of the 1-hexene feed flow rate on the KPI's.

8.3.5 Variables not affecting the KPI's

The following variables were found not to have an appreciable effect on the KPI's:

- Condenser temperature.
- Hydrogen feed location.
- 1-Hexene feed location.

All of them share the common fact that they do not appreciably affect the column temperature.

The *condenser temperature* (Figure 8.8) has little effect due to sufficiently high vapour-liquid heat transfer coefficients that allow the entering reflux to quickly adjust to the temperature of the rising vapour (see Figure 8.3).

Since *hydrogen* is non-condensable, shifting its *feed location* (Figure 8.10) has a negligible effect on the temperature within the reactive zone - as long as it is fed below the reaction. It is clear, however, that the hydrogen feed location must become significant at some point as, if the hydrogen is fed above the reactive zone, the VLE and hydrogen concentration within the reactive zone would be significantly different. To ensure a significant amount of hydrogen, it must be fed below the reactive zone, otherwise only the small amount of dissolved hydrogen (cf. Figures 8.10e) from the condenser will be recycled back into the column.

The *1-hexene feed location* (Figure 8.9) can at best shift the 1-hexene concentration within the reactive zone. However, this has little effect on the reactive zone temperature since the organic components present (namely 1-hexene, 2-hexene and n-hexane) are very close boiling. Thus, a change in their composition has little effect on the column temperature profile. In any event, Figure 8.9e indicates that a change in the 1-hexene feed location has negligible effect on the 1-hexene concentration in the reactive zone.

8.4 Summary of results

The CD system was operated and generated data successfully. The highest quality data was then identified and used to fit the deviation factors of the reaction kinetic and vapour-liquid mass transfer coefficients for the specific system.

It proved to be difficult to fit the model to experimental data. This was due to several factors:

- Inaccuracies introduced by instrumentation.
- Complex, non-linear reaction kinetics.
- Long required computer calculation times.

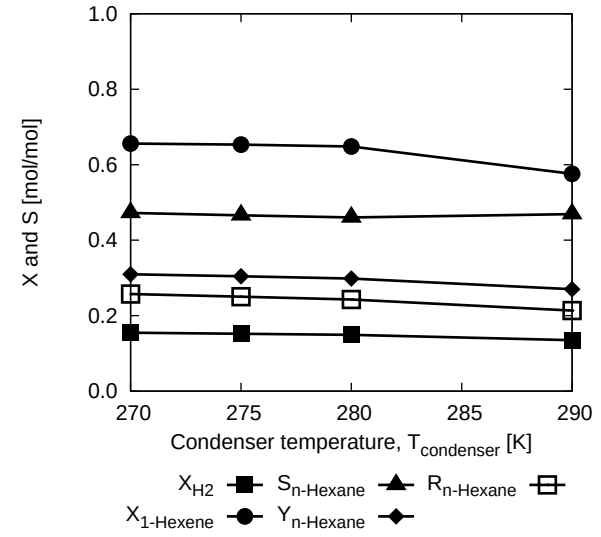

(a) Conversion and selectivity

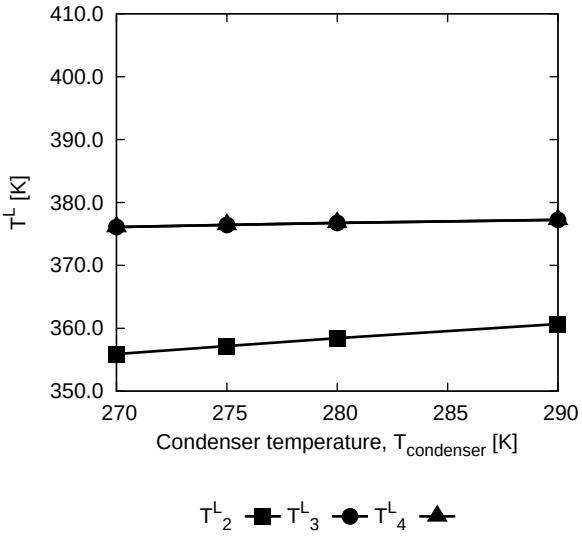

(b) Liquid temperature on stages 2 to 4

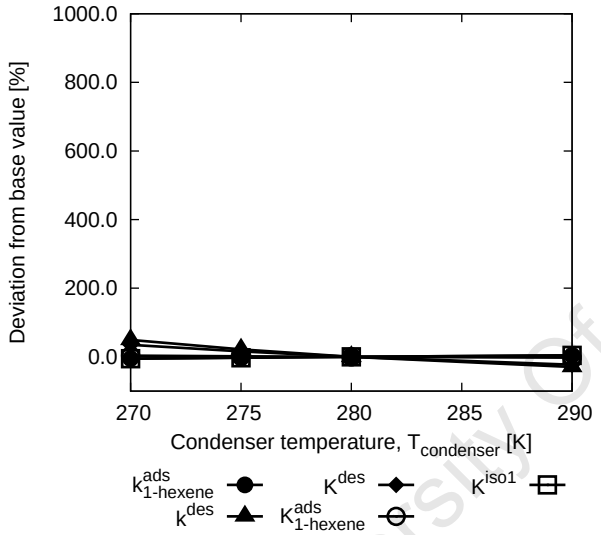

(c) Reaction kinetics

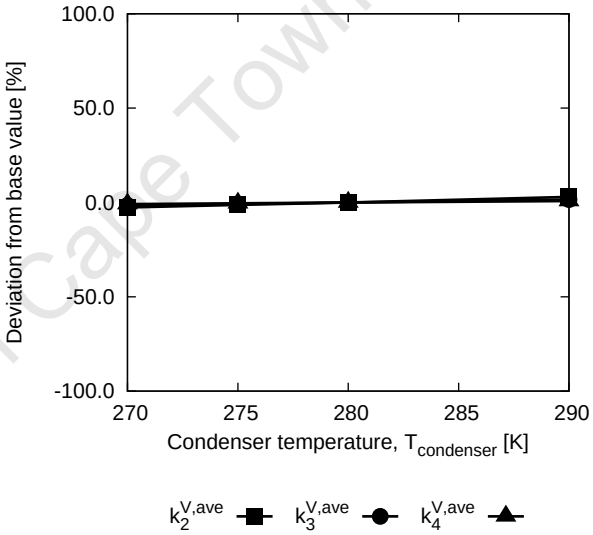

(d) Vapour phase mass transfer coefficient

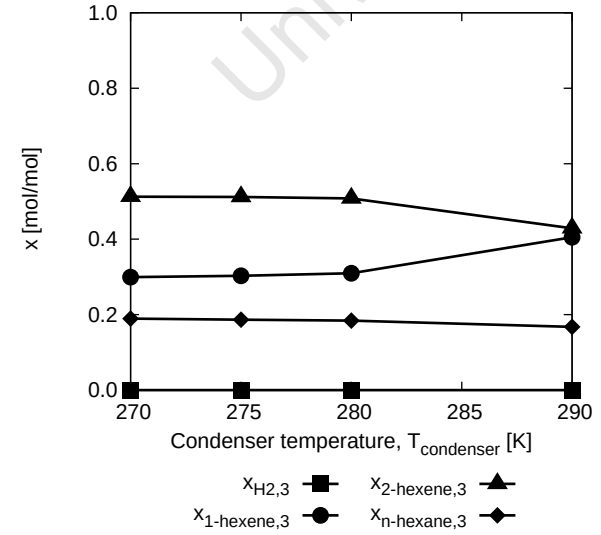

(e) Middle reactive zone liquid phase compositions

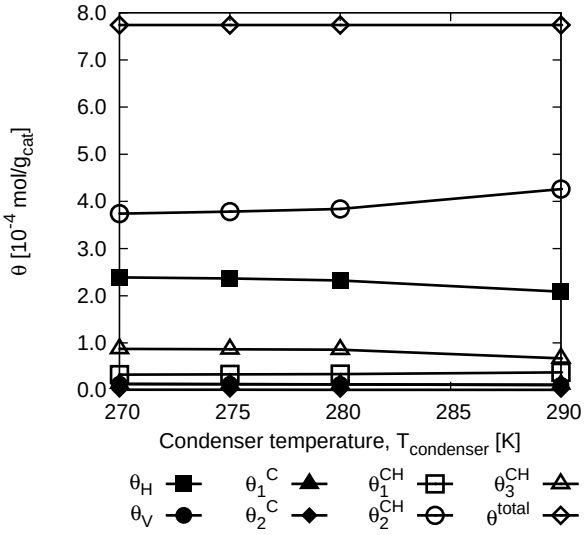

(f) Surface species concentrations

Figure 8.8: Effect of the condenser temperature on the KPI's.

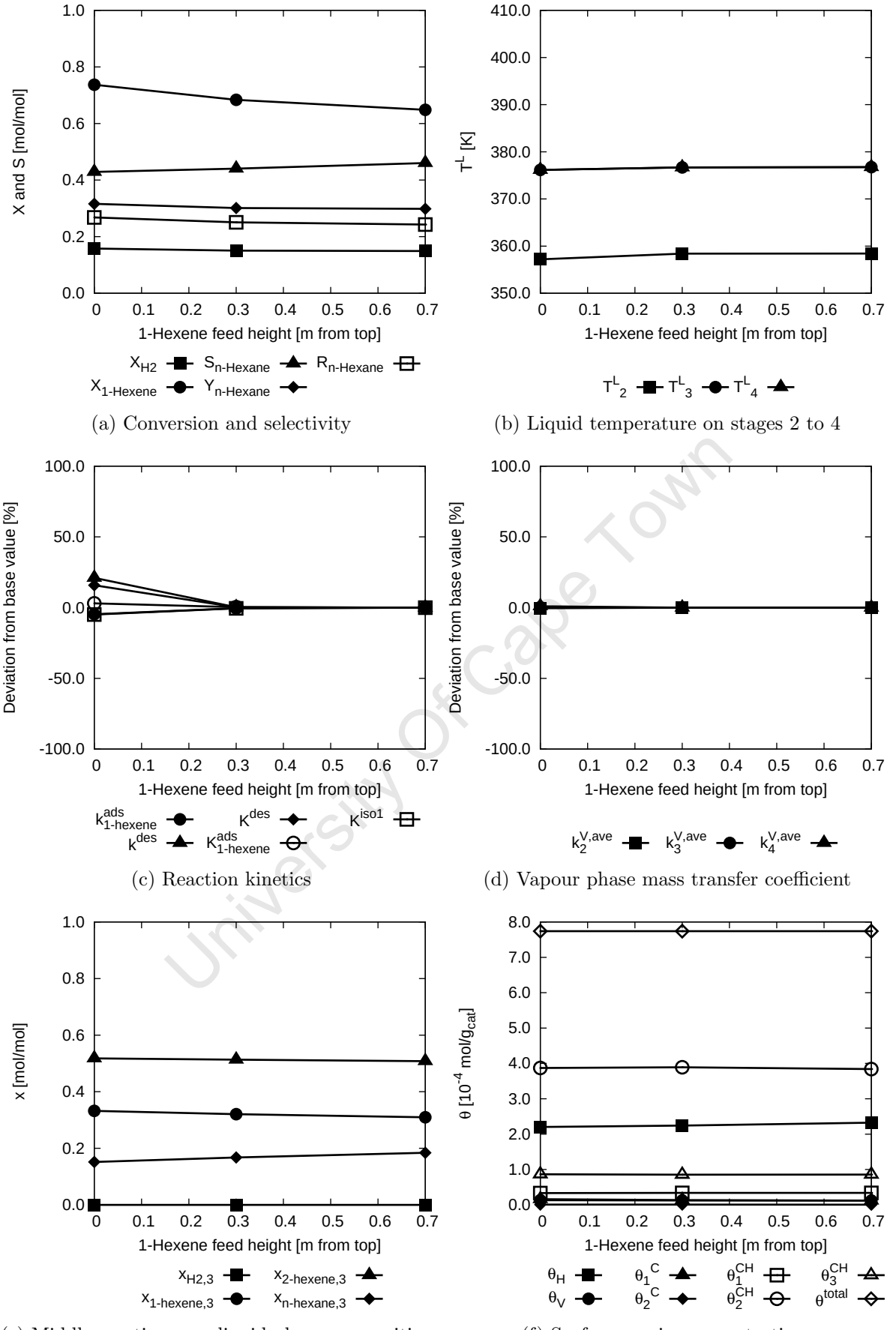

(a) Conversion and selectivity

(b) Liquid temperature on stages 2 to 4

(c) Reaction kinetics

(d) Vapour phase mass transfer coefficient

(e) Middle reactive zone liquid phase compositions

(f) Surface species concentrations

Figure 8.9: Effect of the 1-hexene feed location on the KPI's.

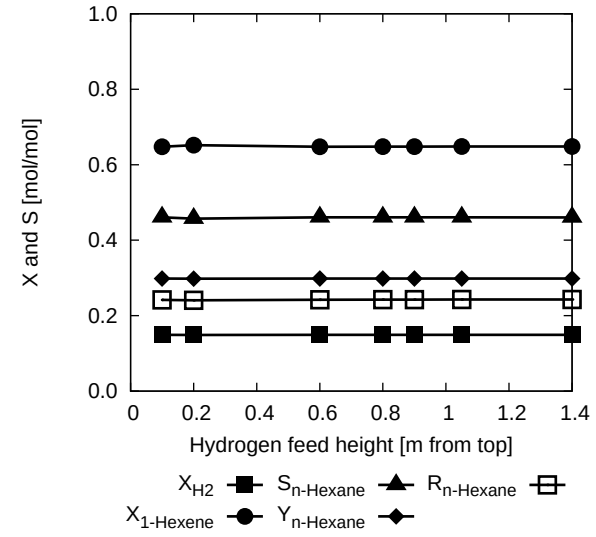

(a) Conversion and selectivity

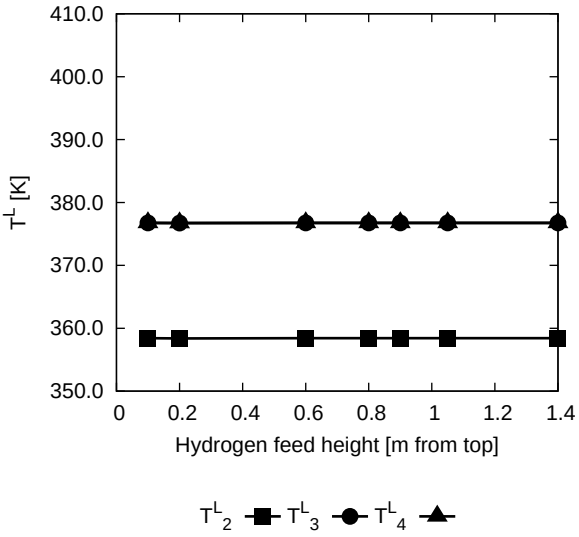

(b) Liquid temperature on stages 2 to 4

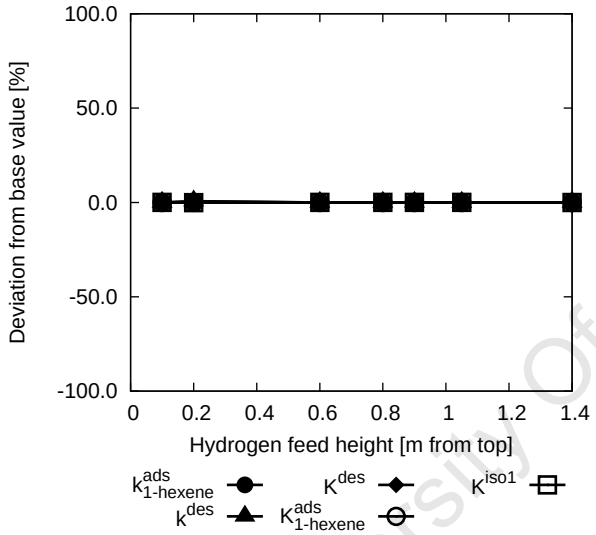

(c) Reaction kinetics

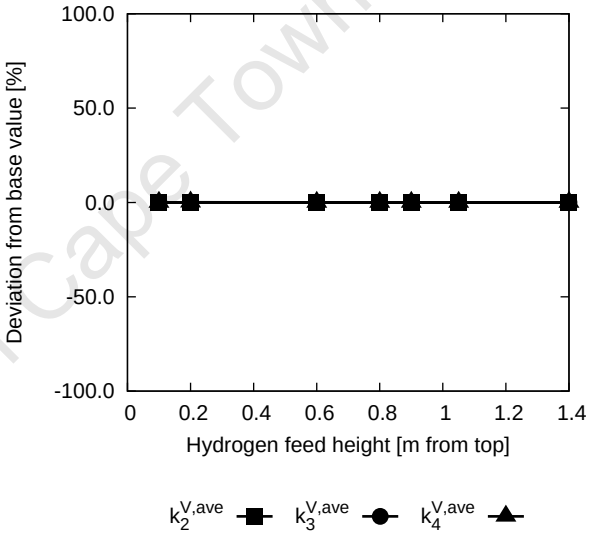

(d) Vapour phase mass transfer coefficient

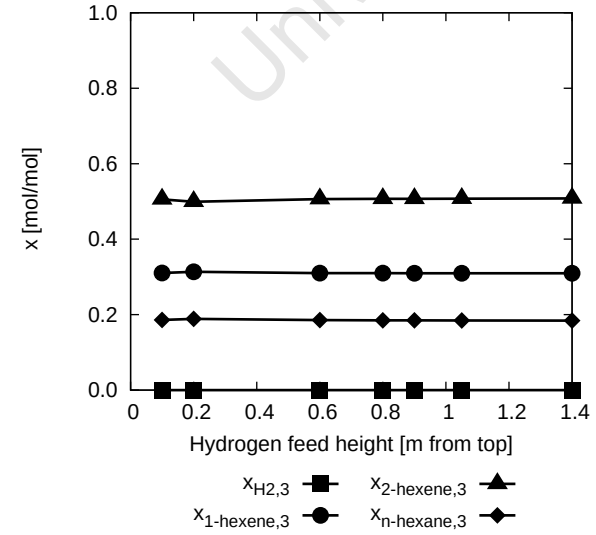

(e) Middle reactive zone liquid phase compositions

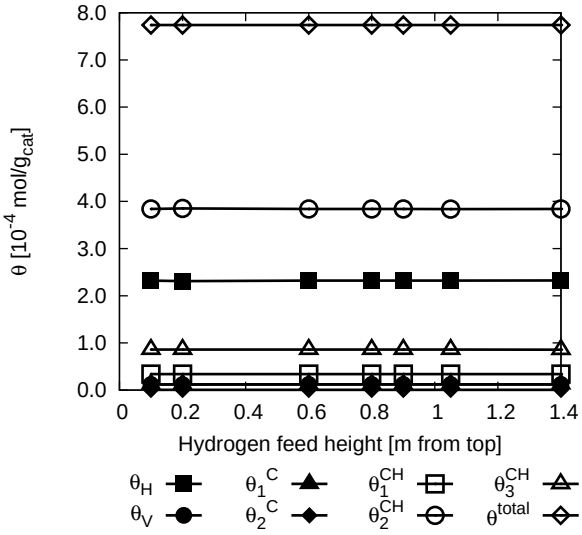

(f) Surface species concentrations

Figure 8.10: Effect of the hydrogen feed location on the KPI's.

To eleviate these issues, the following can be recommended for future work:

- Installation of a larger quantity of temperature measuring devices in and around the reactive zone to increase the temperature resolution in the zone.
- More detailed, separate studies of the vapour-liquid mass and heat transfer on the catalyst.
- The use of analytical derivatives during calculation of the Jacobian.

The resulting mathematical description of the model fit the data to a reasonable accuracy (CV $< 40\%$) and exhibited the correct trends in the KPI's. The KPI's were less well predicted at the lower pressures and were out by as much as 36%. At higher pressures, the conversions were predicted to within several percent.

Significant adjustments were necessary to the mass transfer and reaction rate constants in order to make the model fit the experimental data. Adjustment to the vapour-liquid mass transfer coefficients was not unexpected due to the different catalyst geometry used in the CD column compared to the semi-batch kinetics experiments (see Section 4). Adjustments to the reaction rate constants suggested the possibility of internal and external catalyst heat and mass transfer limitations.

The KPI's were found to be sensitive to the vapour-liquid mass transfer coefficients as expected.

Pressure and the hydrogen feed flow rate were found to influence the KPI's significantly. In both cases it appeared that the temperature was the main driving force for change as it significantly affected the reaction kinetics and mass transfer coefficients.

It was found that inclusion of Langmuir-Hinshelwood kinetics can elucidate macroscopically observed effects by explaining the catalyst surface coverage.

The following is recommended for future research:

- Inclusion of internal and external mass and heat transfer effects.
- Testing of the wetting characteristics of the catalyst.
- Experimental verification of the findings.
- Adjustment of the catalyst properties to the compliment kinetics and mass transfer trends. A better understanding of the Langmuir-Hinshelwood kinetics and the way they interact with the rest of the system could allow the design of catalysts tailored for a specific CD application.

Chapter 9

Conclusions

Fundamental Langmuir-Hinshelwood kinetics were derived for the particular reactive system and fit to experimental data with an acceptably accurate coefficient of variation of less than 40%. It was shown that the 1-hexene and hydrogen adsorption rates were rate controlling in this particular case. A rigorous CD model was also developed based on a standard non-equilibrium model with the included fundamental reaction kinetics. The deviations of the predicted mass transfer coefficients and reaction kinetics were then determined by fitting predictions to the experimentally generated 1-hexene CD hydrogenation data for a low ($1.7 \cdot 10^5$ Pa) and high pressure ($6 \cdot 10^5$ Pa) case. Although the non-linearity of the system made regression difficult, it was possible to fit a low and high pressure case with a coefficient of variation of less than 40%.

The sensitivity of the model to the reaction kinetics and vapour-liquid mass transfer coefficients could be determined. The system appeared to be most sensitive to the column pressure and the hydrogen feed flow rate. Both have a significant effect on the average temperature in the reactive zone, which in turn as a strong effect on the reaction kinetics and vapour-liquid mass transfer coefficients. In contrast, the condenser temperature, 1-hexene feed flow rate, 1-hexene feed location and hydrogen feed location had a negligible effect, while the reflux ratio was (as expected) only significant at low values where it influences the column's separation efficiency.

Thus, it is believed that the goal has been met.

In terms of the key questions, internal and external catalyst mass and heat transfer were found to be significant in the CD experiments. Their effects could be compensated for via empirically fitting the deviation of their observed values to that predicted. The validity of the regressed process parameters was tested via several statistical techniques, including the coefficient of variation, which is an indication of the "goodness" of the fit. The impacts of the process parameters were considered via case studies and sensitivity analyses.

Using the final CD model, it was shown at lower pressure that the hydrogen conversion is relatively sensitive to the 1-hexene adsorption rate, hydrogen adsorption rate

and the liquid phase mass transfer coefficient. The 1-hexene conversion is also sensitive to these parameters, but twice as sensitive to the 1-hexene adsorption equilibrium. Additionally, the reaction step involved in the first hydrogen addition is also significant. In terms of selectivity, it is this reaction step and the 1-hexene adsorption that controls n-hexane selectivity.

Towards higher pressures, vapour-liquid mass transfer dominates both the hydrogen and 1-hexene conversions. Selectivity appears largely insensitive to any of the parameters, though it is most affected by the 1-hexene adsorption and n-hexane desorption.

An increase in the hydrogen feed flow rate increases the recovery of n-hexane to the bottoms product. However, it also decreases the bottoms flow rate and the hydrogen conversion, which indicates that there must be an optimal economic operating point. An increase in the 1-hexene feed flow rate causes the n-hexane recovery to the bottoms to pass a maximum. This is caused by competitive adsorption between the hexenes and hydrogen, which diminishes the hydrogen surface coverage on the catalyst.

Thus, it is believed that the hypothesis has been met: rigorous modelling of vapour-liquid mass transfer and reaction kinetics add value to our understanding of the macroscopically observed phenomena in 1-hexene hydrogenation CD.

Chapter 10

Future research

It is recommended that effort be expended towards analytically calculating as much of the Jacobian as possible. This upfront time investment can greatly facilitate analysis later.

Analysis of the data has highlighted several aspects that may be improved upon in future experiments.

In terms of the physical system, a more accurate, online manometer is suggested to measure the pressure fall across the reactor. Pressure drop can then be included in the model for data fitting purposes. It can also be used to monitor column flooding and liquid holdup. The temperature profile resolution in the reactor should also be increased, especially in the reactive zone where calculations show a sharp temperature gradient. Liquid mass flow meters may also improve the mass balance.

Most importantly, it is recommended to make predictions based on the regressed model and to experimentally verify the model at other values within the data space considered. The pressure and temperature range can also be expanded. Considering very different reaction systems, such as e.g. etherification, is not currently recommended.

The kinetics model should be reassessed. Though it describes the data, the negative activation energies are most probably not fundamentally interpretable. This could be due to numerical convergence errors, experimental errors, activation energies close to zero that direct the search algorithm to negative values, the insensitivity of the model to those parameters within the region of interest, a high degree of correlation between parameters (see Section 6.1) and/or the fact that the model is fundamentally not an accurate description of the system. Since a high degree of correlation has been found and since the model is insensitive to several of the reaction steps after the initial hydrogen and alkene adsorption, the problem could be there. More experimental data, including data at more severe conditions, may elucidate the true reaction kinetics.

Several variables may still be considered without alteration to the CD column or the reaction system itself. These include experimentally changing the 1-hexene feed location, hydrogen feed location, reactive zone location, reactive zone designs, the addition of a

third hydrocarbon feed component such as one with a lower hydrocarbon number, say n-pentane, that will increase the temperature gradient in the column, but not the operating pressure, which has only been tested up to $6{\cdot}10^5$ Pa(a).

Lastly, the external and internal mass transfer effects within the catalyst should be better understood, both via predictive modelling and experimentation. It is recommended that this be approached in a separate experimental system (similar to the approach followed to determine the reaction kinetics) and then built into the CD column model. Additionally, a better understanding of the degree of wetting of the catalyst is required.

REFERENCES

Adams, I.I., Thomas, A., & Seider, Warren D. 2009. Semicontinuous Reactive Extraction and Reactive Distillation. Chemical Engineering Research and Design, **87**(3), 245 – 262.

Al-Arfaj, Muhammad A., & Luyben, William L. 2000. Effect of Number of Fractionating Trays on Reactive Distillation Performance. AIChE Journal, **46**(12), 2417 – 2425.

Alejski, Krzysztof, & Duprat, Franoise. 1996. Dynamic Simulation of the Multicomponent Reactive Distillation. Chemical Engineering Science, **51**(18), 4237 – 4252.

Alver, Morten O., Batada, Nizar N., Baylac, Michel, Brix, Kolja, Darboux, Fréd'eric, Gardey, Guillaume, d'Haese, Cyrille, Murshed, S M Mahbub, Nagel, Raik, Oezbek, Christopher, Reitmayr, Ellen, Renckens, Gert, Rudert, Andreas, Spiegel, Michael, Stervbo, Ulrik, Waβenhoven, Dominik, Wegner, Joerg K., Wrighton, Michael, Willighagen, Egon, & Zieren, Jörg. 2008. JabRef version 2.4.2.

Anderson, E., Bai, Z., Bischof, C., Blackford, S., Demmel, J., Dongarra, J., Du Croz, J., Greenbaum, A., Hammarling, S., McKenney, A., & Sorensen, D. 1999. LAPACK Users' Guide. Third edn. Philadelphia, PA: Society for Industrial and Applied Mathematics.

Atkins, P.W. 1998. Physical Chemistry. Oxford University Press.

Augustine, Robert L. 1996. Heterogeneous Catalysis for the Synthetic Chemist. Marcel Dekker, Inc.

Backhaus, Arthur A. 1922. Apparatus for Producing High Grade Esters. United States Patent Number 1403224.

Backhaus, Arthur A. 1923a. Apparatus for Producing High Grade Esters. United States Patent Number 1454462.

Backhaus, Arthur A. 1923b. Process of Esterification. United States Patent Number 1454463.

Backhaus, Arthus A. 1921. Continuous Process for the Manufacture of Esters. United States Patent Number 1400849.

Barbosa, D., & Doherty, M.F. 1987. A New Set of Composition Variables for the Representation of Reactive Phase Diagrams. Proceeding of the Royal Society A, **413**, 459–464.

Barbosa, Domingos, & Doherty, Michael F. 1988. The Simple Distillation of Homogeneous Reactive Mixtures. Chemical Engineering Science, **43**(3), 541–550.

Baur, R., & Krishna, R. 2003. Distillation Column with Reactive Pump Arounds: an Alternative to Reactive Distillation. Catalysis Today, **79-80**(Apr.), 113–123.

Baur, R., & Krishna, R. 2004. Distillation Column with Reactive Pump Arounds: an Alternative to Reactive Distillation. Chemical Engineering and Processing, **43**(3), 435–445.

Baur, R., Higler, A. P., Taylor, R., & Krishna, R. 2000a. Comparison of Equilibrium Stage and Nonequilibrium Stage Models for Reactive Distillation. Chemical Engineering Journal, **76**(1), 33–47.

Baur, R., Taylor, R., & Krishna, R. 2000b. Development of a Dynamic Nonequilibrium Cell Model for Reactive Distillation Tray Columns. Chemical Engineering Science, **55**(24), 6139 – 6154.

Baur, R., Taylor, R., & Krishna, R. 2001. Dynamic Behaviour of Reactive Distillation Tray Columns Described with a Nonequilibrium Cell Model. Chemical Engineering Science, **56**(4), 1721 – 1729.

Bird, R. Byron, Stewart, Warren E., & Lightfoot, Edwin N. 2002. Transport Phenomena. Second edn. John Wiley & Sons, Inc.

Bond, G. C., & Winterbottom, J. M. 1969. Hydrogenation of olefins. Part 6.Reaction of n-butenes with hydrogen and with deuterium over alumina- supported palladium. Trans. Faraday Soc., **65**, 2779 – 2793.

Bond, G.C., & Wells, P.B. 1964. The Hydrogenation of Olefins. Advances in Catalysis, **15**, 92–221.

Bravo, Jose L., & Fair, James R. 1982. Generalized Correlation for Mass Transfer in Packed Distillation Columns. Industrial & Engineering Chemistry Process Design and Development, **21**(1), 162–170.

Buchaly, Carsten, Kreis, Peter, & Gorak, Andrzej. 2007. Hybrid Separation Processes-Combination of Reactive Distillation with Membrane Separation. Chemical Engineering and Processing, **46**(9), 790–799.

Campelo, J.M., Garcia, A., Luna, D., & Marinas, J.M. 1982. Liquid Phase Catalytic Hydrogenation of 1-Hexene on AlPO4-supported nickel catalysts. Applied Catalysis, **1982**(3), 315–325.

CDTech. 2009. CDTech webpage. http://www.cdtech.com/.

Chandra, P. V. S. Ravi, & Venkateswarlu, Ch. 2007. Multistep Model Predictive Control of Ethyl Acetate Reactive Distillation Column. Indian Journal of Chemical Technology, **14**(4), 333–340.

Chemtech, Sulzer. 2003. Structured Packings for Distillation, Absorption and Reactive Distillation. Sulzer.

Chen, Jian, Fischer, Kai, & Gmehling, Jürgen. 2002. Modification of PSRK Mixing Rules and Results for Vapor-Liquid Equilibria, Enthalpy of Mixing and Activity Coefficients at Infinite Dilution. Fluid Phase Equilibria, **200**(2), 411–429.

Christmann, K., Schober, O., Ertl, G., & Neumann, M. 1974. Adsorption of Hydrogen on Nickel Single Crystal Surfaces. The Journal of Chemical Physics, **60**(11), 4528–4540.

Corporation, DIGITAL Equipment. 1997-1998. Visual Fortran Professional Edition 6.0A.

Dennis, JE, & Schnabel, RB. 1996. Numerical Methods for Unconstrained Optimisation and Non-linear Equations. Classics in Applied Mathematics, vol. 16. Society of Applied and Industrial Mathematics.

Dennis, John E., Gay, David M., & Welsch, Roy E. 1981. Algorithm 573 NL2SOL - An Adaptive Nonlinear Least-Squares Algorithm. ACM Transactions on Mathematical Software, **7**(3), 369–383.

Doherty, M.F., & Buzad, G. 1992. Reactive Distillation By Design. Trans IChemE, **70 (PartA)**, 448 – 458.

ESKOM. 2009. ESKOM webpage. http://www.eskom.co.za/live/content.php?Category_ID=4/.

Farkas, A., Farkas, L., & Rideal, E.K. 1934. Experiments On Heavy Hydrogen IV - The Hydrogenation and Exchange Reaction of Ethylene With Heavy Hydrogen. Proceedings Royal Society of London Series A, **146**, 630–639.

Fendt, Alexander. 2008. Dynamic Fault Analysis and Modification of a Catalytic Distillation Hydrogenation Column. Tech. rept. University of Cape Town.

Fischer, K., & Gmehling, J. 1995. Further Development, Status and Results of the PSRK Method for the Prediction of Vapor-Liquid Equilibria and Gas Solubilities. Fluid Phase Equilibria, **112**(1), 1–22.

Fogler, H. Scott. 1999. Elements of Chemical Reaction Engineering. Third edn. New Jersey: Prentice-Hall International Inc.

for Statistical Computing, The R Foundation. 2008. R version 2.8.1 RC (2008-12-15 r47212). http://www.r-project.org/.

Gear, C.W., & Petzold, L.R. 1983. Differential Algebraic Systems and Matrix Pencils. Lecture Notes in Mathematics, **973**, 75–89.

Gmehling, J. 1995. From UNIFAC to Modified UNIFAC to PSRK with the Help of DDB. Fluid Phase Equilibria, **107**(1), 1–29.

Gmehling, J., Wittig, R., Lohmann, J., & Joh, R. 2002. A Modified UNIFAC (Dortmund) Model. 4. Revision and Extension. Industrial & Engineering Chemistry Research, **41**(6), 1678–1688.

Gmehling, Jürgen, Rasmussen, Peter, & Fredenslund, Aage. 1982. Vapor-Liquid Equilibriums by UNIFAC Group Contribution. Revision and Extension. 2. Industrial & Engineering Chemistry Process Design and Development, **21**(1), 118–127.

Gmehling, Jürgen, Li, Jiding, & Schiller, Martin. 1993. A Modified UNIFAC Model. 2. Present Parameter Matrix and Results for Different Thermodynamic Properties. Industrial & Engineering Chemistry Research, **32**(1), 178–193.

Grüner, S., Mohl, K. D., Kienle, A., Gilles, E. D., Fernholz, G., & Friedrich, M. 2003. Nonlinear Control of a Reactive Distillation Column. Control Engineering Practice, **11**(8), 915 – 925. Process Dynamics and Control.

Hansen, Henrik K., Rasmussen, Peter, Fredenslund, Aage, Schiller, Martin, & Gmehling, Jürgen. 1991. Vapor-Liquid Equilibria by UNIFAC Group Contribution. 5. Revision and Extension. Industrial & Engineering Chemistry Research, **30**(10), 2352–2355.

Harmsen, G. Jan. 2006. Industrial Reactive Distillation a Review of Applications, Research, Development, Design and Operation Paper for CHISA 2006.

Harmsen, G. Jan. 2007. Reactive Distillation: The Front-runner of Industrial Process Intensification - A Full Review of Commercial Applications, Research, Scale-up, Design and Operation. Chemical Engineering and Processing, **46**(9), 774–780.

Hartmann-Petersen, Preben, Gerrans, Gus, & Hartmann-Petersen, Rasmus. 2001. Sasol Science and Technology Resource. Infosource Publishers and New Africa Education Publishing.

Hauan, Steinar, Ciric, Amy R., Westerberg, Arthur W., & Lien, Kristian M. 2000. Difference Points in Extractive and Reactive Cascades. I - Basic Properties and Analysis. Chemical Engineering Science, **55**(16), 3145 – 3159.

Heath, MT. 2002. Scientific Computing : an Introductory Survey. Second edn. McGraw-Hill.

Hernandez, Salvador, Sandoval-Vergara, Rodrigo, Omar Barroso-Munoz, Fabricio, Murrieta-Duenas, Rodolfo, Hernandez-Escoto, Hector, Gabriel Segovia-Hernandez, Juan, & Rico-Ramirez, Vicente. 2009. Reactive Dividing Wall Distillation Columns: Simulation and Implementation in a Pilot Plant. Chemical Engineering and Processing, **48**(1), 250–258.

Higler, A., Krishna, R., & Taylor, R. 2000. Nonequilibrium Model of Reactive Distillation: A Dusty Fluid Model for Heterogeneously Catalyzed Processes -. Industrial and Engineering Chemistry Research, **39**, 1597–1607.

Higler, Arnold Peter. 1999. A Nonequilibrium Model for Reactive Distillation. Ph.D. thesis, Clarkson University.

Hiwale, Rameshwar S., Bhate, Nitin V., Mahajan, Yogesh S., & Mahajani, Sanjay M. 2004. Industrial Applications of Reactive Distillation: Recent Trends. International Journal of Chemical Reactor Engineering, **2**(R1), 1–52.

Hoffmaster, Warren R., & Hauan, Steinar. 2004. Difference Points in Reactive and Extractive Cascades. III–Properties of Column Section Profiles with Arbitrary Reaction Distribution. Chemical Engineering Science, **59**(17), 3671–3693.

Hoffmaster, Warren R., & Hauan, Steinar. 2005. Difference Points in Reactive and Extractive Cascades: IV–Feasible Regions for Multisection Columns with Kinetic Reactions and Side Streams. Chemical Engineering Science, **60**(24), 7075–7090.

Horiuti, I., & Polanyi, M. 1934. Exchange Reactions of Hydrogen on Metallic Catalysts. Transactions of the Faraday Society, 1164–1172.

Horstmann, Sven, Jabloniec, Anna, Krafczyk, Jörg, Fischer, Kai, & Gmehling, Jürgen. 2005. PSRK Group Contribution Equation of State: Comprehensive Revision and Extension IV, Including Critical Constants and [alpha]-Function Parameters for 1000 Components. Fluid Phase Equilibria, **227**(2), 157–164.

Jackson, S. David, & Monaghan, Andrew. 2007. Hydrogenation of Unsaturated Hydrocarbons–40 years on: Hydrogenation of 1,3-pentadiene over Pd/alumina. Catalysis Today, **128**(1-2), 47–51.

Jasper, Joseph J. 1972. The Surface Tension of Pure Liquid Compounds. Journal of Physical Chemistry, **1**, 841–1009.

Jenkins, M. A. 1975. Algorithm 493: Zeros of a Real Polynomial [C2]. ACM Trans. Math. Softw., **1**(2), 178–189.

Jenkins, M. A., & Traub, J. F. 1972. Algorithm 419: zeros of a complex polynomial [C2]. Commun. ACM, **15**(2), 97–99.

Jonker, Gerald H., Veldsink, Jan-Willem, & Beenackers, Antonie A. C. M. 1997. Intrinsic Kinetics of 9-Monoenic Fatty Acid Methyl Ester Hydrogenation over Nickel-Based Catalysts. Industrial & Engineering Chemistry Research, **36**(5), 1567–1579.

Kaymak, Devrim B., & Luyben, William L. 2008. Quantitative Comparison of Dynamic Controllability Between a Reactive Distillation Column and a Conventional Multi-Unit Process. Computers & Chemical Engineering, **32**(7), 1456–1470.

Kolodziej, Andrzej, Jaroszynski, Mieczyslaw, & Bylica, Irena. 2004. Mass Transfer and Hydraulics for KATAPAK-S. Chemical Engineering and Processing, **43**(3), 457–464.

Kolodziej, Andrzej, Jaroszynski, Mieczyslaw, Schoenmakers, Hartmut, Althaus, Klaus, Geiβler, Elke, Übler, Christoph, & Kloeker, Markus. 2005. Dynamic Tracer Study of Column Packings for Catalytic Distillation. Chemical Engineering and Processing, **44**(6), 661 – 670. Intelligent Column Internals for Reactive Separations.

Kooijman, H.A., & Taylor, R. 1998. The Chemsep Book: Technical Documentation.

Kooijman, Harry, & Taylor, Ross. 2005. Chemsep version 5.1. http://www.chemsep.org.

Kooijman, Hendrik A., & Taylor, Ross. 1991. Estimation of diffusion coefficients in multicomponent liquid systems. Industrial & Engineering Chemistry Research, **30**(6), 1217–1222.

Kooijman, Hendrik Adriaan. 1995. Dynamic Nonequilibrium Column Simulation. Ph.D. thesis, Clarkson University.

Krishna, R., & Wesselingh, J.A. 1997. The Maxwell-Stefan Approach to Mass Transfer. Chemical Engineering Science, **52**(6), 861–911.

Kumar, M. V. P., & Kaistha, N. 2007. Temperature Based Inferential Control of a Methyl Acetate Reactive Distillation Column. Chemical Engineering Research & Design, **85**(A9), 1268–1280.

Kumar, M. V. Pavan, & Kaistha, N. 2008a. Internal Heat Integration and Controllability of Double Feed Reactive Distillation Columns, 1. Effect of Feed Tray Location. Industrial & Engineering Chemistry Research, **47**(19), 7294–7303.

Kumar, M. V. Pavan, & Kaistha, N. 2009a. Evaluation of Ratio Control Schemes in a Two-Temperature Control Structure for a Methyl Acetate Reactive Distillation Column. Chemical Engineering Research & Design, **87**(2A), 216–225.

Kumar, M. V. Pavan, & Kaistha, Nitin. 2008b. Decentralized Control of a Kinetically Controlled Ideal Reactive Distillation Column. Chemical Engineering Science, **63**(1), 228–243.

Kumar, M. V. Pavan, & Kaistha, Nitin. 2008c. Role of Multiplicity in Reactive Distillation Control System Design. Journal of Process Control, **18**(7-8), 692–706.

Kumar, M. V. Pavan, & Kaistha, Nitin. 2008d. Steady-State Multiplicity and its Implications on the Control of an Ideal Reactive Distillation Column. Industrial & Engineering Chemistry Research, **47**(8), 2778–2787.

Kumar, M.V. Pavan, & Kaistha, Nitin. 2009b. Reactive Distillation Column Design for Controllability: A Case Study. Chemical Engineering and Processing: Process Intensification, **48**(2), 606 – 616.

Lai, I-Kuan, Liu, Yan-Chun, Yu, Cheng-Ching, Lee, Ming-Jer, & Huang, Hsiao-Ping. 2008. Production of High-Purity Ethyl Acetate using Reactive Distillation: Experimental and Start-up Procedure. Chemical Engineering and Processing: Process Intensification, **47**(9-10), 1831 – 1843.

Le Chatelier, H.L. 1884. Comptes Rendus, **99**, 786.

Le Chatelier, H.L. 1888. Anales des Mines, **13**, 157.

Lee, Jae W., Hauan, Steinar, Lien, Kristian M., & Westerberg, Arthur W. 2000. Difference Points in Extractive and Reactive Cascades. II – Generating Design Alternatives by the Lever Rule for Reactive Systems. Chemical Engineering Science, **55**(16), 3161 – 3174.

Lei, Zhigang, Li, Chengyue, Li, Jianwei, & Chen, Biaohua. 2004. Suspension Catalytic Distillation of Simultaneous Alkylation and Transalkylation for Producing Cumene. Separation and Purification Technology, **34**(1-3), 265–271.

Lei, Zhigang, Yang, Jianfeng, Gao, Jinji, Chen, Biaohua, & Li, Chengyue. 2007. Gas-Liquid and Gas-Liquid-Solid Reactors for the Alkylation of Benzene with Propylene. Chemical Engineering Science, **62**(24), 7320 – 7326. 8th International Conference on Gas-Liquid and Gas-Liquid-Solid Reactor Engineering.

Liu, D.C., & Nocedal, J. 1989. On the Limited Memory Method for Large Scale Optimization. Mathematical Programming B, **45**(3), 503–528.

Luyben, William L. 2007. Control of Ternary Reactive Distillation Columns with and without Chemically Inert Components. Industrial & Engineering Chemistry Research, **46**(17), 5576–5590.

Lylykangas, M. S., Rautanen, P. A., & Krause, A. O. I. 2003. Liquid-Phase Hydrogenation Kinetics of Isooctenes on Ni/Al2O3. AIChE Journal, **49**(6), 1508–1515.

Lylykangas, Mikko. 2004. Kinetic Modeling of Liquid-Phase Hydrogenation Reactions. Ph.D. thesis, Helsinki University of Technology (Espoo, Finland).

Manduca, Efrain, Gonzalez, J. Castor, & Elman, Hinda. 2003. Mass Transfer Characteristics of Bale-Type Catalytic Distillation Packings. Separation Science and Technology, **38**, 3535–3552.

Miller, Alan. 2009. Alan Miller's Fortran Software. `http://jblevins.org/mirror/amiller`.

Morachevskii, A. G. 2004. Paul Sabatier (to 150th Anniversary of His Birthday). Russian Journal of Applied Chemistry, **77**(11), 1909–1912.

Moré, Jorge J., Garbow, Burton S., & Hillstrom, Kennet E. 1980. User Guide for Minpack-1. Argonne National Laboratory: Applied Mathematics Division.

Mueller, Ivo, & Kenig, Eugeny Y. 2007. Reactive Distillation in a Dividing Wall Column: Rate-Based Modeling and Simulation. Industrial & Engineering Chemistry Research, **46**(11), 3709–3719.

Mulopo, Jean Lubilanji, Hildebrandt, Diane, & Glasser, David. 2008. Reactive Column Profile Map Topology: Continuous Distillation Column with Non-Reversible Kinetics. Computers & Chemical Engineering, **32**(3), 622 – 629.

National Instruments. 2007. Labview 7.1. http://www.ni.com.

Nieuwoudt, Josias Jakobus. 2005. Design and Application of a Catalytic Distillation Column. Stellenbosch: University of Stellenbosch.

Nieuwoudt, Josias Jakobus. 2008. Personal experience.

Nocedal, J. 1980. Updating Quasi-Newton Matrices with Limited Storage. Mathematics of Computation, **35**, 773–782.

Onda, Kakusaburo, Takeuchi, Hiroshi, & Okumoto. 1968. Mass Transfer Coefficients Between Gas and Liquid Phases in Packed Columns. Journal of Chemical Engineering of Japan, **1**, 56.

Oudshoorn, O. L., Janissen, M., van Kooten, W. E. J., Jansen, J. C., van Bekkum, H., van den Bleek, C. M., & Calis, H. P. A. 1999. A Novel Structured Catalyst Packing for Catalytic Distillation of ETBE. Chemical Engineering Science, **54**(10), 1413 – 1418. International symposium on multifunctional reactors.

Peng, Jianjun, F. Edgar, Thomas, & Bruce Eldridge, R. 2003. Dynamic Rate-Based and Equilibrium Models for a Packed Reactive Distillation Column. Chemical Engineering Science, **58**(12), 2671–2680.

Perry, Robert H., Green, Don W., & Maloney, James O. 1997. Perry's Chemical Engineers' Handbook. Seventh edn. New York: McGraw-Hill.

Pines, H. 1981. The Chemistry of Catalytic Hydrocarbon Conversions -. Academic Press.

Podrebarac, G.G., Ng, F.T.T., & Rempel, G.L. 1997. More Uses for Catalytic Distillation. CHEMTECH, **27**(5), 37–45.

Poling, Bruce E., Prausnitz, John M., & O'Connell, John P. 2007. The Properties of Gases and Liquids. McGraw-Hill.

Radulescu, Gabriel, Gangadwala, Jignesh, Paraschiv, Nicolae, Kienle, Achim, & Sundmacher, Kai. 2009. Dynamics of Reactive Distillation Processes with Potential Liquid Phase Splitting Based on Equilibrium Stage Models. Computers and Chemical Engineering, **33**(3), 590 – 597.

Rautanen, P.A., Lylykangas, M.S., Aittamaa, J.R., & Krause, A.O.I. 2002. Liquid-Phase Hydrogenation of Naphthalene and Tetralin on Ni/Al2O3: Kinetic Modeling. Ind. Eng. Chem. Res., **41**(24), 5966–5975.

Roberts, Steve. 2007. Personal communication. University of Cape Town.

Rock, K., Gildert, R., & McGuirk, T. 1997. Catalytic Distillation Extends Its Reach. Chemical Engineering, **July 1997**, 78–84.

Rosales-Quintero, A., & Vargas-Villamil, F. D. 2009. On the Multiplicities of a Catalytic Distillation Column for the Deep Hydrodesulfurization of Light Gas Oil. Industrial & Engineering Chemistry Research, **48**(3), 1259–1269.

Rylander, P.N. 1994. Hydrogenation Methods. Academic Press.

Sabatier, Paul. 1912. The Method of Direct Hydrogenation by Catalysis. In: Nobel Lectures, Chemistry 1901-1921. Elsevier Publishing Company.

Saito, Shozaburo, Michishita, Tsuguo, & Maeda, Siro. 1971. Separation af Meta- and Para-Xylene Mixture by Distillation Accompanied by Chemical Reactions. Journal of Chemical Engineering of Japan, **4**(1), 37–43.

Sander, S., Flisch, C., Geissier, E., SchoenmakerS, H., Ryll, O., & Hasse, H. 2007. Methyl Acetate Hydrolysis in a Reactive Divided Wall Column. Chemical Engineering Research & Design, **85**(A1), 149–154.

Sandler, Stanley I. 1999. Chemical and Engineering Thermodynamics. John Wiley & Sons, Inc.

Scenna, N. J., Ruiz, C. A., & Benz, S. J. 1998. Dynamic Simulation of Start-up Procedures of Reactive Distillation Columns. Computers & Chemical Engineering, **22**(Supplement 1), S719 – S722. European Symposium on Computer Aided Process Engineering-8.

Schmitt, Markus, Blagov, Sergej, & Hasse, Hans. 2008. Mastering the Reaction is the Key to Successful Design of Heterogeneously Catalyzed Reactive Distillation: A Comprehensive Case Study of Hexyl Acetate Synthesis. Industrial & Engineering Chemistry Research, **47**(16), 6014 – 6024.

Seader, J.D., & Henley, E.J. 1998. Separation Process Principles. John Wiley and Sons.

Segovia-Hernndez, Juan Gabriel, Hernndez, Salvador, & Jimnez, Arturo. 2005. Analysis of Dynamic Properties of Alternative Sequences to the Petlyuk Column.

Computers & Chemical Engineering, **29**(6), 1389 – 1399. Selected Papers Presented at the 14th European Symposium on Computer Aided Process Engineering.

Sharrock, Cayle J., & Coetzer, Roelof. 2007. Selecting Robust Kinetic Models on Noisy Data Using the Bootstrap. International Journal of Chemical Reactor Engineering, **5**, A103.

Siegel, Stanley, Butler, Patrick H, & Egger, Gerald. 2005. Houston, The Supercity of Buffalo Bayou. American Historical Press.

Singh, Utpal K., & Vannice, M. Albert. 2001. Kinetics of Liquid-Phase Hydrogenation Reactions over Supported Metal Catalysts – a Review. Applied Catalysis A: General, **213**(1), 1–24.

Smith, J.M., Van Ness, H.C., & Abbott, M.M. 1996. Introduction to Chemical Engineering Thermodynamics. Fifth edn. McGraw-Hill International Editions.

Sneesby, Martin G., Tade, Moses O., & Smith, Terence N. 1999. Two-Point Control of a Reactive Distillation Column for Composition and Conversion. Journal of Process Control, **9**(1), 19 – 31.

Stark, Nicolaus Ladislaus, & Swart, Josias Sevass De Kock. 2006 (March). Hydrogenation of Olefinic Feed Stocks.

Steyer, Frank, Freund, Hannsjoerg, & Sundmacher, Kai. 2008. A Novel Reactive Distillation Process for the Indirect Hydration of Cyclohexene to Cyclohexanol Using a Reactive Entrainer. Industrial & Engineering Chemistry Research, **47**(23), 9581–9587.

Sumana, C., & Venkateswarlu, C. 2007. Development of a Software Sensor for Compositions in Continuous Reactive Distillation. Journal of Scientific & Industrial Research, **66**(11), 898–904.

Taylor, R., & Krishna, R. 1993. Multicomponent Mass Transfer. John Wiley and Sons.

Taylor, R., & Krishna, R. 2000. Modelling Reactive Distillation. Chemical Engineering Science, **55**(22), 5183 – 5229.

Thompson, Della (ed). 1996. The Pocket Oxford Dictionary of Current English. Clarendon Press.

Turton, Richard, Bailie, Richard C., Whiting, Wallace B., & Shaeiwitz, Joseph A. 1998. Analysis, Synthesis, and Design of Chemical Processes. First edn. New Jersey: Prentice Hall, PTR.

Twigg, G.H., & Rideal, F.R.S. 1939. The Exchange Reaction Between Ethylene and Deuterium on a Nickel Catalyst. Proceeding of the Royal Society A, **171**, 55–69.

Uchytil, Jan, Kocova, Eva, & Kraus, Milos. 1981. Hydrogenation of Alkenes on a Nickel-Tungsten-Alumina Catalyst. Collection Czechoslovak Chemical Community, **46**, 2076–2082.

van Baten, J. M., & Krishna, R. 2002. Gas and liquid phase mass transfer within KATAPAK-S structures studied using CFD simulations. Chemical Engineering Science, **57**(9), 1531 – 1536.

van Baten, J. M., Ellenberger, J., & Krishna, R. 2001. Radial and Axial Dispersion of the Liquid Phase within a KATAPAK-S Structure: Experiments vs. CFD Simulations. Chemical Engineering Science, **56**(3), 813 – 821.

Vignes, Alain. 1966. Diffusion in Binary Solutions. Variation of Diffusion Coefficient with Composition. Industrial & Engineering Chemistry Fundamentals, **5**(2), 189–199.

Vodopivec, Andrej. 2004-2008. wxMaxima 0.8.0. http://www.wxmaxima.sourcforge.net/.

Wang, G.Q., Yuan, X.G., & Yu, K.T. 2005. Review of Mass-Transfer Correlations for Packed Columns. Industrial & Engineering Chemistry Research, **44**(23), 8715–8729.

Wang, Jinfu, Ge, Xudong, Wang, Zhanwen, & Jin, Yong. 2002. Development of a Novel Catalytic Distillation Column. Chemical Engineering and Processing, **41**(2), 115 – 121.

Weinkauf, Tino, Norris, Chris, Schrader, Stephan, Selormey, Paul, Vacha, Pavel, Welzel, Christian, Wiegand, Sven, & Wieland, Oliver. 1999-2008. TEXnicCenter 1 Beta 7.5. http://TeXnicCenter.org.

Welker-Nieuwoudt, Cathrin A. 2008. Personal communication. University of Cape Town.

Wen, L.Y., Min, E.Z., Pang, G.C., & Yu, W.Y. 2000. Synthesis of Cumene by Suspension Catalytic Distillation Process. Journal of Chemical Industry and Engineering (China), **51**, 2000.

Wentink, A.E., Kuipers, N.J.M., de Haan, A.B., Scholtz, J., & Mulder, H. 2007. Olefin Isomer Separation by Reactive Extractive Distillation: Modelling of Vapour-Liquid Equilibria and Conceptual Design for 1-Hexene Purification. Chemical Engineering and Processing, **46**(9), 800 – 809. Selected Papers from the European

Process Intensification Conference (EPIC), Copenhagen, Denmark, September 19-20, 2007.

Wittig, R., Lohmann, J., & Gmehling, J. 2003. Vapor-Liquid Equilibria by UNIFAC Group Contribution. 6. Revision and Extension. Industrial & Engineering Chemistry Research, **42**(1), 183–188.

Xu, Y., Ng, F.T.T., & Rempel, G.L. 2005. Comparison of a Pseudo-Homogeneous Nonequilibrium Dynamic Model and a Three-Phase Nonequilibrium Dynamic Model for Catalytic Distillation. Ind. Eng. Chem. Res., **44**(16), 6171–6180.

Yuxiang, Z, & Xien, X. 1992. Study on Catalytic Distillation Processes. Part I: Mass Transfer Characteristics in Catalyst Bed within the Column. Chemical Engineering Research & Design, **70**, 459–464.

Znak, Leszek, & Zielinski, Jerzy. 2008. Effects of support on hydrogen adsorption/desorption on nickel. Applied Catalysis A: General, **334**(1-2), 268 – 276.

Part IV

APPENDICES AND INDEX

Appendix A

CD system specifications

A.1 Changes to the existing CD system

The improved CD system P&ID is supplied in Section 4 and may be compared to the original supplied in Nieuwoudt [2005]. For convenience, equipment specifications supplied in this reference are updated in Appendix A.2 and updated operating procedures are supplied in Appendix A.3. Front and back views of the final system are shown in Figure A.3.

A decision was made to reduce the *reboiler liquid inventory* to facilitate faster process dynamics. The internal heating element was thus replaced with an external band heater for this smaller reboiler, which also addressed some safety concerns regarding a possible fire hazard.

In the previous *reboiler level detection* design, a vertical glass tube spanning most of the height of the reboiler was connected near the top and bottom of the reboiler and three optical level sensors used to test for the presence of liquid at point locations. However, this design functioned only intermittently. After it was established that this was due to a thermosiphon effect that circulated liquid through the glass tube used for optical level detection, the glass tube was moved to the bottom of the reboiler and a float with an aluminium rod hanging down into the glass tube used. As the aluminium rod passed between the optical level transmitter and receiver, the electronic circuit was opened and the rod and level simultaneously detected. Experimentation with different floating devices and materials found a hollow aluminium cylinder (see Figure A.2) to be most suited to this application.

The original *solenoid valves* were found not to be resistant against 1-hexene/n-hexane operation and were replaced by pneumatically actuated Swagelok valves. The backpressure regulator was found to have insufficient accuracy at the lower pressures of interest and was similarly replaced by a pneumatically controlled backpressure regulator.

An *ampoule off-gas sampling* point was found to leak excessively during operation.

(a) Design 1.

(b) Design 2.

Figure A.1: Photos of the reactive zones used in the CD column.

Figure A.2: Photo of the final float used in the reboiler.

(a) Front view.

(b) Rear view.

Figure A.3: Photos of the CD system.

A tie-in was thus made to a nearby micro-GC-TCD for analyses and a nitrogen reference gas with known flow rate fed into the of-gas stream via an additional mass flow controller to later determine the total flow of the mixture and to sufficiently dilute the organics present in the off-gas to meet the GC-TCD input requirements (see Section 4.4).

Fendt [2008] suggested an alternative operating philosophy for the *partial condenser level control*. Instead of on/off opening of the condenser drain line (via Sol-D) the manipulated variable was shifted to the reflux pump rate and a constant distillate flow rate chosen. One of the redundant reboiler optical sensors was moved to the condenser. The resulting 4 point level optical sensors were then used as follows: 1 to protect the pump against a low level (LLA) in the condenser; 3 used to estimate the required pump flow rate. The LLA tripped the system. The result was much stabler operation, though some manual fine-tuning was required to choose a suitable distillate rate. The dynamics of the condenser level control system improved considerably.

Due to the *Eskom power crisis*[a] in South Africa during many of the experiments, the system was fully shifted to the uninterrupted power supply (UPS). As the pneumatic valves were dependent on an air compressor that was not on UPS, the pneumatic system was tied into pressurized cylinder gas. When the compressor output pressure dropped below 3-4·10^5 Pa(g), the cylinder gas would take over from the compressor to drive the pneumatic system (typically for 2-3 hours).

Fluctuating *tap water pressure* resulted in unacceptable variations in the tap water coolant flow through the partial condenser. This was solved by purchasing a water tank kept level by a float valve. A submerged centrifugal pump in the tank than pumped water through a control valve, a rotameter and the condenser and out to drain independent of the tap water feed pressure. The water was not circulated back to the tank as calculations showed that heat would build up in the circulation loop.

The *refrigerator* was replaced after breaking down and the new refrigerator placed on the ground in the frame to reduce the vibrations transmitted to the frame. The *reboiler outlet tank and balance* was also moved off the frame to the ground to ensure a liquid level below the reboiler liquid level and proper drainage for low pressure operation. Both the reboiler and condenser drain line diameters were increased to $\frac{1}{4}$" (ca. 6 mm) to reduce frictional losses.

Other changes were small or software related. In terms of *software* the computer algorithm and data logging were optimized to reduce their resource requirements and several enhancements were made to the GUI and error handling system to simplify the controls for other users. The partial condenser level control was significantly augmented. *Electronic* problems were few and mainly concerned with inconsistencies in the electrical

[a]Eskom is an electricity supplier that provides 95% of the electricity used in South Africa [ESKOM, 2009]. By the year 2007 its supply margin available for peak usage had shrunk considerably, in part leading to electricity shortages and load shedding [Nieuwoudt, 2008].

power supply rather than the electrical designs themselves.

A.2 Selected equipment datasheets

Table A.1: Catalytic Distillation column data sheet.

CATALYTIC DISTILLATION COLUMN DATA SHEET			Tag(s) Description	CD-1 Simultaneous reaction-separation	
Operating data					
No. required	1	None			
Non-reactive section	Structured packing	None			
Reactive section	Ni/Al_2O_3 catalyst	None			
Column shell					
Sections			Section type 1		
Amount available	3	None	–Length	490	mm
Types	2	None	–Amount used	3	None
Inner diameter	49.25	mm	Section type 2		
Outer diameter	60.33	mm	–Length	416	mm
Thickness	5.54	mm	–Amount used	0	None
Corrosion allowance	None	mm	Total height	1470	mm
Volume	2.5	dm^3	MOC	SS AISI 316	None
Non-reactive structured packing					
Type	Sulzer CY	None	Channel		
Void fraction	0.965	None	–Base	7.5	mm
Packing surface area	708	m^2/m^3	–Side	5.65	mm
Crimp height	4.25	mm	–Flow angle rel. horiz.	45	°
Layer height	160	mm	Packing height	1440	mm
Diameter	50	mm	MOC	SS AISI 316	None
Reactive section					
Type	“Tea bag”	None	Catalyst	Ni/Al_2O_3	None
Reaction	Hydrogenation	None	Catalyst weight	21	g
Reboiler					
Type	Heating band	None	Heating element		
Vessel			–Geometry	Band	None
–Diameter	60	mm	–Maximum power	1000	W
–Height	200	mm	–Nominal power	650	W
–Volume	0.57	dm^3			
–MOC	SS AISI 316	None			
Glass level indicator					
Location	Reboiler bottom	None	Glass tube		
Metal connections			–Nominal pressure	2-6	bar
–Inner diameter	0.194	inch	–Length	166.5	mm
–Outer diameter	0.250	inch	–Outer diameter	6	mm
–Thickness	0.028	inch	–Inner diameter	3	mm
–MOC	SS AISI 316	None	–Thickness	1.5	mm
–Working pres. (max.)	276	bar	–MOC	Glass	None
Glass-metal connection	Graphite ferrules	None	–Safe working pressure	30	bar
Other related equipment					
Partial condenser	C-DP	None	Storage tanks	T-HC, T-DC6, T-BC6	None
Refrigerator	E-1	None	Pumps	P-HF, P-RD	None
Office purposes					
N/A					

Table A.2: Partial condenser data sheet.

PARTIAL CONDENSER DATA SHEET			Tag(s) Description	C-DP Partial condenser for distillate	
Operating data					
No. of units required	1	None	Sections (top to bottom)		
Type	Shell and tube	mm	–Number	4	None
Shells per unit	2	None	–Section 1	Gas inlet chamber	None
Surface area per unit	57453	mm^2	–Section 2 (shell)	Tap water	None
Surface area per shell	See below	mm^2	–Section 3 (shell)	Glycol	None
Total heat removed	650	W	–Section 4	Reflux chamber	None
Performance of section 2					
Shell side			Tube side		
Fluid circulating	Tap water	None	Fluid circulating	N/A	-
Vapour	N/A	-	Vapour	1-Hexene	None
	N/A	-		n-Hexane	None
Liquid	Water	None	Non-condensables	Hydrogen	None
Heat removed	250	W			
Performance of section 3					
Shell side			Tube side		
Fluid circulating	50/50 Glycol/Water	None	Fluid circulating	N/A	-
Vapour	N/A	-	Vapour	1-Hexene	None
	N/A	-		n-Hexane	None
Non-condensables	N/A	-	Non-condensables	Hydrogen	None
Heat removed	400	W			
Construction of section 1: Gas inlet chamber (top)					
MOC	SS AISI 316	None	Baffles		
Shell			–Amount	0	None
–Number of shells	1	None	–Spacing	N/A	mm
–Inner diameter	50	mm	–Diameter	N/A	mm
–Outer diameter	56	mm	–Baffle cut	N/A	mm
–Thickness	3	mm	–Thickness	N/A	mm
–Length (excl. flanges)	21.44	mm	–MOC	N/A	None
–Volume	42	ml	Inlet and outlet		
Flanges			–Outer diameter	0.875	inch
–Outer diameter	106	mm	–Inner diameter	0.745	inch
–Height	10	mm	–Thickness	0.083	inch
Total section height	34.44	mm			
Construction of section 2: Tap water					
MOC	SS AISI 316	None	Baffles		
Shell			–Amount	2	None
–Number of shells	1	None	–Spacing	19.33	mm
–Inner diameter	50	mm	–Diameter	50	mm
–Outer diameter	56	mm	–Baffle cut	15	mm
–Thickness	3	mm	–Thickness	1	mm
–Length (excl. flanges)	60	mm	–MOC	SS AISI 316	None
–Volume	118	ml	Inlet and outlet		
Flanges			–Outer diameter	0.500	inch
–Outer diameter	106	mm	–Inner diameter	0.402	inch
–Height	10	mm	–Thickness	0.049	inch
Total section height	80	mm			
Construction of section 3: Glycol					
MOC	SS AISI 316	None	Baffles		
Shell			–Amount	7	None
–Number of shells	1	None	–Spacing	21.5	mm
–Inner diameter	50	mm	–Diameter	50	mm
–Outer diameter	56	mm	–Baffle cut	15	mm

Table A.2: Partial condenser data sheet (cont'd).

–Thickness	3	mm	–Thickness	1	mm
–Length (excl. flanges)	180	mm	–MOC	SS AISI 316	None
–Volume	353	ml	Inlet and outlet		
Flanges			–Outer diameter	0.500	inch
–Outer diameter	106	mm	–Inner diameter	0.402	inch
–Height	10	mm	–Thickness	0.049	inch
Total section height	200	mm			
Tubes					
Number of tubes	12	None	Working pres. (max.)	276	bar
Configuration	Staggered	None	Outer diameter	0.250	inch
Material of construction	SS AISI 316	None	Inner diameter	0.194	inch
Bundle diameter		mm	Thickness	0.028	inch
Shell bundle clearance	10.58	mm	Length (excl. flanges)		
Surface area			–Section 2	60	mm
–Section 2	14363	mm^2	–Section 3	180	mm
–Section 3	43090	mm^2	–Section 4 (from top)	17	mm
–Total	57453	mm^2	Pitch	8	mm
Section 4: Reflux chamber (bottom)					
Total volume	273	ml	Off-gas outlet		
Liquid vol. (nominal)	196	ml	–Outer diameter	0.125	inch
Liquid height (nominal)	100	mm	–Inner diameter	0.069	inch
Material of construction	SS AISI 316	None	–Thickness	0.028	inch
Chamber dimensions			–Angle with horizontal	30	°
–Inner diameter	50	mm	Liquid outlets		
–Outer diameter	56	mm	–Amount	2	None
–Thickness	3	mm	–Outer diameter	0.125	inch
–Length (excl. flanges)	142	mm	–Inner diameter	0.069	inch
Flanges			–Thickness	0.028	inch
–Outer diameter	106	mm			
–Height	10	mm			
Total section height	155	mm			
Glass level indicator					
Location	Side of section 4	None	Glass tube		
Metal connections			–Nominal pressure	2-6	bar
–Inner diameter	0.194	inch	–Length	110	mm
–Outer diameter	0.250	inch	–Outer diameter	6	mm
–Thickness	0.028	inch	–Inner diameter	3	mm
–MOC	SS AISI 316	None	–Thickness	1.5	mm
–Working pres. (max.)	276	bar	–MOC	Glass	None
Glass-metal connection	Graphite ferrules	None	–Safe working pressure	30	bar
Other related equipment					
Refrigerator	E-1	None			
Office purposes					
N/A					

Table A.3: Reflux pump data sheet.

Reflux Pump			Tag(s)	P-RD	
DATA SHEET			Description	Refluxes distillate to column	
Operating data					
Number required	1	None	Available NPSH	1	m
Type	Metering pump	None	Required output	14.2	l/h
Fluid			Operating pressures	5	bar
–Viscosity	3.02E-04	Pa.s	Working temperature	7	°C
–Density	683	kg/m^3	Analysis	None	None
			Electrical supply	230V (3phase)	None
Technical data					
Pump			Lubricants		
–Drawing no.	See manual	None	–Pump case, gear box		
–Type	Cucchi Hydraulic Diaphragm Pump	None	– Type	SAE140, 23°E (ca. 160 mPa.s)	None
–Model	CMP-2/12 X 118	None	– Volume	300	ml
–Maximum load	0-14.2	l/h	– Oil used	Shell Spirax A85 W 140	None
–Max. head	20	bar	–Oil chamber		
–Efficiency		None	– Type	1 or 2 °E Pharma	ml
Piston			– Volume	72	ml
–Diameter	8	mm	– Oil used	Glycerol	None
–Max. stroke speed	118	spm	Water required		
–Motor			–Cooling	None	None
–Type	H71A4-40050	None	–Sealing	None	None
–Serial no.	4601	None	MOC		None
–Year	2004	None	–Head	SS316	None
–Max. power delivery	0.25	kW	–Valves	SS316	None
Electrical supply			–Diaphragm	PTFE	None
–Voltage	230/380	V	Phonometric		
–Phase	3	None	–Max. sound	76.6	dB(A)
Relief valve pressure	N/A	None	–Av. surface pressure	73.2	dB(A)
Type of baseplates	Two-plate double vibration dampener	None	–Sound power	76.7	dB(A)
Dimensions (box)					
–Volume	23.52	dm^3			
–Width	140.00	mm			
–Length	400.00	mm			
–Total Heigth	420.00	mm			
Related equipment: Variable speed drive					
Type	Emotron	None	Model	VSD-DFE23-02	None
Description	DFE Frequency Inverter	None	Function	230(1)-230(3)	V(ph)
Office purposes					
REMARKS: When filling the oil chamber the stroke length must be set to 0% with the adjustment knob. Ensure that no air remains in the poured oil. Gear box oil to be initially changed after 500 hours and then 3000 hours.					

Table A.4: Balances data sheet.

ELECTRONIC BALANCES DATA SHEET			Tag(s) Description	W-D and W-B Product balances for mass flow rates	
Operating data					
No. required	2	None	Ambient temperature		
Input rate			Minimum	5	°C
W-D	50	g/h	Maximum	40	°C
W-B	47	g/h	Relative humidity		
Capacity (nominal)			Minimum	25	%
W-D	12	hours	Maximum	85	%
W-B	12	hours	Criterium	Non-condensing	None
Technical data					
Supplier	Cape Scientific Services	None	Weighing pan		
Make	Precisa	None	Form	Square	None
Type	XB 4200C	None	Length	170	mm
Minimum weight			Breadth	170	mm
Weight	0.50	g	Electrical		
e	0.01	g	Voltage	115 or 230	V
Maximum weight			Voltage tolerance	-20 to +15	%
Weight	4200.00	g	Frequency	50 to 60	Hz
Readability (d)	0.10	g	Power consumption		
Linearity	0.15	g	Without peripheral	6.0	VA
Reproducibility	0.10	g			
Data transfer to peripheral devices					
Interface	RS232/V23	None			
Safety characteristics					
Maintenance period	Regular	None			
Office purposes					
N/A					

A.3 Operating procedures

The CD system itself was and is a dynamic, experimental system that is modified on a regular basis. Thus, the operating procedures presented here do not attempt to direct the user according to a set recipe that strictly identifies each valve and the action to be taken. Rather, it presents the user with the necessary operating philosophy and background to successfully run the system.

Table A.5: General safety considerations.

Duration	No.	Action
	1	Safety goggles, laboratory coat, closed shoes and long pants to be worn at all times.
	2	Latex gloves to be worn when working with the chemicals (such as during sampling or loading).
	3	Glass fume hood doors must be closed when no work is being performed on the system to ensure proper extraction in the fume hood.
	4	MSDS information must be available at the system.

Table A.6: Temperature programmed reduction (TPR) analysis of the catalyst.

Duration	No.	Action
	1	Take the supplied glass U-tube with gloved hands. Place a small amount of high temperature glass wool in the bottom of the thick section of the tube.
	2	Weigh out the approximate amount of desired catalyst in a weighing boat.
	3	Take the sample holder, the glass U-tube and plastic funnel and weigh precisely.
	4	Pour the catalyst into the glass U-tube. Re-weigh and subtract the previous weight to get the sample weight.
	5	Connect the U-tube to the TPR machine, using high temperature O-rings as sealant, making sure to connect the glass tubes to the correspondingly sized stainless steel tubes leading into the TPR.
00:30	1	Heat the sample to 100°C in argon at 10°C/min.
01:00	1	Leave for an hour to cool down to 60°C.
	1	Switch to 5% hydrogen in argon.
01:00	2	Heat up at 10°C/min to 1000°C.
	3	Close the gas lines and cool the sample down to ambient temperature.

Table A.7: Pre-reduction of the catalyst.

Duration	No.	Action
	1	Measure out the desired amount of catalyst in a weighing cup.
	2	Place clean, fine glass wool at the bottom of a clean calcination tube and fill with the weighed catalyst.
	3	Insert the calcination tube into the heating block.
	4	Insert the tip of the thermocouple into the center of the catalyst mass through the clean normal glass wool filled plug at the top of the calcination tube.
	5	Clamp the thermocouple plug shut to the tube.
	6	Connect the calcination tube gas inlet via a flexible silicon tube to the gas supply.
	7	Open the hydrogen valve and adjust the actual hydrogen flow rate until the particles fluidize or the MFC reaches its maximum (e.g. 70 ml/min).
04:00	8	Ramp the temperature from ambient to 350°C during a 4 hour time period.
16:00	9	Maintain 350°C for 16 hours.
02:00	10	Discontinue heating and allow the catalyst to cool down to ambient. Choose a sufficiently long cooling period to prevent automatic repetition of the heating cycle by the controller.
	11	Set hydrogen flow to 0 on the mass flow controller and close the hydrogen connection valve.
	12	Open the argon connection valve and set set the argon mass flow controller to 70 ml/min to maintain the inert atmosphere in the calcination tube.
	13	Take a small glass beaker sufficiently large to submerse the entire catalyst cage. Fill the glass beaker with tetradecane.
	14	The system has a tube to atmosphere connected to the calcination tube feed. Make sure the metering valve in this line is closed, open the in-line ball valve and then open the metering valve slowly. Bubble this argon through the glass beaker for several minutes and then hold it inside the glass beaker to ensure an inert atmosphere.
	15	Remove the thermocouple from the glass wool filled plug.
	16	Disconnect the flexible silicon feed tube and close it with a thumb. Unclamp the calcination tube from the support structure.

Table A.7: Pre-reduction of the catalyst (cont'd).

Duration	No.	Action
	17	Bring the opening of the calcination tube close to the glass beaker. Swiftly remove the glass plug and pour the catalyst into the beaker under the argon atmosphere.
	18	Close the submerged cage and load timeously into the reactor vessel.

Table A.8: Pressure test of the column body, gas system and utility loops.

Duration	No.	Action
	1	Procure a leak detector or prepare a simple soap bubble solution to seek for leaks.
	2	Close all the outlet valves, including sample needle valves, reflux line drain ball valve, reboiler level indicator drain ball valve, off-gas shut-off valve, catchpot drain ball valves, reboiler and reflux drum filling ball valves and the low pressure outlet gauge isolation valve (to prevent damage to the low pressure gauge).
	3	Ensure that the column isolation and reboiler drain shut-off valves are open. The former allows pressurization with argon via the condenser; the latter allows pressure testing up to the bottoms solenoid valve.
	4	To also pressure test up to the MFC with argon, set the 3-way valve to the argon supply.
	5	Close the pressure regulator fully to isolate the argon supply line from the system.
	6	Open the argon mains supply shut-off ball valve and allow the supply line to pressurize.
	7	Set the argon pressure regulator to a pressure between the previous pressure tested and 6 bar(g). It is recommended to do several pressure test with increasing severity.
	8	Allow the column pressure to stabilize and close the argon mains supply.
	9	If the column pressure drops very rapidly there is a big leak(s). Open the argon supply again, quickly search for big leaks, close them if possible and close the argon mains supply. Repeat test if necessary.
	10	Isolate the column from the gas system by closing the column isolation shut-off valve.

Table A.8: Pressure test of the column body, gas system and utility loops (cont'd).

Duration	No.	Action
01:00	11	The column pressure and gas system pressure must stay constant for at least 1 hour. If not, test for leaks, take remedial actiona and repeat the pressure test if necessary.
	12	Once the pressure test is successful, set to a higher pressure if required and re-test or continue with testing of the hydrogen gas system.
	13	To pressure test the hydrogen supply system, set the three-way valve to the hydrogen supply.
01:00	14	Follow the same procedures as for the main system
	1	To pressure test the tap water coolant, open the mains tap water utility shut-off ball valve supply.
	2	Check for big leaks between the mains supply and the float valve tank inlet.
	3	Commence tap water circulation through the coolant loop by switchin on the submerged pump.
00:30	4	Monitor the tap water line from the mains to the drain for 20-30 minutes and deal with leaks appropriately.
00:30	1	To pressure test the refrigerator coolant loop, commence circulation, monitor for 20 or 30 minutes and deal with leaks appropriately.
	1	To pressure test the compressed air utility, simply open the mains air supply and use leak detector or soap solution to detect leaks. Leaks in the compressed air supply are not critical.

Table A.9: Loading of the catalyst.

Duration	No.	Action
	1	Perform a pressure test.
	2	Close the bottoms ball drain valve and disconnect the outlet line.
	3	Pressurize the system with argon, close the argon supply and the open the off-gas valve to allow the system to reach ambient pressure.
	4	Open the flange nearest to the catalyst insertion or removal point and move it down the threaded rods being careful of obstructions.
	5	Remove the previous catalyst if necessary. NOTE: The amount of catalyst is small and it was found that passivation was not necessary. However, the catalyst is pyrophoric and deactivation is recommended when working with larger quantities.
	6	Start flowing argon from the bottom through the system via using the gas feed mass flow controller. The flow rate must be sufficient to displace any atmospheric oxygen.
	7	Bring the liquid tetradecane submerged reduced catalyst closer.
	8	Swiftly remove the catalyst from the liquid and place it in the column. Tetradecane has a high viscosity and the catalyst remains coated with a layer of tetradecane for a sufficiently long period of time to avoid deactivation.
	9	Close the opened flange as quickly as possible.
	10	Discontinue the argon flow via the mass flow controller and pressurize the system to ca. 5 bar(g) with argon.
	11	Reconnect the reboiler outlet line and open the bottoms ball drain valve.
	12	Pressure test the reconnected flange and outlet line.

Table A.10: Pre-start-up.

Duration	No.	Action
	1	Load the catalyst into the column (see catalyst loading procedures).
	2	Do a pressure test (see pressure test procedures). This will also ensure that all the valves are in the correct positions.
	3	Check that the water and compressed air utility line shut-off valves are in the open position.
	4	Check that both the normal and UPS power supply sockets at the wall are set to "on".
	5	Check that the reference, hydrogen and argon gas utility shut-off valves are closed.
	6	Set the electronics and refrigerator electricity supply switches in the "on" position.
	7	On the electronic box, set all to "manual" and "off".
	8	On the electronic box, set the balances, multiplug, reflux pump and HPLC pump and MFC switches to "on".
	9	Switch the main electricity supply switch to "on".
	10	Load 1-Hexene and n-Hexane to the reboiler via the HPCL pump.

Table A.11: Start-up and Operation.

Duration	No.	Action
	1	Start-up the computer program, follow the prompts and engage the red ignition switch on the electronics box when the graphical user interface (GUI) has loaded, is displaying the temperature profile and the toggle switch is flashing. If the pressure setpoint is lower than the current pressure, first depressurize the column by opening the valves in the off-gas line, which lead to atmosphere. NOTE: depressurization to a lower pressure setpoint during operation is not advised as the liquid in the column will flash. Engage the ignition switch and press start-up on the GUI.
	2	Monitor that each instrument has started up correctly: it's background on the GUI will turn green. Check the column pressure. Set a flowrate at the argon-MFC to protect the catalyst from oxygen.

Table A.11: Start-up and Operation (cont'd).

Duration	No.	Action
		Set the solenoid valves to auto on the electronics box and start the reflux pump by pushing the start button on the Emotron frequency inverter. The display should show: SP0 (no speed) or the current pump speed.
	3	Check that the tap water and refrigerator water cooling mediums are flowing through the respective rotameters. Check the reboiler level. If it is below the high level, load additional feed via the HPCL pump. If the amount of condensables that can be lost via the off-gas during batch start-up is significant, start proactively replenishing the hydrocarbons via the HPLC pump.
	4	Set the element to the desired power on the GUI and set the heating element switch on the electronics box to "auto".
	5	A temperature wave will start to move up the column from the reboiler. Set the reflux pump rate control to "method 1 control" on the GUI. This will automatically adjust the reflux pump speed to compensate for the boil-up rate. Set the operating mode in both level controls to "forced unless shutdown" and "closed". Allow the column to reach steady state as a batch system.
	6	Take the relevant samples (see sample procedures).
	7	If the system is to be run in batch mode, choose the new desired setpoint, wait for steady state and take the required samples.
	8	If the system is to be run as a continuous non-reactive distillation column, set the bottoms solenoid valves to "auto" on the electronic box. Switch the distillate solenoid valve to "manual" and "on". Adjust the distillate flow rate via fine metering valve Fm-1 and set the reflux flow rate control to control the condenser liquid level.
	9	If not started yet, set the HPLC pump to the required hydrocarbon feed flow rate and start feeding the liquid feed.
	10	Use the feed sample valve to check that the liquid is being fed. If not, prime the HPLC pump by connecting a silicon tube and syringe to the sample outlet and sucking out any existing gas lodged in the HPLC supply line.
	11	Allow the column to reach a steady state.
	12	Take the relevant samples (see sample procedures).
	13	Choose a new desired setpoint, unless the system is to be run as a reactive distillation column.

Table A.11: Start-up and Operation (cont'd).

Duration	No.	Action
	14	If the system is to be run as a continuous reactive distillation column, open the hydrogen supply shut-off valve.
	15	Pressurize the hydrogen supply line to a pressure higher than that in the system itself.
	16	Set the desired MFC mass flow rate on the GUI and choose hydrogen on the dropdown menu. Switch the three way valve from the argon to the hydrogen supply.
	17	Allow the system to reach a steady state.
	18	Take the relevant samples (see sample procedures).
	19	Choose a new desired setpoint and repeat.

Table A.12: Maintenance while in operation.

Duration	No.	Action
	1	The system is largely automated and requires minimal operator intervention.
	2	Monitor the liquid feed and product tanks to respectively prevent emptying and overfilling.
	3	Check, and if necessary empty, the hydrogen, argon and off-gas catchpots on a regular basis.
	4	Monitor periodically that the tap water pump is not exceeding the tap water mains supply flow rate.

Table A.13: Sampling.

Duration	No.	Action
	1	Access the manual input parameters from the CD control program GUI and enter the required manual values.
	2	To sample the reboiler liquid, ensure that the silicon cooling tube is wound around the sampling needle valve to prevent flashing of the liquid to atmospheric pressure.
	3	Open the needle valve and measure out a small sample directly into a GC compatible sampling bottle. Close the lid immediately and label "B".
	4	To sample the reflux line, open the needle valve slightly, position a GC compatible sampling bottle and quickly flip the 3-way sampling valve between the sampling point and reflux line. Close the lid immediately and label "D".
	5	In the case of a continuous system, open the feed sampling needle valve and measure out a small sample directly into a GC compatible sampling bottle. Close lid immediately and label "F".
	6	Write the RUN-ID and time displayed on the CD control program GUI onto each sample bottle.
	7	To sample the off-gas check that the condenser is not overfilled. NO LIQUID MAY ENTER THE micro GC-TCD!
	8	Open the reference gas manifold shut-off valve, which is connected to the reference gas supply line.
	9	Open the reference gas cylinder and set the supply pressure to at least 3 bar(g) via the pressure regulator.
	10	Activate the reference gas mass flow controller and set the flow rate to the same order of magnitude (or as close as possible) to that of the off-gas.
	11	Turn the 3-way valve to bypass the off-gas catchpot and wait 5 minutes so that the 1/8" feed line to the micro GC-TCD is purged with the current off-gas composition.
	12	Switch the 4-way valve to the CD column (points to the wall if GC is connected) and run the micro GC-TCD sampling program.
	13	When the sampling program is complete, reroute the off-gas through the off-gas catchpot via the 3-way valve and switch the 4-way valve back to the other system.
	14	Switch off the reference gas mass flow controller and close the reference gas manifold shut-off valve.
	15	Liquid samples are to be analysed in any available GC or the GC-MS.

Table A.14: Shutdown.

Duration	No.	Action
	1	Shutdown is triggered either by the user or the control program itself.
	2	The column shuts down based on a user set sequence.
	3	Once the control program GUI indicates that the equipment are shut down, close the off-gas shut-off valve to isolate the system and especially the catalyst from the outside air.
	4	Close all the sample needle valves, reflux line drain ball valve, reboiler level indicator drain ball valve, off-gas shut-off valve, catchpot drain ball valves, reboiler and reflux drum filling ball valves and the low pressure outlet gauge isolation valve.
	5	Pressurize the system with argon to above its current setting or the vacuum created in the column by the cooling liquid will suck liquid (and possibly air) in through the HPLC pump.
	6	Close the gas utility lines. The compressed air line may be left open unless the column will be out of use for and extended period of time.
	7	Allow the tap water to siphon through the submersible pump and condenser for a while to expedite cooling of the system before closing the tap water utility mains shut-off valve.

Table A.15: Emergency shutdown.

Duration	No.	Action
	1	An emergency shutdown may be software triggered either by the user or control program, or hardware triggered by the user by flipping the main electrical supply switch to the "off" position.
	2	Essentially, the emergency shutdown cuts power to the entire system, excluding the computer which will run the required shutdown scripts and exit normally.
	3	After an emergency shutdown, follow the standard shutdown procedures.
	4	Do a fault analysis to determine the reason for the shutdown and take remedial action.

Appendix B

xPVT Property estimation techniques

B.1 Properties

Table B.1: Property estimation techniques - Liquid.

Limitation	Method	Equation	Source
Heat capacity, c_p^L, J/kmol.K			
Ideal, $T < T_c$	Correlation	$c_{p,i}^L = c_{i,0}T^0 + c_{i,1}T^1 + c_{i,2}T^2 + c_{i,3}T^3 + c_{i,4}T^4$	Perry et al. [1997]
$T > T_c$	(Hypothetical)	$c_{p,i}^L = c_{p,i}^V$	-
Mixtures	Mole weighted averages	$c_{p,mix}^L = \sum_{i=1}^{c} x_i c_{p,i}^L$	-
Heat conductivity, k_c^L			
$T_r \leq 0.8$, $P \leq 3.4 \times 10^6$ Pa, Organics	Pachaiyappan et al., Riedel	$k_{c,i}^L = c_1 \rho_{293.15K,i} M_i^{c_2} \frac{3 + 20(1 - T_{r,i})^{2/3}}{3 + 20(1 - 293.15/T_c)^{2/3}}$, $c_1 = 4.407 \times 10^{-4}$, $c_2 = 0.7717$	Perry et al. [1997]
$T > T_c$	(Hypothetical)	$k_{c,i}^L = k_{c,i}^V$	-
Mixtures	Mole weighted averages	$k_{c,mix}^L = \sum_{i=1}^{c} x_i k_{c,i}^L$	-
Diffusion, $D_{i,j}^L$			
Infinite dilution	Wilke and Chang	$D_{i,j}^{L,inf} = 1.1728 \times 10^{-16} \frac{\sqrt{f_{ass,j} M_j} \cdot T}{\eta_j V_{bp,i}^{0.6}}$, $f_{ass,j} = 2.0$	Taylor & Krishna [1993]
Finite dilution	Vignes equation	$D_{i,j}^L = \prod_{i=1}^{c} (D_{i,k}^{L,inf} D_{j,k}^{L,inf})^{x_k/2}$	Vignes [1966] generalized by Kooijman & Taylor [1991]

Table B.1: Property estimation techniques - Liquid.

Limitation	**Method**	**Equation**	**Source**
Density, ρ^L			
Ideal, $T < T_c$	Correlation	$\rho_i^L = \frac{c_{i,1}}{c_{i,2}^{1+(1-T/c_{i,3})^{c_{i,4}}}}$	Perry et al. [1997]
Ideal mixtures, $T < T_c$	-	$\rho_{mix}^L = \left(\sum_{i=1}^{c} \frac{x_i}{\rho_i^L} \right)^{-1}$	First principles
Non-ideal mixtures, $T > T_c$	EOS: vdW, RK, SRK, PR, PSRK-Unifac	see section B.2	Seader & Henley [1998], Sandler [1999]
Surface Tension			
$T < T_{high}^{Jasper}$	Regression	$\sigma_i^L = [c_{i,1} - c_{i,2}(T - 273.15)]1 \times 10^{-5}100$	Jasper [1972]
$T_{high} < T < T_c$	Extrapolation	$\sigma_i^L = [d(1 - T_{r,i})^e]1 \times 10^{-5}100$	Perry et al. [1997]
		$e = \frac{c_{i,2}[(T_{c,i} - 273.15) - (T_{high}^{Jasper} - 273.15)]}{c_{i,1} - c_{i,2}(T_{high}^{Jasper} - 273.15)}$	
		$d = [c_{i,1} - c_{i,2}(T_{high}^{Jasper} - 273.15)](1 - T_{r,i})^{-e}$	
$T > T_c$	-	0	Perry et al. [1997]
Mixtures	Mole weighted averages	$\sigma_{mix}^L = \sum_{i=1}^{c} x_i \sigma_i^L$	-
Vapour pressure, P_{vap}			

Table B.1: Property estimation techniques - Liquid.

Limitation	**Method**	**Equation**	**Source**
$T < T_c$	Correlation	$P_{vap} = exp\left[c_1 + c_2/T + c_3/\log(T) + c_4 T^{c_5}\right]$	Perry et al. [1997]
Viscosity, η^L			
$T < T_c$, Hydrocarbons	Letsou and Stiel	$\eta_i^L = \frac{\lambda_1 + \omega_i \lambda_2}{\lambda}$ $\lambda = 2173.424 \frac{T_{c,i}^{1/6}}{M_i^{0.5} P_{c,i}^{2/3}}$ $\lambda_1 = (1.5174 - 2.135 T_{r,i} + 0.75 T_{r,i}^2) 1 \times 10^{-5}$ $\lambda_2 = (4.2552 - 7.674 Tr_{r,i} + 3.4 T_{r,i}^2) 1 \times 10^{-5}$	Perry et al. [1997]
$T > T_c$	(Hypothetical)	$\eta_i^L = \eta_i^V$	Perry et al. [1997]
Mixture, $T < T_c$, Hydrocarbons	Letsou and Stiel	$\eta_{mix}^L = \sum_{i=1}^{c} x_i \cdot \log\left(\eta_i^L\right)$	Perry et al. [1997]

Table B.2: Property estimation techniques - Vapour.

Limitation	Method	Equation	Source
Heat capacity, c_p^V			
Ideal	Correlation	$c_{p,i}^V = c_{i,1} + c_{i,2}\left[\frac{c_{i,3}/T}{sinh(c_{i,3}/T)}\right]^2 + c_{i,4}\left[\frac{c_{i,5}/T}{cosh(c_{i,5}/T)}\right]^2$	Perry et al. [1997]
Mixtures	Mole weighted averages	$\sum_{i=1}^{c} y_i c_{p,i}^V$	-
Heat conductivity, k_c^V			
Pure non-hydrocarbon gases, linear non-associating molecules, $P < 101325$ Pa	Method of Stiel and Thodos	$k_{c,i}^V = \eta_i^V / M_i \cdot [1.3(c_{p,i}^V - 8314) + 14644 - 2928.8/T_{r,i}]$	Perry et al. [1997]
Pure non-hydrocarbon gases, linear non-associating molecules, $P > 101325$ Pa	Method of Stiel and Thodos	$k_{c,i}^V = \eta_i^V / M_i \cdot [1.3(c_{p,i}^V - 8314) + 14644 - 2928.8/T_{r,i}]$ if $\rho_r \leq 0.5 : c = [2.702, 0.535, -1.000]$ if $0.5 \leq \rho_r \leq 2 : c = [2.528, 0.670, -1.069]$ if $\rho_r > 2 : c = [0.574, 1.155, 2.016]$ $k_{c,i}^V = k_{c,i}^V + \frac{c_1 10 \times 10^{-4}(e^{c_2\rho_r} + c_3)}{\frac{T_{c,i}^{1/6} M_i^{0.5}}{(P_{c,i} 1 \times 10^{-6})^{2/3}} Z_{c,i}^5}$	Perry et al. [1997]

Table B.2: Property estimation techniques - Vapour.

Limitation	Method	Equation	Source
Methane and cyclic compounds, $P < 350000$ Pa; $T_r < 1$	Misic and Thodos	$\lambda = T_{c,i}^{1/6} M_i^{0.5} \left(\frac{101325}{P_{c,i}}\right)^{2/3}$ $k_{c,i}^V = 4.45 \times 10^{-7} T_{r,i}(c_{p,i}^V/\lambda)$	Perry et al. [1997]
$P > 101325$ Pa	Method of Chung	$k_{c,i}^V = 3.75\psi\eta_i^V 8314/M_i$ $\alpha = (c_{i,p}^V - 8314)/8314 - 3/2$ $\beta = 0.7862 - 0.7109\omega_i + 1.3168\omega_i^2$ $Z = 2.0 + 10.5T_{r,i}^2$ $\psi = 1 + \alpha\frac{0.215 + 0.28288\alpha - 1.061\beta + 0.26665Z}{0.6366 + \beta Z + 1.061\alpha\beta}$	Poling et al. [2007]
Gas mixtures, $P < 101325$ Pa, non-polar		For H_2, He and Ne $S_i = 79.0$, else $S_i = 1.5T_{nbp,i}$ $A_{i,j} = 0.25\left[\frac{1 + \sqrt{\eta_i^V/\eta_j^V}(M_j/M_i)^{0.75}(T + S_i)}{T + S_j}\right]^2 \frac{T + \sqrt{S_i S_j}}{T + S_i}$ $k_{c,mix}^V = \sum_{i=1}^{c} \frac{y_i k_{c,i}^V}{\sum_{i=1}^{c} y_j A_{i,j}}$	
Diffusion, $D_{i,j}^V$			

Table B.2: Property estimation techniques - Vapour.

Limitation	Method	Equation	Source
Low pressures	Kinetic theory of gases	$D_{i,j}^V = \frac{1.013 \times 10^{-2} T^{1.75} \sqrt{1/Mr_j + 1/Mr_j}}{P(V_{Fuller,j}^{1/3} + V_{Fuller,j}^{1/3})^2}$	Kooijman & Taylor [1998]
Density, ρ			
Mixtures, Ideal gases	Ideal gas law	$\rho_{mix}^V = \frac{P \cdot M_{mix}}{R_0 \cdot T}$	-
Non-ideal mixtures and $T > T_c$	EOS: vdW, RK, SRK, PR, PSRK-Unifac	see Appendix B.2	Seader & Henley [1998], Sandler [1999]
Viscosities, ν			
Hydrocarbons, $T_r < 0.6$	Stiel and Thodos	$\eta_i^V = \left[\frac{4.6 \times 10^{-4}(0.0003400 T_{r,i}^{0.94}) M_i^{0.5} P_{c,i}^{2/3}}{T_{c,i}^{1/6}}\right] \frac{1}{1000}$	Perry et al. [1997]
Hydrocarbons, $T_r > 0.6$	Dean and Stiel	$\eta_i^V = \eta_i^V + \left[\frac{5 \times 10^{-8}(M_i^{0.5} P_{c,i}^{2/3})(e^{1.439\rho_{r,i}} - e^{-1.11\rho_{r,i}^{1.858}})}{T_{c,i}^{1/6}}\right] \frac{1}{1000}$	Perry et al. [1997]

Table B.2: Property estimation techniques - Vapour.

Limitation	Method	Equation	Source
Non-hydrocarbon gases	Yoon and Thodos	$\eta_i^V = \frac{1 + c_1 T_r^{c_2} - c_3 e^{c_4 T_r} + c_5 e^{c_6 Tr}}{(1 \times 10^8 curly)}$	
		Constants used in the equations:	
		$H_2 : C = [47.65, 0.657, 20.0, -0.858, 19.0, -3.995]$	
		$He : C = [52.57, 0.656, 18.9, -1.144, 17.9, -5.182]$	
		$else : C = [46.10, 0.618, 20.4, -0.449, 19.4, -4.058]$	
		$curly = 2173.4241 T_{c,i}^{1/6} / (\sqrt{M_i} P_{c,i}^{2/3})$	
Mixture		$\eta^V_{intaction,i,k} = \frac{(1 + \sqrt{\eta_i^V / \eta_k^V}(M_k/M_i)^{0.25})^2}{\sqrt{8(1 + M_i/M_k)}}$	Kooijman & Taylor [1998]
		$\eta^V_{mix} = \sum_{i=1}^{c} \frac{y_i \eta_i^V}{\sum_{k=1}^{c} y_k \eta^V_{interaction,i,k}}$	

Table B.3: Property estimation techniques - Other.

Limitation	Method	Equation	Source
Mixture molar masses, Mr_{mix}			
None		$Mr^{mix} = \sum_{i=1}^{c} x_i Mr_i$	First principles
Reduced variables, T_r, P_r, V_r, ρ_r			
None		$T_r = \frac{T}{T_c}$ $P_r = \frac{P}{P_c}$ $V_r = \frac{V}{V_c}$ $\rho_r = \frac{1}{V_r}$	Per definition
Dimensionless number			
None		$\text{Re} = \frac{\rho_{mix}^{mass} v d_{eq}}{\nu_{mix}}$ $\text{Sc} = \frac{\nu_{mix}}{\rho_{mix}^{mass} D}$ $\text{Le} = \frac{k_{c,mix}}{D c_{p,mix} \rho_{mix}^{mass}}$	Per definition
Superficial velocities			

Table B.3: Property estimation techniques - Other.

Limitation	Method	Equation	Source
None		$u^{phase} = \frac{F^{phase}}{\rho_{mix}^{phase} A_{\text{perpendicular to flow}}}$	Per definition

B.2 Equations of state

It can be shown that all the cubic equations of state discussed here can be written as a cubic polynomial in the Z-form (where Z is the compressibility factor).

$$0 = f_3(A,B)Z^3 + f_2(A,B)Z^2 + f_1(A,B)Z^1 + f_0(A,B)Z^0 \tag{B.1}$$

where A and B are defined as follows:

$$A = a\frac{P}{(R_0T)^2} \tag{B.2}$$

$$B = b\frac{P}{R_0T} \tag{B.3}$$

Here, a and b can be either pure component values defined for each EOS or mixture values calculated by using an appropriate mixing rule. Smith et al. [1996] and Seader & Henley [1998] discuss the different EOS's and solutions obtainable. In general, physically feasible solutions are positive, real and greater than b. At supercritical conditions, $T > T_c$, 1 real and 2 conjugated imaginary roots exist. At the supercritical point, $T = T_c$, 3 equivalent real roots exist. If $T < T_c$ and a VLE exists, 3 real roots exist, where the largest root corresponds to the vapour and the smallest root to the liquid phase, while the intermediate value can be ignored.

B.2.1 Redlich-Kwong (RK)

The Redlich-Kwong (RK) equation is defined as follows:

$$P = \frac{R_0T}{\upsilon - b} - \frac{a}{\upsilon^2 + b\upsilon} \tag{B.4}$$

$$a_i = 0.42748\frac{R_0^2T_{c,i}^{2.5}}{P_{c,i}T^{0.5}} \tag{B.5}$$

$$b_i = 0.08664\frac{R_0T_{c,i}}{P_{c,i}} \tag{B.6}$$

where $a = a_i$ and $b = b_i$ in the case of a pure component. Mixtures require a suitable mixing rule as discussed in section B.2.4. The Z-form is calculated as follows:

$$0 = (1)Z^3 + (-1)Z^2 + (A - B - B^2)Z + (-AB) \tag{B.7}$$

B.2.2 Soave-Redlich-Kwong (SRK)

The Soave-Redlich-Kwong (SRK) equation is defined as follows:

$$P = \frac{R_0 T}{\upsilon - b} - \frac{a}{\upsilon^2 + b\upsilon} \tag{B.8}$$

$$f_w = 0.48 + 1.57\omega_i - 0.176\omega_i^2 \tag{B.9}$$

$$a_i = 0.42748 \frac{R_0^2 T_{c,i}^2 (1 + f_w(1 - \sqrt{T/T_{c,i}}))^2}{P_{c,i}} \tag{B.10}$$

$$b_i = 0.08664 \frac{R_0 T_{c,i}}{P_{c,i}} \tag{B.11}$$

where $a = a_i$ and $b = b_i$ in the case of a pure component. Mixtures require a suitable mixing rule as discussed in section B.2.4. The Z-form is calculated as for the RK EOS.

B.2.3 Peng-Robinson (PR)

The Peng-Robinson (PR) equation is defined as follows:

$$P = \frac{R_0 T}{\upsilon - b} - \frac{a}{\upsilon^2 + 2b\upsilon - b^2} \tag{B.12}$$

$$f_w = 0.37464 + 1.54226\omega_i - 0.26992\omega_i^2 \tag{B.13}$$

$$a_i = 0.45724 \frac{R_0^2 T_{c,i}^2 (1 + f_w(1 - \sqrt{T/T_{c,i}}))^2}{P_{c,i}} \tag{B.14}$$

$$b_i = 0.07780 \frac{R_0 T_{c,i}}{P_{c,i}} \tag{B.15}$$

where $a = a_i$ and $b = b_i$ in the case of a pure component. Mixtures require a suitable mixing rule as discussed in section B.2.4. The Z-form is calculated as follows:

$$0 = (1)Z^3 + (B-1)Z^2 + (A - 2B - 3B^2)Z + (B^2 + B^3 - AB) \tag{B.16}$$

B.2.4 Mixing rules

General mixing rule

Seader & Henley [1998] supply the following mixing rule for mixtures of hydrocarbons and/or light gases:

$$a_{i,j} = \sqrt{a_i a_j}(1 - \aleph_{i,j}) \tag{B.17}$$

$$a = \sum_{i=1}^{c} \sum_{j=1}^{c} x_i x_j a_{i,j} \tag{B.18}$$

$$b = \sum_{i=1}^{c} x_i b_i \tag{B.19}$$

where $\aleph_{i,j}$ is an interaction parameter that compensates for modest polarity in the components and which will be assumed zero for a mixtures of hydrogen, n-hexane, 1-hexene and 2-hexene. Equations B.2 and B.3 can now be applied:

$$A_{i,j} = a_{i,j}\frac{P}{(R_0T)^2} \tag{B.20}$$

$$B_i = b_i\frac{P}{R_0T} \tag{B.21}$$

$$A = a\frac{P}{(R_0T)^2} \tag{B.22}$$

$$B = b\frac{P}{R_0T} \tag{B.23}$$

PSRK mixing rule

For a VLE containing supercritical gases and highly non-ideal liquids the EOS's in section B.2 are inadequate. In such cases a G^E method such as the PSRK method [Fischer & Gmehling, 1995; Gmehling, 1995; Chen et al., 2002; Horstmann et al., 2005] is used in an attempt to bridge the gap between an EOS and activity coefficient model.

The PSRK calculates $a_{i,j}$ and b as before (equations B.17 and B.19 respectively). However, a is then calculated via the use of G^E (eq. B.24), which is in turn calculated from a suitable activity coefficient model.

$$a = bR_0T\left[\sum_{i=1}^{c}\frac{x_ia_{i,i}}{b_iR_0T} + \frac{G^E/(R_0T) + \sum_{i=1}^{c}x_ilog(b/b_i)}{log(1.1/(1.1+1.0))}\right] \tag{B.24}$$

B.3 Activity coefficient model

B.3.1 UNIFAC

Since its conception in the 1970's, the original UNIFAC has been continuously developed and updated (e.g. Gmehling et al. [1982]; Hansen et al. [1991]; Wittig et al. [2003]) as well as a modified UNIFAC (Dortmund) which was propounded in 1987 (e.g. Gmehling et al. [1993, 2002]). The UNIFAC method is a group contribution method similar to the UNIQUAC method that calculates the activity coefficient and Gibbs excess energy as the sum of a combinatorial and residual term.

$$\gamma_i = exp\left(ln\gamma_i^C + ln\gamma_i^R\right) \tag{B.25}$$

$$G^E = R_0T\sum_{i=1}^{c}x_i(ln\gamma_i^C + ln\gamma_i^R) \tag{B.26}$$

An extensive list of PSRK/UNIFAC parameters are available to the public and published by Horstmann et al. [2005]. Essentially, a component is broken down into main groups, each of which can be broken down further into substituent subgroups. The behaviour of a component is described by manipulation of the R_k and Q_k values of a subgroup (equations B.27 and B.28), while the interaction between components are described by the main groups associated to the subgroup via the main groups' three parameter equation, eq. B.29.

$$r_i = \sum_{k=1}^{n_{subgroups}} n_{i,k}^{subgroups} R_k \tag{B.27}$$

$$q_i = \sum_{k=1}^{n_{subgroups}} n_{i,k}^{subgroups} Q_k \tag{B.28}$$

$$\psi_{n,m} = exp\left(-(C_{n,m,1}^{UNIFAC} + C_{n,m,2}^{UNIFAC} T + C_{n,m,3}^{UNIFAC} T^2)/T\right) \tag{B.29}$$

where $\mathbf{C_{n,m}^{UNIFAC}}$ are the 3 constants describing the interaction between main groups m and n.

The *combinatorial* part of the equation is calculated as follows:

$$ln\gamma_i^C = 1 - V_{emp} + log(V_{emp}) - 5q_i \left[1 - \frac{V_{aux}}{F_{aux}} + log\left(\frac{V_{aux}}{F_{aux}}\right)\right] \tag{B.30}$$

The auxiliary and empirical values depend on whether the original or modified UNIFAC approach is used. In general the following holds:

$$V_{aux} = \frac{r_i}{\sum_{j=1}^{c} x_j r_j} \tag{B.31}$$

$$V_{emp} = V_{aux} \tag{B.32}$$

$$F_{aux} = \frac{q_i}{\sum_{j=1}^{c} x_j q_j} \tag{B.33}$$

However, if the modified approach is used, V_{emp} is calculated as follows:

$$V_{emp} = \frac{r_i^{0.75}}{\sum_{j=1}^{c} x_j r_j^{0.75}} \tag{B.34}$$

Calculation of the *residual* term is slightly more involved and requires calculation of

several variables, including an interaction parameter. The residual is defined as follows:

$$ln\gamma_i^R = \sum_{k=1}^{n_{subgroups}} n_{i,k}^{subgroups}(ln\Gamma_k - ln\Gamma_k^I) \tag{B.35}$$

$$ln\Gamma_k^I = Q_k \left[1 - log\left(\sum_{m=1}^{n_{subgroups}} \theta_m \psi_{m,k} \right) - \sum_{m=1}^{n_{subgroups}} \frac{\theta_m \psi_{k,m}}{\sum_{n=1}^{n_{subgroups}} \theta_n \psi_{n,m}} \right] \tag{B.36}$$

The difference between $ln\Gamma_k$ and $ln\Gamma_k^I$ lies in the calculation of X_m,which is used in the calculation of θ_m as defined in eq B.37.

$$\theta_m = \frac{Q_m X_m}{\sum_{n=1}^{n_{subgroups}} Q_n X_n} \tag{B.37}$$

When calculating X_m via eq. B.38, $\mathbf{x} = \mathbf{x}$ for $ln\Gamma_k$ and $\mathbf{x} = \mathbf{I}$ (where $\mathbf{I}$ is the identity matrix) for $ln\Gamma_k^I$.

$$X_m = \frac{\sum_{i=1}^{c} n_{i,m}^{subgroups} x_i}{\sum_{i=1}^{c} \sum_{n=1}^{n_{subgroups}} n_{i,n}^{subgroups} x_i} \tag{B.38}$$

B.4 Equilibrium coefficients

From Smith et al. [1996] VLE in a non-ideal solution may be expressed as follows for component i:

$$\phi_i^V y_i P = \gamma_i x_i P_i^{sat} \phi_i^{sat} exp\left[\frac{v_i^L (P - P_i^{sat})}{R_0 T} \right] \tag{B.39}$$

where the term in square brackets is known as the Poyinting correction factor. For ideal systems at low pressures, Raoult's law can be used with the fugacities, activity coefficients and Poynting correction factor approximated as unity:

$$K_i^{eq} = \frac{y_i}{x_i} = \frac{P_i^{vap}}{P_t} \tag{B.40}$$

However, this does not hold for non-ideal systems or systems containing supercritical gases which by definition do not have vapour pressures. In such cases, EOS's were used to calculate the liquid and vapour fugacities and the following definition of equilibrium

applied [Smith et al., 1996; Seader & Henley, 1998]:

$$K_i^{eq} = \frac{y_i}{x_i} = \frac{\phi_i^L}{\phi_i^V} \tag{B.41}$$

The fugacities for the liquid and vapour phases can be calculated by using an equation of state to calculate respectively Z^L, Z^V and the associated mixture constants. The Z value and constants are then used to calculate ϕ. For the PR EOS, Sandler [1999] shows that:

$$\phi_i = exp\left[\frac{B_i}{B(Z-1)} - log(Z-B) - \frac{A}{2\sqrt{2}B}\left(2\sum_{i=1}^{c}\frac{x_j A_{i,j}}{A} - \frac{B_i}{B}\right) log\left(\frac{Z+(1+\sqrt{2})B}{Z+(1-\sqrt{2})B}\right)\right] \tag{B.42}$$

Using the same methodology, a similar equation can be derived for the RK and SRK EOS's:

$$\phi_i = exp\left[\frac{(Z-1)B_i}{B} - log(Z-B) - \frac{A}{B}\left(2\sqrt{\frac{A_{ii}}{A}} - \frac{B_i}{B}\right) log\left(1+\frac{B}{Z}\right)\right] \tag{B.43}$$

Appendix C

Geometrically dependent properties

The properties in this section differ from those in Section B in that, apart from composition, pressure and temperature, they are also dependent on they're geometric environment.

C.1 Random Packings

The liquid and gas phase mass transfer coefficients for random packing are given by the correlations of Onda et al. [1968]:

$$k_{i,k}^{L,\text{random}} = 0.0051 \left(\text{Re}^{I,L}\right)^{0.667} (Sc^L)^{-0.5} (a_p d_p)^{0.4} \left(\frac{\rho_{mix}^L}{\eta_{mix}^L g}\right)^{-0.33} \tag{C.1}$$

$$k_{i,k}^{V,\text{random}} = A(\text{Re}^V)^{0.7}(Sc^V)^{0.333} (a_p d_p)^{-2} \left(a_p D_{i,k}^V\right) \tag{C.2}$$

The Schmidt numbers and superficial liquid and gas velocities are calculated as before in Table B.3, using liquid or vapour properties depending on the phase. $A = 2$ if $d_p < 0.012$ m, else $A = 5.23$, with d_p being the diameter of a sphere with the same surface area as that of the packing. Calculation of the liquid and vapour Reynolds numbers are expressed in terms of the packing's interfacial area:

$$Re^{phase} = \frac{\rho_{mix}^{phase} u_{phase}}{\eta_{mix}^{phase} a_p} \tag{C.3}$$

The liquid phase Reynolds number based on the interfacial area density (a_d) is defined in eq C.4. Here, the method of Bravo & Fair [1982] will be used to calculate a_d as in

Taylor & Krishna [1993] [a].

$$\mathrm{Re}^{I,L} = \frac{\rho^L_{mix} u_L}{\eta^L_{mix} a_d} \tag{C.4}$$

$$a_d = 19.78 a_p (Ca_L Re^V_{mix})^{0.392} \sigma^{0.5}_{mix} H^{-0.4} \tag{C.5}$$

$$Ca_L = \frac{u_L \eta^L_{mix}}{\sigma_{mix}} \tag{C.6}$$

$$\tag{C.7}$$

Note that H refers to the height of the section of packing.

C.2 Structured packings

The method followed here is that of Bravo, Fair and Rocha (1985) as described in Taylor & Krishna [1993], which expresses the liquid and vapour mass transfer coefficients as follows:

$$k^{L,\text{structured}}_{i,k} = 2\sqrt{\frac{D^L_{i,k}}{\pi t_L}} \tag{C.8}$$

$$k^{V,\text{structured}}_{i,k} = \frac{Sh^V D^V_{i,k}}{d_{eq}} \tag{C.9}$$

To calculate the dimensionless Reynolds and Schmidt numbers it is firstly necessary to calculate the effective diameter and superficial velocities of the packing. The effective diameter is defined as follows (also see Table 4.2):

$$d_{eq} = Bh_c \left(\frac{1}{B + 2S} + \frac{1}{2S} \right) \tag{C.10}$$

The effective superficial gas velocity is defined in terms of the packing voidage (ϵ) and packing angle relative to the horizontal (θ). The effective superficial liquid velocity is then calculated based on the "perimeter per unit cross-sectional area" (P) and Γ, the liquid flow rate per P.

$$u_{V,effective} = \frac{V}{\rho^V_{mix} A_{column}} \cdot \frac{1}{\varepsilon \sin(\theta)} \tag{C.11}$$

[a] Note the correct form of Ca_L on p.61 of Taylor & Krishna [1993].

$$P = \frac{4S + B}{Bh_c} \tag{C.12}$$

$$\Gamma = \frac{\rho^{L,mix} u_L}{P} \tag{C.13}$$

$$u_{L,effective} = \frac{3\Gamma}{2\rho^L_{mix}} \left[\frac{\left(\rho^L_{mix}\right)^2 g}{3\eta^L_{mix}\Gamma} \right]^{1/3} \tag{C.14}$$

The Schmidt number is defined in Table B.3 while the resulting vapour phase Reynolds number is:

$$\mathrm{Re}^V = \frac{d_{eq}\rho^V_{mix}\left(u_{V,effective} + u_{L,effective}\right)}{\eta^V_{mix}} \tag{C.15}$$

Finally, to complete the liquid phase mass transfer coefficient via the penetration model, the exposure time must be calculated.

$$t_L = \frac{S}{u_{L,effective}} \tag{C.16}$$

Appendix D

Constant molar overflow (CMO)

From eq 5.27 it can be shown that:

$$(1+r_j^V)V_j - V_{j+1} = L_{j-1} - (1+r_j^L)L_j + F_j^L - r_{i,j}^L + F_j^V \tag{D.1}$$

From eq. 5.38 and the assumptions that $H_j^L \approx H_{j+1}^L$, $H_j^V \approx H_{j+1}^V$ and $H_j^{vap} \approx H_{j+1}^{vap}$:

$$eqE_j = H_j^L\left[(1+r_j^L)L_j - L_{j-1}\right] + H_j^V\left[(1+r_j^V)V_j - V_{j+1}\right] - F_j^L H_j^{LF} - F_j^V H_j^{VF} - Q_j^T \tag{D.2}$$

Then, from eq. D.1:

$$\begin{aligned} eqE_j &= H_j^L\left[+(1+r_j^L)L_j - L_{j-1}\right] + \\ &\quad H_j^V\left[-(1+r_j^L)L_j + L_{j-1} + F_j^L - r_{i,j}^L + F_j^V\right] \\ &\quad -F_j^L H_j^{LF} - F_j^V H_j^{VF} - Q_j^T \end{aligned} \tag{D.3}$$

Rearranging:

$$\begin{aligned} eqE_j &= \left[(1+r_j^L)L_j - L_{j-1}\right](H_j^L - H_j^V) \\ &\quad +H_j^V(F_j^L + F_j^V) - r_{i,j}^L H_j^V - F_j^L H_j^{LF} - F_j^V H_j^{VF} - Q_j^T \end{aligned} \tag{D.4}$$

From $\Delta H^{vap} = H^V - H^L$ and rearranging:

$$(1+r_j^L)L_j - L_{j-1} = \frac{H_j^V F_j^T - (F_j^L H_j^{LF} + F_j^V H_j^{VF})}{\Delta H^{vap}} - \frac{r_{i,j}^L H_j^V}{\Delta H^{vap}} - \frac{Q_j^T}{\Delta H^{vap}} \tag{D.5}$$

The q-factor relates the change in the internal flow rates to the feed flow rate. Thus,

dividing by the total feed:

$$\frac{(1+r_j^L)L_j - L_{j-1}}{F_j^T} = \frac{H_j^V - (\frac{F_j^L}{F_j^T}H_j^{LF} + \frac{F_j^V}{F_j^T}H_j^{VF})}{\Delta H^{vap}} - \frac{r_{i,j}^L H_j^V}{F_j^T \Delta H^{vap}} - \frac{Q_j^T}{F_j^T \Delta H^{vap}} \tag{D.6}$$

Assuming no reaction nor heat exchange on the feed stage, eq D.6 reduces to eq. 7-20 in Seader & Henley [1998].

Appendix E

Selected CD Experimental Data

Table E.1: Summary of generated experimental data

Run No			1.1	2.1	2.2
Run ID		-	071206-0827	071214-1114	071214-1114
Sample time		s	114881	74226	130632
Reboiler duty		W	150	250	350
Condenser pressure		$\cdot 10^5$ Pa(a)	1.6	1.6	1.7
Cage design		-	2	2	2
Mass balance error			-3.2	-3.1	0.6
Conversion	Hydrogen	%	0.4	0.8	2.9
	1-Hexene	%	11.6	-4.4	0.6
Selectivity	n-Hexane	%	1.5	-0.2	-3.5
	2-Hexene	%	0.1	-0.3	2.4
Hydrogen feed rate		kg/s	1.09E-06	1.09E-06	1.09E-06
		kmol/s	5.43E-07	5.43E-07	5.43E-07
Liquid feed	Flow rate	kg/s	4.40E-05	4.41E-05	4.40E-05
		kmol/s	5.20E-07	5.22E-07	5.21E-07
	n-Hexane	mol/mol	50.0	50.3	49.9
	1-Hexene	mol/mol	49.3	48.9	49.3
	2-Hexene	mol/mol	0.2	0.3	0.3
	Total	mol/mol	99.5	99.5	99.6
Bottoms	Flow rate	kg/s	3.28E-05	1.11E-05	2.45E-05
		kmol/s	3.86E-07	1.30E-07	2.87E-07
	n-Hexane	mol/mol	64.1	84.0	69.0
	1-Hexene	mol/mol	34.9	14.6	29.6
	2-Hexene	mol/mol	0.4	0.7	0.9
	Total	mol/mol	99.4	99.2	99.5
Distillate	Flow rate	kg/s	5.97E-06	2.80E-05	1.29E-05
		kmol/s	7.07E-08	3.31E-07	1.53E-07
	n-Hexane	mol/mol	33.5	39.3	26.5
	1-Hexene	mol/mol	65.5	59.8	72.7
	2-Hexene	mol/mol	0.6	0.6	0.5
	Total	mol/mol	99.6	99.6	99.7
Off-gas	Flow rate	kg/s	7.77E-06	7.45E-06	7.42E-06
		kmol/s	6.19E-07	6.13E-07	6.03E-07
	1-Hexene	mol/mol	7.4	8.1	9.8
	n-Hexane	mol/mol	5.3	4.1	2.7
	Hydrogen	mol/mol	87.3	87.8	87.5
	2-Hexene	mol/mol	0.0	0.0	0.0
	Total	mol/mol	100.0	100.0	100.0
Reflux rate		m^3/s	4.98E-06	7.34E-06	1.22E-05
Condenser duty		W	-81.5	-156.2	-244.9
Temperature profile	T-0	K	315.2	340.8	342.9
	T-1	K	337.6	343.4	344.0
	T-2	K	338.8	343.5	343.8
	T-3	K	339.5	344.7	345.1
	T-4	K	341.0	345.7	345.9
	T-5	K	341.9	346.1	346.2
	T-6	K	342.2	346.8	346.8
	T-7	K	342.5	347.3	347.3
	T-C	K	285.5	287.0	285.8
	T-R	K	348.1	350.6	349.8

2.3	2.4	2.5	3.1	3.2
071214-1114 176872	071214-1114 218413	071214-1114 263673	080116-0836 96411	080116-0836 184972
250	250	250	350	350
1.7	2.0	20.0	4.5	6.3
2	2	2	2	2
-0.2	1.3	1.5	3.2	5.6
1.1	1.2	1.4	12.3	21.8
-0.2	4.7	5.5	29.0	46.7
6.5	0.1	0.3	0.4	0.5
-7.6	0.4	0.3	0.5	0.4
1.09E-06	1.09E-06	1.09E-06	1.09E-06	1.09E-06
5.43E-07	5.43E-07	5.43E-07	5.43E-07	5.43E-07
4.41E-05	4.41E-05	4.42E-05	4.45E-05	4.45E-05
5.22E-07	5.22E-07	5.25E-07	5.31E-07	5.31E-07
49.3	48.7	33.8	0.1	0.1
50.0	50.6	65.5	99.7	99.7
0.3	0.3	0.4	0.0	0.0
99.6	99.7	99.8	99.8	99.8
2.21E-05	2.84E-05	2.86E-05	2.90E-05	2.80E-05
2.60E-07	3.33E-07	3.37E-07	3.44E-07	3.31E-07
73.2	65.4	46.7	0.1	0.0
25.3	33.0	51.5	69.2	53.6
1.0	1.2	1.6	15.1	21.4
99.5	99.6	99.7	84.4	75.0
1.56E-05	9.81E-06	9.63E-06	1.28E-05	1.35E-05
1.85E-07	1.16E-07	1.14E-07	1.53E-07	1.59E-07
25.9	22.5	16.5	0.1	0.0
73.2	76.6	82.5	79.5	60.8
0.6	0.7	0.8	10.0	18.4
99.7	99.7	99.8	89.5	79.1
7.45E-06	6.41E-06	6.44E-06	2.35E-06	1.57E-06
6.12E-07	6.00E-07	5.99E-07	4.93E-07	4.33E-07
9.8	8.7	9.6	3.3	1.8
2.5	1.8	1.0	0.1	0.2
87.7	89.5	89.4	96.6	98.0
0.0	0.0	0.0	0.0	0.0
100.0	100.0	100.0	100.0	100.0
7.83E-06	6.00E-06	9.63E-06	4.52E-06	4.59E-06
-148.4	-159.6	-148.6	-156.9	-161.6
339.9	340.5	338.9	349.4	345.1
343.5	349.2	348.9	383.4	399.1
344.1	350.0	349.9	384.8	400.9
344.9	350.7	350.4	384.9	400.6
345.8	351.6	351.1	385.2	400.9
346.3	352.1	351.5	385.3	401.1
346.9	352.7	352.0	385.7	401.4
347.4	353.2	352.5	386.1	402.0
286.4	286.4	286.4	282.2	282.1
351.0	356.5	356.0	389.0	405.2

Run No			4.1	4.2	4.3
Run ID		-	080121-0827	080121-0827	080121-0827
Sample time		s	98026	196292	294249
Reboiler duty		W	350	350	350
Condenser pressure		$\cdot 10^5$ Pa(a)	1.7	1.7	6.0
Cage design		-	1	1	1
Mass balance error			1.4	-0.8	5.9
Conversion	Hydrogen	%	2.8	1.7	21.8
	1-Hexene	%	5.2	4.8	66.0
Selectivity	n-Hexane	%	0.4	0.5	0.6
	2-Hexene	%	0.4	0.9	0.4
Hydrogen feed rate		kg/s	1.09E-06	1.09E-06	2.19E-06
		kmol/s	5.43E-07	5.43E-07	1.09E-06
Liquid feed	Flow rate	kg/s	4.44E-05	4.40E-05	4.44E-05
		kmol/s	5.30E-07	5.21E-07	5.30E-07
	n-Hexane	mol/mol	0.1	48.9	0.1
	1-Hexene	mol/mol	99.6	50.5	99.5
	2-Hexene	mol/mol	0.0	0.3	0.0
	Total	mol/mol	99.8	99.7	99.6
Bottoms	Flow rate	kg/s	2.92E-05	2.96E-05	3.05E-05
		kmol/s	3.48E-07	3.47E-07	3.60E-07
	n-Hexane	mol/mol	0.1	0.0	0.0
	1-Hexene	mol/mol	94.5	33.3	35.9
	2-Hexene	mol/mol	2.3	2.7	22.7
	Total	mol/mol	96.9	36.0	58.7
Distillate	Flow rate	kg/s	9.28E-06	9.67E-06	1.01E-05
		kmol/s	1.11E-07	1.15E-07	1.20E-07
	n-Hexane	mol/mol	1.1	23.5	37.2
	1-Hexene	mol/mol	0.5	1.0	16.5
	2-Hexene	mol/mol	97.8	74.7	37.3
	Total	mol/mol	99.5	99.1	91.0
Off-gas	Flow rate	kg/s	6.41E-06	6.18E-06	3.26E-06
		kmol/s	5.91E-07	5.94E-07	8.72E-07
	1-Hexene	mol/mol	10.8	8.3	1.1
	n-Hexane	mol/mol	0.0	1.9	1.0
	Hydrogen	mol/mol	89.2	89.8	97.3
	2-Hexene	mol/mol	0.0	0.0	0.0
	Total	mol/mol	100.0	100.0	99.4
Reflux rate		m^3/s	2.36E-05	2.12E-05	3.98E-06
Condenser duty		W	-222.4	-219.6	-167.6
Temperature profile	T-0	K	341.3	341.9	346.8
	T-1	K	342.4	343.0	392.2
	T-2	K	342.9	343.4	394.9
	T-3	K	343.3	344.0	394.0
	T-4	K	343.4	344.6	394.2
	T-5	K	343.4	345.0	394.4
	T-6	K	343.4	345.4	395.0
	T-7	K	343.5	345.7	395.7
	T-C	K	281.1	280.1	280.7
	T-R	K	346.0	348.6	401.6

4.4	4.5
080121-0827	080121-0827
359799	402775
350	350
6.0	6.3
1	1
8.0	5.9
22.2	22.6
66.2	66.7
0.5	0.6
0.3	0.4
2.19E-06	2.19E-06
1.09E-06	1.09E-06
4.44E-05	4.44E-05
5.31E-07	5.30E-07
0.1	0.1
99.5	99.5
0.0	0.0
99.6	99.6
2.90E-05	2.73E-05
3.43E-07	3.22E-07
38.2	39.4
36.9	36.0
23.0	22.7
98.1	98.0
1.07E-05	1.34E-05
1.26E-07	1.58E-07
37.7	39.1
34.0	32.6
25.0	25.1
96.8	96.7
3.21E-06	3.11E-06
8.67E-07	8.57E-07
1.1	1.0
1.0	1.0
97.5	98.1
0.0	0.0
99.6	100.0
4.33E-06	4.28E-06
-169.0	-153.7
346.4	345.9
393.0	395.5
395.3	397.5
394.7	396.8
394.8	396.9
395.1	397.2
395.6	397.8
396.3	398.3
280.5	280.5
402.1	404.4

Appendix F

Supplementary results

F.1 Kinetic Analyses

F.1.1 Sensitivity analyses

The sensitivity analyses that were generated for Section 7 are supplied in Tables F.1.

F.1.2 Correlation matrices

The correlations matrices that were generated in this thesis are supplied in Tables F.2 to F.5.

Table F.1: Sensitivity analyses for runs 10-13 and the change in sensitivity as the temperature decreases from runs 13 to 10 to elucidate the rate controlling reaction step(s).

Parameter[a]	Sensitivity analysis				Change in sensitivity		
	10	11	12	13	10	12	13
k^{H2}	2.62	2.9	1.89	1.39	1.88	1.36	1.00
	2.66	2.88	1.88	1.36	1.96	1.38	1.00
K^{H2}	0.00	0.01	0.01	0.04	0.00	0.25	1.00
	0.00	0.01	0.01	0.04	0.00	0.25	1.00
k_1^{ads}	1.35	1.49	0.80	0.77	1.75	1.04	1.00
	1.33	1.48	0.80	0.77	1.73	1.04	1.00
k_2^{ads}	0.19	0.15	0.14	0.08	2.38	1.75	1.00
	0.19	0.15	0.13	0.08	2.38	1.63	1.00
K_1^{ads}	0.58	0.53	0.38	0.44	1.32	0.86	1.00
	0.58	0.53	0.37	0.43	1.35	0.86	1.00
K_2^{ads}	0.24	0.22	0.25	0.11	2.18	2.27	1.00
k_1^{iso1}	0.02	0.04	0.02	0.09	0.22	0.22	1.00
	0.02	0.04	0.02	0.09	0.22	0.22	1.00
k_2^{iso1}	0.00	0.00	0.05	0.03	0.00	1.67	1.00
	0.00	0.00	0.05	0.03	0.00	1.67	1.00
K_1^{iso1}	0.12	0.08	0.05	0.08	1.50	0.63	1.00
	0.12	0.08	0.05	0.08	1.50	0.63	1.00
K_2^{iso1}	0.06	0.07	0.04	0.07	0.86	0.57	1.00
	0.06	0.06	0.04	0.07	0.86	0.57	1.00
k_1^{iso2}	0.02	0.01	0.03	0.07	0.29	0.43	1.00
	0.02	0.01	0.03	0.07	0.29	0.43	1.00
k_2^{iso2}	0.01	0.01	0.04	0.03	0.33	1.33	1.00
	0.01	0.01	0.04	0.03	0.33	1.33	1.00
K_1^{iso2}	0.07	0.15	0.06	0.05	1.40	1.20	1.00
	0.07	0.15	0.06	0.05	1.40	1.20	1.00
K_2^{iso2}	0.09	0.09	0.09	0.01	9.00	9.00	1.00
	0.09	0.09	0.09	0.01	9.00	9.00	1.00
k_1^{des}	0.05	0.01	0.01	0.21	0.24	0.05	1.00
	0.05	0.01	0.01	0.21	0.24	0.05	1.00
k_2^{des}	0.04	0.01	0.04	0.18	0.22	0.22	1.00
	0.04	0.01	0.04	0.18	0.22	0.22	1.00
k_3^{des}	0.02	0.00	0.02	0.03	0.67	0.67	1.00
	0.02	0.00	0.02	0.03	0.67	0.67	1.00
K_1^{des}	0.09	0.10	0.08	0.02	4.50	4.00	1.00
	0.08	0.09	0.08	0.02	4.00	4.00	1.00
K_2^{des}	0.09	0.24	0.10	0.02	4.50	5.00	1.00
	0.09	0.24	0.10	0.02	4.50	5.00	1.00
K_3^{des}	0.07	0.12	0.13	0.01	7.00	13.00	1.00
	0.07	0.12	0.13	0.01	7.00	13.00	1.00
Pressure	3.61	3.53	2.78	2.31	N/A	N/A	N/A
	3.68	3.50	2.75	2.25	N/A	N/A	N/A
W_{cat}	1.64	1.66	1.25	1.25	N/A	N/A	N/A
	1.65	1.65	1.24	1.24	N/A	N/A	N/A
V_{T0}	0.02	0.01	0.02	0.02	N/A	N/A	N/A
	0.02	0.01	0.02	0.02	N/A	N/A	N/A

[a] see Table 7.2 for parameter units. Pressure, W_{cat} and V_{T0} as in Nomenclature.

Table F.2: Correlation matrix for run 10.

	k^{H2}	K^{H2}	k_1^{ads}	k_2^{ads}	K_1^{ads}	K_2^{ads}	k_1^{iso1}	k_2^{iso1}	K_1^{iso1}	K_2^{iso1}	k_1^{iso2}	k_2^{iso2}	K_1^{iso2}	K_2^{iso2}	k_1^{des}	k_2^{des}	k_3^{des}	K_1^{des}	K_2^{des}	K_3^{des}
k^{H2}	1.00																			
K^{H2}	0.47	1.00																		
k_1^{ads}	0.63	0.46	1.00																	
k_2^{ads}	0.66	0.40	0.36	1.00																
K_1^{ads}	0.17	0.21	0.17	0.21	1.00															
K_2^{ads}	0.49	0.21	0.36	0.25	0.25	1.00														
k_1^{iso1}	0.62	0.37	0.43	0.74	0.01	0.49	1.00													
k_2^{iso1}	0.62	0.75	0.51	0.45	0.03	0.05	0.20	1.00												
K_1^{iso1}	0.02	0.62	0.38	0.09	0.40	0.31	0.02	0.30	1.00											
K_2^{iso1}	0.13	0.46	0.21	0.39	0.01	0.53	0.38	0.37	0.61	1.00										
k_1^{iso2}	0.14	0.65	0.12	0.19	0.48	0.58	0.12	0.64	0.36	0.47	1.00									
k_2^{iso2}	0.70	0.84	0.70	0.65	0.12	0.10	0.62	0.65	0.46	0.23	0.34	1.00								
K_1^{iso2}	0.15	0.63	0.08	0.00	0.51	0.26	0.09	0.64	0.55	0.44	0.80	0.30	1.00							
K_2^{iso2}	0.28	0.41	0.77	0.17	0.02	0.20	0.30	0.21	0.48	0.38	0.18	0.64	0.09	1.00						
k_1^{des}	0.56	0.57	0.58	0.20	0.09	0.07	0.11	0.71	0.56	0.43	0.49	0.51	0.56	0.25	1.00					
k_2^{des}	0.01	0.48	0.06	0.30	0.26	0.68	0.02	0.44	0.23	0.37	0.67	0.27	0.43	0.09	0.33	1.00				
k_3^{des}	0.30	0.15	0.29	0.32	0.09	0.23	0.37	0.05	0.30	0.05	0.18	0.28	0.14	0.19	0.15	0.01	1.00			
K_1^{des}	0.25	0.70	0.57	0.12	0.04	0.06	0.39	0.30	0.72	0.37	0.03	0.72	0.21	0.71	0.30	0.01	0.38	1.00		
K_2^{des}	0.25	0.15	0.02	0.27	0.19	0.01	0.33	0.31	0.17	0.37	0.21	0.05	0.46	0.12	0.10	0.02	0.45	0.10	1.00	
K_3^{des}	0.35	0.79	0.29	0.18	0.26	0.45	0.01	0.79	0.54	0.67	0.86	0.55	0.76	0.20	0.71	0.62	0.07	0.31	0.21	1.00

Table F.3: Correlation matrix for run 11.

k^{H2}	1.00																							
K^{H2}	0.73	1.00																						
k_1^{ads}	0.30	0.10	1.00																					
k_2^{ads}	0.36	0.32	0.52	1.00																				
K_1^{ads}	0.63	0.48	0.37	0.67	1.00																			
K_2^{ads}	0.31	0.18	0.48	0.42	0.46	1.00																		
k_1^{iso1}	0.41	0.24	0.55	0.40	0.35	0.66	1.00																	
k_2^{iso1}	0.94	0.66	0.40	0.42	0.67	0.26	0.46	1.00																
K_1^{iso1}	0.65	0.64	0.50	0.70	0.65	0.69	0.75	0.68	1.00															
K_2^{iso1}	0.66	0.67	0.42	0.68	0.68	0.63	0.64	0.68	0.97	1.00														
k_1^{iso2}	0.03	0.33	0.02	0.30	0.11	0.53	0.68	0.06	0.58	0.48	1.00													
k_2^{iso2}	0.37	0.27	0.61	0.71	0.63	0.72	0.59	0.40	0.78	0.75	0.41	1.00												
K_1^{iso2}	0.70	0.54	0.59	0.75	0.81	0.73	0.69	0.73	0.92	0.89	0.41	0.86	1.00											
K_2^{iso2}	0.48	0.23	0.68	0.64	0.62	0.79	0.81	0.51	0.81	0.71	0.50	0.82	0.87	1.00										
k_1^{des}	0.61	0.27	0.10	0.29	0.14	0.31	0.23	0.58	0.13	0.06	0.54	0.31	0.05	0.21	1.00									
k_2^{des}	0.81	0.56	0.45	0.57	0.79	0.44	0.27	0.80	0.67	0.71	0.08	0.62	0.82	0.56	0.37	1.00								
k_3^{des}	0.49	0.36	0.58	0.48	0.40	0.65	0.69	0.54	0.77	0.64	0.56	0.65	0.74	0.85	0.08	0.47	1.00							
K_1^{des}	0.72	0.57	0.54	0.69	0.69	0.68	0.71	0.72	0.91	0.87	0.42	0.81	0.96	0.84	0.04	0.80	0.74	1.00						
K_2^{des}	0.04	0.12	0.35	0.53	0.23	0.67	0.63	0.03	0.62	0.54	0.70	0.63	0.55	0.61	0.76	0.12	0.46	0.57	1.00					
K_3^{des}	0.13	0.22	0.83	0.66	0.42	0.59	0.35	0.20	0.43	0.37	0.01	0.73	0.60	0.67	0.28	0.48	0.51	0.54	0.44	1.00				

Table F.4: Correlation matrix for run 12.

	k^{H2}	K^{H2}	k_1^{ads}	k_2^{ads}	K_1^{ads}	K_2^{ads}	k_1^{iso1}	k_2^{iso1}	K_1^{iso1}	K_2^{iso1}	k_1^{iso2}	k_2^{iso2}	K_1^{iso2}	K_2^{iso2}	k_1^{des}	k_2^{des}	k_3^{des}	K_1^{des}	K_2^{des}	K_3^{des}
k^{H2}	1.00																			
K^{H2}	0.43	1.00																		
k_1^{ads}	0.00	0.04	1.00																	
k_2^{ads}	0.55	0.47	0.08	1.00																
K_1^{ads}	0.43	0.88	0.04	0.36	1.00															
K_2^{ads}	0.52	0.82	0.31	0.36	0.87	1.00														
k_1^{iso1}	0.27	0.18	0.28	0.74	0.15	0.22	1.00													
k_2^{iso1}	0.03	0.05	0.30	0.25	0.01	0.11	0.50	1.00												
K_1^{iso1}	0.63	0.51	0.38	0.73	0.48	0.32	0.50	0.41	1.00											
K_2^{iso1}	0.05	0.06	0.38	0.45	0.14	0.14	0.27	0.09	0.09	1.00										
k_1^{iso2}	0.28	0.33	0.32	0.04	0.20	0.44	0.10	0.69	0.24	0.17	1.00									
k_2^{iso2}	0.40	0.90	0.31	0.32	0.82	0.68	0.02	0.12	0.58	0.06	0.04	1.00								
K_1^{iso2}	0.18	0.33	0.68	0.32	0.33	0.52	0.24	0.56	0.14	0.45	0.70	0.04	1.00							
K_2^{iso2}	0.74	0.71	0.08	0.59	0.67	0.70	0.35	0.22	0.75	0.12	0.02	0.77	0.02	1.00						
k_1^{des}	0.07	0.50	0.56	0.07	0.36	0.17	0.16	0.23	0.22	0.28	0.17	0.70	0.44	0.31	1.00					
k_2^{des}	0.33	0.43	0.57	0.06	0.33	0.24	0.04	0.47	0.43	0.39	0.23	0.68	0.60	0.58	0.76	1.00				
k_3^{des}	0.42	0.43	0.08	0.41	0.40	0.28	0.36	0.31	0.34	0.06	0.20	0.36	0.23	0.17	0.39	0.01	1.00			
K_1^{des}	0.70	0.75	0.09	0.68	0.62	0.65	0.32	0.31	0.60	0.29	0.46	0.59	0.48	0.75	0.13	0.15	0.03	1.00		
K_2^{des}	0.22	0.73	0.35	0.41	0.60	0.66	0.34	0.05	0.36	0.31	0.07	0.62	0.37	0.56	0.26	0.19	0.41	0.55	1.00	
K_3^{des}	0.37	0.31	0.60	0.59	0.25	0.38	0.43	0.47	0.09	0.47	0.59	0.03	0.81	0.17	0.35	0.45	0.09	0.66	0.34	1.00

Table F.5: Correlation matrix for run 13.

k^{H2}	1.00																														
K^{H2}	0.51	1.00																													
k_1^{ads}	0.94	0.35	1.00																												
k_2^{ads}	0.58	0.60	0.26	1.00																											
K_1^{ads}	1.00	0.51	0.94	0.57	1.00																										
K_2^{ads}	0.02	0.43	0.13	0.50	0.02	1.00																									
k_1^{iso1}	0.87	0.72	0.73	0.64	0.87	0.09	1.00																								
k_2^{iso1}	0.90	0.32	0.75	0.70	0.90	0.12	0.83	1.00																							
K_1^{iso1}	0.21	0.48	0.33	0.29	0.21	0.93	0.19	0.39	1.00																						
K_2^{iso1}	0.81	0.49	0.62	0.70	0.80	0.22	0.93	0.93	0.39	1.00																					
k_1^{iso2}	0.17	0.22	0.36	0.49	0.17	0.95	0.25	0.18	0.87	0.28	1.00																				
k_2^{iso2}	0.38	0.40	0.25	0.33	0.38	0.54	0.74	0.55	0.50	0.81	0.56	1.00																			
K_1^{iso2}	0.65	0.06	0.54	0.59	0.65	0.25	0.32	0.74	0.12	0.46	0.26	0.12	1.00																		
K_2^{iso2}	0.41	0.24	0.11	0.81	0.41	0.03	0.58	0.74	0.22	0.80	0.08	0.64	0.48	1.00																	
k_1^{des}	0.31	0.37	0.54	0.35	0.32	0.04	0.19	0.12	0.14	0.13	0.26	0.17	0.23	0.68	1.00																
k_2^{des}	0.10	0.75	0.16	0.08	0.10	0.22	0.30	0.24	0.46	0.04	0.03	0.13	0.57	0.40	0.74	1.00															
k_3^{des}	0.50	0.11	0.62	0.19	0.50	0.80	0.59	0.45	0.77	0.56	0.93	0.70	0.09	0.09	0.37	0.18	1.00														
K_1^{des}	0.74	0.53	0.86	0.02	0.74	0.20	0.69	0.44	0.20	0.46	0.49	0.34	0.05	0.16	0.81	0.59	0.72	1.00													
K_2^{des}	0.69	0.51	0.50	0.64	0.68	0.29	0.91	0.84	0.40	0.98	0.34	0.91	0.28	0.80	0.18	0.03	0.59	0.41	1.00												
K_3^{des}	0.02	0.16	0.30	0.79	0.02	0.60	0.06	0.27	0.43	0.22	0.76	0.04	0.48	0.69	0.73	0.41	0.66	0.59	0.19	1.00											

Appendix G

Used programs and subroutines

The programs and subroutines listed here are by no means the exhaustive list of those considered, tried, tested and/or used. This is especially true with regards to the Fortran packages which contain many auxilliary subroutines called by a main subroutine. Furthermore, the programs and Fortran packages are often concerted efforts by numerous individuals and/or groups spanning decades of updates and refinements.

In terms of the programs used, they are referenced with the information on their individual "About" menu items.

Fortran packages are referenced with regards to publications or user manuals detailing the algorithm and associated subroutines. Subroutines not associated with a package were referenced directly based on information supplied in the codes. The purposes of the individual surboutines were copied directly from the code and shortened where required. Most of these codes can be found readily after a search on the internet. Useful websites include: `www.netlib.org`, `www.netlib.org/lapack/`, `http://jblevins.org/mirror/amiller/`, `http://people.sc.fsu.edu/~burkardt` and `groups.google.com/group/comp.lang.fortran`, though there are many more.

Table G.1: Main computer programs used during this project (references list the information on the "About" menu item).

Program	Comment	References
Digital Visual Fortran 6.0	Platform for coding in Fortran 95 and earlier Fortran formats.	Corporation [1997-1998]
Visual Basic for Applications (Excel)	Programming language linked to Excel spreadsheet data.	Microsoft Corporation
LabVIEW 7.1	Programming language (graphical) for process control	National Instruments [2007]
R	Programming language and packages for statistical analyses.	for Statistical Computing [2008]
Excel 2003	Spreadsheeting.	Microsoft Corporation
Excel 2007	Spreadsheeting.	Microsoft Corporation
wxMaxima 0.80	Computer algebraic program.	Vodopivec [2004-2008]
Chemsep 5.1	Distillation simulation.	Kooijman & Taylor [2005]
JabRef 2.3.1	Literature database.	Alver et al. [2008]
TEXnicCenter 1 Beta 7.50	Platform for report writing in Latex.	Weinkauf et al. [1999-2008]

Table G.2: Fortran subroutines referenced in the thesis.

Name	Purpose	Reference/Author
GREG		
...DDASAC	Solves a DAE system. Limited to lower index problems.	Mike Caracotsios and W. E. Stewart
LAPACK		Anderson et al. [1999]
...SGBSV	Computes the solution to a real system of linear equations $\mathbf{AX} = \mathbf{B}$.	
...SGESV	Computes the solution to a real system of linear equations $\mathbf{AX} = \mathbf{B}$.	
...DGESV	Double precision version of SGESV.	
...DGETRI	Computes the inverse of a matrix using LU factorization.	
LBFGS		Nocedal [1980] and Liu & Nocedal [1989]
...SETULB	Solves bound constrained optimization problems via the BFGS method.	
MINPACK	Library: solves sets of nonlinear equations/performs least squares minimization.	Moré et al. [1980]
...FDJAC1	Estimates an N by N Jacobian matrix using forward differences.	
...FDJAC2	Estimates an M by N Jacobian matrix using forward differences.	
...HYBRD	Seeks a zero of N nonlinear equations in N variables.	
...LMDIF	Minimizes M functions in N variables using the Levenberg-Marquardt method.	
NL2SOL	Library: least squares minimization via an adaptive, nonlinear algorithm.	Dennis et al. [1981]
...DN2FB	NL2SNO modified to handle simple bounds on the variables.	David M. Gay
...NL2SNO	Minimizes nonlinear sum of squares using a finite difference Jacobian.	David M. Gay
SLATEC	Library: includes (amongst others) MINPACK	
...DFZERO	Searches for a zero of a function F(X) in a given interval (B,C).	L.F. Shampine and H. A. Watts
...RPQR79	Find the zeros of a polynomial with real coefficients.	W.H. Vandevender
Miscellaneous		
...BESIRK2	Solves a DAE system. Can handle higher index problems.	Kooijman [1995]
...CPOLY	Finds the zeros of a complex polynomial[a].	Jenkins & Traub [1972]
...NLEQ1S	Solves systems of highly nonlinear equations with a sparse Jacobian matrix.	U. Nowak and L. Weimann

[a] Code converted to Fortran90 by Miller [2009] using *TO_F90*.

Table G.2: Fortran subroutines referenced in the thesis.

Name	Purpose	Reference/Author
...NLEQ1	Solves systems of highly nonlinear equations.	U. Nowak and L. Weimann
...POLZEROS	Finds the zeros of a polynomial with complex coefficients[a].	Dario Andrea Bini
...RPOLY	Finds the zeros of a polynomial with real coefficients[a].	Jenkins [1975]

Appendix H

CV - February 2010

Current contact details	
Name:	Josias Jakobus Nieuwoudt
Address:	*Supplied if requested
Phone:	*Supplied if requested
E-mail:	jako.nieuwoudt@sasol.com
Personal details	
General:	30 years of age, male, married.
Birth:	11 January 1980, Citrusdal, Western Cape, South Africa.
Nationality:	South African
Languages:	Afrikaans, English (fluent); German, IsiXhosa (third languages)
Occupation:	Process Engineer, Process Development, Sastech R&D, Sasol (Sasolburg), South Africa.
Time line	
1987-1993	Primary school education at Gene Louw, Durbanville, South Africa.
1994-1998	Secondary school eduation at Stellenberg, Bellville, South Africa.
1998	Matriculated *summa cum laude* with exemption with the Cape Senior Certificate in: Afrikaans Eerste Taal, English First Language, Mathematics, Science, IsiXhosa Third Language, and Accounting.
1999-2002	Studied Chemical Engineering at the University of Stellenbosch, Chemical Engineering Department, South Africa.
2000	6 weeks vacation training at the Sasol Polymers Cyanide plant, Sasolburg, South Africa.
2001	6 weeks vacation training at Schümann Sasol, Sasolburg, South Africa.
2002	Completed final year undergraduate project titled "Computer-aided Molecular Design with SolvGen Multi GA: Designing Polymers by Using Genetic Algorithms" with supervisor Prof. I. Nieuwoudt (unrelated).

2002	Received a B.Eng. (Chem. Eng.) degree *cum laude* at the University of Stellenbosch, Chemical Engineering Department, South Africa.
2003-2005	Worked on an M.Sc.Eng. degree entitled "Design, Construction and Commissioning of a Catalytic Distillation System" on a joint project between the Universities of Cape Town and Stellenbosch (South Africa) with respectively A/Prof. Klaus P. Möller and Dr. Linda H. Callanan as supervisors.
2003	Completed several postgraduate courses - especially in catalysis.
2003-2007	Tutored various undergraduate courses including: Fluid Dynamics, Process Control, Mass Transfer (senior tutor) and Separation Technology (senior tutor).
2005	Received an M.Sc.Eng. (Process Engineering) degree *cum laude* at the University of Stellenbosch, Process Engineering Department, South Africa.
2005-2009	Worked on a PhD in Chemical Engineering at the University of Cape Town entitled "Kinetics and Mass Transfer Effects in 1-Hexene Hydrogenation CD" with supervisor Prof. K.P. Möller.
2008	Commenced work at Process Development, Sastech R&D, Sasol (Sasolburg), South Africa.
2008-2009	Worked as a team member on commissioning and running of a pilot plant slurry bed reactor system, including the coding of several tools to assist in data analyses for fundamental research and daily plant operation. Gained specific experience in slurry filtration, which includes statistical data analyses and planning and execution of an experimental plan to elucidate filtration in a slurry bed.
2009	On 1 September 2009, started a 6 month rotation to Sasol Wax, Sasolburg, South Africa to gain commercial plant experience and to assist in several optimization studies.

Achievements	
1999	Best First Year Chemical Engineering Student; Given membership of the Golden Key National Honour Society.
2001	Best Thermodynamics Student; Best Process Design Student.
2002	Best Final Year Technology Management Student; Best Final Year Project Poster; Best Final Year Chemical Engineering Design; Best Final Year Chemical Engineering Student; Final Year Project Innovation Prize (Chemical Engineering Departmental Winner); Bachelor of Engineering *cum laude*; Best Presentation (SAIChE R&D Day).
2003	Best Presentation (SAIChE R&D Day).

2005	M.Sc.Eng. *cum laude*.
2007	Best CATSA Poster.
Presentations and poster snapshots given at conferences.	
2003	Western Cape SAIChE R&D day: "Computer-aided Molecular Design with SolvGen Multi GA: Designing Polymers by Using Genetic Algorithms".
2003	South African Chemical Engineering Congress: "Computer-aided Molecular Design with SolvGen Multi GA: Designing Polymers by Using Genetic Algorithms".
2005	7th World Chemical Engineering Congress: "Olefin Hydrogenation in a Catalytic Distillation Column".
2007	CRE XI: Green Chemical Reactor Engineering: "Influence of a Reaction on the Mass Transfer Characteristics of a Catalytic Distillation System".
2007	CATSA: "Influence of a Reaction on the Mass Transfer Characteristics of a Catalytic Distillation System".

* Contact details are not supplied for privacy reasons.